Track substructure inclusions for reducing the risk of mud pumping in heavy haul tracks

by Joseph Arivalagan

Thesis submitted in fulfilment of the requirements for the degree of

Doctor of Philosophy

under the supervision of Professor Cholachat Rujikiatkamjorn and Distinguished Professor Buddhima Indraratna

University of Technology Sydney
Faculty of Engineering and Information Technology

December 2022

CERTIFICATE OF ORIGINAL AUTHORSHIP

I, Joseph Arivalagan, declare that this thesis, is submitted in fulfilment of the requirements for the award of Doctor of Philosophy, in the School of Civil and Environmental Engineering/Faculty of Engineering and Information Technology at the University of Technology Sydney.

This thesis is wholly my own work unless otherwise referenced or acknowledged. In addition, I certify that all information sources and literature used are indicated in the thesis. This document has not been submitted for qualifications at any other academic institution.

Production Note:
Signature removed prior to publication.

Joseph Arivalagan,

02 December 2022.

I would like to dedicate my thesis to my beloved parents

ACKNOWLEDGEMENTS

Pavithira Sivabalan, for her constant love, patience, and respect during the highs and lows of this PhD study. Finally, I would like to take this opportunity to thank everyone who has contributed to making this journey a successful one.

TABLE OF CONTENTS

LIST OF FIGURES

LIST OF TABLES

LIST OF SYMBOLS

ε_a - Cyclic axial strain

N – Number of cycles

N_c - Critical number of cycles

f - Frequency

O_f - Filtration opening size (f%)

d_f - Filament diameter (geotextile)

n - Porosity

t_{GT} – Thickness of the geotextile

μ_{GT} - Mass per unit area of the geotextile

ρ_f - Density of the fibres

i_{LG} – Hydraulic gradient across a soil thickness (L) and the geotextile

i_s – Rereference gradient in the soil

γ_d - Dry density

D_x - Soil particle size in mm for which x% of the soil is finer

C_u - Coefficient of uniformity of the subgrade soil

k_H - Horizontal permeability

k_V – Vertical permeability

O_{95} - Apparent opening size of geotextile filter

K_a - Reduction factor considering the effect of loading and partial clogging (geotextiles)

m_{vr} - Coefficient of volume compressibility

K_S - Hydraulic conductivity of the soil

K_{GS} - Hydraulic conductivity of a soil/geotextile composite

S_r - Degree of Saturation

V_w - Volume of water

V_v - Volume of voids

P_a' - Average contact pressure at the sleeper and the ballast interface

P_d - Design wheel load incorporating dynamic effects

P_s - Static wheel load

D_w - Diameter of the wheel

$\emptyset$ - Dimensionless impact factor (>1.0).

F - Factor depending on the type of sleeper and the track maintenance

U_h - Average degree of consolidation

T_h – Time factor

q_r - Maximum rail seat load

LIST OF ABBREVIATIONS

- ADR - Amplitude Domain Reflectometry
- AOS - Aperture Opening Size
- BDT – Basic Dynamic Test
- BFI - Ballast Fouling Index
- CL - Low Plasticity Clay
- CPT - Cone Penetration Test
- CSL - Critical State Line
- CSR - Cyclic Stress Ratio
- CSRc - Critical Cyclic Stress Ratio
- DBPF - Dirty Ballast Pumping Failure
- DFA - Dynamic Filtration Apparatus
- DFT - Dynamic Filtration Test
- EARS - Energy Absorbing Rubber Seam
- EPF - Erosion Pumping Failure
- EPP/EPWP - Excess Pore Water Pressure
- EPPG - Excess Pore Pressure Gradient
- FE - Finite Element
- FI - Fouling Index
- GPR - Ground Penetration Radar
- GR - Gradient Ratio
- HCR - Hydraulic Conductivity Ratio
- HS - Hardening Soil
- ICS - Instrumented Control Section
- LL - Liquid Limit
- LVDT - Linear Variable Differential Transformer
- MC - Mohr-Coulomb
- MP - Miniature Pressure Transducer
- NC - Normally Consolidated
- OC - Over Consolidated
- OCR – Over Consolidation Ratio
- OMC - Optimum Moisture Content
- P - Body Pressure Transducer

- PF - Percent Fouling

- PI - Plastic Index

- PL - Plastic Limit

- PP - Percent Passing

- PSD - Particle Size Distribution

- PVC - Percentage Void Contamination

- PVD - Prefabricated Vertical Drains

- RC – Relative Compaction

- RIBS - Rubber Intermixed Ballast System (RIBS)

- SPT – Standard Penetration Test

- SS – Soft Soil

- USCS - Unified Soil Classification System

- VCI - Void Contamination Index

- VWC - Volumetric Water Content

LIST OF PUBLICATIONS

1. Arivalagan, J., Rujikiatkamjorn, C., Indraratna, B., and Warwick, A. (2021). 'The Role of Geosynthetics in Reducing the Fluidisation Potential of Soft Subgrade under Cyclic Loading', Geotextiles and Geomembranes, vol. 49, no. 5, pp. 1324-38. https://doi.org/10.1016/j.geotexmem.2021.05.004.

2. Arivalagan, J., Rujikiatkamjorn, C., Indraratna, B., and Warwick, A. (2022). 'Effectiveness of a Geocomposite-PVD System in Preventing Subgrade Instability and Fluidisation under Cyclic Loading', Geotextiles and Geomembranes, vol. 50, no. 4, pp. 607-617. https://doi.org/10.1016/j.geotexmem.2022.03.001.

3. Indraratna, B., Singh, M., Nguyen, T., Rujikiatkamjorn, C., Malisetty, R. S., Arivalagan, J., Nair, L (2021). 'Internal Instability and Fluidisation of Subgrade Soil under Cyclic Loading', Indian Geotechnical Journal. https://doi.org/10.1007/s40098-022-00616-0.

4. Arivalagan, J., Rujikiatkamjorn, C., Indraratna, B., and Warwick, A. (2023). 'Effectiveness of Geosynthetics at Preventing Subgrade Instability under Cyclic Loading', Geo-Congress 2023 (Paper submitted).

5. Arivalagan, J., Rujikiatkamjorn, C., Indraratna, B., and Warwick, A. (2023). 'Cause-and-Effect of Subsoil Fluidization and Preventive Measures by Geosynthetic Drainage' 14th Australia and Newzealand Conference on Geomechanics (under preparation).

6. Arivalagan, J., Rujikiatkamjorn, C., Indraratna, B., and Warwick, A. (2022) 'Effectiveness of geosynthetics in preventing subgrade instability and fluidization under heavy haul loading', Australian Geomechanics Journal. (Under preparation).

AWARDS: Winner of AGS NSW Research Award 2022, Australian Geomechanics Society (Jul 2022) and Runner-up of the 2021 UTS FEIT Research Showcase (Nov 2021)

ABSTRACT

In recent times the demand for railway transportation has increased rapidly all over the world because a sustainable mode of transportation is needed to convey passengers and other commodities. However, subgrade soil with low bearing capacity is susceptible to instability under unfavourable drainage conditions. Subgrade soils with low/medium plasticity characteristics that undergo high cyclic stress levels are prone to fluidisation due to the rapid increase in excess pore water pressure (EPWP). Subsequently, subgrade can become unstable which leads to fines being pumped into the ballast/subballast layer (mud pumping). Excessive fine content, EPWPs, applied cyclic stress and frequency are the primary factors that induce particle migration and associated mud pumping. However, the actual mechanisms and cost-effective solutions to prevent subgrade fluidisation were not thoroughly understood due to its complexity and limitations.

In this study, a series of laboratory experiments were carried out to examine the following aspects of mud pumping: (1) the occurrence of subgrade fluidisation by simulating various drainage conditions, (2) the role geotextiles play in stabilising subgrade/ballast interface, and (3) the effectiveness of a prefabricated vertical drain (PVD) and geocomposite system in reducing the fluidisation potential using dynamic filtration apparatus (DFA). Soil specimens were tested at loading frequencies ranging from 1.0 to 5.0 Hz and cyclic deviator stresses from 40 to 70 kPa, simulates a maximum axle load of 35 tonnes. The axial strain (ε_a), EPWPs, and time-dependent excess pore pressure gradient (EPPG) that developed under undrained (impermeable) and free drained (no capping) conditions were used to define the failure criteria. The results showed that geocomposite with an effective filter membrane could prevent the migration of particles under typical train loading (25 tonnes). However, when the cyclic deviatoric stress increased (up to 35-40 tonnes of axle loading), the ability of geocomposites to alleviate the EPWP diminished.

The effectiveness of PVDs was also assessed under various loading conditions. The combined PVD-geocomposite system could reduce the accumulation of EPWPs and continuously dissipate them as the number of cycles increases, thereby providing a viable solution for mitigating the effects of subgrade fluidisation. Design guides were introduced with the field applications at Chullora, NSW. Finally, a numerical study was carried out to evaluate the use of geosynthetics under typical rail track conditions. The predictions revealed the efficiency of geosynthetics at regulating and dissipating the generation of EPWPs under train loading.

Keywords: Subgrade fluidisation; Mud pumping; Geosynthetics; Excess pore water pressure

CHAPTER 1: INTRODUCTION

1.1 Study Background

The increasing demand over the past few decades for railway transportation requires a faster and more reliable rail network for transferring people and goods. However, railway tracks built on weak subgrade soil are vulnerable to instability due to the induced and repeated dynamic stress during the passage of heavy-haul trains and passenger trains. The railway authority spends hundreds of million dollars on frequent remedial measures and costly maintenance, mainly for the deterioration of the track geometry caused by poor drainage. Indeed, the rapid generation of Excess Pore Water Pressure (EPWP) during cyclic load leads to a significant reduction in effective stress and an increase in the void ratio where the dislocated/separated finer particles can be pumped up under critical hydraulic conditions (mud pumping). A severe mud pumping site near Wollongong city is shown in Figure 1. 1.

Figure 1. 1: Subgrade mud pumping (Courtesy: Prof. Indraratna)

The capping layer or the sub-ballast is generally expected to: (1) reduce the cyclic stress transferred from the ballast to the subgrade, and (2) provide appropriate drainage conditions in railway tracks that can prevent subgrade fines from upward pumping. Railway embankments which are constructed on subgrade where the groundwater table is close to the subgrade surface are more prone to instability under cyclic load. Moreover, the critical hydraulic gradient induced by cyclic EPWPs inside the subgrade (at different depths) leads to the onset of subgrade instability/fluidisation. For these reasons, conventional capping which often becomes impermeable, fails to perform its primary function and leads to excessive settlements and track degradation, as has been reported at various sites including NSW, Australia. A brief description of the pumping of fines in railway tracks which highlights the significant difference between soil fluidisation and liquefaction is given below.

1.2 Soil Fluidisation (Mud Pumping) and Soil Liquefaction

The shallow subgrade below a railway can become unstable due to the migration of moisture and fine (silt) particles towards the top surface due to the EPWPs that develop under a cyclic load. Subsequently, the moisture content of subgrade at the surficial layers can increase to the liquid limit, thus forming a slurry. However, cohesive soil with a high clay content can resist fabric instability by preventing the segregation of fine particles and moisture migration within the fabric. Soil liquefaction during earthquakes is a deep-seated phenomenon that is caused by the inevitable build-up of EPWP due to low-frequency seismic accelerations. The excessive pore water pressures generated by seismic shaking can affect the non-linear dynamic soil response. Subsequently, the soil loses its bearing capacity (zero effective stress) during liquefaction, and the overlying structures can sink into the ground.

Mud pumping is a shallow layer phenomenon where the water content can reach its liquid limit before the effective stress becomes zero. Laboratory tests carried out by Indraratna et

al. (2020) reported that the rapid internal migration of very fine particles carrying moisture exacerbated by increased hydraulic gradients can very quickly make the soil close to the surface have a liquidity index (LI) approaching one. In this case, the soil becomes a liquid or slurry because its water content is equal to the liquid limit (LL). This mainly occurred due to the build-up of EPWP in the soil so further laboratory analysis is needed to investigate the mud pumping phenomenon more closely.

1.3 Problem Statement

Although some previous research studies addressed the mud pumping issue, the factors that cause mud pumping, such as water associated with drainage conditions, fines properties, and cyclic load parameters, have not been addressed very well (Duong et al. 2013; Kuo et al. 2017; Nguyen et al. 2019). In most cases, the failure mechanism of compacted granular capping and other model tests used to assess ballast degradation and ballast/subgrade interaction were captured under cyclic loading conditions (Indraratna et al. 2018; Indraratna & Raut 2006; Israr & Indraratna 2018; Liu & Xiao 2010; Tennakoon & Indraratna 2014; Trani & Indraratna 2010). Due to its complex nature, the mechanism of subgrade fluidisation must be investigated using laboratory experiments and mathematical and numerical models. To investigate the performance of weak soil, large-scale laboratory tests are required (primary method) to simulate typical train-induced cyclic loading.

The conventional solution for mud pumping is often to clean and/or replace the fouled material at mud pumping sites. However, this approach is costly and still does not prevent the chance of mud pumping occurring again (i.e., it is not a permanent solution for mud pumping). To alleviate the occurrence of mud pumping, the drainage capacity at the ballast/subgrade must be considered during construction and maintenance activities. The other solution is chemical stabilisation, which may reduce subgrade fluidisation (Karol 2003), but this approach is not environmentally friendly because it has adverse effects on the natural ground (Lenart et al. 2018). The best solution for mitigating the migration of

fines is to install geosynthetics or geocomposites and provide additional drainage to prevent subgrade fluidisation.

Geosynthetics are one of the most effective and sustainable approaches used in railway tracks to mitigate the migration of particles under dynamic loading conditions. The installation of prefabricated vertical drains (PVDs) and geotextiles in railway tracks are shown in Figure 1. 2. The justification for using a geotextile as a capping layer in railway tracks has not been emphasised in previous studies. It is important to assess how well geosynthetics can prevent particle separation and upward pumping into the ballast layer and the governing factors that cause subgrade fluidisation under critical loading conditions. Geotextiles can prevent fine particles from moving towards the overlying layer and provide adequate drainage if clogging can be prevented (Chawla & Shahu 2016; Kermani et al. 2018). The design criteria of a geotextile should satisfy filtration, drainage, and clogging in terms of the aperture opening size (AOS) and any other properties under critical hydro-mechanical circumstances (Ayres 1986; Luettich et al. 1992).To decelerate EPWP generation at a greater depth within subgrade soil, PVDs can be installed; they provide a short radial drainage path and also increase the stability of soft weak soils. The use of PVDs combined with geotextiles/geocomposites to mitigate mud pumping phenomena has not really been well established or understood comprehensively in previous studies.

1.4 Research Hypotheses

The research hypothesis is developed based on research questions and previously published research based on the theory. The following research hypotheses clearly define the focus of the experiment and expected outcomes.

- The dynamic filtration tests can be used to assess the primary factors that cause subgrade fluidisation by simulating various drainage conditions (e.g., Undrained, free drainage, and partially drained conditions)

- Geosynthetics (geotextile, geocomposite and PVDs) can be used to dissipate the generation of EPWPs (the primary factor which causes subgrade instability in soft soils) during the train loading and even after the passage of the train.

- The generation of time-dependent excess pore pressure gradient plays a crucial role in inducing the migration of fine particles from the middle towards the subgrade surface.

- The effectiveness of geotextiles and geocomposites will diminish under higher axle loads and increased train speeds.

- The combined PVD-Geocomposite system can be used to alleviate the development of critical EPWPs and control soil softening at the ballast/subgrade interface.
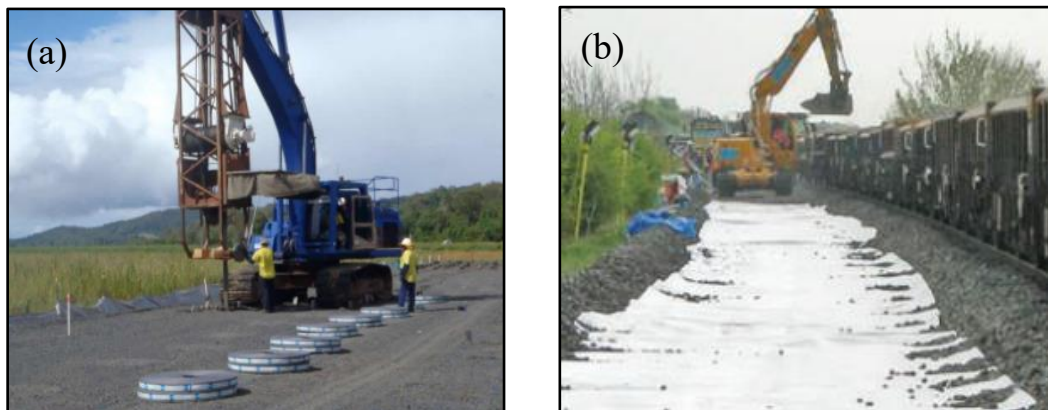
Figure 1. 2: (a) The installation of PVDs (b) geotextiles (Courtesy: Global Synthetics)

1.5 Objectives and Scope of the Present Study

This research is aimed to investigate the role of geosynthetics in reducing the fluidisation potential of soft subgrade under adverse hydro-dynamic conditions. A series of dynamic filtration tests can be used to assess the effectiveness of geosynthetics to alleviate critical pore water pressure generation and migration of fine particles at the ballast/subgrade interface.

The specific objectives of this research are as follows:

- o To study the inception of subgrade instability under the cyclic loading conditions and identify the key factors causing the mud pumping while addressing the generation of Excess Pore Pressure Gradient (EPPG) and critical flow conditions.

- o To evaluate how well the geosynthetics placed in weak subgrade soil can alleviate the development of EPWPs and prevent particles from migrating across the soil/geotextile interface. Large-scale dynamic filtration tests were carried out to simulate the in-situ hydraulic conditions in railway tracks.

- o To determine how effective geosynthetics are in terms of filtration and drainage and evaluate the effects of the loading characteristics (different axle loads and speed of heavy haul trains).

- o To analyse the role of a combined PVD-Geocomposite system in mitigating or controlling the onset of subgrade instability and fluidisation under cyclic loading.

- o To develop the numerical models to assess the performance of geosynthetics in a typical railway track environment; the drainage capacity of the track at ballast/subgrade interface can be captured by carrying out FEM analysis.

1.6 Innovations and Salient Outcomes

- o Although geotextiles are being used as a filter and separator in highway and railway embankments, their ability to prevent the fluidisation potential of soft soils has not been well established in previous studies. The Dynamic Filtration Apparatus (DFA) was designed and built at the University of Technology Sydney in order to assess the key factors that cause subgrade fluidisation under adverse drainage conditions and the effectiveness of geosynthetics to prevent mud pumping.

- o This study shows that the application of geocomposite with a filter membrane can be an effective way to stabilize the railway tracks by preventing particle migration

and dissipating the EPWPs, especially near the subgrade surface. A continual dissipation was also observed with the inclusion of geocomposites during cyclic loading, and this can make the track more stable.

o The inclusion of PVDs has shown promising signs of dissipating the quick rise of EPWPs at deeper subgrade soil while geocomposite can provide adequate surficial drainage at the interface. From a practical perspective, the stabilization of rail tracks with a PVD-geocomposite system can be employed to prevent the fluidisation potential of soft soils.

o The practical guidelines for improved track performance in weak soils were established for industry practitioners, and the design criteria for geotextiles are included in the guidelines.

o The geocomposites and geotextiles were included in Chullora filed trail because the subgrade soil had a high fine content and the rail track was flooded due to heavy rainfall. The geosynthetics can improve the drainage capacity and prevent particle separation and upward migration of fines.

1.7 Organisation of Dissertation

There are ten chapters in this thesis. A brief description of the ten chapters is as follows:

o Chapter 1 starts with a brief introduction on the failure mechanisms of mud pumping and associated remedial action required to prevent interruptions to train transport systems.

o Chapter 2 provides a comprehensive literature review of subgrade fluidisation and the associated mud pumping phenomenon. The experiments and theoretical analysis carried out by numerous researchers on mud pumping projects are summarised, and then the mitigation measures for mud pumping and previously proposed guidelines are briefly described in Chapter 2.

- Chapter 3 describes the methodology proposed for the dynamic filtration tests (DFT). The research approach and testing procedures for evaluating the performance of geosynthetics are detailed in this chapter.

- Chapter 4 describes the experimental program which consists of preliminary hydraulic tests and dynamic filtration tests. The results of cyclic tests conducted to assess the performance of geotextiles/geocomposites using slurry are presented.

- Chapter 5 contains the experimental results of undrained and free drainage conditions. The rapid change in moisture content and upward migration of fine particles towards the ballast layer under cyclic loading are reported.

- Chapter 6 explains the role of geotextiles/geocomposites in preventing particle migration and subgrade fluidisation. This section describes the cyclic tests carried out on a large soil specimen (240 mm diameter by 200 mm high) using the geotextiles and geocomposites having different filtration and drainage properties.

- Chapter 7 contains the design guidelines for the appropriate selection of geotextiles and geocomposites under cyclic loading conditions. The characteristics of subgrade soils vulnerable to mud pumping and the function of geotextiles are elaborated.

- Chapter 8 reports the performance of PVDs and geocomposites under rail tracks. The effectiveness of geocomposites and PVDs installed to alleviate the rapid generation of EPWPs and prevent the potential for early soil softening/fluidisation is discussed in conjunction with plotted test results from a series of laboratory experiments.

- Chapter 9 proposes an FEM analysis to capture the generation of EPWPs with and without geosynthetic inclusions. The ability of geotextiles, PVD and PVD-geotextile systems in dissipating the EPWPs and preventing subgrade instability are discussed under adverse hydro-dynamic conditions.

- Chapter 10 explains the design and construction stages of the Chullora Field Trial. The geosynthetics tested in this study were used in the real field. A suite of instruments placed in four different sections and techniques used to measure the performance of geosynthetics under the typical train loading are discussed.

- Chapter 11 provides conclusions, research highlights, discussions, and recommendations for future research work. It also discusses the applicability of the research and the possible practical implications. A list of references follows Chapter 11.

CHAPTER 2: LITERATURE REVIEW

2.1 General

The Australian railway network is over 43,000 km long and carries some of the world's heaviest and longest freight trains (*Australian Trade and Investment Commission*). In recent times, railway transport has become more competitive than road and other modes of transportation (Road and Rail Freight 2018) and as such plays a key role in Australia's economy by supporting mobility and job creation (ARA 2020). However, track instability caused by mud pumping, ballast breakages, differential settlement, and track misalignment requires millions of dollars for the frequent maintenance needed to ensure safety and passenger comfort.

Undoubtedly, the stability of the substructure is greatly affected by the cyclic stresses caused by the increased speed of the train and axle load. These dynamic stresses can induce the migration of fines into the ballast and subballast (mud pumping) under poor drainage conditions. Mud pumping sites from all over the world are shown in Figure 2. 1. These pumped-up fines or slurry into the ballast layer can drastically reduce the drainage properties, and moreover, the fouled ballast particles coated by clay slurry immediately lose their shear strength and can no longer resist the dynamic stresses developed under repeated cyclic loading (Tennakoon & Indraratna 2014). The particle size distribution, relative density, plasticity characteristics of the soil, water content, effective stress, and the various type of loading should be considered when trying to prevent mud pumping in railway tracks (Nguyen & Indraratna 2021; Nguyen et al. 2019).

This chapter reviews past and recent research studies with special reference to subgrade fluidisation and the prevention techniques or mitigation measures used in railway tracks. While compacted sand blankets and geosynthetics (capping layer) have been used to prevent subgrade failures, the complex process of degradation involves various mechanical aspects, which means that mud pumping and cost-effective prevention measures are still not understood completely and nor are they well established (Nguyen et al. 2019). Several laboratory tests, site investigations, and theoretical models that capture the fundamental concepts of mud pumping in railway tracks are still needed to understand the mechanism of subgrade mud pumping.

Figure 2. 1: Mud pumping sites in (a) Ashfield, New South Wales (Tennakoon et al. 2014) (b) Queensland (Indraratna et al. 2012), (c) The United Kingdom (Ghataora et al. 2017) and (d) Mansfield, Massachusetts (Aw 2007)

2.2 Rail Track Structure

2.2.1 Track Components

The superstructure and substructure of rail tracks consists of rails, sleepers, ballast, sub-ballast, and subgrade. The superstructure includes the rails, ties (sleepers), and fastening systems that can withstand train loading. Rails are laid on concrete, steel, or timber sleepers to guide the wheels of the train. Concrete/Timber sleepers are mainly used to distribute the loads into the coarse ballast. Ballast is the uppermost layer in the substructure, it is about 250 mm - 350 mm thick, and acts as the load-bearing platform and uniformly distribute the load into the subballast and subgrade. The subballast or sand blanket is the granular layer compacted on the subgrade. Subballast consists of well-graded crushed rock with a thickness that can vary from 100 mm – 150 mm. The sub-ballast layer prevents the ballast from penetrating the subgrade and also reduces the fine migration. The bottom layer is subgrade, i.e., the foundation for the track bed. Subgrade can be a treated soil or fill material if the natural soil does not have enough bearing capacity to withstand train-induced loads. Any loss of stiffness in the subgrade soil can significantly affect the substructure and superstructure and lead to the degradation of ballast and differential rail settlement.

2.2.2 Track Response under Heavy Haul Loading

The ballast layer in railway tracks provides a dynamic resilience against huge axle loads and the increasing speed of freight trains (Indraratna & Salim 2005), whereas the subballast acts as a filter and separation layer that evenly transfers cyclic stress from the coarse ballast to the subgrade. The filtration characteristics of the subballast layer are increasingly important because it must provide adequate drainage and retention capacity (Selig & Waters 1994). Figure 2. 2 shows the stress distribution on track structure where concrete and wood ties are used (Li et al. 2015) and the maximum vertical stress (>340 kPa) is generated directly beneath the rail in both sleepers.
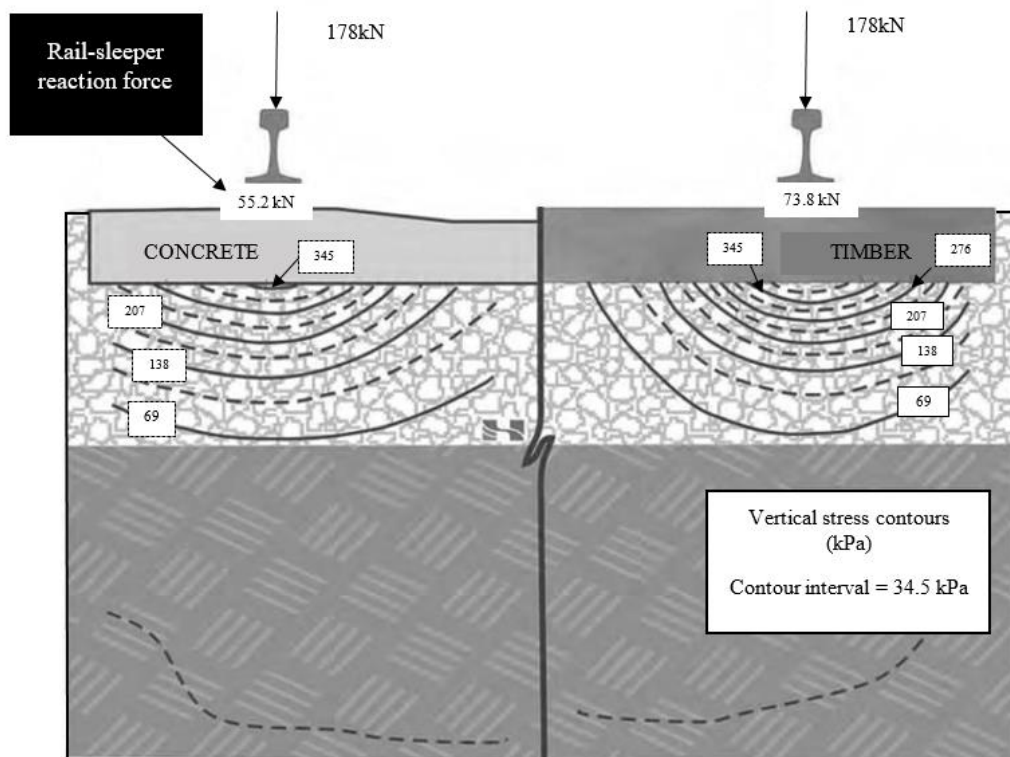
Figure 2. 2: The vertical stress transmission under concrete and wood ties (modified after Li et al. (2015))

2.2.2.1 Maximum Vertical Stress

During the passage of trains, the loading pulses generated by trucks (bogie) are transferred to the substructures. The amount of stress transmitted to the substructure may determine the type of track/subgrade failures. Maximum stress at the ballast surface can be observed when the wheel is directly over the sleeper-ballast interface (Indraratna et al. 2011b). The vertical stress developed at the sleeper/ballast contact area by a coal train with wagons (100 tons) with wheel irregularities is shown in Figure 2. 3. It is clear that the maximum vertical cyclic stress increased up to 230 kPa, in fact one peak reached more than 415 kPa; this corresponds to the arrival of wheel-flats. This implies that large dynamic impact stresses can be developed due to wheel imperfections and should be assessed in track designs.
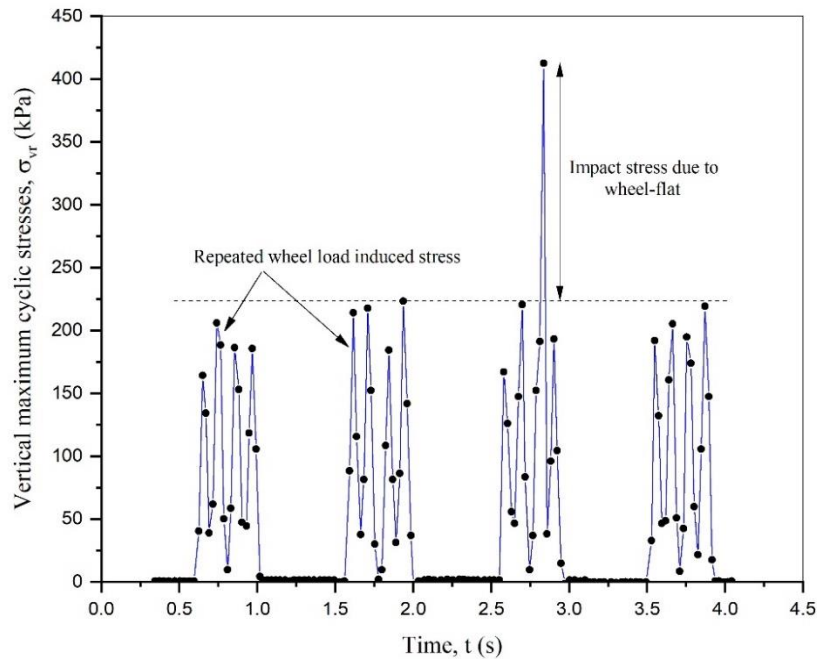
Figure 2. 3: Vertical cyclic stresses σ_{vr} generated at the ballast layer (modified after Indraratna et al. (2010a))

2.2.2.2 Stress Attenuation

The dynamic stress exerted onto subgrade soil attenuates rapidly from the subgrade surface. Liu & Xiao (2010) reported that the stress pulses caused by 120 km/h freight trains and 200 km/h passenger trains are different from the stress imparted onto the subgrade as the depth increases. Field measurements reveal that the dynamic stress caused by a passing train attenuates within shallow depths. For instance, the dynamic stress that develops 2.5 m below the subgrade surface can drop to 20% of the surface mean value. Furthermore, the loading frequency can affect the threshold stress, and the railway subgrade also has the potential for shear failure under frequent loading with increased train speed (Liu 2006).

2.2.3 Track Instability and Characteristics of Subgrade Problems

The deterioration of subgrade soil dramatically affects the performance of the superstructure and substructure, it also results in ballast fouling, track misalignment and

degradation, ballast pockets, mud pumping, and differential settlements. Subgrades with fine-grained material under continuous train-induced loads may fail by attrition from the ballast, progressive shear failure, or excessive settlement due to the accumulation of excessive plastic strain (Li & Selig 1995; Li & Vanapalli 2021). Subgrade soil attrition associated with mud pumping is mainly due to repetitive dynamic loads, excessive water content, and the existence of fine particles in the subgrade. The cyclic EPWPs induce high hydraulic gradients across different soil layers that can cause fines to migrate with increased seepage, thereby forming slurry on the subgrade surface (Boomintahan & Srinivasan 1988). Once the fine particles migrate upwards and fill the voids in the ballast layer, it can no longer provide structural stability.

2.3 Mechanisms of Mud Pumping/Subgrade Fluidisation

2.3.1 The Occurrence of Mud Pumping

Numerous research studies have been carried out over the previous decades to study the occurrence of mud pumping and it is still not well understood how the mechanism of subgrade fluidisation varies with different loads and the characteristics of the soil.

2.3.1.1 Mud pumping Induced by Localised Suction

Takatoshi (1997) reported that mud pumping is caused by suction under four stages, as shown in Figure 2. 4. There are gaps between the sleepers and ballast beds due to dilation and breakage as ballast degrades due to long term cyclic loading. When a train passes over the ties the train loads impart high EPWPs in the subgrade. During unloading, the space left by the sleepers generate negative EPWPs or suction that cause upward fine migration. This suction force is repeated under cyclic loading, causing the fines to accumulate inside

the ballast layer, as shown in Figure 2. 4. The poor sleeper-ballast contact creates an upward

suction in the ballast layer that can draw fine particles into the ballast layer, thereby causing

fouled ballast. This was first proposed by Takatoshi (1997) and was further complemented

by later studies (Liu et al. 2013; Wheeler et al. 2017). Hudson et al. (2016) reported that

voids under sleepers combined with localised stress and cyclic deformation accelerate mud

pumping in railway tracks. A similar mechanism was observed in slab tracks where the

gaps between the concrete slabs and subgrade caused a fluidised subgrade surface that

subsequently accelerated mud pumping near the base plate expansion joints during the next

train loading (Cai et al. 2015).
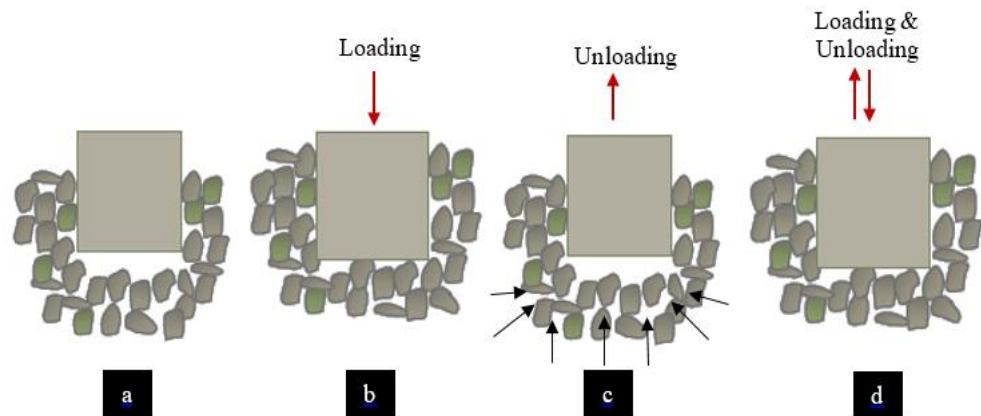
Figure 2. 4: Initiation of mud pumping proposed after Takatoshi (1997) (a) Floating tie

between sleeper and ballast, (b) High pore water pressure, (c) Fine migration by suction,

and (d) Mud pumping

2.3.1.2 Subgrade Fluidisation under Cyclic Loads

Cyclic loads generate EPWPs under rail tracks and induce fines to move upwards through

the surface layers. The penetration of ballast and associated fine migration leads to an

'interlayer creation,' i.e. a layer with a mixture of materials at the ballast/subgrade interface

(Duong et al. 2014a). Aw (2007) reported that mud pumping can be identified in the zone

with excess water, thus weakening the base and allowing fine particles to migrate into the

16

voids. Subsequent ballast penetration into the subgrade was also reported under repeated cyclic loading conditions. Unit cells with a rigid wall (physical model) test were also used in past studies to examine the mechanism under different loading conditions (Boomintahan & Srinivasan 1988; Ghataora et al. 2006).

Duong et al. (2014) carried out tests using a 550 mm transparent thermoplastic cell to observe the 'interlayer creation'. A 220 mm thick subgrade consisting of an artificial mixture of 70% crushed sand and 30% kaolinite clay by dry weight was compacted to 1500 kg/m^3 of dry unit mass, and then a 160 mm thick ballast was placed onto the subsoil. No fines were pumped up during the unsaturated tests or no changes observed at the interface between these two layers even after 500,000 cycles (5Hz). However, the ballast immediately penetrated in subgrade and created upward migration of fine particles under saturated conditions. Permanent displacement continues to increase rapidly during cyclic loading. There was a significant amount of fine particle migration during cyclic loading compared to monotonic/static constant loading, as shown in Figure 2. 5. This shows that the migration of fines occurs due to not only ballast penetration (i.e., interlayer creation) but also the generation of EPWP combined with induced local hydraulic gradient.
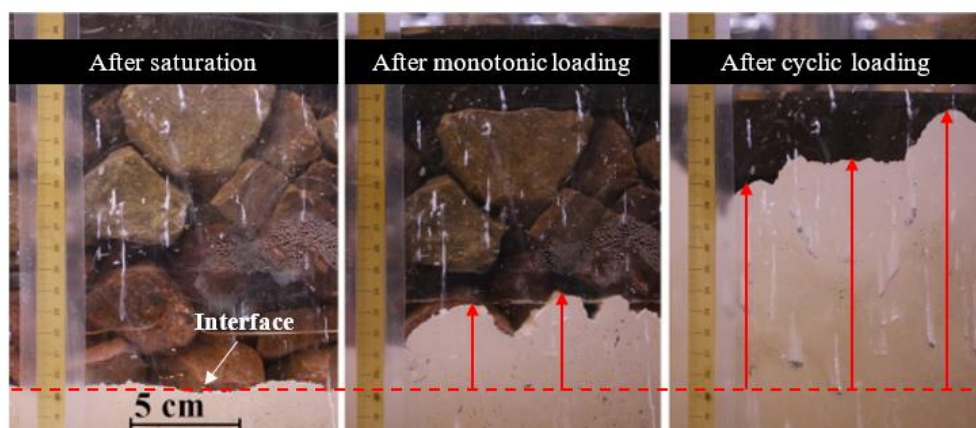
Figure 2. 5: Photos showing the evolution of the interface (a) after saturation, (b) after monotonic loading, and (c) after cyclic loading (after Duong et al. (2014a))

The cyclic load generates more EPWP than monotonic loading, and the EPWP that developed into the subgrade exceeded the effective stress, thereby causing the surface of the soil to rise towards the ballast particles. The transformation of subgrade soil into slurry depends mainly on the drainage capacity of the foundation. Insufficient drainage at the ballast/subgrade interface (limited or strictly undrained conditions) increases the water content near the top subgrade surface and leads to a significant rise in EPWP under repeated loads (Indraratna et al. 2020d).

Indraratna et al. (2020d) carried out cyclic triaxial tests under undrained conditions using low-plastic soil with a PI of about 11%. The effects of the cyclic stress ratio (CSR), speed of trains, and relative density of soils were determined by carrying out cyclic triaxial tests. The CSR can be defined as the ratio between the applied cyclic stress and twice the effective confining pressure. The fluidisation of soft soils under undrained cyclic loading was examined under different frequencies (1 to 5 Hz), CSRs (0.1 to 1.0), and relative densities (1600, 1680, and 1790 kg/m^3). The results shows that 'internal redistribution of moisture' can explain the phenomenon of mud pumping under cyclic loading. The rapid increase in moisture content approaches the liquid limit (LL) and it reveals that a slurry-like state is developed at the surface under repetitive loading.

Subgrade fluidisation can be triggered when the CSR exceeds a threshold level, but it also depends on the dry density. Figure 2. 6(a) shows that a soil specimen compacted to lower densities are more prone to subgrade fluidisation, even under lower critical CSRs, with an increased number of cycles. However, the soil specimen with around 95% of relative density and subjected to higher CSRs (0.4 and 0.5), failed under a lower number of cycles. Figure 2. 6(b) shows the residual axial strain under different CSRs and relative densities. The rapid increase in axial strain observed for lower density soil, but it rose to above 0.25% when the CSRs increased. Although stable samples with an increased fine content showed a decreasing incremental rate of EPWPs and axial strain, the fluidised samples resulted a

rapid increase in EPWPs and strain with an increased number of cycles (Indraratna et al. 2020d).

According to Indraratna et al. (2020a) the fines content (Kaolin) in subgrade increase the cyclic resistance of subgrade. Subsequently, soil with 10% kaolin changed its failure mode to conventional undrained shear failure. However, an excessive fines content (above 30% of kaolin) reduced soil resistance dramatically. Aw (2007) carried out field investigations and showed that the correlation between EPWP in subgrade soils was not clear compared to the laboratory experiments. Therefore, more studies are needed to understand the mud pumping phenomenon under cyclic loading while considering different field variables.
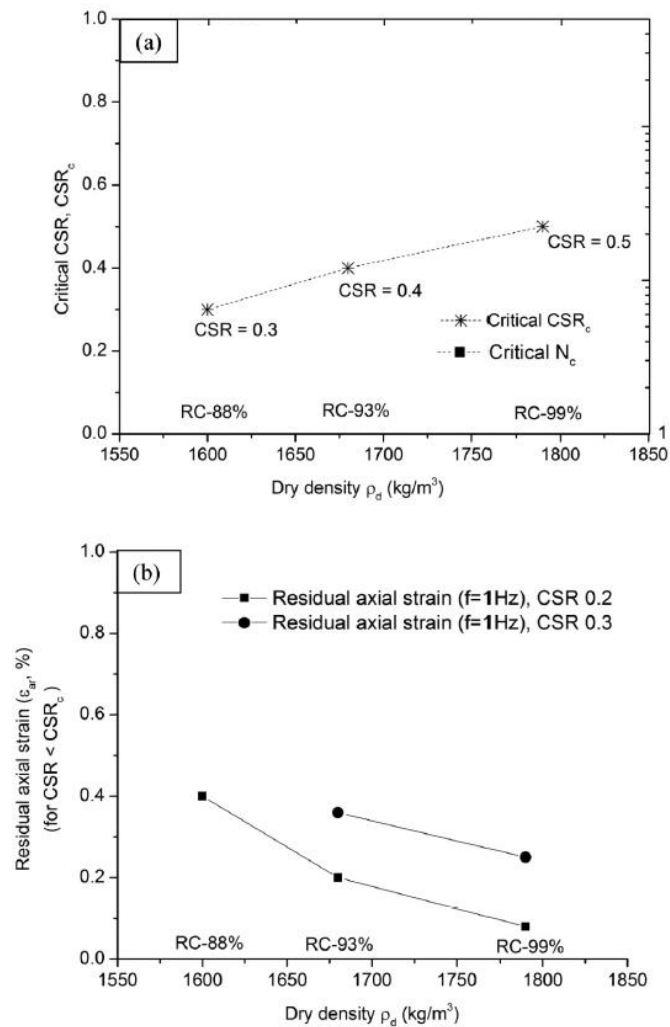
Figure 2. 6: The effect of dry density inducing subgrade fluidisation (a) Critical CSRs and (b) residual axial strain (after Indraratna et al. 2020d)

2.3.1.3 Effects of Weather on Mud Pumping

Changes in the weather conditions such as significant rainfall and very low temperatures also affects the occurrence of mud pumping because water is the vital component needed to initiate mud pumping. The drainage capacity of a track foundation can be hindered during typical rainfall events (>67.5 mm/hour). Several studies were carried out to predict how these adverse weather conditions created more potential for mud pumping (Duong et al. 2014a; Hudson et al. 2016; Indraratna et al. 2020a; Ito 1984; Kuo et al. 2017). The test results showed that railway tracks became more vulnerable during high rainfall periods due to a higher groundwater table and water ponding in railway foundations. Li & Wilk (2020) investigated a 'Rainy Section' test zone in order to understand the mechanisms of mud pumping. The stability of track-substructure can be characterised by drainage capacity and resistance to induced cyclic stress under repeated dynamic wheel loads. Figure 2. 7 shows the 6.1m long rainy test section, where the ballast contains around 40% fines (degraded ballast material and pumped-up fines). The field investigations showed that the pumped-up fines from the subgrade becoming weaker under 40 million gross tons (MGT) of traffic loading.

Figure 2. 7: Rainy test section with fouled ballast (Li & Wilk 2020)

Figure 2. 8: Peat boils and voids between the sleeper and the ballast (after Wheeler et al. 2017)

2.3.1.4 Unstable Soft Foundations and Transition Zones

Issues due to the instability of soft foundations has been reported in Canada, Australia, France, India, and other European countries because the cyclic load could induce large rail displacements, differential settlements, and increased risk of derailments (Duong et al. 2014b; Hendry et al. 2013; Powrie 2014; Trinh et al. 2012; Wong et al. 2006). Wheeler et al. (2017) reported that subgrade soil with very low stiffness was particularly prone to create voids between the rail and sleeper due to pore water pressures and associated pumping of fines. As shown in Figure 2. 8, the pumping of mud directly from a peat soil creates piping hole formations (peat boils) accompanied by large voids beneath rail and

sleepers, as well as between the sleeper and ballast layer. The soft soil foundation was vulnerable to progressive shear failure under static loads and subsequently caused mud/slurry at the subgrade surface. It tends to pump-up onto the surface during cyclic loading under increasing EPWP as the train loads squeeze the mud. The deterioration of tracks and potential for mud pumping is commonly found in vulnerable sections of rail lines such as switches and crossings, expansion joints, and transition zones (Li et al. 2015; Powrie 2014; Wang & Markine 2019; Yang et al. 2018). According to Coelho et al. (2011), a train passing through the transition zones can lead to significantly larger impact loads and abruptly reduce the track stiffness.

2.3.1.5 Ballast Mud Pumping

Unlike subgrade mud pumping (Section 2.3.1.2), the mechanism of ballast mud pumping is based on an increasing EPWP inside the ballast layer caused by accumulated fines and ballast degradation (Brown & Selig 1991). The ballast becomes contaminated with fines, and also contains crushed particles and coal fines which can infiltrate and accumulate in the ballast layer (Aw 2007; Ayres 1986; Selig et al. 1992). The degradation of ballast is primarily due to the infiltration of coal particles spilled from coal wagons. However, voids in the ballast mixed with infiltrated fines impair the drainage capacity, which means the ballasted track may not withstand greater axle loads in the long term (Gundavaram & Hussaini 2021; Indraratna et al. 2010b).

Ionescu (2004) investigated the characteristic degradation of the ballast layer in railway tracks. This study also reported on how the deposition of fines in the voids of the ballast layer reduced its drainage capacity under continuous train loading. As a result, the permeability of fouling ballast decreased much more than typical fresh ballast due to the intrusion of fines such as coal, clay, and silt. Tennakoon et al. (2012) introduced a Void Contaminant Index (VCI) and investigated the correlation between the percentage of fouling and the drainage properties of the ballast layer.

2.3.2 Key Factors Inducing Mud Pumping

According to Nguyen et al. (2019), there are three primary factors, excessive fines, water content, and dynamic load that contribute to mud pumping in railway tracks. The evolution of EPWP in soils, the migration of fine particles under cyclic loading, and the factors affecting the generation of cyclic pore water pressure are also discussed in this section.

2.3.2.1 The Source of Excess Fines

Excess fines can come from (1) the subgrade and subballast, (2) ballast breakage, and (3) external sources such as dust, waste materials, and wagon spillage (Nguyen et al. 2019). Figure 2. 9 shows the primary sources of fines inducing mud pumping in railway tracks. Subgrade pumping and ballast breakage are induced by the internal processes of a railway foundation, whereas dust and wagon spillage come from external sources. During subgrade degradation, the subgrade soil develops a higher EPWP which leads to particle migration. Ayres (1986) classified these factors as: 'Erosion Pumping Failure' (EPF) and 'Dirty Ballast Pumping Failure' (DBPF). Under EPF, pumped-up slurry is formed under two mechanisms; (1) the penetration of ballast and 'interlayer creation', and (2) the generation of greater cyclic stresses. The pumped-up fines from the subgrade are the common source of mud pumping and they significantly affect the internal friction of ballast particles (Hudson et al. 2016; Sussmann et al. 2012). The mud pumping sites reported in previous studies and the characteristics of soils used for laboratory testing are listed in Table 2. 1. It is clear that most of the subgrade soil falls above the A-line and can be classified as inorganic clay soils, as shown in Figure 2. 10. Moreover, the liquid limit (LL) mainly varies from 20 to 50 while the plasticity index (PI) is less than 30, i.e. low to medium plasticity soils.
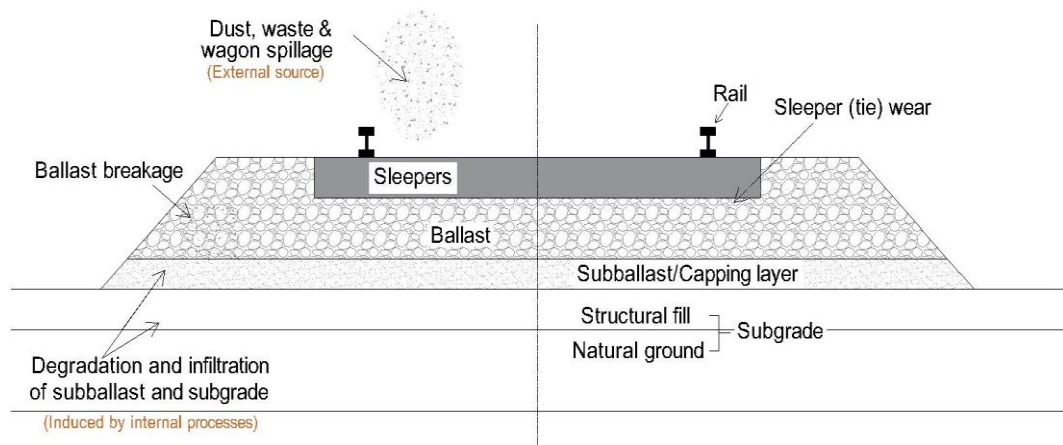
Figure 2. 9: Sources of excess fines inducing mud pumping under loads

On the other hand, Dirty Ballast Pumping Failure (DBPF) also occurs due to ballast particle breakage, sleeper wear, and the deposition of wind-blown sediments. Ballast particles can slide and roll over each other under train loading, thus leading to ballast breakage and attrition. Many studies showed that ballast breakage was predominant compared to subgrade fines so they only adopted mechanical degradation in their studies (Feldman & Nissen 2002; Indraratna et al. 2011b; Ionescu 2004). Moreover, fines can build up when transporting coal and this contribute to ballast fouling (Tutumluer et al. 2008). Feldman & Nissen (2002) reported that ballast fouling in the Queensland rail line is mainly caused by the infiltration of coal, which contains around 70 to 95% of contaminated ballast. In contrast, the performance of ballast-less tracks depends mainly on subgrade infiltration during the critical EPWP that develops under cyclic loads in slab tracks. In other words, the accumulation of fines due to ballast breakage and external sources can be absent or insignificant under slab tracks (Hayashi & Shahu 2000; Muramoto et al. 2006).

2.3.2.1.1 Migration of Fines and Change in Particle Size Distribution

The particle size distribution tests on samples collected at mud pumping sites revealed that fines which accumulated at the top surface could be observed under subgrade fluidisation (Korkitsuntornsan 2020; Nguyen & Indraratna 2021). The fine particles had traversed from the middle layers and experienced a loss of fines. More recent studies proved that accumulated fines could turn into slurry because the lower part of the specimen had densified and released the EPWP while carrying fines under repeated cyclic loading. These separated fines can be migrated into the granular layers due to the developed excessive hydraulic gradients (Abeywikrama 2020; Indraratna et al. 2020a).
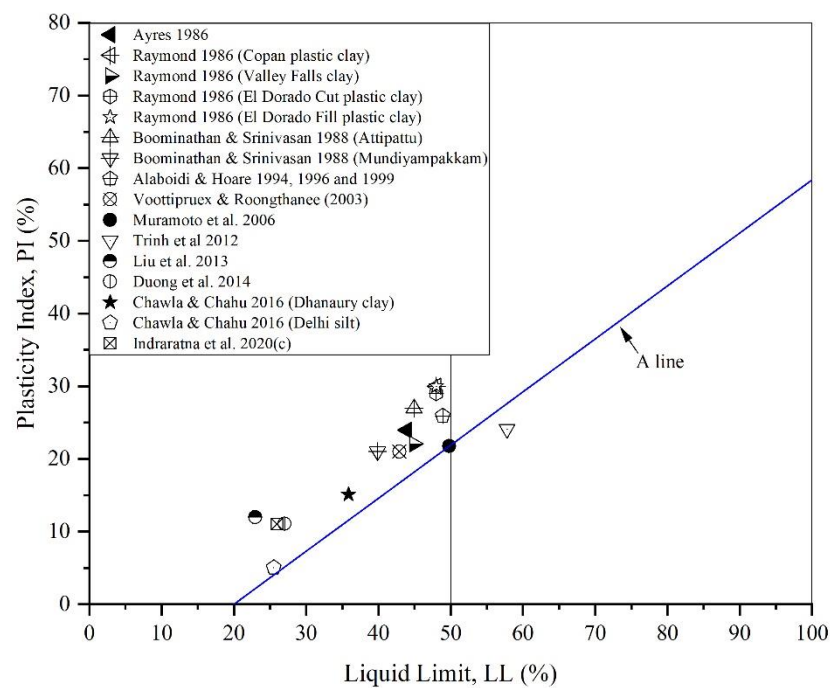
Figure 2. 10: Plasticity chart of soft soil at mud pumping sites (Arivalagan et al. 2021)

Table 2. 1: Characteristics of soil subjected to mud pumping reported in previous studies

Mud pumping sites/References	Soil description	Country/location	LL	PI	Particle size
Ayres (1986)	Marine deposited calcareous clay	Lower Lias, UK	44	24	95% finer than 63 μm
Raymond (1986a)	Copan plastic clay	Kansas, USA	48	30	83% finer than 60 μm
Raymond (1986a)	Valley Falls plastic clay	Kansas, USA	45	22	79% finer than 60 μm
Raymond (1986a)	El Dorado Cut plastic clay	Kansas, USA	48	29	95% finer than 60 μm
Raymond (1986a)	El Dorado Fill plastic clay	Kansas, USA	48	30	99% finer than 60 μm
Boomintahan & Srinivasan (1988)	Attipattu Clayed silt	Attipattu, India	45	27	67% silt and 12% clay
Boomintahan & Srinivasan (1988)	Mundi-yampakkam Clayed silt	India	40	21	
Rollin et al. (1990)	Non-plastic silt (S1 & S2) & plasctic clay (C3)	Canada			75% finer than 75 μm
Alobaidi & Hoare (1994),(1999)	Silty clay with medium plasticity (Keuper Marl)	Birmingham, UK	49	26	
Hayashi & Shahu (2000)	Shirasu soil (SW)	Kagoshima, Japan			10% silt and 82% sand

Voottipruex & Roongthanee (2003)	Inorganic clay with low to medium plasticity	Thailand	43	21	77% finer than 75 μm
Muramoto et al. (2006) & Muramoto & Nakamura (2011)	Arakida clay	Japan	49.9	21.7	50.6% silt and 46.6% clay
Trinh et al. (2012)	Finely grained soil (CH)	Lyon, France	57.8	24.1	98% finer than 100 μm
Liu et al. (2013)		China	23	12	
Duong et al. (2014a)	70% crushed sand & 30% kaolin	France	27	11	95% finer than 80 μm
Chawla & Shahu (2016a)	Dhanaury clay (CI)	India	36	15	99% finer than 60 μm
Chawla & Shahu (2016a)	Delhi Silt (ML)	India	25.5	5	40% finer than 70 μm
Hudson et al. (2016)	Alluvial clay, silt and sand	UK			
Kuo et al. (2017)	Out of 30 sites 50% are ML (mud) others are clay (CH) and sand (SM)	Hsinchu, Taiwan			25-80% finer than 75 μm
Wheeler et al. (2017)	Peat subgrade	Canada			
Indraratna et al. (2020d)	Low plasticity clay (CL)	Australia	26	11	30% finer than 75 μm

2.3.2.2 Dynamic Loading

Several studies carried out to investigate the effects of dynamic and repeated traffic loads revealed that the critical load that causes subgrade fluidisation/mud pumping has still not been understood very well due to the complex mechanism (Nguyen et al. 2019). Duong et al. (2014a) reported that the pumping of fines, penetration of ballast into the subgrade, and associated 'interlayer creation' under cyclic loading were significant compared to monotonic loading. Furthermore, a rapid increase in EPWP and axial strain initiated fluidisation type failures when the CSR exceeded a certain level (i.e. Critical Cyclic Stress Ratio – CSR_c) under undrained conditions (Indraratna et al. 2020d; Selig & Li 1994).

2.3.2.3 Role of Water, Drainage, and Effects of Degree of Saturation

Mud pumping can only occur under adverse hydraulic conditions such as during heavy rainfall and high groundwater levels in the foundation (Do 2021), but poor drainage at the surface, inside ditches, ballast shoulders, and culverts can also induce adverse hydraulic conditions in railway tracks (Cantrell 2009; Latvala et al. 2016). A high groundwater table can saturate subgrade soil, so most laboratory investigations used saturated samples to study mud pumping (Chawla & Shahu 2016a; Duong et al. 2013; Li Dingqing 2020). The potential for mud pumping with low water contents or under unsaturated conditions has not yet been proven, but according to Duong et al. (2013), more fines migrated rapidly under a saturated state (water content > 14%), and no pumping occurred under unsaturated conditions. The EPWPs that accumulate over time could separate the fines and induce particle migration (Alobaidi & Hoare 1999; Alobaidi & Hoare 1996), and fines transported into ballast can dramatically reduce its permeability.

Table 2. 2: Cyclic response of soft subgrade and potential failures in a Nutshell – Key themes

Theme description	Selected key References
1. Effect of CSR$_c$, Development of excess pore pressure (EPWP) and axial strain (ε) under cyclic loading	Larew & Leonards (1962), Sangrey et al. (1969), Andersen et al. (1980), Yasuhara et al. (1982), Ansal & Erken (1989), Yasuhara et al. (1992), Zergoun & Vaid (1994), Christopher et al. (2006), Guo et al. (2013), Wang et al. (2013), Paul et al. (2015), Indraratna et al. (2015), Ni et al. (2015), Lei et al. (2016), Thian & Lee (2017), Martínez et al. (2017), Głuchowski et al. (2019), Do (2021)
2. Effect of frequency (train speed)	Brown et al. (1975), Matsui et al. (1980), Procter & Khaffaf (1984), Konrad & Wagg (1993), Liu & Xiao (2010), Mortezaie & Vucetic (2013), Wichtmann et al. (2013), Yang et al. (2019), Zhou & Gong (2001), Indraratna et al. (2020a), Ansal & Erken (1989), Lei et al. (2016), Ni et al. (2015), Yang et al. (2019), Dash & Sitharam (2016), Zhang et al. (2021), Jiang et al. (2010), Shen et al. (2017)
3. Effect of water content and Drainage capacity under cyclic loading	Alobaidi (1991), Alobaidi & Hoare (1996), Miller et al. (2000), Cantrell (2009), Indraratna et al. (2009), Tennakoon et al. (2012), Duong et al. (2013), Chawla & Shahu (2016a), Latvala et al. (2016), Li Dingqing (2020)
4. Stiffness degradation under cyclic loading	Idriss et al. (1978), Andersen et al. (1980), Zhou & Gong (2001), Vucetic & Dobry (1991), Kagawa (1992), Lee & Sheu (2007), Guo et al. (2013), Cai et al. (2018), Singh et al. (2021)

2.3.3 Cyclic Response of Soft Subgrade and Potential Failures

Soft subgrade is more vulnerable to higher axle loads and it cannot withstand any cyclic stress exerted from the top layers. A dynamic load significantly reduces track stability by inducing EPWPs and diminishing the seepage hydraulics (Trani & Indraratna 2010b). The following sections discuss the effect of cyclic load (CSR), frequency, water content/adverse drainage conditions on weak subgrade soil. Most outcomes in this regard can be categorised into four themes, as shown in Table 2. 2.

2.3.3.1 Excess Pore Water Pressure and Axial Strain under Cyclic Load

Many studies have been carried out over the years to find out the threshold cyclic stress ratio (CSR_t) for undisturbed and remoulded samples by analysing the development of plastic strain and EPWPs (Andersen et al. 1980; Ansal & Erken 1989; Ni et al. 2015). When soil specimens were subjected to well below the threshold stress levels, the soil behaved elastic, and there was no loss in stiffness; however the specimens experienced plastic failures when the cyclic stress reached its limiting value (Larew & Leonards 1962). A rapid generation of EPWPs at the subgrade/subballast interface could lead to erosion and subsequent particle migration (Christopher et al. 2006). Kermani et al. (2018) reported that the number of pumped-up fines increased with simulated traffic loading cycles.

Sangrey et al. (1969) performed an array of cyclic triaxial tests to assess the behaviour of fully saturated clayey soil under cyclic load. As predicted, the pore pressure that was generated under cyclic loading brings the soil to the effective stress failure envelope under critical stress levels. The cyclic strain and EPWP were measured and showed that each loading cycle subjects to non-recoverable deformation and failure. Figure 2. 11 explains the relationship between the level of cycled stress and the maximum pore pressure under the peak of a non-failure equilibrium cycle. Wang et al. (2013) performed triaxial tests on soft marine clays to investigate the generation of axial strain and EPWPs. The resilient strain rapidly increased at the beginning and then reached a steady value. Figure 2. 12

shows that the pore pressure rapidly increases during the first hundreds of cycles but then the rate of increment in EPWP decreases. The axial strain is more than 4% at 50,000 cycles (CSR=0.40), and there is a significant increase in EPWP as the CSR increased from 0.14 to 0.40. However, the increment of EPWP over a long time is small, irrespective of the stress magnitude (Figure 2. 12). Similar observations in shear strains and EPWP were reported at different cyclic stress ratios (Thian & Lee 2017; Zergoun & Vaid 1994). In addition, Głuchowski et al. (2019) reported that EPWPs generated in the first few cycles play a key role in the accumulation of plastic strains and constitutes the major amount of EPWP.
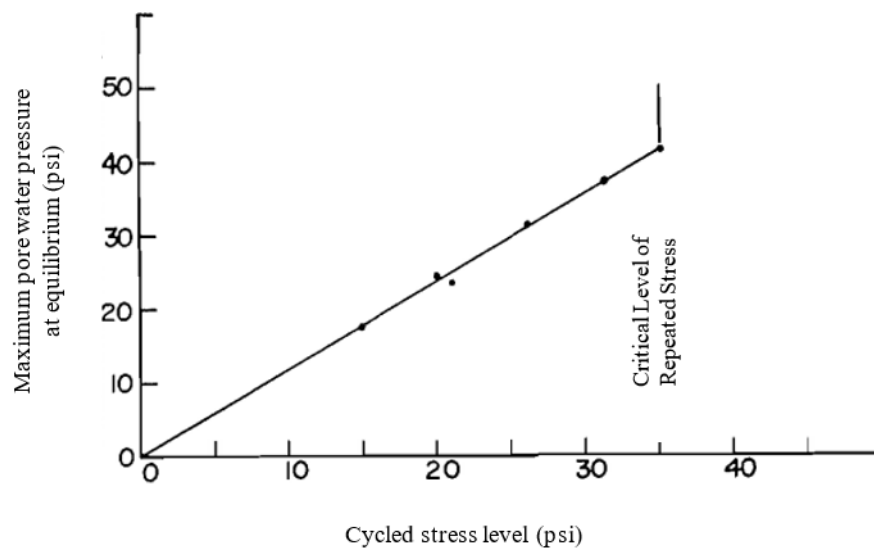
Figure 2. 11: The relationship of equilibrium pore pressure to the level of cycled stress (after Sangrey et al. (1969))

Yasuhara et al. (1992) performed the stress-controlled triaxial tests to assess the cyclic strength and deformation of clay thereby defining cyclic failure at critical state line (CSL). There was a positive generation of EPWP when NC clay was subjected to undrained cyclic loading, and moreover, the clay specimens behaved differently subjected to one-way and two-way cyclic load.
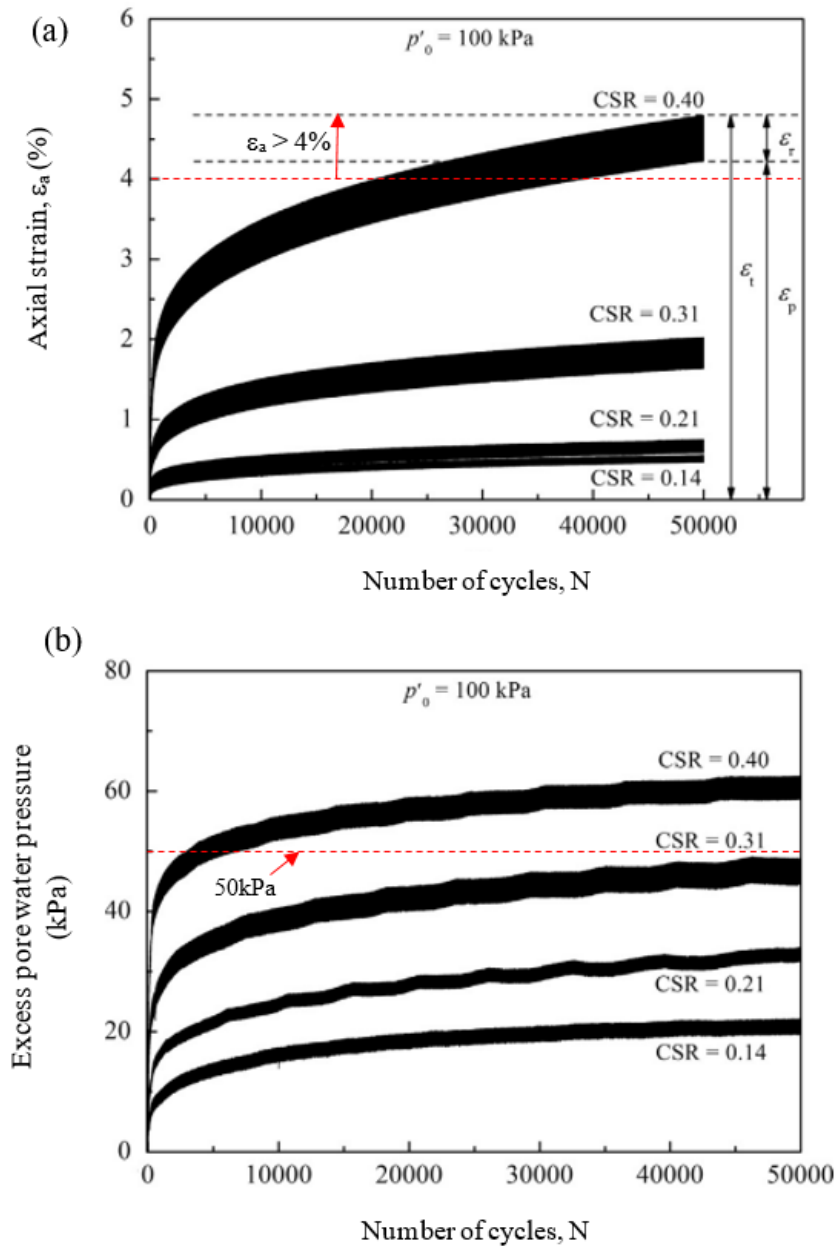
Figure 2. 12: Triaxial tests under confining pressure of 100 kPa (a) Axial strain and (b) EPWPs (modified after Wang et al. (2013))

2.3.3.2 Loading Frequency

The cyclic frequency on subgrade soil is mainly affected by the train speed, the carriage length, the bogies, and the distance between axles. In general, larger axial strains and EPWP can be developed at lower frequencies with increasing loading cycles (Indraratna et al.

2020d; Konrad & Wagg 1993; Procter & Khaffaf 1984; Wichtmann et al. 2013; Zhou & Gong 2001). Zhou and Gong (2001) reported on the effect of axle load and frequency on normally consolidated (NC) and over consolidated (OC) samples and found that axial strain developed at lower frequencies was more prominent than at larger frequencies. Jiang et al. (2010) also obtained similar results, i.e., a continual increase in axial strain and EPWPs with an increased time per loading cycle. Zhang et al. (2021) investigated the effects of frequency on a sand and silt mixture and reported that a rapid failure with severe particle migration occurred as the loading frequency increased. The influence of frequency varies on a wide range of soils, so predictions can only be made by conducting a series of laboratory tests.

2.3.3.3 Drainage Conditions

Yasuhara et al. (1992) investigated the changes in undrained strength with and without drainage under cyclic loading and reported that the soil decreased in strength under undrained cyclic conditions (no drainage). However, once drainage was allowed, the specimen continued to dissipate the pore pressure, thereby increasing the undrained strength (i.e., the clay experienced secondary compression).

Migrating fines can clog the pores of subbase (road) or subballast (railway tracks) and thus impede its drainage capacity. As the drainage capability of tracks decreases (i.e., poor drainage/undrained conditions), the EPWP cannot be dissipated and thus reduce the shear strength and stiffness of the subgrade soil. According to Alobaidi & Hoare (1996), the pumping of fines depended mainly on the EPWPs that developed at the subgrade/subbase interface. Moreover, a significant hydraulic gradient that was generated during the dissipation of pore pressure could separate the fines and pump the fine particles into the top layers. However, the inclusion of geosynthetics significantly reduced the generation of EPWP and continuously alleviated the EPWP under cyclic loading (Attya et al. 2007b). Geosynthetics as a filter successfully prevented the pumping of fines in highway

embankments (Kermani et al. 2018; Palmeira et al. 1997). Ni (2012) also reported that prefabricated vertical drains installed in soft soils dissipated the cyclic EPWPs during rest periods (Figure 2. 13).
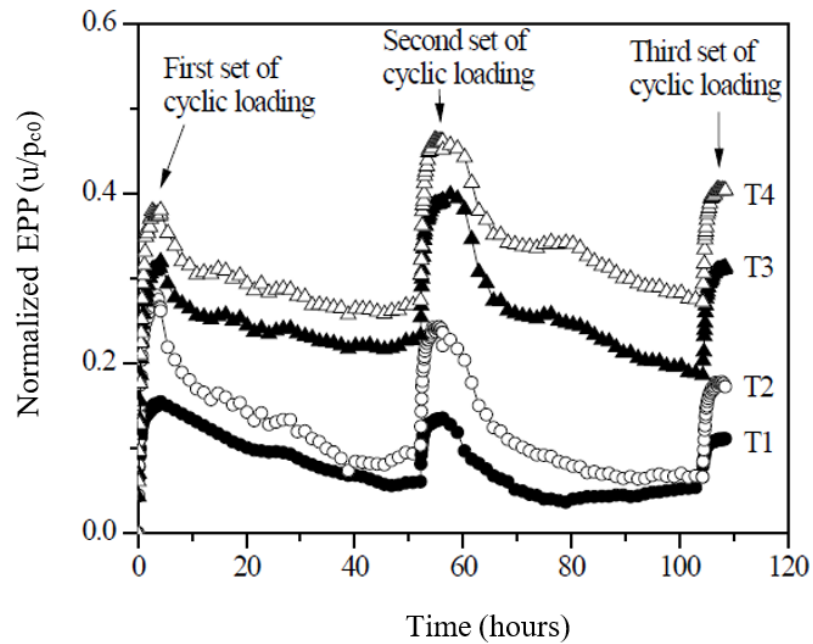
Figure 2. 13: Dissipation of EPWP after cyclic loads (after Ni (2012))

2.3.3.4 Stiffness Degradation

The stiffness of soft subgrade soil decreases in the first few cycles and then undergoes excessive degradation due to the rapid increase in cyclic stress and strain. Zhou & Gong (2001) investigated the role of CSR, with regards to its frequency and over consolidation ratio (OCR) in developing cyclic strain/degradation. Figure 2. 14 shows how the Cyclic Stress Ratio (CSR) affects stiffness degradation of a normally consolidated soil (under F=1 Hz and OCR = 1). The lower the degradation index, the higher the degradation in soils. Figure 2. 14 shows significant reduction in the degradation index as the CSR increases; and it is not linear. Zhou & Gong (2001) also reported that the rate of degradation was significant under at low frequency, and became lower as the frequency increases. Singh et al. (2021) investigated the stiffness degradation of vulnerable soft soils under different

loading conditions and proposed a quasi-linear relationship between the threshold strain and threshold number of cycles.
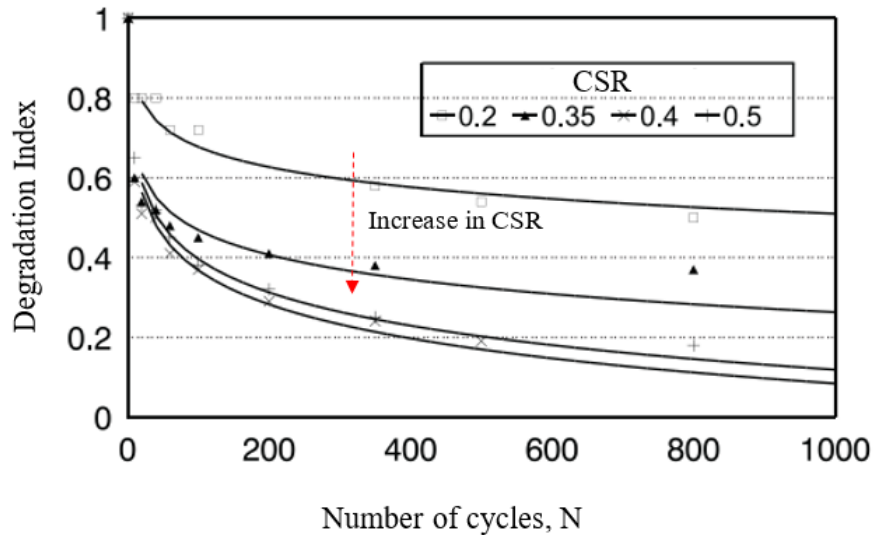
Figure 2. 14: The effect of cyclic stress ratio on the degradation index (f=1 Hz, OCR=1 modified after Zhou & Gong (2001))

2.3.4 Internal Erosion Associated with the Filtration Process

Mud pumping is a complex intrinsic process that interacts with different geomaterials such as fines, subballast, and ballast. Therefore, conventional filtration tests such as pumping water through the bottom of the specimen to simulate the critical hydraulic gradient, cannot be used to study the actual mud pumping mechanism. Moreover, filtration tests carried out in the past experimented with granular soils such as fine to coarse sand, which differ entirely from the characteristics of typical subgrade soils with low to medium plasticity (Israr et al. 2016; Nguyen et al. 2019; Skempton & Brogan 1994; Trani & Indraratna 2010a).

2.4 Assessment of Mud Pumping

The assessment of mud pumping sites assists in navigating the appropriate and practical solutions to mitigate mud pumping. This section includes the assessments carried out with

and without visible mud pumping in tracks by highlighting theoretical models and laboratory experiments. Governing factors such as the loading conditions, drainage characteristics, the properties of track materials, and the severity of damage to the foundation should be addressed while assessing the mud pumping sites. The fouled ballast and pumped-up slurry on the surface of the track are the visible evidence needed to determine the occurrence of mud pumping because there are no effective methods or strategies that can be used to identify mud pumping before it can occur while trains are passing over the track (Nguyen et al. 2019). There are no user-friendly numerical codes and practical guidelines available in previous literature in order to prevent mud pumping under cyclic loading (ARTC 2013; Transport for NSW 2016).

While numerous studies have been carried out to quantify ballast fouling using the fouling indices, the severity of mud pumping can also be assessed by evaluating ballast fouling. The percent passing (PP), fouling index (FI), percentage void contamination (PVC), and void contamination index (VCI) are the current methods proposed to quantify the level of fouling (Bruzek et al. 2016; Tennakoon et al. 2012), but they cannot determine how fine properties such as material mineralogy, plasticity, and the moisture content affect the performance of ballast during subgrade mud pumping.

The mechanism of mud pumping can be determined to quantify the predominant fines associated with visual observations. These visual observations and laboratory studies on field samples could be used to determine the failure of subgrade. Field work includes excavating and sampling ballast, subballast, and subgrade soil, and investigating the drainage conditions. The laboratory tests determine the properties of track materials such as the water content, the plasticity index, and the PSD. Advanced physical model tests can also be used to assess the ballast/subgrade interactions, subgrade softening and ballast degradation, and to capture the mud pumping mechanism (Liu et al. 2013; Sun et al. 2016; Toyota & Takada 2021). Although several studies highlight the common aspects of mud pumping such as ballast breakage and deformation, subgrade softening and internal erosion

(Indraratna et al. 2014b; Israr & Zhang 2021; Li & Selig 1998; Shire & O'Sullivan 2013; Sun et al. 2016), the theoretical approach to fully capture the mud pumping mechanism is still limited. Therefore, comprehensive geotechnical investigations and complex theoretical models are needed to address the wide range of mechanical issues related to mud pumping issues as well as cost-effective solutions (Nguyen et al. 2019; Read et al. 2011).

Assessing mud pumping sites without visible slurry or ballast fouling can be more challenging, in which case the deterioration of ballast tracks, differential settlement, and derailment are the only visible signs for identifying invisible mud pumping. The deflection-load profile generally represents track stiffness, and the measurement of vertical deflection is also a cost-effective way to identify track problems. Ground Penetration Radar (GPR) can be used to inspect the condition of tracks and substructure, as well as the behaviour of the ballast and sub-ballast layer, moisture and Ballast Fouling Index (BFI) (Li & Wilk 2020). Ballast pockets in the track can be detected using a GPR (Basye & Li 2015). This approach is simple to use in practice and can identify the mud pumping locations that cannot be detected by the naked eye (Kuo 2021). Implementing other methods such as field inspections and collecting soil samples during the rainy season is more challenging, whereas GPR can be used to investigate mud pumping under various weather conditions (Lenart et al. 2018).

2.5 Solutions for Mud Pumping

The solutions for mud pumping and restore the strength and adequate drainage capacity of tracks are important. Although numerous studies have proposed a variety of solutions, the most reliable and cost-effective solution for mud pumping is still a critical question.

2.5.1 Clean and Fouled Ballast

The common method used to maintain a mud pumping track is to remove the fouled ballast and replace it with fresh ballast. Tennakoon & Indraratna (2014) reported that a VCI of

50% can produce an excessive amount of clay in the ballast and thus induce significant EPWP generation. Fouled ballast can be removed, cleaned, and replaced unless the fouling is excessive or the ballast has deteriorated badly with severe particle breakage. Numerous studies have been carried out to assess ballast fouling, they are reported in Section 2.4 (Chapter 2), the ballast should be clean so it can provide acceptable drainage. According to Hudson et al. (2016), renewing fouled ballast and removing the voids through tamping under the sleepers cannot always prevent the risk caused by subgrade mud pumping. However, increasing the thickness of ballast helps to minimise the stress exerted on the subgrade surface, and reduces the pressure on the subgrade by almost half when the ballast increases from 25 cm to 35 cm thick (Ito 1984). This approach, including replacing ballast or renewing the subgrade (slurry), is expensive but it is currently used in practice due to its simplicity and long-life effectiveness (Transport for NSW 2016).

2.5.2 Enhanced Drainage Conditions

Most subgrade failures, including mud pumping in railway tracks, are associated with high water content and poor drainage conditions (Aw 2007). After significant heavy rainfalls the groundwater table rises to the surface and induces potential failure under cyclic loading. While conventional methods such as renewing the fouled ballast, maintaining the ballast shoulders, side ditches, and drainage system can improve the overall drainage capacity of the track, these methods are ineffective under adverse hydraulic conditions and cannot prevent the infiltration of fines and subgrade fluidisation (Mamou et al. 2017). The installation of geosynthetics is an alternative way to provide adequate drainage and maintain the structural stability of tracks (Figure 2. 15).

2.5.2.1 Use of Prefabricated Vertical Drains

Short wick drains can be installed into the soft subgrade to mitigate mud pumping by continually alleviating EPWPs, even after train passing. Therefore, the EPWP for the next

train loading would be less, and the potential for fluidisation or infiltration of the subgrade cannot be triggered (Indraratna et al. 2009; Singh et al. 2020a). Moreover, horizontal (i.e., transverse) drains can also be installed to facilitate horizontal drainage by dissipating EPWP induced by train loads (Ito 1984).

2.5.2.2 Geosynthetic Composites/Inclusion

The use of geosynthetics to prevent track substructures from failing has been studied over the past few decades. Although various geotextiles and geocomposites have been tested in the field and undergone large-scale laboratory testing, their effectiveness to prevent particle migration and fluidisation varies widely. Some studies reported that geosynthetics have a limited efficiency and their performance could diminish quite significantly over the years (Ayres 1986; Faure et al. 2006; Selig & Waters 1994; Sharpe 1988).
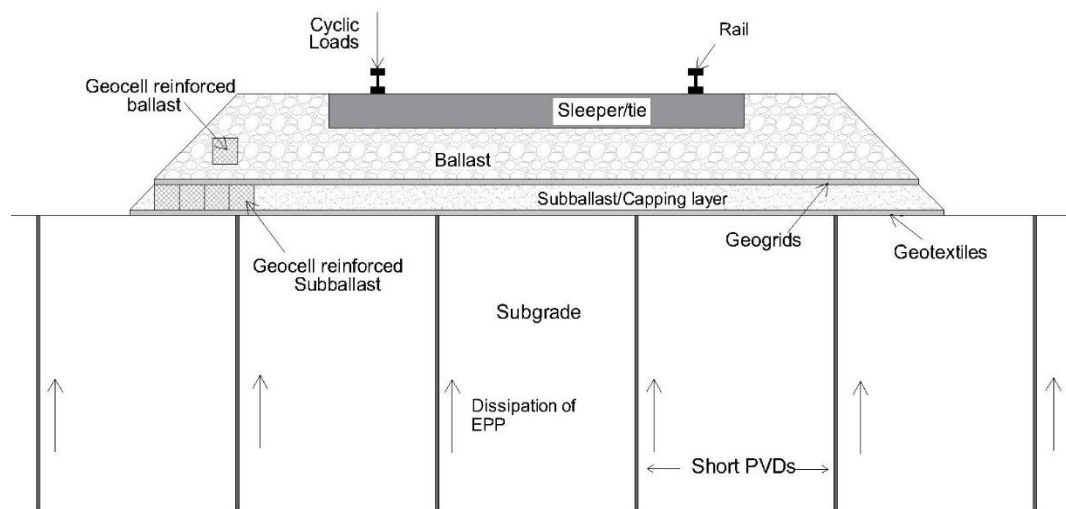
Figure 2. 15: Geosynthetic installation into the soft subgrade

Recent studies show that the installation of effective geosynthetics could prevent particle migration and potential track failures under dynamic loading (Chawla & Shahu 2016a; Kermani et al. 2018; Lenart et al. 2018). Moreover, geogrids can substantially reduce stress and ballast degradation. Other than that, under-sleeper pads, under-ballast mats and other

ballast/subballast reinforcements (geocells) have also been used to reduce the cyclic stress transferred to the ballast and subgrade (Indraratna et al. 2014a; Indraratna et al. 2020b; Navaratnarajah et al. 2018). Geotextiles can also be combined with a capping layer and/or geogrids to enhance the drainage and accelerate the rate of dissipation of EPWP (Alobaidi 1991; Sharpe et al. 2014).

2.5.2.3 Chemical Stabilisation of Railway Foundation

Chemical stabilisation is commonly used to increase the stability and cyclic resistance of substructures by adding or injecting lime, or a mixture of lime and fly ash. These chemicals react with the track materials and generate bonds between the soil/ballast particles and/or minimise voids (Karol 2003). A composition of lime and clay significantly reduces plasticity characteristics and the potential for swelling in wet conditions, and also increases the stiffness. Wang et al. (2012) investigated the dynamic properties of soil treated with lime by simulating high speed railway track conditions and found that while it tends to reduce the plasticity of subgrade soil, it can make the soil susceptible to brittle fracture.

This means the long-term effectiveness of lime stabilisation could be affected by environmental factors and therefore cannot be used for maintenance purposes (too time consuming). According to Wheeler et al. (2017), jet grouting a cement binder increased the track modulus and stability by preventing the occurrence of peat boils. The mass stabilisation technique doubled the track bed modulus and satisfied the minimum track modulus of 28 MPa that was proposed by Selig & Li (1994). In addition to lime, adding a mixture of fly-ash and Portland cement could also increase the subgrade stiffness and reduce the stress transferred on the subgrade surface (Modarres & Nosoudy 2015; Voottipruex & Roongthanee 2003). While these studies with chemical stabilisation subjected to train loads are limited, further investigations are needed to address the cyclic behaviour of stabilised subgrade under adverse hydraulic conditions.

2.6 Use of Geosynthetics in Practice

Geosynthetics can be used to stabilise soft soils and facilitate construction all over the world. The application of geosynthetics is a cost-effective solution to enhance the structural stability of ballasted rail tracks. It can also be used to reduce the lateral movement of ballast particles and permanent deformation. Furthermore, numerous studies and field investigations reported that geotextiles can control subgrade erosion by providing adequate surficial drainage over the years (Aw 2007; Kermani et al. 2020; Kermani et al. 2018; Selig & Waters 1994). Most outcomes in this regard can be categorised into five themes, as shown in Table 2. 3.

2.6.1 Geometry of Geotextile Filters

Woven geotextile filters have a simple geometry and constant opening size, unlike nonwoven geotextiles. However, the geometry may vary widely due to irregularities in manufacturing and the movement of yarns (Giroud 1996). Woven geotextiles are characterised by the width of their yarns, their opening size, and the relative aperture opening area. The geometry of nonwoven geotextiles can also be defined according to their porosity, thickness, and fibre diameter. The relative open area of a woven geotextile is the ratio between the surface area of the openings and the surface area of the geotextile.

The specific surface area for a woven geotextile per unit area of geotextile (m^2/m^2) can be expressed as follows;

$$S_a = \frac{2\pi d_f}{O_f + d_f} \qquad \qquad \text{Equation 2.1}$$

where: O_f = filtration opening size and d_f = filament diameter

Table 2. 3: Application of geotextiles/geocomposites in a Nutshell – Key themes

Theme Description	Selected key References
1. Standards, Design procedures and Practice Guides for geosynthetics, Review of test methods	Lawson (1982), Gerry & Raymond (1983), Ayres (1986), Koerner (2012), Koerner et al. (1987), Williams & Abouzakhm (1989), Montero & Overmann (1990), Luettich et al. (1992), Ghoshal & Som (1993), Bhatia & Smith (1996), Giroud (1996), Elsharief & Lovell (1996), Holz et al. (1998), Aydilek et al. (2002), Narejo (2003), Narejo (2004), Aydilek et al. (2005), Christopher et al. (2006), ISO/TR 20432 - 07 (2007), AASHTO M288 - 08 (2008), Zornberg & Thompson (2012), Khan et al. (2018), Palmeira & Trejos Galvis (2018), Tavakoli Mehrjardi & Amjadi Sardehaei (2019)
2. Performance of geosynthetics/track substructure (structural stability, Filtration, permeability, Clogging, Durability, Survivability criteria)	Raymond (1986b), Rollin et al. (1990), Montero & Overmann (1990), Bhatia & Huang (1995), Richardson (1998), Elvidge & Raymond (1999), Koemer & Koemer (1990), Mlynarek et al. (1990), Christopher & Fischer (1992), Hameiri (2000), Palmeira & Gardoni (2000), Faure et al. (2006), Ghosh & Yasuhara (2004), Xiao & Reddi (2000), Faure et al. (2006), Rosete et al. (2013), Yong et al. (2013), Palmeira & Trejos Galvis (2017), Palmeira et al. (2019), Sañudo et al. (2019), Sabiri et al. (2020), Ghosh & Yasuhara (2021), Khan et al. (2021)

42

3. Geosynthetics in transportation applications	Raymond (1984), Martinek (1986), Meccai & Hasan (2004), Hausmann et al. (1990), Hudson & East (1991), Al-Qadi et al. (1994), Austin & Gilchrist (1996), Raymond (1999), Fernandes et al. (2008), Kumar & Rajkumar (2012), Nithin et al. (2015), Arulrajah et al. (2015), Fuggini et al. (2016), Raut et al. (2016), Sudarsanan et al. (2018), Eller & Fischer (2019), Singh et al. (2020b), Wu et al. (2020)
4. Use of geosynthetics to prevent particle migration and mud pumping under cyclic loading conditions	Alobaidi (1991), Alobaidi & Hoare (1996), Alobaidi & Hoare (1998a), Alobaidi & Hoare (1998b), Kermani et al. (2020), Alobaidi & Hoare (1999), Carlos et al. (2015), Chawla & Shahu (2016a), Chawla & Shahu (2016b), Kermani et al. (2018), Feng et al. (2019), Kermani et al. (2019), Yahaya et al. (2020), Arivalagan et al. (2021)
5. Soft soil stabilisation and Other applications	Koerner et al. (1984), Raymond (1986a), Brons (1987), Degoutte (1987), Henry (1990), Greenwood & Brady (1992), Kaniraj & Rao (1994), Bouazza (2002), Palmeira (2009), Subaida et al. (2009), Wang et al. (2011), Palmeira et al. (2012), Portelinha et al. (2013), Hosseinpour et al. (2015), Miszkowska & Koda (2017), Gül (2020), Rowe (2020)

The specific surface area of a nonwoven geotextile per unit area of geotextile (m²/m²) is as follows;

$$S_a = \frac{4(1-n)t_{GT}}{d_f} \qquad \text{Equation 2.2}$$

$$n = 1 - \frac{\mu_{GT}}{\rho_f t_{GT}} \qquad \text{Equation 2.3}$$

where: n is the porosity of the geotextiles, t_{GT} = thickness, μ_{GT} = mass per unit area of the geotextile and ρ_f = density of the fibres

2.6.1.1 Aperture Opening Sizes

The characteristics of geotextiles rely primarily on the Aperture Opening Sizes (AOS), and this may vary under tension and confinement (Palmeira & Trejos Galvis 2018). According to Giroud (1996), the size of the filtration opening can be categorized as;

(1) The sieving method (sand particles or glass beads): dry sieving, wet sieving, and hydrodynamic sieving

(2) The capillarity method: Moisture desorption, Mercury intrusion and Bubble point method

(3) A morphologic analysis: Image analysis

Sieving methods such as dry sieving and wet sieving are direct methods. The shape and gradation of the particles are the two main aspects involved in sieving methods. Sieving results are related to the size of the constrictions between the pores and govern the filtration behaviour of geotextile. On the other hand, the capillarity methods and the image analysis method are indirect methods that require additional calculations to derive the filtration opening sizes from the measurements.

The filtration opening size measured using the sieving method suffers greatly due to electrostatic attraction, entrapped particles, and energy (Giroud 1996). The glass beads may remain attached to the synthetic fibres instead of passing through a geotextile filter under

dry sieving (**electrostatic attraction**), however, wet sieving method prevents electrostatic attraction. The relatively large particles of glass beads may become trapped within the geotextile (nonwoven), block some filtration paths (**entrapped particles**) and significantly affect the percentage of O_{90} to O_{100}. The definition of O_{90} is as follows: O_{90} is the geotextile opening size such that 90% of the geotextile openings are smaller than 90 μm. Gravity force is not enough to transport the particles, so some energy must be provided by utilising vibration or water flow (**energy**). Dry sieving should not be used with glass beads (electrostatic attraction) while using needle-punched nonwoven geotextiles (entrapping). The wet sieving method depends mainly on the operator, and hydrodynamic sieving is the most reliable method. The image analysis method provides the entire filtration opening size distribution curve, not the specific filtration opening size, so it cannot be applied in filtration applications. The capillary method essentially provides data on pore space and cannot be used to determine the filtration parameters. The bubble point method helps to provide the filtration opening size and the entire filtration opening size distribution curve. Giroud (1996) recommended more laboratory work on the bubble point test. However, at the present time, there is a substantial amount of research validating the capability of the bubble point test.

The pore openings of geotextiles should provide adequate seepage and yet be small enough to minimise the migration of particles. Based on the literature, the filtration criteria for non-woven geotextiles are as follows (Koerner 2012; Narejo 2003);

$$AOS \leq 0.5 D_{85}$$ Equation 2.4

$$AOS < \frac{18}{C_u} D_{50}$$ Equation 2.5

where: Dx is the soil particle size in mm for which x% of the soil is finer; and C_u is the coefficient of uniformity (Kermani et al. 2019).

2.6.1.2 Thickness of the Geotextiles

The thickness of granular and geotextile filters varies significantly and is typically 200 mm to 3 m thick for granular filters, 1 to 10 mm thick for needle punched nonwoven geotextile, and 0.5 to 1 mm thick for woven and heat bonded nonwoven geotextile (Giroud 1996). However, the relationship between the filtration opening size and thickness needle punched nonwoven geotextile filters may vary because nonwoven geotextiles are compressible and granular filters have negligible compressibility. The particles moving through a nonwoven geotextile are generally surrounded by voids, whereas they are more channelised in granular filters. Another significant difference is that granular filters usually contain particles of different sizes and shapes, while geotextile filters usually have identical fibre arrangements. Giroud (1996) proposed the variation of the filtration opening size as a function of geotextile thickness when developing a rationale for a minimum thickness of geotextile filters in use.

2.6.2 Design Criteria and The Performance of Geotextile Filter

Several methods have been adopted to define filtration, retention, and clogging criteria of geotextiles (Bhatia & Huang 1995; Faure et al. 2006; Ghataora et al. 2006; Ghosh & Yasuhara 2004; Hameiri 2000; Michael 2014; Palmeira et al. 1997; Xiao & Reddi 2000). Filter fabrics should satisfy two conflicting requirements: (1) the pore openings of filter should prevent particle dislocation at the interface and piping, and (2) the pore sizes allow sufficient drainage and alleviate excessive pore water pressure. A good filter should have openings large enough to allow water (free flow) to flow, but be small enough to prevent excessive particle migration. According to Williams & Abouzakhm (1989), the effectiveness of filters mainly depends on the following factors;

  (1) Properties of the geotextile: porosity, thickness, primary and secondary bonding mechanism, pore opening size, pore and constriction size distribution, etc.

(2) Characteristics of the soils: water content, plasticity, porosity, particle size distribution, etc.

(3) Drainage capacity across the soil/geotextile interface

2.6.2.1 Retention Criterion

The common geotextile retention criterion for uni-directional flow based on different pores opening sizes has been proposed in previous studies (Lafleur et al. 1996). Failures such as piping and excessive clogging could happen when the geotextile retains base soil particles, which is why a good filter must withstand the pressure applied by the soil and the water flow while retaining the soil particles within the subgrade. There can be initial particle migration through the geotextiles following a stable bridging network at the geotextile/subgrade soil interface. Internally unstable soils are more prone to excessive particle migration (fines). Based on laboratory observations, the uniformity coefficient of soil was utilised to propose the retention criteria (Giroud 1982; Holtz et al. 1997; Lafleur et al. 1996; Luettich et al. 1992).

2.6.2.2 Permeability Criterion

The permeability criterion ensures good drainage capacity; therefore the geotextile should allow enough water to pass through the filter. It has been considered as the minimum permittivity of the geotextile relative to the permeability of the soil. The most well-known requirement is $k_{geotextile} \geq 10k_{basesoil}$; $k_{geotextile} \geq k_{basesoil}$ can also be used when the base soil becomes highly permeable. The permeability of the filter can be calculated by assuming that the soil as parallel tubes separated by impermeable material, and then applying Poiseuille's equation (Giroud 1996). A geotextile filter must retain sufficient permeability even after fine particles have migrated into the filter.

2.6.2.3 Clogging Criterion

The clogging resistance of a geotextile is the minimal understood design criterion and significantly affects its performance over time (Palmeira & Gardoni 2008). The amount of soil that can pass through the geotextile, the amount of fines that become clogged, and the water flow rate are the critical parameters needed for a successful drainage system. Carroll (1983) reported that the retention and permeability criteria did not produce sufficient guidelines for a better filter design because the filter could still fail due to clogging. Rollin et al. (1990) reported that the clogging potential depends mainly on the Apparent Opening Size (AOS) and the slurry density. Moreover, any chemical or biological activity (biologically clogged by bacteria, algae or moss) in geotextiles can also influence the filtration characteristics. In addition, geosynthetics will be chemically clogged with minerals such as iron, manganese, and carbonate precipitates (Michael 2014).

2.6.2.4 Durability Criterion

The clogging of fines inside the pore structure directly affects the long term performance or the durability criterion. Rollin & Lombard (1988) reported that the deterioration of fibres and/or the bonds between the fibres are the main causes that reduce the tensile strength of geotextiles. Durability of fibres can also be affected by the mechanical, chemical, and environmental actions (Rollin & Lombard 1988). The destruction of fibres is generally a slow process, unless they are exposed to critical weather conditions such as high and low temperatures. Geotextiles in railway tracks make cyclic abrasive contact with ballast particles that can degrade the fibres and bonds. Ultraviolet testing, chemical compatibility testing and abrasion testing can be used to assess the durability of geotextiles prior to the field application.

2.6.2.5 Survivability Criterion

The survivability criteria incorporate a certain robustness based on the application in the field. The selected geotextile must survive during the construction process, whereas a field

evaluation is often necessary. Laboratory tests such as an abrasion test, California Bearing Ratio (CBR), grab strength, tear strength, puncture strength, trapezoidal tear, burst strength, and ultraviolet stability, can be carried out to assess the survivability potential (Christopher & Fischer 1992).

2.6.3 Mitigation of Particle Migration and Hydraulic Properties of Geotextiles

Particle migration occurs when subjected to a increased local hydraulic gradient across the soil/geotextile interface (Figure 2. 16). The finer particles (smaller than the pore opening size of the filter) can be transported upwards and/or trapped in the pores which cause clogging as they become electrostatically attracted to the fibres. The 'filter cake' that developed near the interface may hinder the drainage flow (partially drained to undrained conditions), so a geotextile with good drainage properties is required. This can prevent excessive particle migration and create a stable filter cake at the interface (Williams & Abouzakhm 1989). The Gradient Ratio (GR) and Hydraulic Conductivity Ratio (HCR) are the general methods previously used to study the filtration and drainage characteristics of geotextiles (Khan et al. 2018; Palmeira & Gardoni 2000; Williams & Abouzakhm 1989). The GR method can be used to determine the hydraulic gradient across the soil and geotextile interface and the local hydraulic gradient that generates inside the subgrade.

The HCR can be defined as the ratio between the hydraulic conductivity of soil (K_S) and the hydraulic conductivity of a soil/geotextile composite (K_{GS}). The HCR can be analysed by simulating typical field conditions; that will provide appropriate data for the design. A gradient ratio (GR) test was developed by the US Army Corps of Engineers to evaluate the fouling potential of a geotextile. The GR test setup measures the hydraulic head at different locations inside the subgrade soil. It can be used to assess the compatibility between the soil and a geotextile filter. The effect of geotextile compression and impregnation by subgrade soil particles can also be evaluated. The value of the gradient ratio (GR) can be defined as;

$$GR = \frac{i_{LG}}{i_s} \qquad\qquad \text{Equation 2.6}$$

where i_{LG} is the hydraulic gradient across a soil thickness (L) and the geotextile, and i_s is the reference gradient in the soil, measured in a region away from the geotextile (Palmeira et al. 2005). This method can also be used to assess the onset of suffusion or piping with geotextiles.
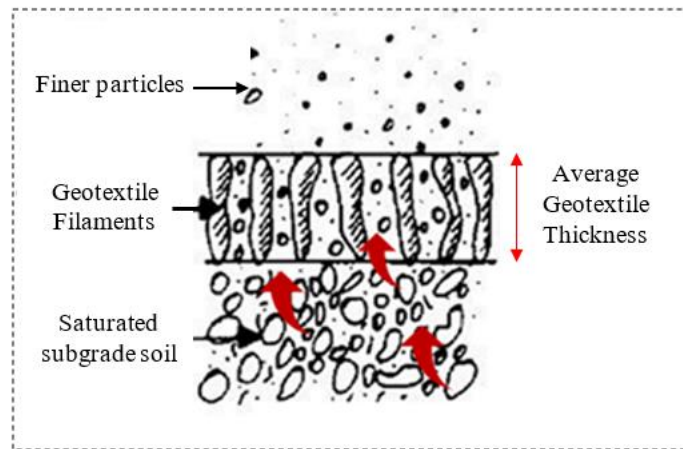
Figure 2. 16: Fine particle migration across soil/geotextile interface (modified after Christopher & Fischer (1992))

2.6.4 Prevention of Mud Pumping using Geosynthetics

The common design guidelines that incorporate filtration, permeability, retention, durability, and survivability criteria have been proposed in previous studies (Ayres 1986; Luettich et al. 1992). Indeed, how to effectively mitigate mud pumping using geosynthetics under rail tracks has been a critical question among academics and practitioners for many years.

2.6.4.1 Performance under Cyclic Loading Conditions

The relevant past studies (Table 2. 3) on the inclusion of geosynthetics are discussed in this section. Alobaidi & Hoare (1998b) carried out a series of laboratory tests using a unit cell to determine the cyclic pore water pressure that develops at the subgrade/subbase interface and the dissipation of pore water pressure (PWP) within one loading cycle. One-dimensional (1D) and three-dimensional loadings (3D) were applied, as shown in Figure 2. 17. The 1D setup had a loaded area which had similar cross-sectional area of the mould (240 mm diameter by 200 mm high). However, the loaded area for the 3D setup was about 1/10 of the mould where the area outside was set to a constant load. Unlike the 1D test, the introduction of geotextiles resulted in subgrade heaving in the 3D test. The test using an impermeable membrane with geotextiles resulted in a high elastic rebound and produced increased axial deformations. Subsequently, this caused higher water movements and induced particle migration under cyclic loading conditions.

Moreover, a gap was observed beneath the geotextile due to a water movement associated with severe erosion. The developed PWPs and deformations were measured using 1D and 3D testing setups (Alobaidi and Hoare 1998). Figure 2.18 shows the significant development in EPWPs and cyclic deformation observed in the 1D (Test 1-x) and 3D (Test 2-x) tests with geotextiles. The results indicated that the 3D test (Test 2-2) gave less pumping than a similar one-dimensional test (Test 1-2). Three-dimensional tests could accurately predict the efficiency of the sand layer in controlling mud pumping. For instance, the amount of pumping in Test 2-2 (geotextile with 15mm sand) was very small and was only 5% in Test 2-1 (geotextile only). Alobaidi and Hoare (1998) reported that there was a continual reduction in PWPs, and no significant difference in pumping behaviour was observed with a sole geotextile and a combination of geotextile with a 15 mm thick layer of sand.

Alobaidi & Hoare (1996) carried out a series of laboratory tests to assess the distribution of PWPs at the interface. The local hydraulic gradients induced under various interface conditions was also measured with increased cycles. They reported that the inclusion of high permeability geotextiles allowed for rapid dissipation of PWPs as the cycles increased, while the mean PWPs were almost zero from the beginning and end of the test. Other geotextiles experienced a maximum of mean PWP at 200 cycles, but this decreased to zero at the end. As predicted, the mean PWP and the axial deformation were increased in the test without geotextiles.

The numerical results also revealed that the pumping of fines under cyclic loading depends mainly on the cyclic stress and drainage conditions. The permeability, thickness, and compressibility of the geotextile were altered in order to capture the critical development of pore water pressure at different time intervals. The EPWP was generated during cyclic loading and dissipated when the load was removed. A rapid increase in the hydraulic gradient can initiate the erosion of subgrade fines and will be pumped up under repetitive cyclic loads (Alobaidi & Hoare 1996; Singh et al. 2020a).

Chawla & Shahu (2016a) reported that the subgrade contained low effective cohesion results in an increased EPWP under dynamic stresses. However, the use of geotextile allowed for in-plane drainage and dissipated the rapid development of EPWP. Chawla & Shahu (2016a) reported that the dissipation rate of EPWP was significant during the first hour, after one train passed. Chawla & Shahu (2016b) developed a numerical approach to investigate the effectiveness of geosynthetics on track performance and the occurrence of mud pumping. Three different constitutive relationships, straight analysis, nonlinear analysis, and coupled analysis, were proposed and the constitutive parameters were evaluated.
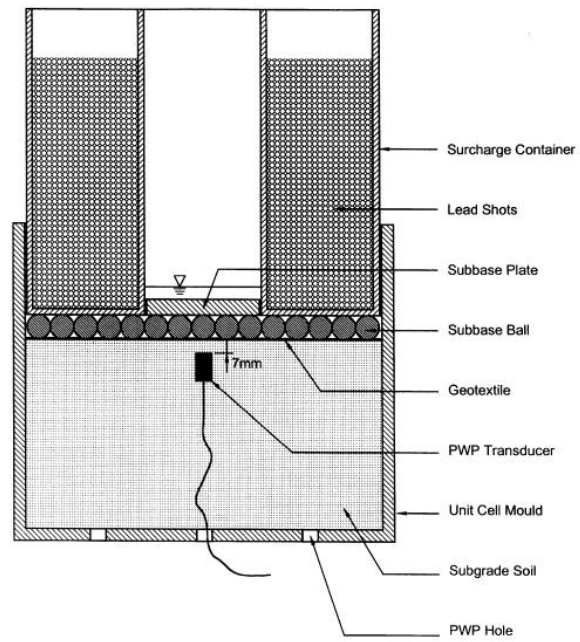
Figure 2. 17: Unit cell equipment for three-dimensional (3D) loading (after Alobaidi & Hoare (1998b))
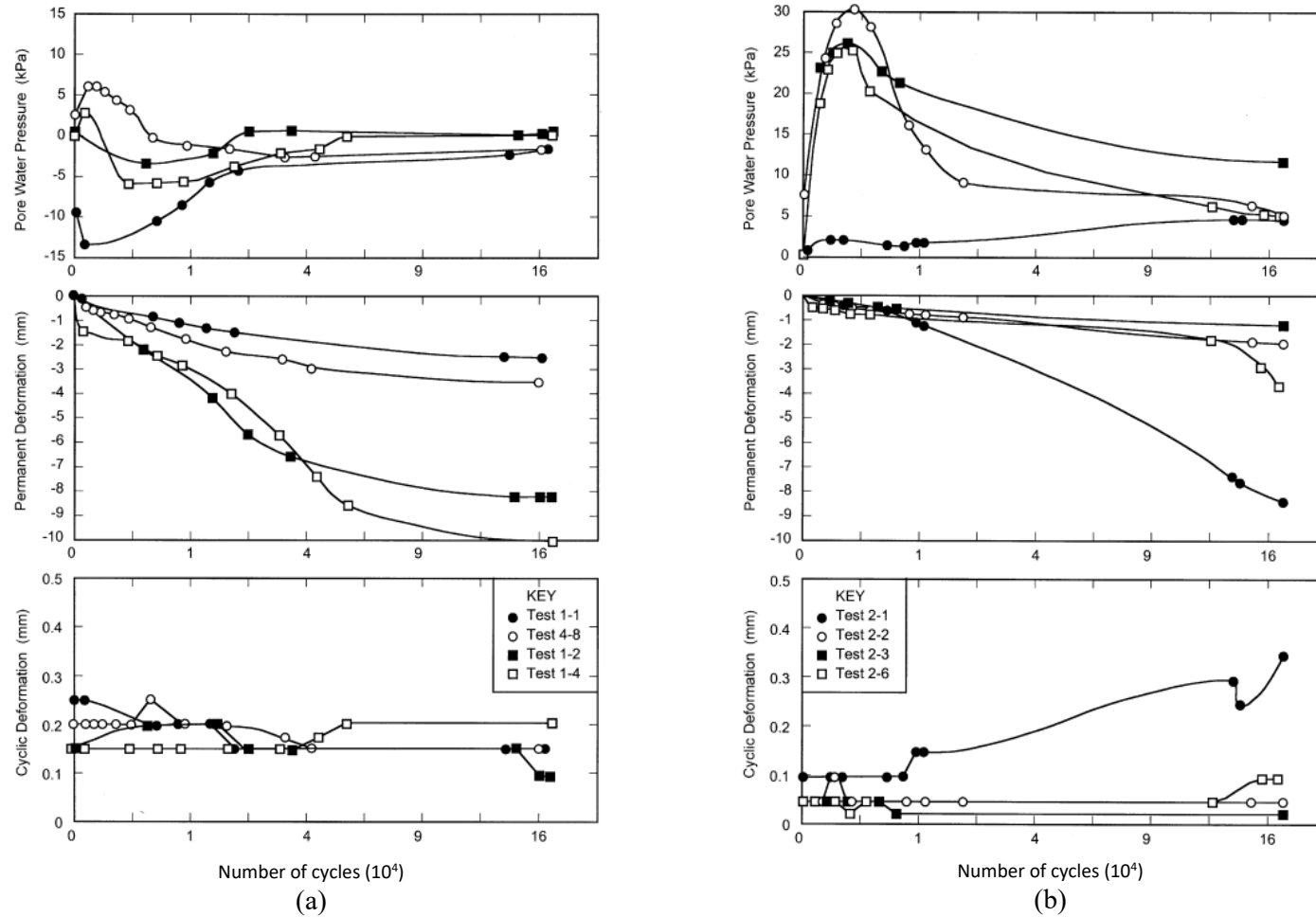
Figure 2. 18: Behaviour of geotextiles (a) One-dimensional unit cell - Left and (b) Three-dimensional unit cell – Right (Alobaidi & Hoare 1998b)

2.6.4.2 Prevention of Particle Migration

Alobaidi & Hoare (1999) used a mean cyclic stress of 20 kPa with a deviatoric cyclic stress of 10 kPa (i.e. 20 ± 10 kPa, f= 2.0 Hz). Alobaidi & Hoare (1999) reported that the increase in the mean and cyclic stresses resulted a rapid development in permanent deformation when granular soil was placed on a cohesive soil (no transition layer). Subsequently, the softening of the subgrade surface becomes significant because of higher stress concentration due to dynamic loading. Moreover, subbase particles immediately penetrated into the subgrade soil and mud pumping observed towards the subbase layer. However, the test with a transition layer or geotextiles reduced the possibility of local shear failure. In this study, the amount of pumping was adopted by determining the weight of fine particles that passed through the pore openings. In addition, pumping occurred at the boundary of each loaded area where the highest hydraulic gradient was recorded. The fine particles that accumulated within and on top of the geotextile significantly affected the compressibility, pore size, and thickness of the geotextile.

Feng et al. (2019) carried out laboratory tests to create sand percolation and fine particle suffusion that occur due to sand filling and consolidation. The travel boundary for fine particle movement was observed with and without a geotextile separator. The tests results indicated that the installation of geotextiles successfully prevented sand percolation and effectively diminished the fine particle suffusion. The rate of particle migration was reduced significantly with geotextiles.

Kermani et al. (2018) performed model tests by simulating typical flexible pavement conditions. The proposed model had an asphalt layer and a subgrade/subbase interface where a non-woven needle-punched geotextile was installed. The amount of fine particles transported were measured at the end of cyclic testing. Particle migration decreased significantly (<2%) due to the installation of geotextile at the top and then it allowed a 30% reduction in pavement rutting. Figure 2. 19 shows the fine migration into the subbase with the number of loading cycles.
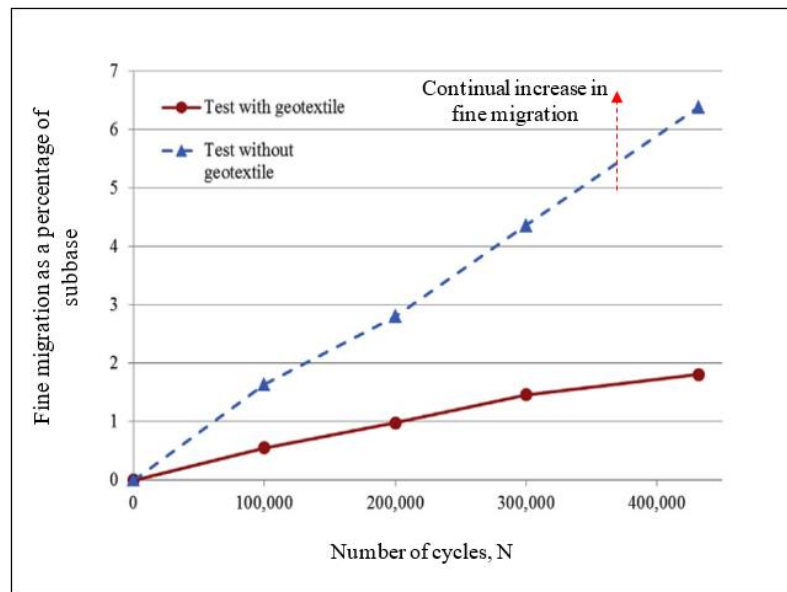
Figure 2. 19: Total mass percentages of subgrade – with and without geotextile (modified after Kermani et al. (2018))

2.6.4.3 Geotextile/Soil Interlayer Characteristics

Duong et al. (2014a) investigated the key factors that cause the migration of fine particles while observing the 'interlayer creation' and the occurrence of mud pumping. This can be prevented by using a geotextile as a capping layer (Kermani et al. 2019). Alobaidi & Hoare (1996) reported that a very thin layer formed during one loading cycle time because the permeability of the cohesive subgrade (without geotextiles) was lower. They also reported a continuous dissipation of EPWPs due to the installation of a geotextile and prevention of soil softening at the subgrade surface. A pore pressure transducer was installed 7 mm below the interface to measure the rate of dissipation. The test results implied that the dissipation of EPWPs depends mainly on the hydraulic properties of the geotextile.

2.6.4.4 Effects of Standing Water

Alobaidi & Hoare (1994) carried out laboratory tests using the unit and triaxial testing apparatus to determine the effects of standing water. A slurry was prepared in the unit cell,

a maximum stress of 320 kPa was applied and then reduced to 10 kPa. 750 ml of standing water was observed after the geotextile layer and subbase plate were placed in situ. They also reported a rapid increase in pumping activity and deformation as the amount of standing water increased as shown in Figure 2. 20. The effect of frequency was captured, and the amount of pumping associated with permanent deformation rapidly increased at higher frequencies. In addition, the rate of pumping became very low after 100,000 cycles, regardless of the frequency. The pumping tests at lower frequencies permitted more time for drainage and more softening may be expected under the same loading conditions (Alobaidi & Hoare 1994).
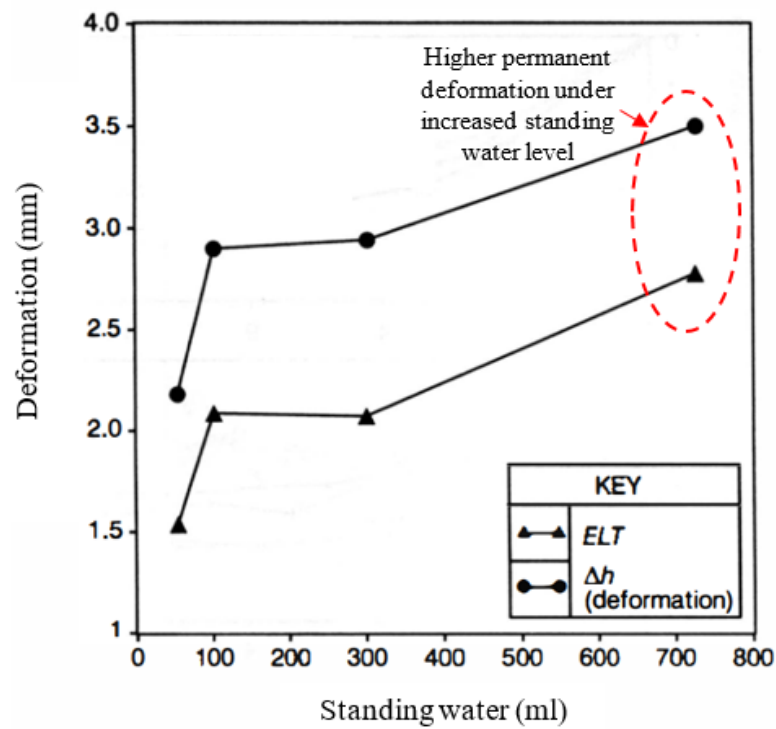
Figure 2. 20: The effect of standing water (modified after Alobaidi & Hoare (1994))

2.7 Use of Prefabricated Vertical Drains

The use of PVDs permits a prudent solution to field problems such as soft soil stabilisation compared to other more expensive ground improvement techniques. From the past, different types of vertical drains, including sand drains, PVDs and stone columns piles have been used to strengthen soft soils prior to the construction and to accelerate consolidation. Prefabricated vertical drains can be made of cardboard, plastic (without a jacket), and fabric (covered drains). Biodegradable drains were also used in previous studies, they were commonly made from natural materials such as coconut coir and jute. PVDs are more cost-effective and can be readily installed in soft soils (vertically up to 40m) and even in non-vertical orientation (Indraratna 2017). Moreover, PVDs can be installed rapidly with minimal environmental implications compared to other ground improvement techniques such as semi-rigid inclusions. Most outcomes in this regard can be categorized into five themes, as listed in Table 2. 4.

2.7.1 Properties of Vertical Drains

PVD normally consists of a plastic core and a filter (sleeve) with a longitudinal channel which is commonly from polymeric materials (Figure 2. 21). The drains that are most available in the market have 90 to 100 mm wide and 3 to 10 mm thick sections. The plastic core should allow water inflowing from the consolidation of cylindrical clay. The accumulated water should be able to pass rapidly through the PVD filter (Karunaratne 2011). The PVD should have an appropriate thickness because a filter that is too thin and/or of a smaller modulus may fail during installation. The proper selection of filter criteria can avoid clogging and subsequent reduction in flow through PVDs (Koerner 2012).

Table 2. 4: Use of prefabricated vertical drains in a Nutshell – Key themes

Theme Description	Selected key references
Consolidation of soft soils using PVDs, Classical theories	Carrillo (1942), Barron (1948), Hansbo (1979), Zeng & Xie (1989), Hansbo (1997), Feng et al. (2017), Tang & Onitsuka (2001), Chu et al. (2006), Indraratna et al. (2007), Chu et al. (2014), Chai et al. (2020), Ngo et al. (2020)
Factors affecting vertical drainage of PVDs, Types of vertical drains and Installation effects	Hansbo (1979), Bo et al. (1998), Chai & Miura (1999), Chai et al. (1995), Basu & Madhav (2000), Hawlader et al. (2002), Chai et al. (2008), Marinucci (2010), Ghandeharioon et al. (2010), Deng et al. (2014), Bo et al. (2016), Zhu et al. (2020), Nguyen (2021)
Theories, Design procedures and Practice Guides	Hansbo (1983), Rixner et al. (1986), Zeng & Xie (1989), Holtz et al. (1991), Bergado et al. (1996), Rawes (1997), Hansbo (1997), Chai & Miura (2000), Seah (2006), Rujikiatkamjorn & Indraratna (2007), Chu & Raju (2012), Mission et al. (2012), Long et al. (2013)
Application of PVDs under Cyclic loading	Attya et al. (2007a), Indraratna et al. (2009), Indraratna et al. (2010c), Ni et al. (2013), Razouki (2016), Indraratna et al. (2015), Kim et al. (2021), Rujikiatkamjorn et al. (2011)
Use of prefabricated vertical drains to prevent mud pumping	Yean-Chin & Peir-Tien (2012), Al-Soud (2016), Singh et al. (2019), Singh et al. (2020a), Abeywikrama (2020)
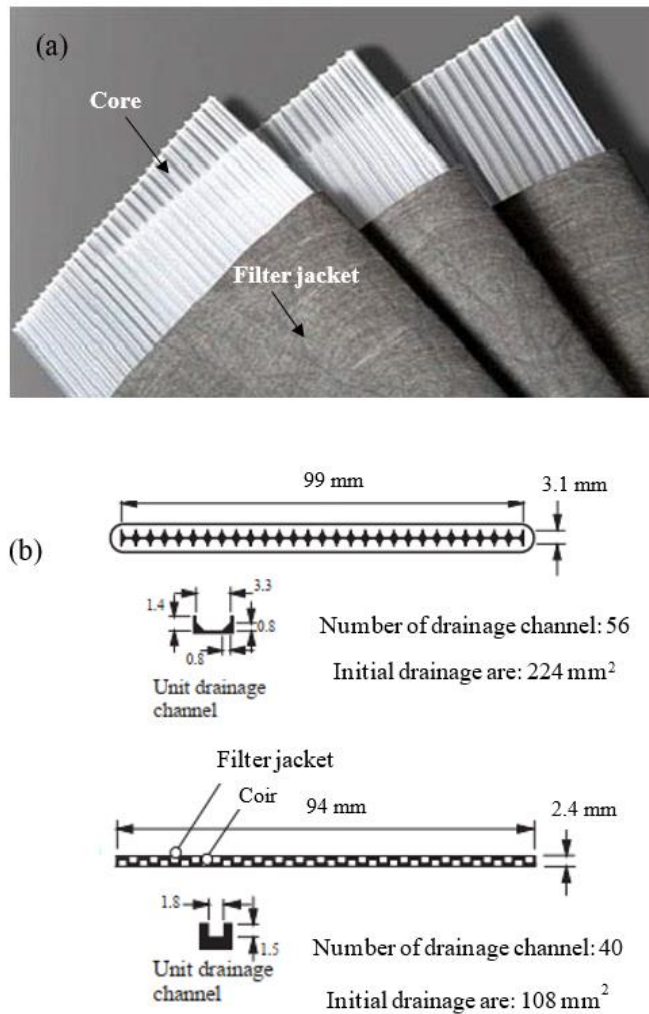
Figure 2. 21: (a) Plastic core and filter of a PVD and (b) Drainage channels and the cross-section of two different PVDs (modified after Chai et al. (2004))

2.7.2 Equivalent Drain Diameter

For a band-shaped vertical drain with a thickness 'b' and a width 'a', Hansbo (1981) proposed an equivalent drain diameter as follows;

$$d_w = \frac{2(a+b)}{\pi}$$ Equation 2.7

Based on a FE approach, the equation for the equivalent drain diameter (d_w) is simplified as (Rixner et al. 1986);

$$d_w = \frac{(a+b)}{2} \qquad \text{Equation 2.8}$$

Based on the flow nets around the soil cylinder of diameter (d_e) Pradhan (1993) suggested a new equation for d_w:

$$d_w = d_e - 2\sqrt{\bar{s}^2} + b \qquad \text{Equation 2.9}$$

where

$$\bar{s}^2 = \frac{d_e^2}{4} + \frac{a^2}{12} - \frac{2ad_e}{\pi^2} \qquad \text{Equation 2.10}$$

2.7.3 Filter Opening Size

The drainage material or the filter jacket of a vertical drain should retain the soil particles and still allow the water to pass through. Effective filtration prevents the particles from moving through the pore openings (Carroll 1983). Care must be taken when selecting geosynthetics (PVDs) based on apparent opening size of the filter and its drainage properties (Ngo et al. 2020). The permeability of a filter must be higher than the soil in order to provide sufficient drainage capacity; the opening size of a vertical drain should also meet the following requirement:

$$O_{95} \leq (4 - 0.75)\frac{D_{85}}{K_a} \qquad \text{Equation 2.11}$$

where O_{95} is the aperture opening size of the filter and K_a is a reduction factor that considers the effect of loading and partial clogging; it can vary from 1.9 to 4.4 (Chu et al. 2006; Palmeira & Gardoni 2002)

2.7.4 Smear Effects and Well Resistance

The efficiency of vertical drains relies on two main parameters, namely; (1) the smear effect, and (2) well resistance. The smear is the disturbed soil area caused by the installation and removal of mandrels when installing vertical drains. The soil area surrounding a drain is restructured when installing a mandrel, while the soil further away from a vertical drain consolidates by dissipating the EPWP. The resistance to water flowing is known as well

resistance. Long vertical drains with limited drainage capacity have increased well resistance. Moreover, a reduction in the cross-sectional area of PVDs, the deformation of PVDs during installation, and trapped fine soil particles into the core of a PVD may induce well resistance (Aboshi et al. 2001; Chu et al. 2006; Holtz et al. 1991).

The arrangement of a vertical drain in a unit cell is shown in Figure 2. 22. The effect of smear and the transition zone, and an analysis of subgrade soil surrounding the mandrel that is disturbed due to the installation of PVDs have been investigated in previous studies (Abuel-Naga et al. 2012; Ghandeharioon et al. 2012; Parsa-Pajouh et al. 2014). According to Sharma & Xiao (2000), the radius of the smear zone is around four times that of the mandrel, and the horizontal permeability (k_H) of the smear zone can be around 1.3 times smaller than the intact zone. As Figure 2. 23 shows, the significant reduction in horizontal permeability observed in the smear zone and change in permeability in the horizontal direction, increases mean consolidation pressure decreases. It is clear that the coefficient of horizontal permeability (k_H) becomes smaller towards the drain and the vertical permeability (k_V) remains almost unchanged, even near the drain interface. The relationship between the change in water content and the change in horizontal permeability inside the smear zone has been reported in previous studies, whereas the permeability depends mainly on the water content and void ratio (Samarasinghe et al. 1982).

2.7.5 Vertical and Radial Consolidation

Vertical drains reduce the EPWPs in subgrade soil and increase the rate of consolidation in road embankments or railway substructures; when needed they can be implemented before starting construction of a railway embankments on an area of soft subgrade. Vertical drains can be used to accelerate the rate of consolidation of soft soil, the relevant literature is tabulated in Table 2. 4.
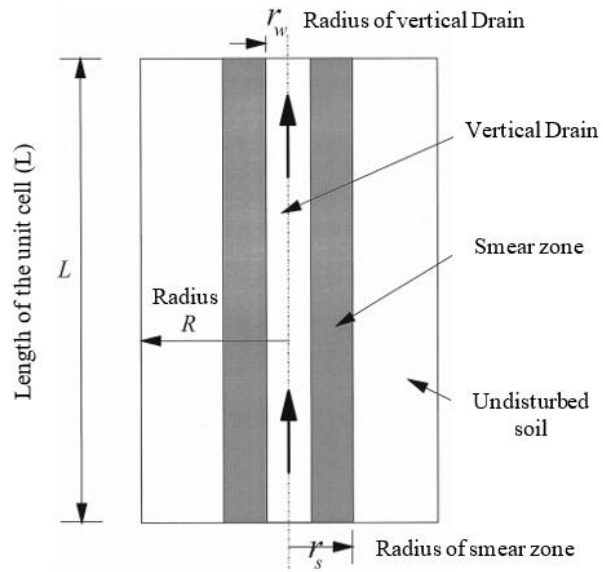
Figure 2. 22: Arrangement of vertical drain in a unit cell, and the smear zone
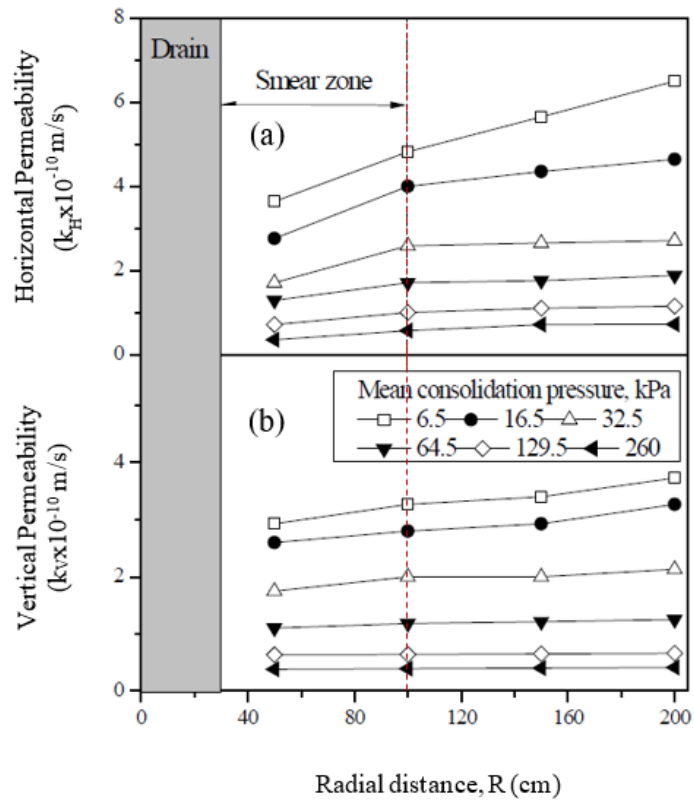
Figure 2. 23: Variations of (a) Horizontal permeability and (b) Vertical permeability (modified after Indraratna & Redana (1998))

The contribution of radial drainage is significant in lower subgrade soils compared to vertical flow under the influence of vertical drains (Ni 2012). The increased surcharge can reduce the stability of soil due to the increased lateral movement on the track. This means a vacuum pressure is needed to reduce the height of surcharge to speed up the consolidation. This combination can prevent subgrade instability and also reduce the lateral movements (Indraratna 2017).

2.7.6 Performance of PVDs under Cyclic Loading

The installation of PVDs stabilises road embankments and rail tracks, especially in coastal areas containing large amounts of clay in the subgrade. A PVD installed at shallow depths within 6-8 m can successfully prevent the generation of excessive EPWP during cyclic loading. Furthermore, a continuous dissipation of EPWP during a rest period can make a track more stable for the next train loading (Indraratna et al. 2009).

2.7.6.1 Effectiveness at Dissipating Pore Water Pressure

The EPWP is the main cause of mud pumping in railway tracks (Duong et al. 2014b), and a high water content in the subgrade soil leads to a rapid increase in EPWPs during cyclic loading (Indraratna et al. 2020d). Prefabricated vertical drains can be used to solve ground problem relating to critical drainage conditions in soft soils. The radial drainage path facilitated by vertical drains can significantly increase the stability of railway foundations, which is why this mechanism is used to assist in soil consolidation under cyclic loading (Indraratna et al. 2011a).

Figure 2. 24 shows the variation of EPWP and the volumetric strain over time under undrained and partially drained conditions. The dissipation of EPWP helps to increase the shear strength of soil. The continuous accumulation of EPWP over time reduced the effective stress under undrained conditions, as shown in Figure 2. 24. However, a partially

drained test can dissipate the EPWP, and lead to an increase in volumetric strain, this can

be given by;

$$\varepsilon_{vr} = m_{vr}\Delta u_d \qquad \text{Equation 2.12}$$

Where m_{vr} is the coefficient of volume compressibility and Δu_d is the dissipation of EPWP

(path B' to C in Figure 2. 24)
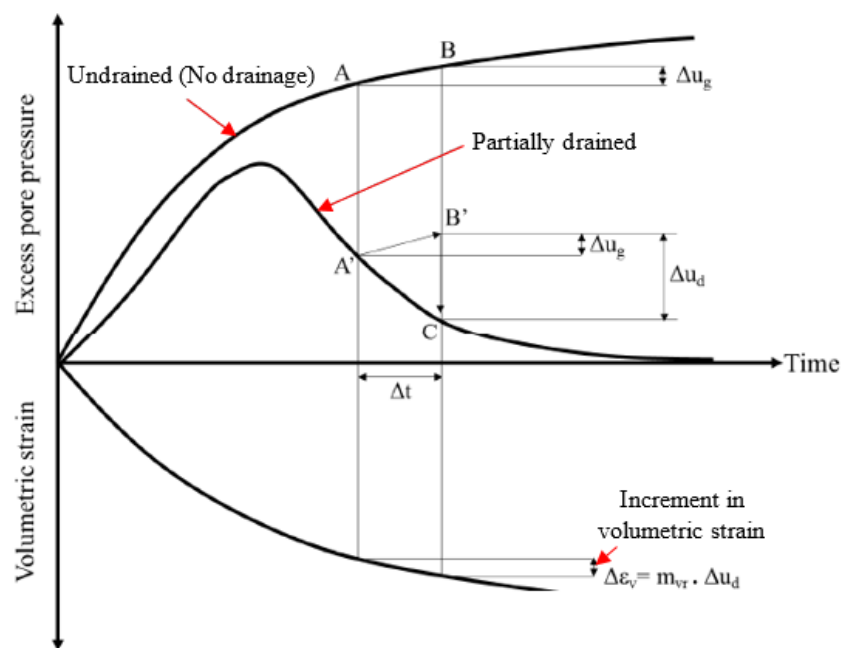
Figure 2. 24: Excess pore pressure and changes in volumetric strain under undrained and

partially drained conditions (modified after Hyodo et al. (1992))

The numerical approaches performed to investigate the cyclic response of subgrade soils

with PVDs in railway tracks are limited (Singh et al. 2020a). Figure 2. 25 shows the

significant reduction in critical pore pressure due to the installation of PVDs. They could

alleviate the EPWP by more than 20%, under cyclic loading conditions, as Abeywikrama

(2020) observed. Thus, the inclusion of PVDs in soft soils can be an effective way of

preventing subgrade failures. However, more laboratory tests are needed to investigate the

key role that geosynthetics play in reducing the subgrade potential under critical hydrodynamic conditions.
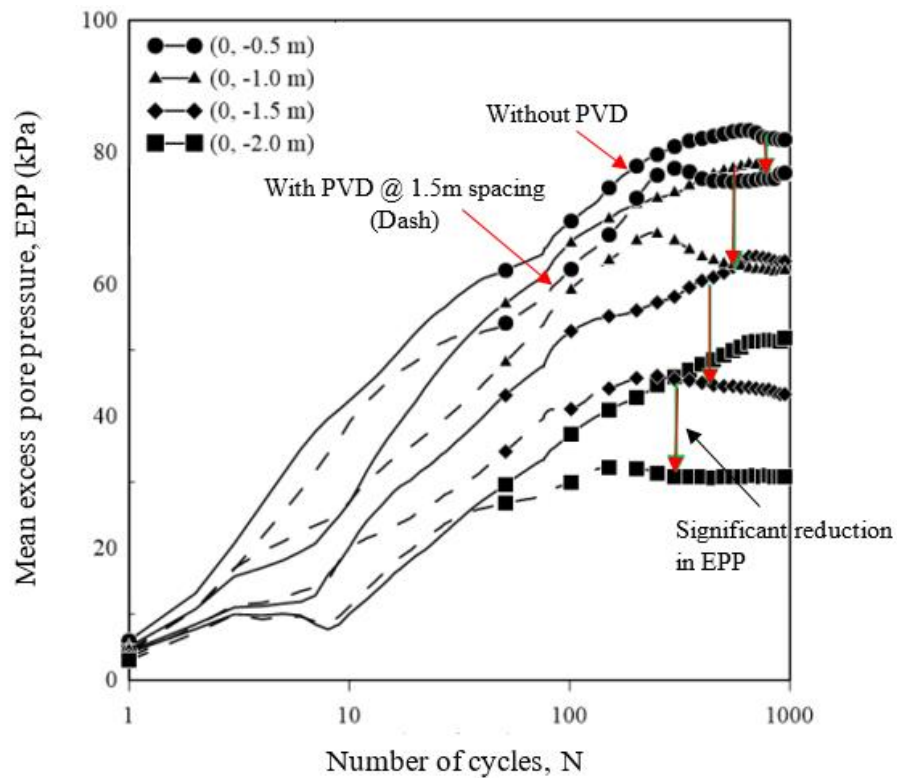
Figure 2. 25: Generation of EPWPs with and without PVDs (modified after Singh et al. (2020a))

2.8 Conventional Capping/Compacted Sand Blanket

The internal instability of granular soils can be categorised based on the type of failure, this includes suffosion, suffusion, backward erosion, segregation piping, and piping (Israr & Indraratna 2018). Adverse hydraulic conditions and huge axle loads may promote premature washout failures. A series of laboratory studies have been conducted to analyse the internal instability of capping under both static and cyclic loading (Haque et al. 2007; Indraratna et al. 1996; Indraratna & Radampola 2002; Israr & Indraratna 2018; Kamruzzaman et al. 2008; Kenny 1985; Phan et al. 2019; Raut & Indraratna 2008; Trani

& Indraratna 2010c). The effectiveness of capping materials was also evaluated by determining the amount of fine particles that eroded, while observing the type of failures (heave or piping). In addition, the appropriate use of geosynthetics with a capping layer can also reduce the thickness of granular subballast in railway tracks (Fatahi et al. 2011). This research has investigated the role geosynthetics play in controlling/preventing subgrade fluidisation potential, it does not report the effectiveness of compacted sand/granular filters.

2.9 Chapter Summary

Mud pumping is one of the most common problems in saturated soft soils. This chapter has summarised previous studies that described the mechanism and key factors that cause mud pumping, the cyclic response of soft soil, and the prevention techniques. The cyclic behaviour of soft subgrade vulnerable to subgrade fluidisation has been investigated in detail. The various types of mud pumping in ballasted tracks that led to track failure were discussed by analysing the rate of strain and the EPWP under cyclic loading conditions. Geosynthetics are currently being used as a filter or separator in railway tracks in order to prevent the particle migration and reduce the stress transferred on subgrade soil. Geosynthetics can also replace a capping layer because of their similar performance, economy, consistent properties, and ease of installation in railway embankments. However, in order to prevent mud pumping, the existing design guidelines for geosynthetics in railway tracks cannot be applied without prior laboratory and field examinations. Finally, the function of geotextiles in terms of filtration, drainage and separation criteria, and the application of vertical drains to enhance the radial drainage of subgrade have been addressed.

CHAPTER 3: RESEARCH APPROACH AND METHODOLOGY

3.1 Introduction

Laboratory modelling is considered to be the most effective and economical way to represent and simulate typical field conditions, albeit with some simplifications. Field testing however, is expensive and it takes time to obtain large quantities of data. The current laboratory experiments were performed to capture the response of track substructures such as geotextiles, geocomposites, prefabricated vertical drains, and conventional capping (compacted sand blanket) under cyclic loading. Chapter 3 mainly discusses the testing materials, the test setup and test program, the experimental phases and the components of dynamic filtration apparatus (DFA), and the methodology used to provide different drainage conditions to assess fluidisation potential under typical rail track conditions. Since the ground conditions, train loading characteristics, and maintenance cycles govern track stability and the occurrence of mud pumping, these factors must be carefully examined. During track design and maintenance activities, these conditions should be examined closely in order to maintain the performance of the track through the design period. The following sections contain detailed descriptions of the methodology and data collection of the experimental study.

3.2 Testing Materials

Railway tracks in Australia are often built on erodible and highly dispersive silty clay soils which are prone to subgrade fluidisation/mud pumping during the passage of trains. The samples of soil collected from the South Coast rail line in NSW by Nguyen & Indraratna

(2021), had a plasticity index (PI) between 10 and 20 (Nguyen & Indraratna 2021; Singh et al. 2020). Samples of disturbed soil that had experienced mud pumping were collected from Wollongong, South Coast Rail line (NSW, Australia) for this study. The test material consisted around 500 kg of subgrade soil that had been carefully sieved through a 2.36 mm sieve and then stockpiled. Particle size distribution (PSD) and basic geotechnical tests were carried out as described below. The PSD of fine soils was measured using the Malvern particle analyser.

3.2.1 Soil Testing

Basic geotechnical tests such as the Atterberg limit (ASTM D4318-00 2003), particle size distribution (ASTM D422-63 2007), permeability (ASTM D5856-95 2002), Proctor compaction (ASTM D698-00 2000) and specific gravity (ASTM D854-02 2002) were carried out. The liquid limit (LL) and plastic limit (PL) of the soil was 42% and 26%, respectively. According to the Unified Soil Classification System (USCS), this soil could be classified as inorganic clay with medium plasticity, and a specific gravity of 2.59. The maximum dry density and optimum moisture content obtained using the standard Proctor test (ASTM D698-00 2000) indicated they were 1682 kg/m^3 and 18.5%, respectively. An in-situ soil density of 1600 kg/m^3 was obtained through compaction, which corresponded to a relative compaction (RC) of 95%. The average water content after saturation was around 32%. A perspex hydraulic cell with a diameter (internal) of 140 mm and a height of 300 mm was used for the permeability tests. D_{cell}/D_{100} is greater than 42 and could avoid the effects of boundary wall friction (i.e. the ratio between the largest particle and the internal diameter of the cell is less than $1/6$ (ASTM D3999-91 2003)). The compacted soil had a permeability of 8.9x10^{-7}m/s, as determined using the falling head method. The PSD and plasticity index charts are shown in Figure 3. 1 and Figure 3. 2, respectively.

3.2.2 Ballast Material

The fresh ballast material commonly used in NSW tracks was selected. The properties of the latite ballast have been provided elsewhere by Indraratna et al. (1998). The maximum and mean particle sizes were 37.5 mm and 30 mm, respectively, and the coefficient of uniformity is 1.34. For the dynamic filtration tests, 30-35 mm thick ballast was placed onto the geotextiles to create a ballast/geotextile interface and to represent typical field conditions.
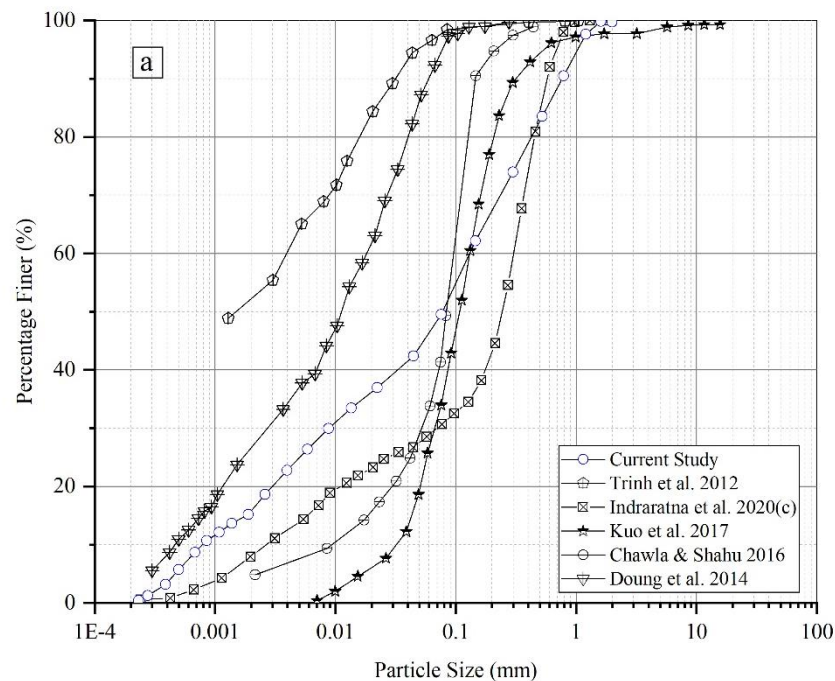
Figure 3. 1: PSD of subgrade soils (after Arivalagan et al. (2021))

3.2.3 Geotextiles

Three nonwoven geotextiles (G2, G3 and G4) and two geocomposites (G1 and G5) with pore opening sizes from less than 1 μm to 80 μm, were used for the laboratory experiments because they were specifically designed for railway tracks (Track bed separators, robust geotextiles, and geocomposite with filter membrane). Most available geotextiles are made of polyester (PET), polypropylene (PP) and Polythene. In this study, all the nonwoven geotextiles were made from polypropylene, which is strong, durable, and lighter than water.

Geocomposites G1 and G5 had a filter membrane in between nonwoven geotextile layers with aperture opening sizes (O_{95}) of <10 μm (ASTM D4491-99 1999) and an average permittivity of 5.1×10^{-7} sec^{-1}(ASTM D4491-99 1999). The nonwoven geotextile which covered the filter membrane had an aperture opening size of 75 μm, maximum tensile strength of 50 kN/m (EN ISO 10319 2008). The cone drop test was carried out according to EN ISO 13433 (2006) to measure the resistance of nonwoven geotextile (sandwiched layer) to penetration, and the diameter of the hole made by the cone was 2 mm. The tensile strength of geocomposites G1 and G5 were 50 and 95 kN/m (EN ISO 10319 2008) and they had a maximum CBR puncture resistance of 10 and 18 kN, respectively (EN ISO 12236 2006). Three nonwoven geotextiles (G2, G3 and G4) were used for the laboratory experiments to investigate how well geotextiles/geocomposites help to control excessive particle migration towards the ballast layer and prevent the instability (soil softening) at the ballast/subgrade interface. The aperture opening size of G2, G3, and G4 were 60, 75, and 65 μm, respectively (ASTM F316-03 2011). The tensile strength of G2, G3, and G4 followed EN ISO 10319 (2008) and were 52.5, 30, and 60 kN/m, respectively. G2, G3, and G4 had a maximum CBR puncture resistance of 9 kN, 5 kN, and 4.3 kN, respectively (EN ISO 12236 2006). All other properties of geosynthetics are listed in Table 3.1.

3.2.3.1 Permeability/Permittivity of Geotextiles

Falling head tests (ASTM D4491-99 1999) were carried out on the geotextiles because their permittivity is less than 0.05 sec^{-1}. During the permeability test (geotextile), a perforated plate was placed on top of the inlet valve, and then a wire mesh covered it to provide preferential flow. High vacuum grease was used to seal the contact between the container and geotextile. The average permittivity of the G1 filter media was 5.1×10^{-7} sec^{-1}. The average permeability of G1, G2, G3, G4 and G5 were 0.03, 45, 40, 30 and 0.35 mm/s, respectively (ASTM D4491-99 1999). All the properties of the geotextiles are listed in Table 3. 1 (Fiberweb 2012).
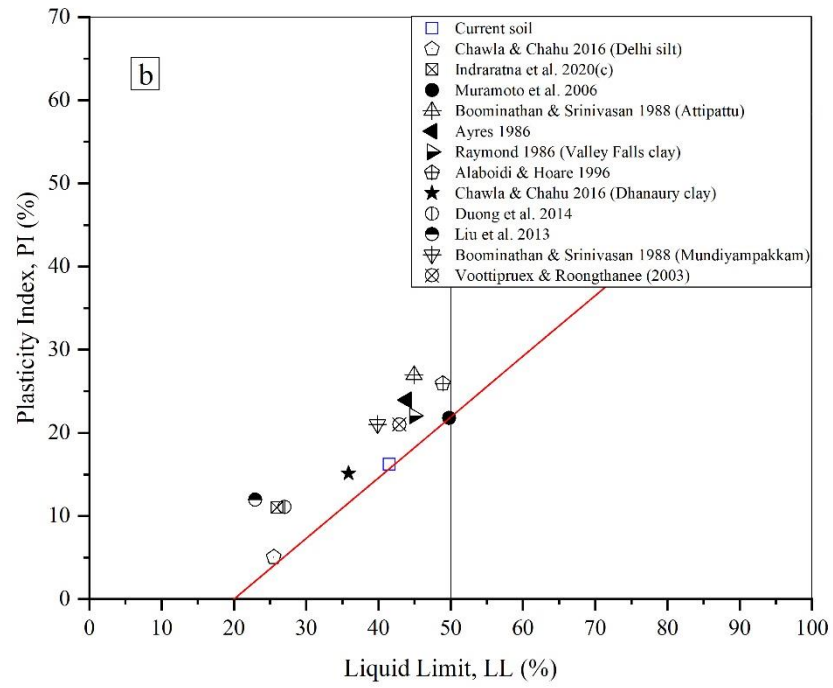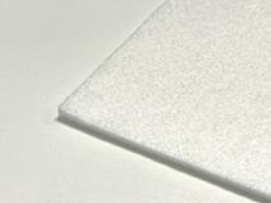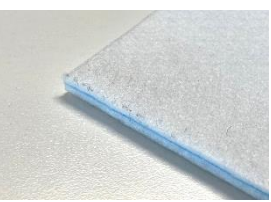
Figure 3. 2: Plasticity Index (modified after Arivalagan et al. (2021))

Table 3. 1: Properties of tested geosynthetics (* Geocomposites)

Geo synthetics	Photos	Thickness (mm)	Mean Peak Tensile strength (kN/m)	AOS (μm)	CBR Puncture Resistance (kN)
G1*		4.5	50	<1	10
G2		2.5	52.5	60	9
G3		3.5	30	75	5
G4		2	60	65	4.3
G5*		9	95	<10	18

3.2.4 Prefabricated Vertical Drain (PVD)

The core was entirely wrapped in a nonwoven geotextile filter, and this filter had an aperture opening size of 75 µm (ASTM D4751-99 1999). The PVD had an assembled drain width of 100 mm (ASTM D3774-96 1996), a thickness of 3.4 mm (ASTM D5199-01 2001) and a grab strength of 2500 N. The assembled drain flow at 200 kPa discharge (ASTM D4716-00 2000) was 2800 m^3/yr. All the properties of PVD (P) are tabulated in Table 3. 2.

Table 3. 2: Properties of tested PVD

PVD (P)	
Photo	
Assembled Drain width (mm)	100
Assembled Drain thickness (mm)	3.4
Drain filter pore size (µm)	75
Assembled Drain grab strength (N)	2500
Assembled Drain flow Discharge at 200kPa (m^3/yr)	2800

3.3 Testing Apparatus

3.3.1 Basic Dynamic Tests

Basic dynamic tests were used to determine how effectively the geotextiles could prevent particle migration and the instability that occurs at the geotextile/subgrade interface. Based on an observation from 'Basic dynamic tests', a modified dynamic test setup (Section 3.3.2) was designed to monitor the generation of EPWP, local changes in porosity and water content, and axial deformation during cyclic loading. The basic dynamic setup with a hydraulic actuator (Case1) and a vibrating table (Case 2) are shown in Figure 3. 3 and Figure 3. 4. The basic dynamic setup contains the following major components:

3.3.1.1 Polycarbonate Cell

The polycarbonate glass cell had a 240 mm internal diameter, and was 300 mm high and 13 mm thick. Its interior wall was coated with Teflon (Rocol – Dry Film Teflon) to reduce friction between the surface and soil particles. Polycarbonate glass was used because its visibility helped to facilitate monitoring the behaviour of base soil under cyclic loading. During the design of this equipment, it was checked that the radial relaxation was relatively small (less than $5 \times 10\text{-}4$ mm) for the lateral pressure induced by applied cyclic loading based on Young's modulus of the 13 mm thick shell (E = 2.6 GPa).

3.3.1.2 Vibrating Table

A Syntechtron vibrating table was used; the TC6B variable rate electronic controller can accurately control the full range of vibration for small vibrators. The range of vibrations per minute (VPM) was 3000 – 3600, which was a frequency of 50 – 60 Hz.

3.3.1.3 Hydraulic Actuator

The load cell actuator can apply a static load of up to 45kN and a cyclic load at frequencies of up to 40Hz. The hydraulic actuator was fixed to a 20 MPa hydraulic system and the applied load was continuously monitored. The monotonic and dynamic loading required can be applied by the hydraulic actuator via a piston connected to the loading plate: thus,

the desired magnitudes of contact normal effective stress could be applied to the specimen. The servo-controlled loading system helped to simulate the cyclic stresses generated during the passage of freight trains at various speeds (Trani & Indraratna 2010a).
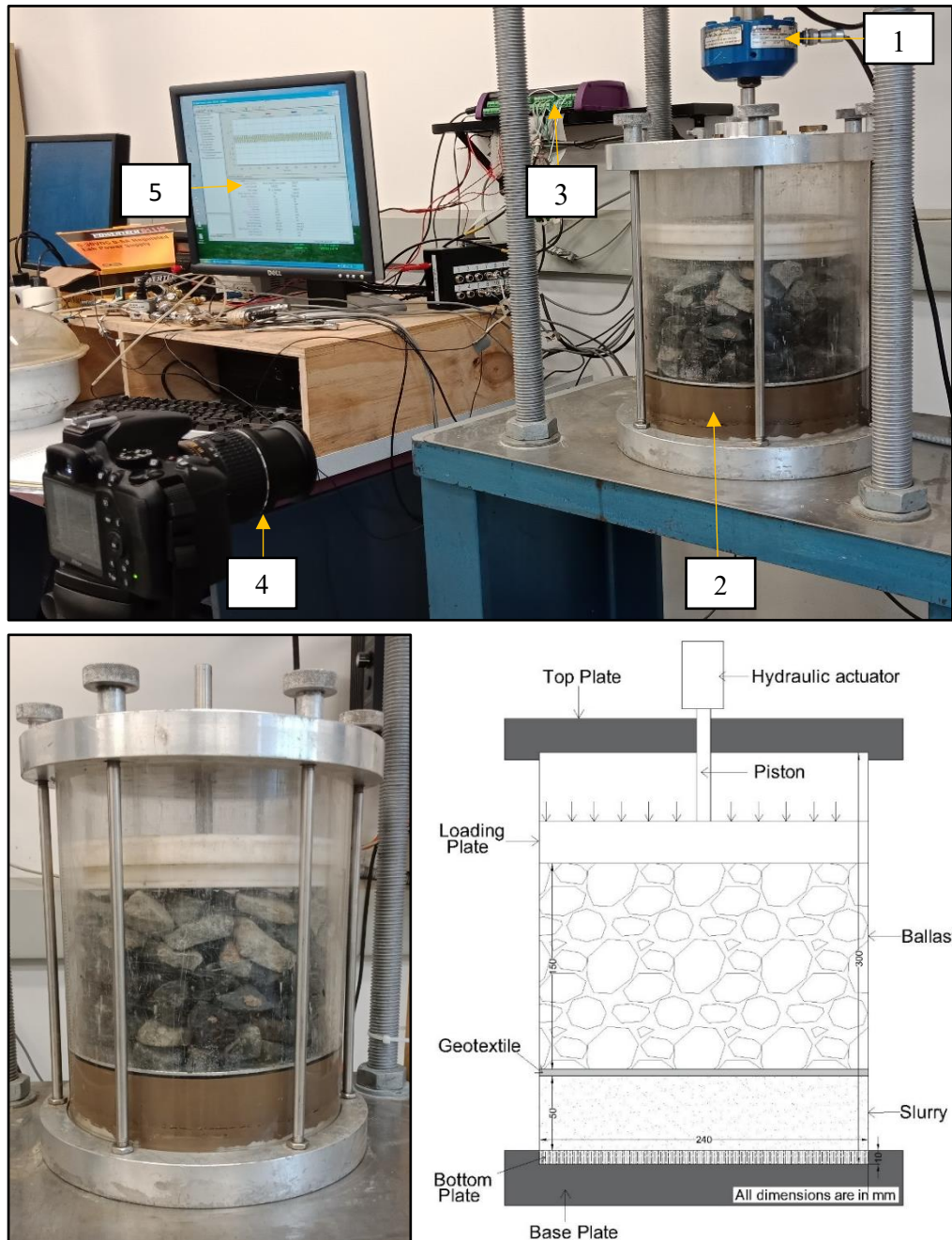
Figure 3. 3: Photos of Basic Dynamic Test (Case 1) and schematic illustration (1) Hydraulic actuator (2) Test sample (3) Data logger (4) Camera (5) Computer
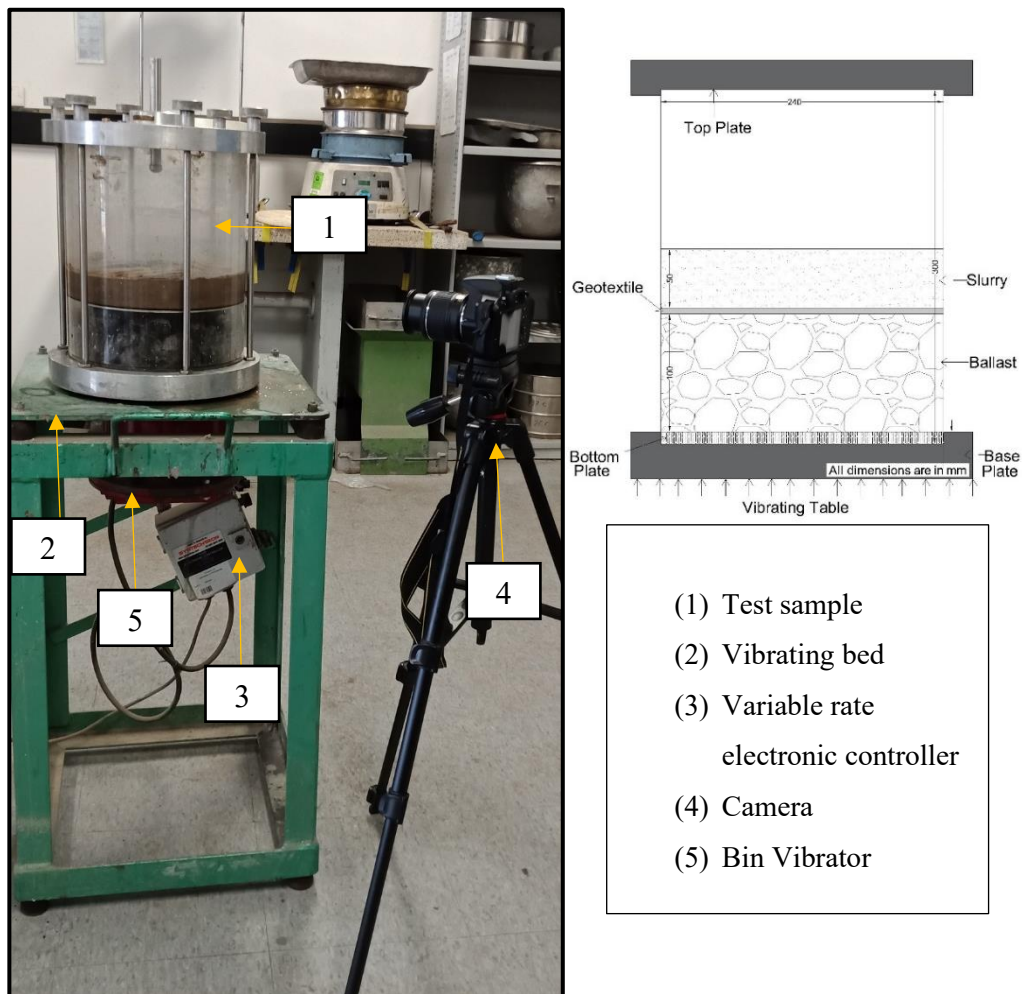
Figure 3. 4: Basic Dynamic Test (Case 2)

3.3.2 Dynamic Filtration Tests (DFT)

3.3.2.1 Modified Dynamic Filtration Apparatus

The filtration apparatus developed by Israr et al. (2016) was modified to monitor the local EPWP, soil porosity, development of EPPG between different soil layers, and deformation under cyclic loading conditions. As Figure 3. 5 shows, the apparatus has ten components, (1) a load cell and linear variable differential transformer (LVDT), (2) Miniature pore pressure transducers (MPs), (3) Body pressure transducers (Ps), (4) Amplitude Domain Reflectometry Probes (ADRs), (5) a Datalogger, (6) a Computer (7) a Camera (8) Power

supply, (9) An inlet for saturating the sample from a de-aired tank, and (10) a Hydraulic

actuator. These components are described as follows:
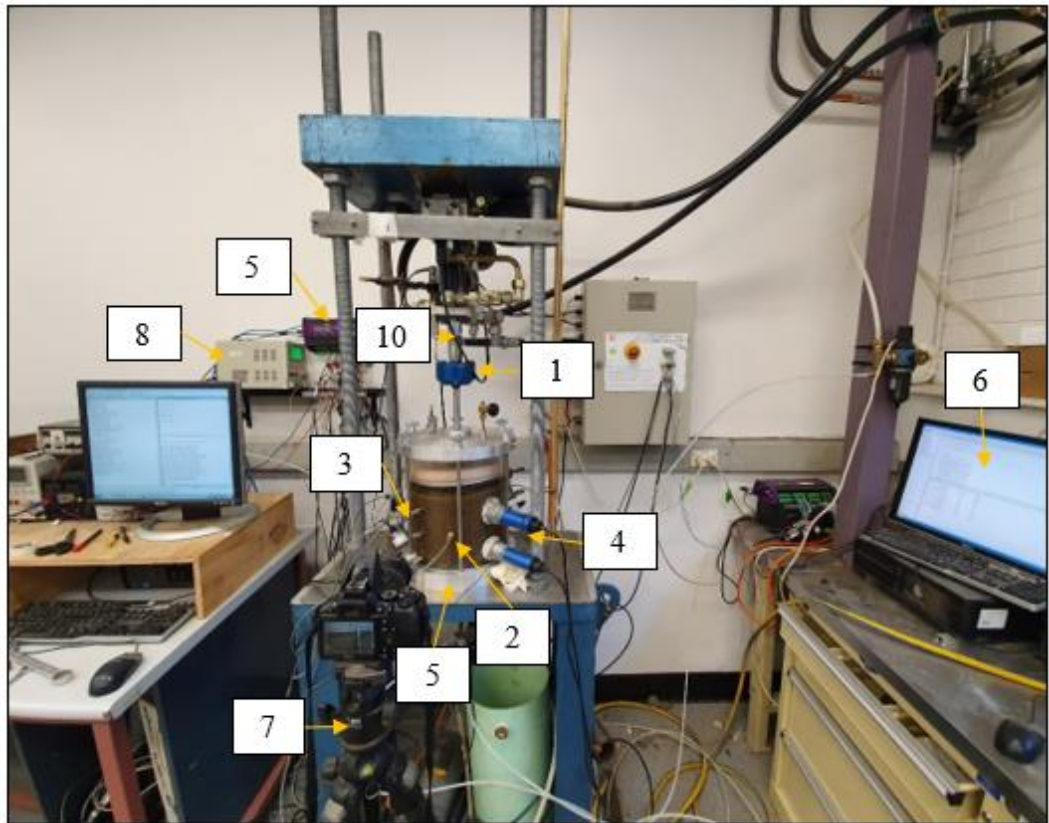
Figure 3. 5: Photo of dynamic filtration apparatus (Arivalagan et al. 2021)

3.3.2.2 Rigid Boundary Polycarbonate Cell

The polycarbonate cell used in the 'basic dynamic test', was modified so it could carry out

dynamic filtration tests on a 300mm high sample. When this equipment was being

designed, it was ensured that the radial relaxation would be less than 5×10^{-4} mm for the

lateral pressure induced by applied cyclic loading based on Young's modulus of the 13 mm

thick shell (E = 2.6 GPa). According to ASTM D3999-91 (2003), the ratio between the

largest particle to the internal diameter of the cell was less than $1/6$, this ensured minimal

boundary effects.

3.3.2.3 Miniature Pressure Transducers (MPs)

Four miniature pore pressure transducers (1 kPa accuracy) were placed on the centreline of the specimen at depths of 20, 40, 80, and 120 mm from the ballast/subgrade interface. The miniature pore pressure transducers (KPE-PB 500kPa) had a dual structure, so they were not affected by the outer lateral pressure. The model KPE-PB was rated as IP68 and measured to an accuracy of 1kPa. Four miniature pore pressure transducers were installed at different heights in the samples to capture the generation of EPWP during cyclic loading.

3.3.2.4 Body Transducers (Ps)

At the edge, six body transducers were placed at depths of 25, 55, 85, 115, 145, and 175 mm from the ballast/subgrade interface. Six body transducers (DGSI Slope Indicator E-120 30 PSI, accuracy 0.5 kPa) were connected to the cell. The local EPPGs that developed inside the specimen can be calculated by measuring the differential hydraulic pressure at each layer. The calibration was carried out using the redetermined magnitudes of hydraulic pressure to obtain accurate measurements. The positions of the miniature pressure transducers and body transducers are shown in Figure 3. 6.

3.3.2.5 Amplitude Domain Reflectometry (ADR) Probes

The MP 406 moisture sensors/ADR probes (ICT international) had a reinforced body and stainless-steel needles, so they were suitable for measuring the volumetric moisture content of soil under different loading conditions. The variations in porosity could be monitored by the three ADR probes installed along the subgrade depths (Israr 2016). The temporal variations in the porosity were measured by the ADR probes; the ADR probes also measure the Volumetric Water Content (VWC), as given by:

VWC (%) = $V_w/V_t = (V_v/V_t)$ x $(V_w/V_v) = n \times S_r$

where,

V_w = Volume of water, V_v = Volume of voids, V_t = Total volume of soil, S_r = Degree of Saturation, and n = Porosity

The variations in porosity could be used to monitor the saturation process, and calibration od ADR sensors was carried out done prior to this testing, in accordance with Trani & Indraratna (2010b).

3.3.2.6 Load Cell

A 50mm diameter load cell was installed at the bottom of the test chamber to monitor the vertical effective stress that was transferred from the applied loading. This load cell could measure the temporal variations caused by the frictional resistance of the side walls (accuracy of 0.1 kPa).

3.3.2.7 Datalogger and Modules

DT85 Data Taker and CMA lab controllers were used for data acquisition purposes. The CMA LTC software can provide full-waveform motion options for all the actuators, the automation feature in the 'Sequence Builder' test enables multi-stage, logic connected test sequences to be constructed and run, signal plotting, and data logging. A burst of data from all 15 sensors (4 miniature transducers, six body pressure transducers, three ADRs, LVDT, and a load cell) was transmitted to the data loggers. This setup could measure the readings from 32 sensors at a given period (3days). The data could be retrieved using data taker programs and could view the response in real time during testing. A minimum permissible time interval of 1 second was set as the default for all the cyclic testing, so the data logger could store test data for up to three days of continuous runtime. The unwanted digital noise in the raw data was smoothed.

3.3.2.8 A Micro-CT scanner

SkyScan 1275 (Belgium) with a 20–100-kV X-ray source and a very high 4-µm voxel resolution was used (SkyScan 1275 2016) to scan the samples of extruded soil after each cyclic test. The cylindrical specimens (20 mm diameter and 100 mm long) can be scanned every 0.5° for 360°, that ensures a high-quality reconstruction with excellent micro characteristics (Nguyen & Indraratna 2019). The porosity at different cross-sections can be captured using CT scanned images.
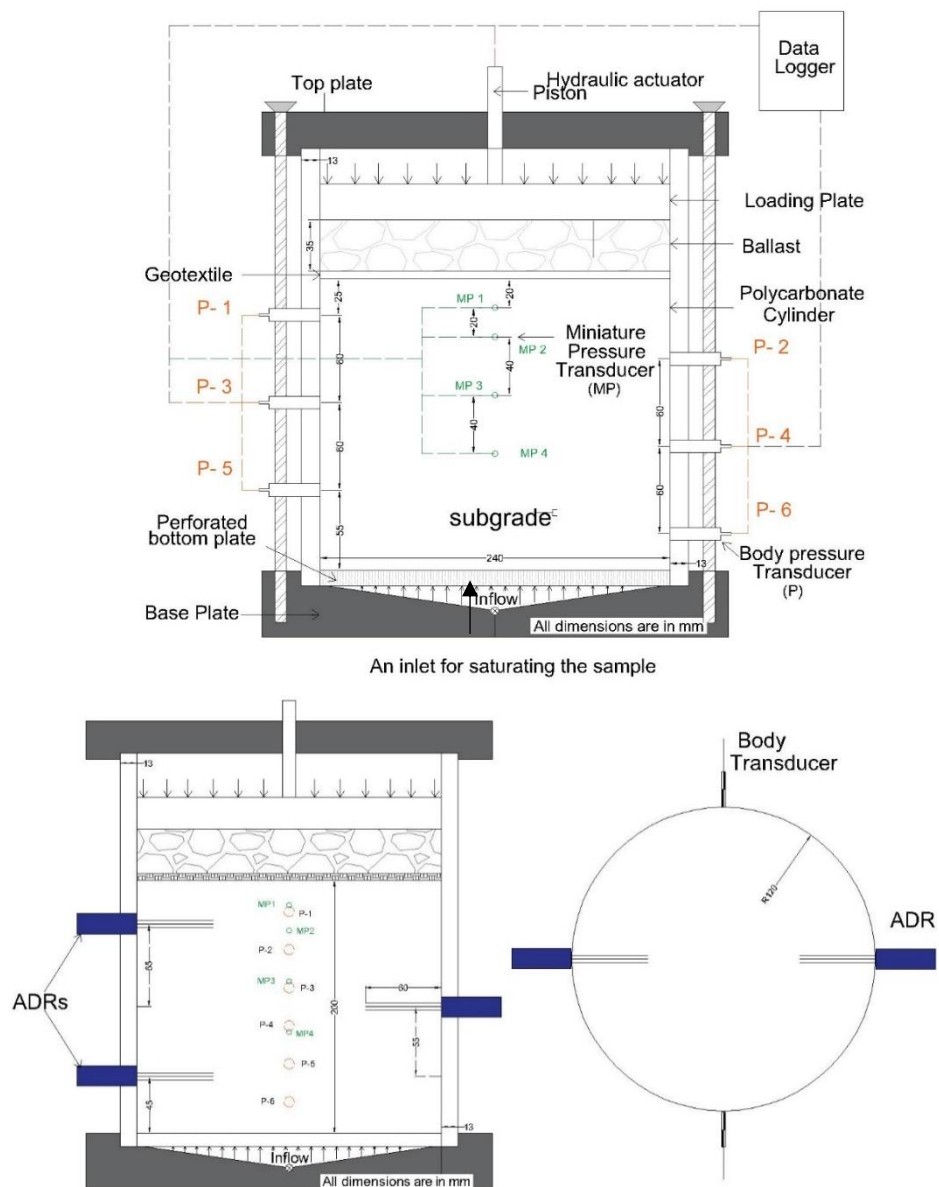
Figure 3. 6: Schematics of Dynamic Filtration Apparatus (DFA)

3.4 Loading Calculation at the Equivalent Depth Beneath the Sleeper

The contact pressure between the sleeper and ballast had been used in the previous studies to simulate the typical railway track conditions (Indraratna & Ngo 2018; Indraratna et al. 2011) and the average contact pressure (σ'_a) at the sleeper and the ballast interface can be expressed as follows:

$$\sigma'_a = \left(\frac{q_r}{BL}\right) F_2 \qquad\qquad \text{Equation 3.1}$$

where q_r = maximum rail seat load; B = width of the sleeper (0.26 m); L is the effective length of sleeper under cyclic load q_r; and F_2 = factor that depends on the type of sleeper and rail track maintenance.

By assuming that 1/3 of the total sleeper length will be effective on the load transfer mechanism, Equation 3.1 will become:

$$\sigma'_a = \left(\frac{3q_r}{Bl}\right) F_2 \qquad\qquad \text{Equation 3.2}$$

where l = nominal length of the sleeper (2.5 m)

For the maximum rail seat load of 85 kN,

$$\sigma'_a = \left(\frac{3q_r}{Bl}\right) F_2$$

$$\sigma'_a = \left(\frac{3*85}{0.26*2.5}\right) F_2 \approx 400 \text{ kPa}$$

The trapezoidal approximation (2:1 i.e., vertical: horizontal) was used to calculate the induced vertical stress at the ballast/subgrade interface under train loading. In a rectangular sleeper, a total concentric vertical load Q can be calculated using the average sleeper-ballast contact pressure (σ_{max}) as shown in Figure 3. 7.
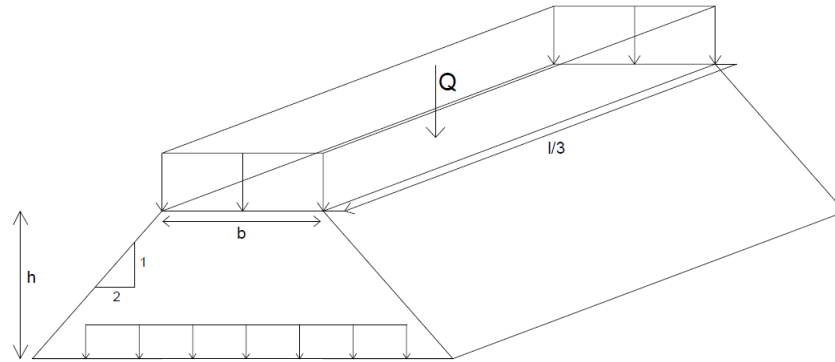
Figure 3. 7: Trapezoidal approximation of load distribution at the ballast/subgrade interface

$$Q = \sigma_{max} x A_e \qquad\qquad \text{Equation 3.3}$$

where A_e is the area of the effective length of sleeper (l/3).

If the $\sigma_{max} = 400 kPa$, Q will be around 86.6 kN

The maximum vertical stress at the equivalent depth (h) beneath the sleeper can be calculated as follows:

$$\sigma_{h\,max} = \frac{Q}{(b+h)\left(\frac{l}{3}+h\right)} \qquad\qquad \text{Equation 3.4}$$

where b and l are width and length of sleeper respectively.

At a depth of 0.3 m, $\sigma_{h\,max} = \frac{86.6}{(0.26+0.3)\left(\frac{2.5}{3}+0.3\right)} = 137 \approx 140$ kPa

In addition, AREMA Engineering Manual also recommended different equations (Talbot equation, Boussinesq equation, Love equation and Japanese National Railways equation) to calculate the contact pressure at the subgrade distributed by ballast layer (AREMA 2003).

3.5 Test Program

3.5.1 Basic Dynamic Tests

Two dynamic loading conditions, namely (1) a cyclic load applied by a hydraulic actuator, and (2) a dynamic load applied by a vibrator, were used to assess the ability of geotextiles to prevent particle migration and to observe the behaviour of the ballast/geotextile/subgrade interlayers. The results of basic dynamic tests are in Chapter 4.

3.5.2 Dynamic Filtration Setup

Although a filtration setup was developed by Israr & Indraratna (2017) to study the failure mechanism of compacted sandy soils, this setup was commissioned on subgrade soil under cyclic loading to evaluate the repeatability of tests, and the reliability of test data. Test repeatability was assessed by carrying out a series of tests. A test procedure similar to the 'dynamic filtration test' was used, it involves applying a cyclic load with deviatoric stress of 40 kPa. The photos of the 'basic dynamic test' and 'modified dynamic filtrations setup' are shown in Figure 3. 8.

3.5.3 Dynamic Filtration Tests (DFT)

The test program consisted of a series of cyclic tests on selected subgrade and geosynthetics, in six distinct experimental phases. These tests capture the key factors that contribute to subgrade fluidisation under critical cyclic loading conditions, as well as prevention techniques and measures to reduce the risk of mud pumping using geosynthetics in railway tracks. The descriptions of each phase are as follows;

3.5.3.1 Phase 1: Undrained and Free Drainage Conditions

To define the failure criteria and subgrade fluidisation, laboratory tests were carried out under (a) undrained conditions where an impermeable boundary was created by a

geomembrane, and (b) free drainage with a layer of ballast directly over the subgrade specimen. A deviator vertical stress (σ_d) of 40 kPa (i.e. σ_{min} = 30 kPa, σ_{max} = 70 kPa) and f = 5.0 Hz were applied.

Figure 3. 8: (a) Basic dynamic test setup (b) Modified Dynamic filtration test setup

3.5.3.2 Phase 2: Performance of Different Geotextiles

The main objective of Phase 2 was to evaluate the performance of 5 different geotextiles/geocomposites (G1, G2, G3, G4, and G5) in terms of controlling the development of EPWP and preventing or delaying the initiation of subgrade fluidisation. Geotextiles were laid at the interface between the ballast and subgrade specimens, and a cyclic loading was applied as described in Phase 1.

3.5.3.3 Phase 3: Influence of Frequency and Amplitude (Geosynthetics)

The laboratory experiments under Phase 3 were needed to investigate the performance of geotextiles under different speeds and axle loads. In this instance, the loading frequency and amplitude applied varied from 1 to 5 Hz and 20-35 kPa (i.e. σ_{min} = 30 kPa, σ_{max} = 70-100 kPa), respectively. The geotextiles at the ballast subgrade interface were selected based on the results under Phase 2.

3.5.3.4 Phase 4: Prefabricated Vertical Drains (PVDs)

The main objective of Phase 4 was to evaluate the performance of PVDs under cyclic loading conditions. The effectiveness of a combined PVD-Geocomposite system was also measured in terms of controlling the development of EPWP and preventing or delaying the initiation of subgrade fluidisation. In phase 4, a deviator vertical stress (σ_d) of 40-70 kPa (i.e. σ_{min} = 30 kPa, σ_{max} = 70 – 100 kPa) and f = 5.0 Hz were applied.

3.5.3.5 Phase 5: Influence of Radial Drainage

A horizontal drainage path was created by the inclusion of PVD within the soil specimen. These experiments were carried out to examine how effectively radial drainage could reduce the EPPG that developed due to cyclic loading (disparity between vertical and horizontal EPPG). Miniature pressure transducers were installed at 0, 30, 60, and 90 mm from the centreline/PVD to measure the EPWPs that developed in a horizontal direction.

3.5.3.6 Phase 6: Effects of Cyclic Stress and Frequency (PVD + Geocomposite)

The laboratory experiments under Phase 6 were carried out to investigate the role of geotextiles and PVDs under different axle loads and speeds. The loading frequency and amplitude varied from 1 to 5 Hz and 40-70 kPa, respectively. In this case, geocomposite G1 was used for the entire test, as illustrated in Table 3. 3.

Table 3. 3: Experimental Phases

Phase	Test Name	Drainage condition at ballast subgrade interface	Tested Geosynthetics	σ_{min} (kPa)	σ_{max} (kPa)	Frequency (Hz)
1	T1	Undrained	Impermeable	30	70	5
	T2	Free drainage (no capping)	NIL	30	70	5
2	G1	Partially drained with G1	Geocomposite 1	30	70	5
	G2	Partially drained with G2	Geotextile 2	30	70	5
	G3	Partially drained with G3	Geotextile 3	30	70	5
	G4	Partially drained with G4	Geotextile 4	30	70	5
	G5	Partially drained with G5	Geocomposite 2	30	70	5
3	G-70-5	Partially drained with G1	Geocomposite 1	30	70	5
	G-85-5	Partially drained with G1	Geocomposite 1	30	85	5
	G-100-5	Partially drained with G1	Geocomposite 1	30	100	5
	G-70-1	Partially drained with G1	Geocomposite 1	30	70	1
	G-70-3	Partially drained with G1	Geocomposite 1	30	70	3
	G-70-5	Partially drained with G1	Geocomposite 1	30	70	5
4	P70	With P	PVD	30	70	5
		With P	PVD	30	85	5

	P85					
	P100	With P	PVD	30	100	5
	G-70	With G1	Geocomposite 1	30	70	5
	PG-70	With P+G1	PVD + Geocomposite 1	30	70	5
5	PG0	With P+G1	PVD + Geocomposite 1	30	70	5
	PG30	With P+G1	PVD + Geocomposite 1	30	70	5
	PG60	With P+G1	PVD + Geocomposite 1	30	70	5
	PG90	With P+G1	PVD+ Geocomposite 1	30	70	5
6	PG-70-5	With P+G1	PVD + Geocomposite 1	30	70	5
	PG-85-5	With P+G1	PVD + Geocomposite 1	30	85	5
	PG-100-5	With P+G1	PVD + Geocomposite 1	30	100	5
	PG-70-1	With P+G1	PVD + Geocomposite 1	30	70	1
	PG-70-3	With P+G1	PVD + Geocomposite 1	30	70	3
	PG-70-5	With P+G1	PVD + Geocomposite 1	30	70	5

3.6 Test Procedures

3.6.1 Basic Dynamic Tests (BDT)

3.6.1.1 Case 1

G1 and G2 were selected for these tests. The soil specimen had a water content of 39% and was poured into the cylinder, and then a saturated geotextile was placed on top of the slurry. A 150 mm thick layer of ballast was then placed on the geotextile to develop a geotextile/ballast contact pressure. Variations in the PSD of the subgrade soil were captured

after cyclic loading by the Malvern particle analyzer. The change in the water content was also measured before and after cyclic testing to investigate how effectively the geotextiles could prevent particle migration and instability at the interface, with enhanced drainage.

3.6.1.1.1 Load Application

A deviator stress of 110 kPa (i.e. σ_{min} = 30 kPa, σ_{max} = 140 kPa) and a frequency of 5 Hz were used. The cyclic stress represents an axle load of 40 tonnes due to the passage of heavy haul trains. The loading frequency of 5 Hz simulated the loading frequency encountered in a typical Australian rail track, and corresponded to train speeds of 80 to 100 km/h (Attya et al. 2007). In this study, a cyclic load was applied continuously for 4500 cycles. The cyclic test was stopped after 15 minutes because it represented 5 train passages.

3.6.1.2 Case 2

These tests were designed to create an extreme case of segregation where coarse particles sink to the bottom and the fine particles and water travels to the top (i.e., bleeding water with micro-fine particles). This generally happens when concrete is being vibrated and if the water/cement ratio is much higher and is based on the packing density of concrete materials. The geotextile at the ballast/slurry interface under Case 2 was based on the results from Case 1. The setup for a basic dynamic test (Case 1) is shown in Figure 3. 3, this test could assess the performance of the selected geotextile under critical loading and adverse hydraulic conditions.

3.6.1.2.1 Slurry Preparation

When fully saturated soft soil approaches its liquid limit due to the load applied, mud pumping can occur because the water content exceeds the liquid limit before the effective stress becomes zero. Two samples of slurry, with water contents of 39% (**Test T39**) and

43% (**Test T43**), were prepared to test the performance of geotextile under constant vibration. A 100 mm thick layer ballast was placed at the bottom, and the saturated geocomposite G1 was placed on top of it. A 50 mm layer of this slurry was then poured on top of the geotextile. The setup for the basic dynamic test (Case 2) is shown in Figure 3. 4. The vibrating speed was 5, and the tests ceased after 60 minutes. The change in the water content and PSD were measured before and after cyclic testing.

3.6.2 Dynamic Filtration Tests (DFT)

3.6.2.1 Testing Material

The collected soil was sieved through 2.36 mm. The required mass of dry soil and volume of water were mixed beforehand and left overnight in a humidity-controlled room, and then compacted inside the test chamber in eight layers. The target bulk density (1600 kg/m^3) and moisture content (17%) were attained by compacting the dry soil and water to the desired volume.

3.6.2.2. Compaction

The 'nonlinear undercompaction' criterion suggested by Jiang et al. (2003) was utilised to obtain a uniform density for the test specimens. As Indraratna et al. (2020) proposed, the height of each layer was calculated using the average predetermined thickness of an individual layer. The specimen was compacted in 8 layers with thicknesses of 27.5, 27.39, 26.98, 26.27, 25.25, 23.9, 22.3, and 20.35 mm (from layer 1 (bottom) to layer 8 (top), respectively. After compaction, the uniformity of each specimen was also assessed by coring additional samples to measure their overall dry density, and the dry density of each layer.

3.6.2.3 Installation of PVD

The equivalent diameter of the soil cylinder for a drain spacing in the field is around 1 to 1.5m; the drain spacing in the dynamic filtration tests was much smaller (240 mm) than the real field requirements. Therefore, PVDs with a modified size were used in the experiments based on the time factor (T_h) and the average degree of consolidation (U_h) for two soil cylinders, as proposed by Ni (2012). The modified PVDs used for laboratory experiments were 17 mm x 3.4 mm. A PVD was driven/inserted through the centre of the subgrade soil using a rectangular mandrel (25 mm x 4.5 mm), to ensure minimum soil disturbance while installing the PVD and removing the mandrel.

3.6.2.4 Saturation

Saturation was carried out in two steps, (1) de-airing the specimen by applying 100 kPa of suction (Kamruzzaman et al. 2008), and (2) saturating the sample with filtered and de-aired water until the water level reached the top of the specimens. The saturation of this specimen was monitored continuously by three ADR probes installed at different depths (Israr et al. 2016; Trani & Indraratna 2010b); these probes remain in situ until uniform readings are attained (i.e., 80 F/m apparent permittivity of water at a room temperature of 20^0). The miniature pore pressure transducers, body pore pressure transducers, and LVDTs were calibrated and then installed after saturating the soil specimen.

3.6.2.5 Consolidation

A total vertical pressure of 30 kPa was applied for 48 hours to consolidate the soil specimen; i.e., until the volume change (ΔV) was considered to be negligible (i.e., < 0.5 mm^3/hour). The interior wall was coated with Teflon (Rocol – Dry Film Teflon) to reduce friction between the surface and soil particles. The soil was subjected to uniform vertical stress, and the corresponding settlements of the consolidating layer were measured. The

pore pressure that developed during the consolidation process was monitored, and the settlement due to the applied loading was recorded continuously for two days.

3.6.2.6 Interface Preparation

The geotextile was saturated before being placed onto the subgrade soil. After placing the ballast and/or geotextile, a sinusoidal load was applied through a servo-controlled actuator.

3.6.2.6.1 Saturation of Geotextile

The geotextile was saturated before the wet run. It is important to have no air bubbles during the saturation process, as proposed in ASTM F316-03 (2011). The sample was saturated by slowly sliding the geotextile into the water at approximately 45° while allowing the water to soak into the sample by capillarity. The testing method suggested in ASTM D4491-99 (1999) was used to remove the air trapped in the specimen. A vacuum chamber was used to assist in wetting the geotextile, as mentioned. A submerged tube that is attached to the source of a vacuum can be used to remove the air trapped in or on the specimen. The sample was soaked in distilled and deaired water for 24 - 48 hours prior to the test setup. No bubbles were on the top surface of the geotextile (during the installation), which confirmed that the geotextile was fully saturated within 24 - 48 hours.

3.6.2.6.2 Entrapped Air in Geosynthetics

During saturation, it was difficult to prevent air from being trapped and air bubbles from forming on the top layer. The method suggested in ASTM D4491-99 (1999) was used to remove the air trapped on the specimen, it is as follows: "A submerged tube which is attached to the source of a vacuum just above the surface of the geotextile can remove the air trapped in or on the specimen ".

3.6.2.7 Cyclic Load Application

A cyclic load was applied to the specimen through a 235 mm diameter loading plate inside a cell with an internal diameter of 240mm. This rigid loading plate could induce uniform stress on the subgrade soil with minimal rigid wall boundary effects (Mohammadinia et al. 2019). Details of this applied loading system are explained elsewhere by Trani & Indraratna (2010b). In this study, a uniform cyclic stress was applied as a minimum vertical stress, and the sinusoidal vertical cyclic stress (σ_{min} = 30 kPa and σ_{max} = 70 – 100/140 kPa) simulates a maximum axle load of 35-40 tonnes. The frequency varied between 1.0 and 5.0 Hz, which corresponds to train speeds of 40-220 km/h (Indraratna et al. 2020; Mamou et al. 2017; Powrie et al. 2007).

3.7 Test Analysis

3.7.1 Basic Dynamic Tests (BDT)

The primary objective of 'basic dynamic tests' is to assess the potential of geotextile to prevent the instability of subgrade soil at the interface (geotextile/subgrade) by providing sufficient drainage capacity. The calculations, observations, and analyses during and after the tests are as follows:

- Pre-test calculations: Pre-test calculations included the preparation of slurry and the loading time considering a typical train passage on railway tracks. Dry mass soil and the volume of water needed to achieve the target moisture content were calculated. The moisture content of the prepared slurry was also measured prior to the tests.

- Mid-test observations: This involved observing the drainage capacity of the geotextile at given time intervals and recording the level of water on top of the geotextile to calculate the average permeability. For reference purposes, photos and videos were taken when applying cyclic loading.

93

- Post-test analysis: The PSD of slurry/water collected at the top was measured using the Malvern Particle Analyzer. Samples of soil were also collected at the middle and the bottom. The water content of the soil beneath the geotextile was also measured.

3.7.2 Dynamic Filtration Tests (DFT)

This section shows the calculations, observations, and analyses made before, during, and after the cyclic tests.

- **Pre-test calculations:** Pre-test calculations included the preparation of specimens and compacted energy imparted for the testing. The mass of dry soil and the volume of water to reach the target density were calculated, and the compaction energy needed to attain uniformly compacted layers was also measured. The nonlinear 'undercompaction' method was used to calculate the thickness of each layer. An additional sample was prepared under different phases to assess the uniformity of each specimen and to measure (a) their overall dry density, and (b) the dry density of each layer.

- **Mid-test observations:** Visual observations were made of the 'interlayer creation', the pumping of fines, and variations in the soil density. This also involved observing the interlayer creation (Sinking ballast particles into subgrade) during cyclic loading and pumping of fine particles (finer particle separation and accumulation at the top surface/segregation). For reference purposes, photos and videos were taken during the application of cyclic loading to capture any changes in the soil specimen.

  Real-time data analysis - The spatial and temporal variations in the porosity (ADRs - during the saturation process), the pore pressure at different depths, and axial deformation were monitored during testing. The stored data can be retrieved at any time.

- **Post-test analysis:** The tested specimen was separated into three distinct layers to capture the PSD (Interface/Top, Middle, and Bottom). The PSD of the slurry collected at the interface was measured using the Malvern Particle Analyzer. Samples of soil were also collected at the middle and the bottom to determine the PSD. Microscopic examination/CT-Scan - Extruded soil samples (0-50mm, 50-100mm, 100-150mm) were used to capture the porosity (i.e. cross-sections of soil columns). Data Acquisition and Processing - The vigorous data recorded from all the channels were processed and smoothed where necessary to examine the response of the specimen under cyclic loading.

3.8 Chapter Summary

This chapter describes the experimental program carried out in this study, it includes the test procedures for all the phases, details about the instrumentation, a schematic of modified apparatus, and related definitions. The experiments were carried out to capture the phenomenon of subgrade fluidisation and using geotextiles/PVDs to reduce the risk of mud pumping by simulating typical loading conditions in railway tracks. Axle loads of 25 - 40 tonnes and train speeds of 40 – 250 km/h were considered. The components and test methodology for all the experimental phases (Basic dynamic tests and Dynamic filtration tests) were described with critical information on instrumentation. The behaviour of the specimens in all the experiment models was evaluated from the continuous-time records of applied load, axial strain, change in EPWPs, and variations in the soil particle arrangement/porosity.

CHAPTER 4: TESTING PROGRAM

BASIC DYNAMIC TESTS AND DYNAMIC FILTRATION TESTS

4.1 Introduction

The capping layer in railway tracks prevents the fine base particles from migrating into the ballast layer and reduces the cyclic stress transferred to the subgrade soil. However, under adverse hydraulic conditions, an overly compacted or impermeable capping layer cannot provide sufficient drainage to reduce EPWPs that develop during the passage of trains; this may lead to subgrade failure and possible mud pumping where fluidised soil particles shoot up through the capping layers. One of the most cost-effective methods for replacing conventional compacted sand layer or reducing the thickness of the capping layer is geosynthetic inclusions (Fatahi et al. 2011). This is why appropriate design guidelines for railway tracks are needed to prevent particle migration and provide acceptable drainage over long periods of time. In this Chapter, dynamic tests were carried out to assess the potential use of geotextiles in railway tracks by simulating heavy haul loading (up to 40-tonne axle load). Tests were also carried out on a vibrating table to assess the soil behaviour at the geotextile/subgrade interface. Based on the results obtained from the 'basic dynamic tests', a 'dynamic filtration apparatus' was modified to measure how effectively geotextiles could alleviate the EPWP that developed at the interface and in shallower subgrade soil. The laboratory results were used to evaluate the effectiveness of geotextiles and geocomposites and the potential for reducing the risk of subgrade fluidisation under critical cyclic loading conditions.

4.2 Basic Dynamic Tests: Results and Discussions

4.2.1 Case 1

Tests were carried out to assess the effectiveness of geocomposite G1 and geotextile G2 at preventing the migration of fine particles under a cyclic load. A soil sample (LL = 42) with a water content of 39% was used for this study. The test procedures for the basic dynamic tests are reported under Section 3.6 in Chapter 3.

4.2.1.1 Reduction in Water content

The migration of fine particles and increased moisture can create a thick slurry at the interface during mud pumping. This slurry can then be pumped up towards the ballast layer under adverse hydraulic conditions such as poor drainage and increased hydraulic gradient. Therefore, geotextiles with increased permeability and filtration characteristics are needed to prevent soil softening (slurry) at the interface. In this instance, the water content of the soil (39%) is close to the liquid limit (LL = 42) of the subgrade. As Table 4. 1 shows, geocomposite G1 reduces the water content of soil near the interface by up to 7% compared to G2, which is only 3.5%. During the test (G1), water inside the subgrade soil moved upwards through the filter media; the water that accumulated on the top geotextile is shown in Figure 4. 1. The collected water on the top was used to calculate the average drainage capacity of the geocomposite/geotextile. The average flow through geocomposite G1 was 4.8 mm^3/s (after 120 minutes of cyclic loading), with a geotextile area of 4.15×10^{-2} m^2. The water flow mainly depends on the rate of clogging (where fine particles accumulate at the bottom of the geotextiles), a phenomenon that is discussed further under Case 2 in the later sections. It is clear that G1 could reduce the increased moisture content of subgrade soil during cyclic loading because the drainage capacity at the soil/geotextile interface was adequate. Permeability tests were also conducted to further understand the hydraulic conductivity of both geotextiles; the amount of trapped fines was also measured (Table 4. 2 and 4.3).

Table 4. 1: Water content for geotextiles G1 and G2

Geotextiles	Description	water content (%)	Reduction (%)
G1	Before Cyclic Testing	(39.3 + 39.4)/2 = 39	7
	After Cyclic Testing	32	
G2	Before Cyclic Testing	(32.1+39.4)/2 = 39	3.5
	After Cyclic Testing	35.5	

Figure 4. 1: Accumulated water at the top of geocomposite G1

4.2.1.2 Permittivity of the Geotextiles

The hydraulic conductivity of the geotextiles was determined by permittivity according to ASTM D4491-99 (1999). As expected, there was a reduction in G1 (around 35%) after cyclic testing due to clogged fines inside the pores of the geotextiles. On the other hand, G2 was severely clogged due to the migration of fines (57% reduction in permittivity), and pumped-up slurry could be seen through the pore openings. Geotextile G2 failed to prevent fines from migrating and the soil from softening under cyclic loading; a photo of geotextile G2 tested after 36,000 cycles is shown in Figure 4. 6.

Table 4. 2: Hydraulic conductivity of the geotextiles

Geotextiles	Description	Permittivity (s^{-1})	Reduction (%)
G1	Before Cyclic Testing	$7.1x10^{-4}$	35
	After Cyclic Testing	$4.6x10^{-4}$	
G2	Before Cyclic Testing	15	57.2
	After Cyclic Testing	6.41	
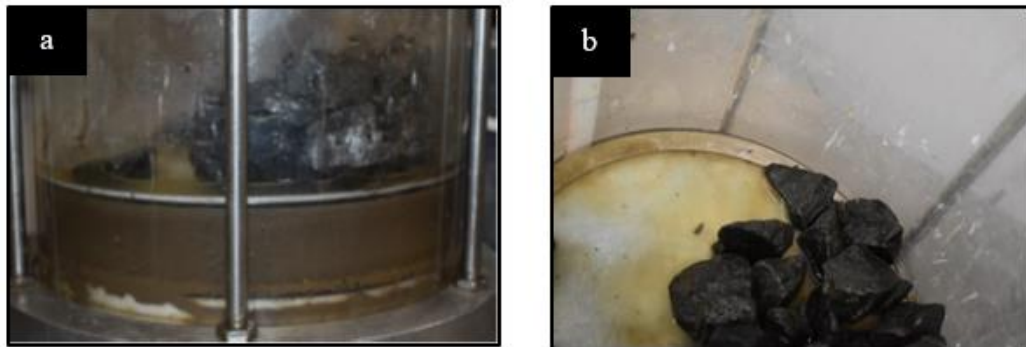
Figure 4. 2: Cyclic test with geocomposite G1 (a) Removal of ballast, (b) Ballast particles with accumulated water

4.2.1.3 The Variations in Particle Size Distribution

The change in particle size distribution (PSD) was assessed using the Malvern particle analyser. After removing the ballast (Figure 4. 2), the water that remained on top of the

geotextile, and the slurry, was collected to determine the PSD of fines that had infiltrated through the pore openings due to the applied load. The changes in the PSD when using geocomposite G1 were insignificant, and geotextile G2 failed to prevent particle pumping (Figure 4. 3and 4.4).

4.2.1.3.1 Estimating Pumped-up Fines from PSD analysis

As Figure 4. 3 and 4.4 show, finer particles of less than 1 micron migrate through the geotextile (G2) under cyclic loading (70 kPa deviator stress). The volume density represents the amount of soil used for PSD testing using the laser diffraction Malvern Particle analyser. The results indicate that particles between 1 – 100 microns could clog the pores, and some fines were pumped up through the pore openings of the geotextiles. Furthermore, slurry pumping was visible through the pores of geotextile G2 and this indicates that geotextile G2 could not prevent particles from migrating under cyclic loading conditions. Although geocomposite G1 performed better than G2 (Figure 4. 4), the potential for subgrade fluidisation under heavy haul trains carrying 35 or 40 tonnes of axle loading should be assessed. Therefore, an array of different cyclic deviatoric stresses (40-70 kPa) were selected in 'Dynamic Filtration Tests' (Chapter 6).

Table 4. 3: The trapped fine particles

Geotextiles	Description	Weight of Oven Dried Geotextile (g)	Trapped Fines (g)
G1	Before Cyclic Testing	40.3	6.39
	After Cyclic Testing	46.69	
G2	Before Cyclic Testing	25.46	12.08
	After Cyclic Testing	37.54	
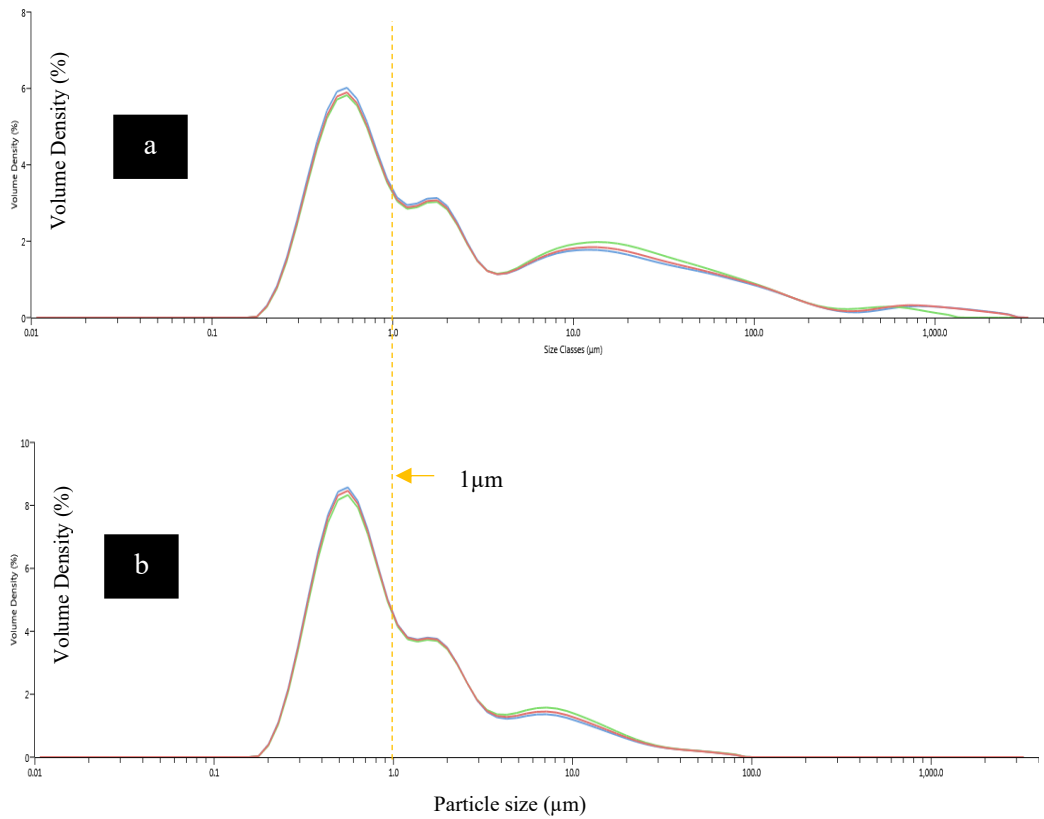
Figure 4. 3: Variations in volume density of (a) soil collected near the interface and (b) slurry collected from the top of geotextile G2

4.2.1.4 Clogging Behaviour of the Geotextile

The weight of trapped fine particles was calculated by taking the differences between the weights of oven-dried (after testing) and clean geotextile (before testing). The geocomposite G1 had 6.8 g of trapped fines; the geotextile/subgrade interfaces after cyclic loading are shown in Figure 4. 5. Geocomposite G2 could not prevent the fine particles from migrating (slurry on the top), and severe clogging was observed (i.e., 12.8g of trapped fines). Geocomposite G1 prevented slurry from being pumped up through the pores, unlike G2. During the 'basic dynamic tests' fines could be seen through the pores after 36,000

cycles (Figure 4. 5), so a cyclic load up to 100,000 cycles were chosen for the 'Dynamic filtration Tests' to assess the performance of geotextiles under various loading conditions.
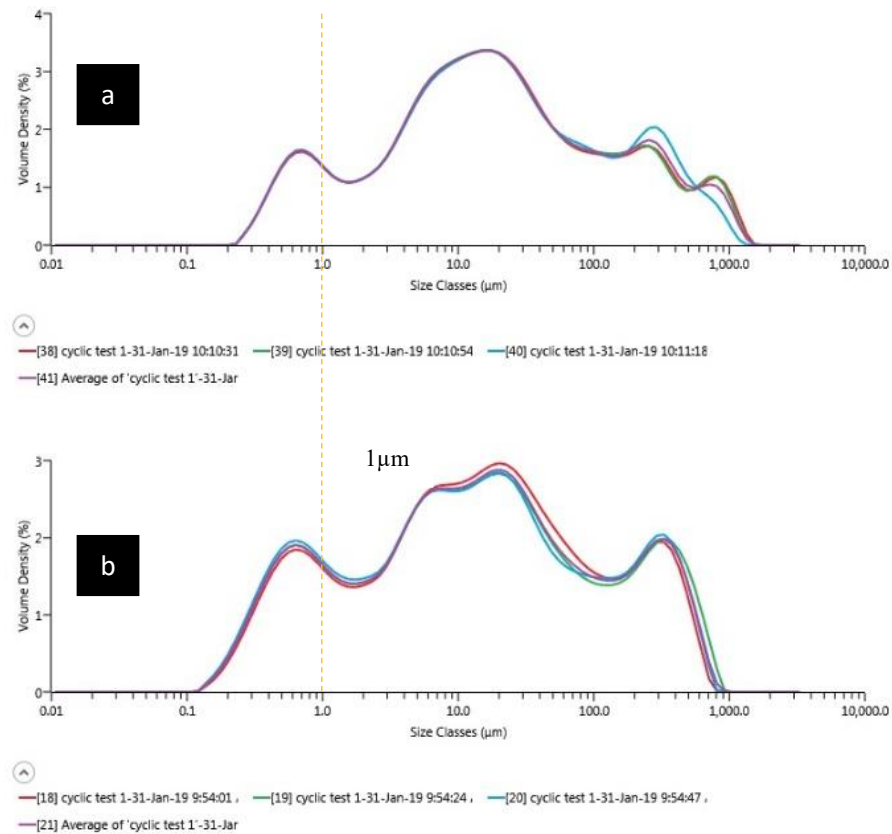
Figure 4. 4: Change in volume density (a) soil prepared for testing and (b) soil collected at the interface after cyclic testing (Geocomposite G1)

4.2.1.5 Issues Encountered during the Test

Air entrapped in geotextiles could affect their performance, so entrapped air and air bubbles were removed during the saturation proposed in ASTM F316-03 (2011). Permeability tests were carried out on the tested geotextiles under cyclic loading conditions. Trapped fine particles started to dislocate from the pore openings due to continuous flow during the 'Falling head tests'; however, there could have been minor errors in the permittivity measured in the geotextiles and geocomposites.
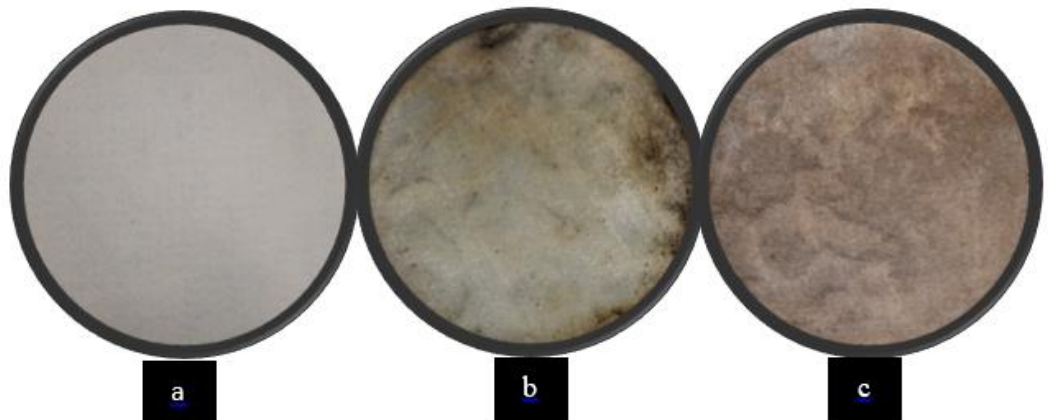
Figure 4. 5: Geocomposite G1 (magnification = 0.209x) (a) After Saturation, (b) Top (after cyclic loading), and (c) Bottom (after cyclic loading)

Figure 4. 6: Geotextile G2 after cyclic testing

4.2.2 Case 2

In Case 2, geocomposite G1 was selected because it could reduce the water content (w/c) and prevent particle migration, as described in Section 4.2.1 (Chapter 4). The primary focus here was to investigate the effectiveness of geotextile under strong vibrations (frequencies up to 60 Hz). In this instance, two separate tests were carried out, namely, **T39** (39% of initial w/c) and **T43** (43% of initial w/c) based on the water content of the slurry. The tests

were stopped after running the vibrating table for 60 minutes (f=50Hz or 300 VPM); the test procedure with a description of the electronic controller can be found in Chapter 3.
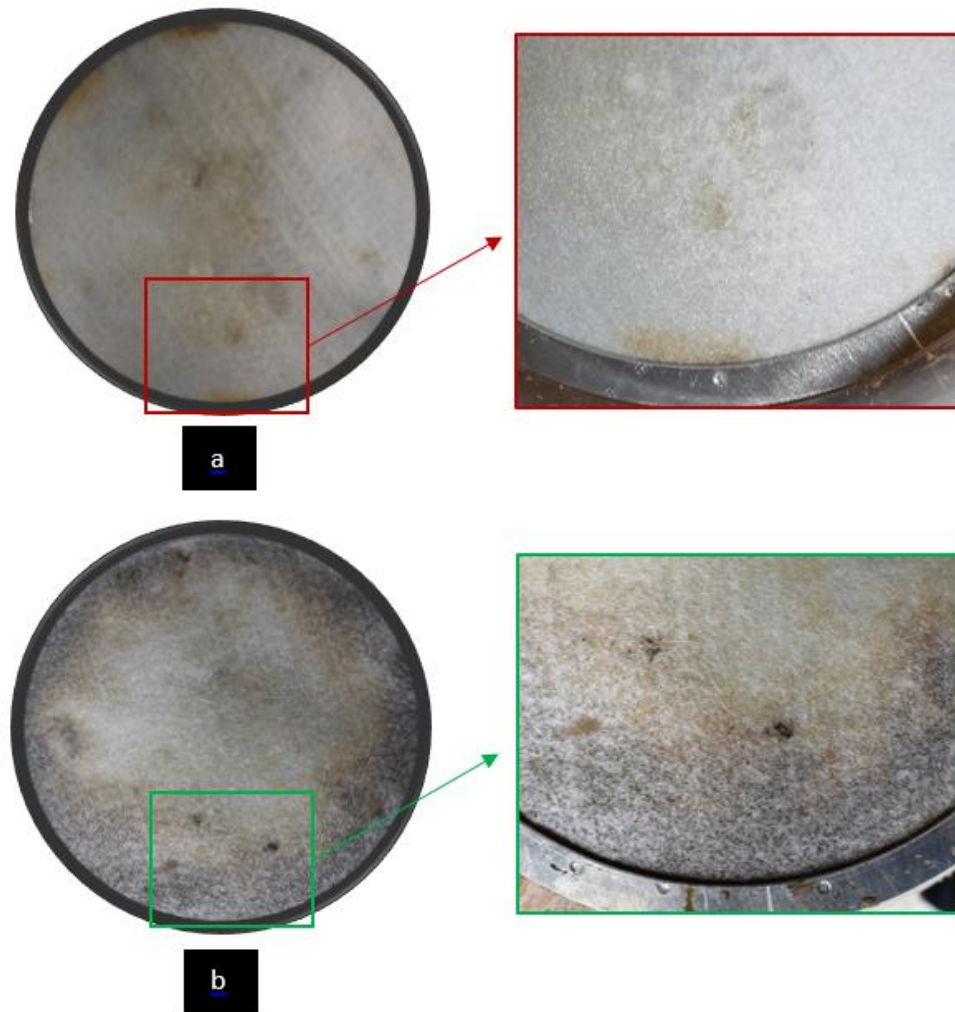
Figure 4. 7: Photos of tested G1 (magnification = 0.209x) in (a) T39, and (b) T43

4.2.2.1 Test Results and Discussions

As Figure 4. 7 shows, no clay particles travelled through geocomposite G1 in Test T39 (initial w/c =39%). However, a lot of fine particles were trapped in the geocomposite in Test T43 (initial w/c = 43%) compared to T39; this was confirmed by the amount of fine

particles transported through the pores during Test T43. The infiltrated water containing fine slurry entered into the ballast layer; this could increase the fouling index. Unfortunately, it was not possible to collect the drained water (mixed with fines) for PSD in this setup. A photo of the slurry tested in T43 (after cyclic loading) is shown in Figure 4. 8(c). The water content of subgrade soil at the geotextile interface was more than 43% in T43, which shows how ineffective the geocomposite was at reducing the water content of fluidised subgrade and preventing finer particles from intruding (clogging) into the pore openings (Table 4. 4). The average permittivity of the severely clogged geocomposites dropped by 46% during T43, and only 35% was observed in T39. This implies that geocomposite (G1) could not provide sufficient drainage and prevent the migration of fines in fluidised subgrade soil. When the moisture of the soil was less than the LL (Test T39), the geotextile could perform well even under a high frequency of loading.

Table 4. 4: Test Results of T39 and T43

Tests	T39		T43	
	Before cyclic testing	After cyclic testing	Before cyclic testing	After cyclic testing
Water content (%)	39	33	43	43.6
Reduction (%)	6		Increased by 1%	
Permittivity (s⁻¹)	7.10×10^{-4}	4.61×10^{-4}	7.12×10^{-4}	3.83×10^{-4}
Reduction (%)	35%		46%	

The continuous water flow in the permeability setup increased the permittivity of the repeated tests (T1 – T5), as shown in Table 4. 5. The fine particles trapped at the bottom of the geotextiles were transported from the clogged pores due to the continuous water flow while using the falling head method. The pressure head (< 0.5m) in the 'falling head permeability setup' was enough to dislodge the fines clogged at the bottom surface. The

flow behaviour of fine specimens during the falling head tests corresponded to Darcy's Law based on laminar flow.
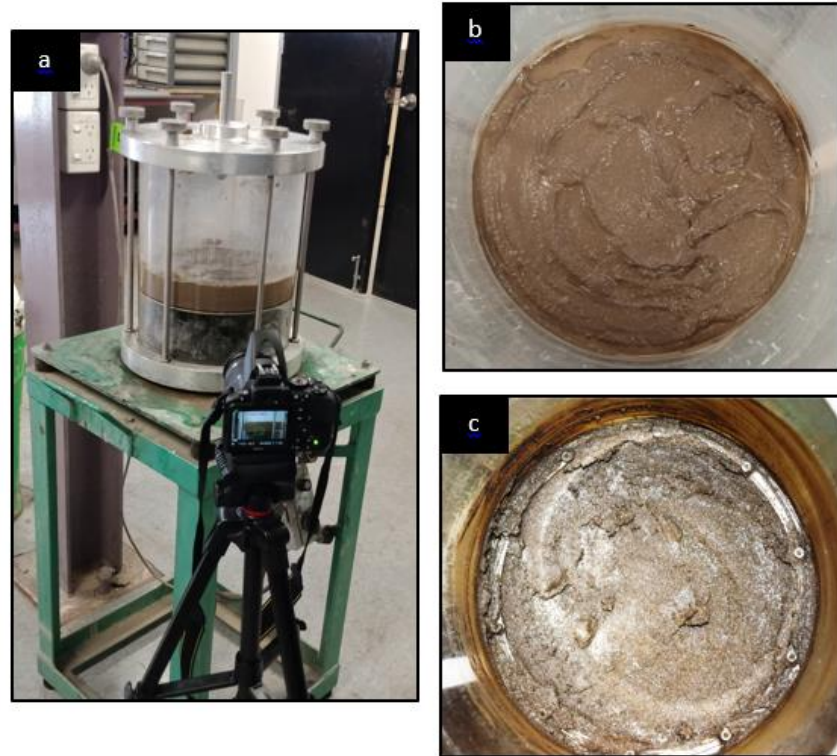
Figure 4. 8: Photos of (a) Test setup, (b) Slurry after testing in T43, and (c) Removal of slurry to determine the water content of soil at the interface (soil/geotextile – T43)

Table 4. 5: Permittivity of G1

Test Name	Permittivity (x10⁻⁴ s⁻¹)	
	Case 1 (w/c=39%)	Case 2 (T39)
T1	4.73	4.63
T2	4.78	4.74
T3	4.92	4.74
T4	5.01	4.75
T5	5.13	4.78

4.2.3 Summary: Filtration and Drainage Capacity of Geotextiles

Geotextile G2 failed to prevent the migration of particles and provide drainage for the subgrade. Ineffective filters eventually create an impermeable layer in the subgrade, leading to undrained conditions. Therefore, various drainage conditions were selected (Chapter 5 and Chapter 6) to illustrate the potential for fluidisation with and without the inclusion of geosynthetics under cyclic loading. G1 had a filter media between two non-woven geotextiles with an aperture opening of <10 µm. It is clear that the effective filter media could prevent particle migration and provide adequate drainage at the interface under cyclic loading conditions. However, the effectiveness of the geocomposite could decrease beyond a threshold cyclic stress value or under increased water content by clogging the fibre network with micro-fine particles. The drainage capacity of the geotextile/geocomposite can also be deduced by carrying out permeability tests and measuring the porosity (CT scan). Transmissivity of geotextiles is better under lower stress levels on fabrics (Koerner et al. 1984), thereby providing adequate drainage at the interface and can quickly direct the water to a nearby ditch.

4.2.4 Proposed Method to Assess the Performance of Geosynthetics in Dynamic Filtration Tests

The development of critical EPWP in railway tracks causes instability under cyclic loading conditions, and the excess pore pressure gradient (EPPG) that develops within the soil can dislocate the finer particles. To prevent particle migration, geotextiles must dissipate the EPWP that develops at the shallow part of the subgrade. The rate of change in the EPWP due to the inclusion of geotextiles must be examined under various loading conditions.

Subgrade fluidisation mainly occurs due to the internal redistribution of water contents and subsequent increment in the fines content in the upper layers of the test specimen under cyclic loading conditions. Therefore, particle size distribution (PSD) and moisture content tests can be carried out in this study to evaluate the migrated fine particles and the

occurrence of soil softening. A micro CT-Scanner can be used measure the porosity of soil specimens and the accumulation of fine particles. A modified dynamic filtration setup can be developed with miniature pore pressure transducers to measure the pore water pressure that develops at different depths. The following key factors obtained from the 'Basic dynamic tests' give a clear picture of these modifications to the Dynamic filtration tests.

- Drainage conditions – Undrained, Free drainage, Using geosynthetics
- Measurement of water content and PSD of the soil at the interface
- Influence of number of cycles – Repeated cyclic loading conditions
- Characteristics of cyclic stress –Amplitude and frequency of cyclic loading
- Drainage capacity – Dissipation of EPWP/hydraulic conductivity
- Filtration – Particle clogging and particle pumping

The dynamic filtration apparatus (DFA) was modified based on these aspects to analyse the above criteria under critical hydrodynamic conditions and is discussed in the following sections.

4.3 Dynamic Filtration Apparatus

4.3.1 Features of Modified Hydraulic Apparatus

This modified hydraulic setup can measure the variations of EPWP, and the local pore pressure gradient, porosity, and deformation. The body transducers connected onto the opposite walls can monitor the local EPPGs generated at different layers of subgrade. Ten millimetre diameter miniature pressure transducers were installed in the middle of the soil specimen to help monitor the excess pore water pressure that develops near the interface. Israr (2016) reported the effects of instrumentation by carrying out static and cyclic tests with and without the sensors (ADRs, Load cells, and Pressure transducers). The primary

objective here is to assess the test repeatability and reliability by carrying out cyclic tests with and without geosynthetics (free drainage).

4.3.2 Experimental Program

A test procedure similar to that in Chapter 3 was used to apply a cyclic loading with and without the inclusion of geotextiles. The EPWPs (measured by the miniature pressure transducers), the EPPGs (measured by the body pressure transducers), the normal effective stress (measured by the load cell at the bottom), the changes in porosity (measured by the ADR Probes), and the axial strain (measured by the LVDT) were monitored and recorded. This proposed methodology simulates the more realistic hydro-mechanical conditions in railway tracks. In this case, the deviatoric cyclic stress and frequency were 40 kPa and 5 Hz, respectively.

4.3.3 Cyclic Tests without Capping/Free Drainage Tests

Free drainage tests were carried out to create/simulate the occurrence of fluidisation under train loading conditions. A layer of ballast was placed directly onto the subgrade soil to investigate the creation of an interlayer that could sink into the subgrade during continual cyclic loading (Duong et al. 2014). The key factors that promote subgrade fluidisation could be assessed by carrying out free drainage tests. The changes in the water content and the particle size distribution of the soil specimens were used to investigate the soil fluidisation phenomenon.

Figure 4.9 shows the test results from Tests G1 and cyclic tests under free drainage conditions. Gecomposite G1 was used to compare the effectiveness of capping at the subgrade interface. As shown in Figure 4. 9 the EPWPs reached a maximum of 20 kPa after 500 cycles and then decreased to 10-15 kPa at the end of 75,000 cycles. The interface of ballast/subgrade soil is shown in Figure 4. 10 after 500 cycles. The axial strain exceeded 5% after 500 cycles, and there was no continual dissipation of EPWP after 15,000 cycles.

This soil has the potential for subgrade fluidisation because the top part of the subgrade (interface) became slurry, together with a rapid increase in axial strain (above 8%). The moisture content of the specimen was more than 39% at the end of cyclic loading. This means that subgrade soil subjected to repetitive cyclic loading generates a higher EPWP without continual dissipation, results in particle separation and increases the potential for subgrade fluidisation under adverse hydraulic conditions in railway tracks.
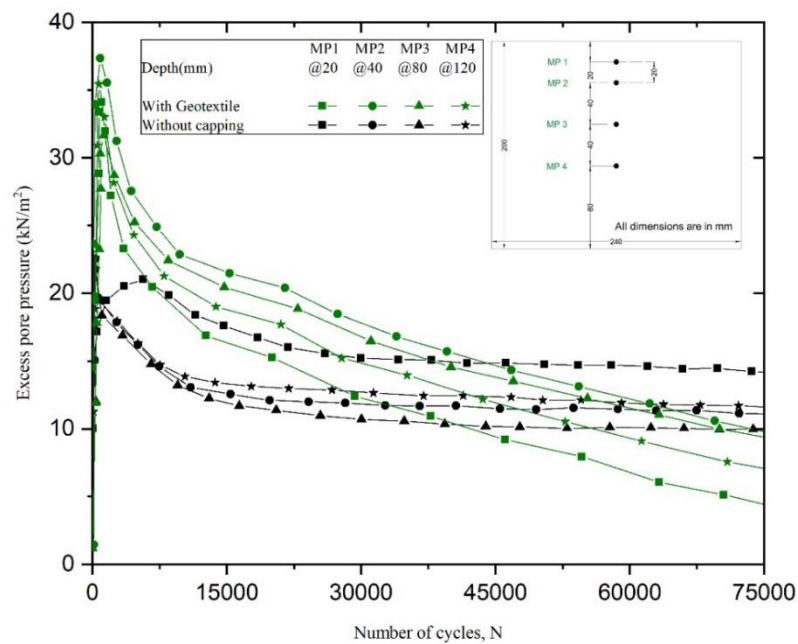
Figure 4. 9: Excess pore water pressure (a) With geotextile and (b) Free drainage test

4.3.4 Cyclic Tests with Geocomposite G1

The potential use of geotextiles at preventing subgrade fluidisation was assessed. These tests were repeated three times under the same loading conditions to commission the dynamic filtration apparatus (Test repeatability).

The EPWPs developed at MP1, MP3, MP3, and MP4 are shown in Figure 4. 9. The EPWPs inside the soil specimen increased rapidly at the beginning (0-3000 cycles) of cyclic loading, but then they decreased as the number of cycles increased. MP1 measures the lowest values due to the influence of the geotextile which continuously dissipated the pore water pressure that developed at the interface. The generation of EPWPs in the middle of

the soil specimen (MP3 and MP4) are higher than those at the interface. The development of axial strain is also controlled because the G1 prevents the formation of an 'interlayer creation' by additional confinement at the interface. The selected geotextile with an effective filter membrane helps to reduce the water content of the soil, unlike the test without a capping layer. Photos of the tested specimens with and without geocomposites after 500 cycles are shown in Figure 4. 11.
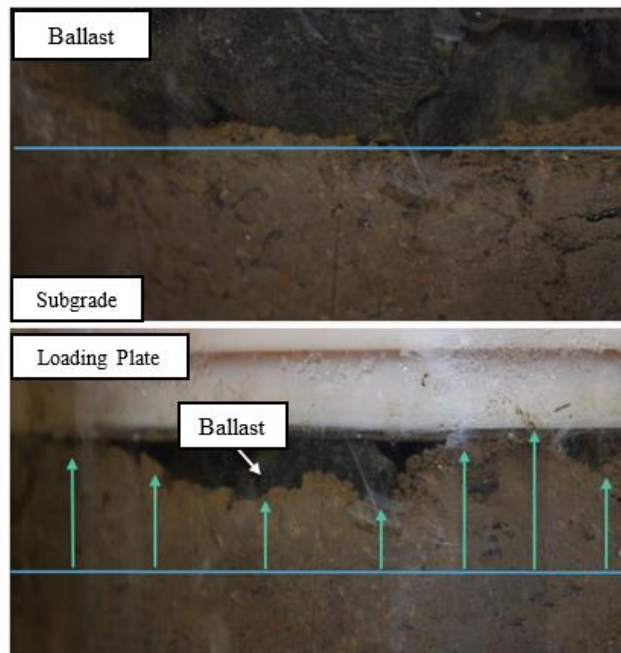
Figure 4. 10: Ballast/Subgrade Interface (a) Before Testing (b) After 500 cycles
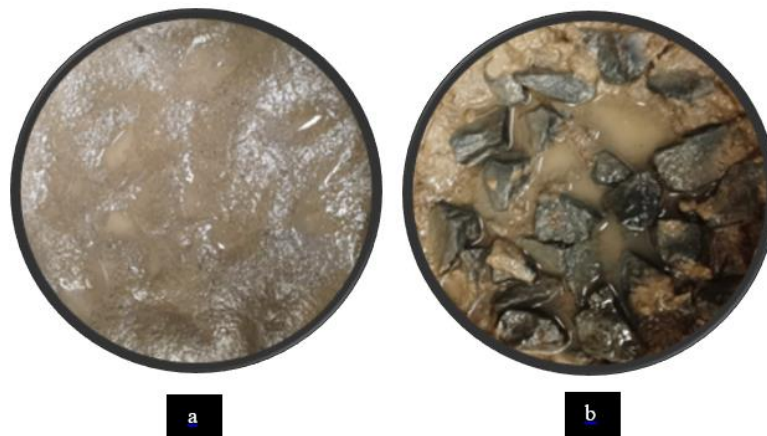
Figure 4. 11: Photo of subgrade surface (magnification = 0.2x) (a) with geotextile (after 100,000 cycles) (b) without geotextile (free drainage – Only after 500 cycles)

4.3.5 Effects of Test Repeatability

As Figure 4. 12 and 4.13 show, cyclic tests were carried out under the same loading conditions to assess test repeatability under similar hydrodynamic conditions. After removing the cyclic loading, the geotextile allowed the EPWPs to be dissipated and similar trend was observed.
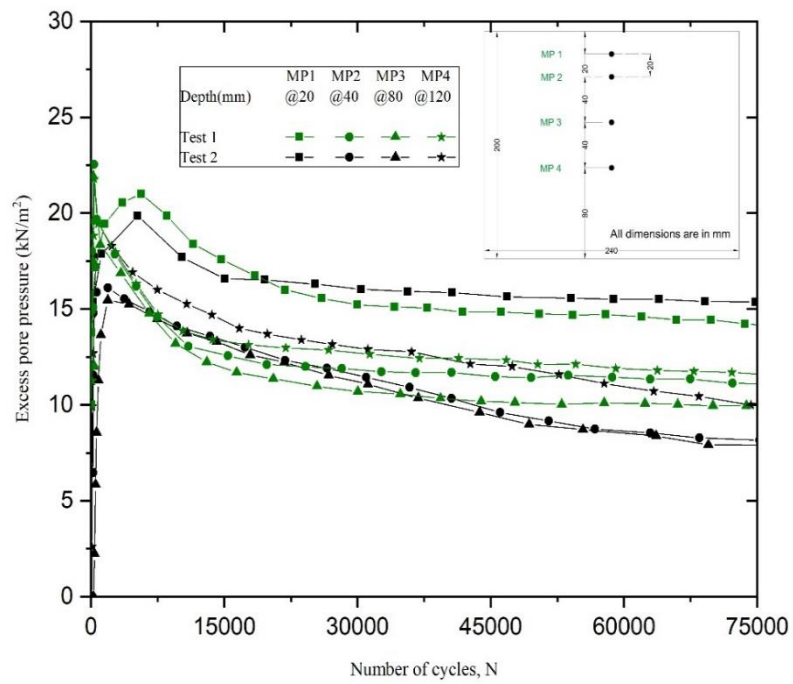
Figure 4. 12: Cyclic tests under free drainage conditions (No geosynthetics/Capping)
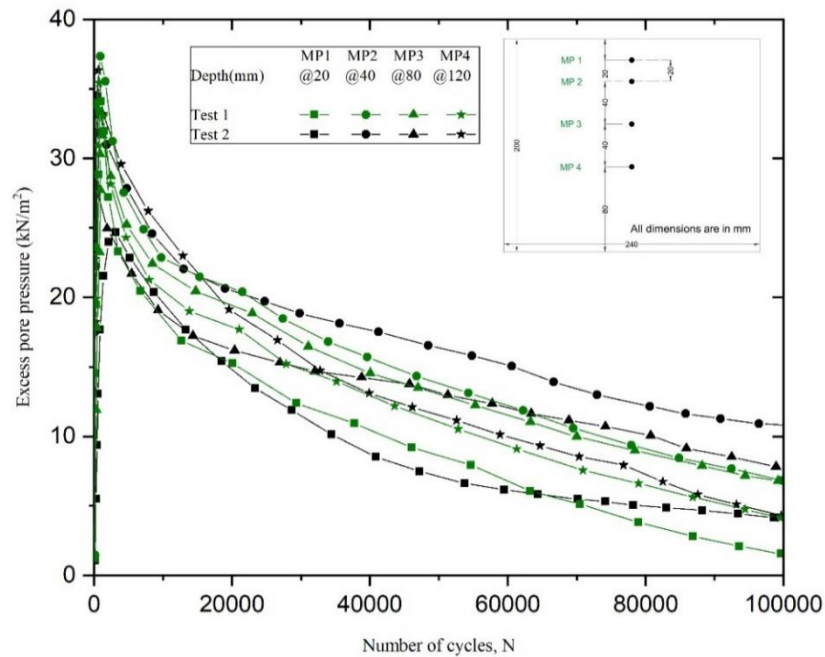
Figure 4. 13: Cyclic tests with geocomposite G1

To observe the change in water content, two cyclic tests under free drainage conditions were also stopped after 500 and 1000 cycles, respectively. The water content of the soil near the interface was approximately 37-39% after 500 – 1000 cycles, thus showing the potential for fluidisation (LL = 42%). The cyclic tests were also repeated twice (up to 100,000 cycles) to measure the rate of change in the EPWP that developed under cyclic loading conditions (with and without geotextiles). Similar trends were also observed during the repeated cyclic loading (Figure 4. 12 and 4.13).

4.4 Chapter Summary

The 'basic dynamic tests' (BDT) were carried out to evaluate the effectiveness of geotextiles under dynamic loading conditions. Based on observations from the 'basic dynamic tests' (BDT) and the progression of instability, a dynamic filtration apparatus (DFA) was designed and built-up at the University of Technology Sydney. The effectiveness of dynamic filtration tests and test repeatability were discussed in this Chapter. The 'dynamic

113

filtration test' (DFT) results showed that the migration of fine particles and associated mud pumping could be mitigated with geocomposites. It was observed that cyclic tests without a capping (free drainage) had an increased potential for subgrade failure due to the rapid increase in axial strain and EPWPs under cyclic load. The application of geotextile could continuously/quickly dissipate the developed EPWP and sustain the stability of interface soil. However, this needs to be further investigated under different loading conditions in order to evaluate the effectiveness of geosynthetics. The occurrence of instability in subgrade soil due to the developed EPWPs can be studied, and the use of geosynthetics at preventing potential failure also can be examined by dynamic filtration tests. Notably, primary factors such as the generation of EPWP, variations in effective stress and water content, and temporal variations in EPPG must be investigated when designing the filters (geosynthetics/capping) under critical loading conditions.

CHAPTER 5: SUBGRADE BEHAVIOUR INFLUENCED BY DRAINAGE CONDITIONS AT THE BALLAST SUBGRADE INTERFACE

5.1 Introduction

In recent times, the undrained behaviour of base soil subjected to cyclic load has been investigated by many researchers to assess fluidisation potential and to evaluate soil response to various cyclic stresses by carrying out cyclic triaxial, hollow cylinder, and cyclic direct shear tests (Abeywickrama et al. 2019; Guo et al. 2018; Indraratna et al. 2020a; Indraratna et al. 2020b; Indraratna et al. 2020c; Nguyen & Indraratna 2021; Singh et al. 2021; Singh et al. 2020a; Truong et al. 2021; Yang et al. 2019; Zhang et al. 2021). The key factors contributing to subgrade fluidisation, such as cyclic stress, fine content, and other characteristics of soil have also been investigated under undrained conditions. In fact, the undrained condition imposed by an impermeable boundary in typical railway tracks is due to overly compacted sand or impermeable capping material with pumped-up fine particles. The impermeable capping underneath ballast cannot provide enough drainage to continuously dissipate the excess pore water pressure (EPWP) that develops under repeated cyclic loading, which means that cyclic tests under undrained conditions can also be used to investigate mud pumping (i.e., it represents adverse hydraulic conditions in railway tracks).

Duong et al. (2014) reported that the 'interlayer creation' and associated subgrade fluidisation could happen when there is no capping layer between ballast and subgrade (free drainage conditions at the interface). Furthermore, ballast particles could penetrate into the

subgrade and the increased cyclic stress at the interface could cause instability. Pumped-up fine particles can cause fouled ballast and also lead to localised failure in subgrade. This indicates that free drainage tests (i.e., without capping) can capture the cyclic response of soil at the interface due to the development of excessive hydraulic gradient. This chapter contains a series of laboratory tests performed while simulating the undrained (impermeable capping) and free drainage (no capping) conditions needed to assess the potential for subgrade fluidisation.

5.2 Experimental Results and Discussion

5.2.1 Undrained Cyclic Tests (Test T1)

Unlike conventional cyclic triaxial apparatus, modified dynamic filtration tests can measure the EPWPs that develop at different depths inside the soil specimen and the excess pore pressure gradients (EPPGs) generated at different layers within the subgrade soil.
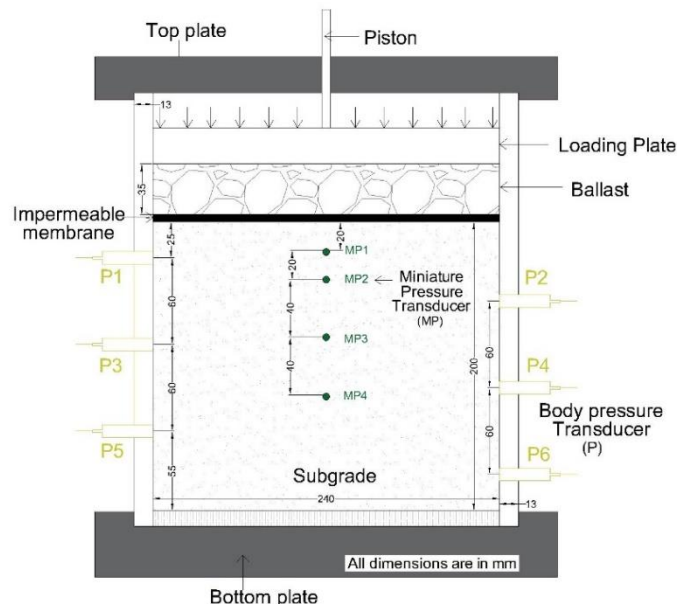
Figure 5. 1: Dynamic filtration test setup for undrained cyclic test

As Figure 5. 1 shows, the miniature pressure transducers are installed in the middle of the subgrade soil and they can capture the rapid generation of EPWP under cyclic load. The EPWP measured by body transducers installed on the opposite faces of the polycarbonate cell can also be used to calculate the EPPGs that develop between two different soil layers. EPPG can be defined as the ratio between changes in the excess pore water pressure head (dU_e) and the corresponding distance between two specified locations (dL).

$$\boldsymbol{EPPG} = \frac{dU_e}{dL} \qquad \text{Equation 5.1}$$

5.2.1.1 Excess Pore Water Pressure (EPWP) and Axial Strain (ε_a)

The EPWPs that developed inside the specimen are measured under undrained conditions because they are the main cause of instability in subgrade under continuous cyclic loading. Figure 5. 2 shows the rapid development of EPWP up to 500 cycles, where all the miniature pressure readings remain above 22 kPa (EPP$_{T1}$) until the end of the test. The transducer MP3 (at 80 mm) measured the maximum EPWP of 27 kPa at 50,000 cycles. The maximum EPWP at MP1 (20 mm from the interface) was less than 24 kPa until 50,000 cycles, which was approximately 15% less than the EPWP developed at MP3. The EPWP at MP3 dissipated approximately 12% of the maximum EPWP (31 kPa) developed at 500 cycles at the end of cyclic testing (27 kPa), while the EPWPs that developed at 40 mm (MP2) and 80 mm deep (MP4) were higher than those that developed near the soil interface. These results confirm that the middle and lower layers can develop higher EPWPs and have more potential for subgrade failure under critical hydrodynamic conditions.

The continual increase in axial strain was observed even after 50,000 cycles under undrained conditions. Unlike the free drainage tests (T2), there was a maximum of 2.2 – 2.8% of axial strain for the undrained cyclic tests (T1) until the test ended (N= 100,000 cycles). The movement of fluidised soil towards the interface could also be seen through

the transparent polycarbonate cell. The water content of subgrade soil near the interface soil approached the LL (42%). This change in the moisture content and particle size distributions at the interface and soil in the middle region are described in Chapter 5, Section 5.2.1.3. Undrained tests were also repeated to assess the repeatability of the cyclic tests. These cyclic tests were stopped at 500, 50,000 and 100,000 cycles to investigate the soil behaviour and to determine the failure criteria.
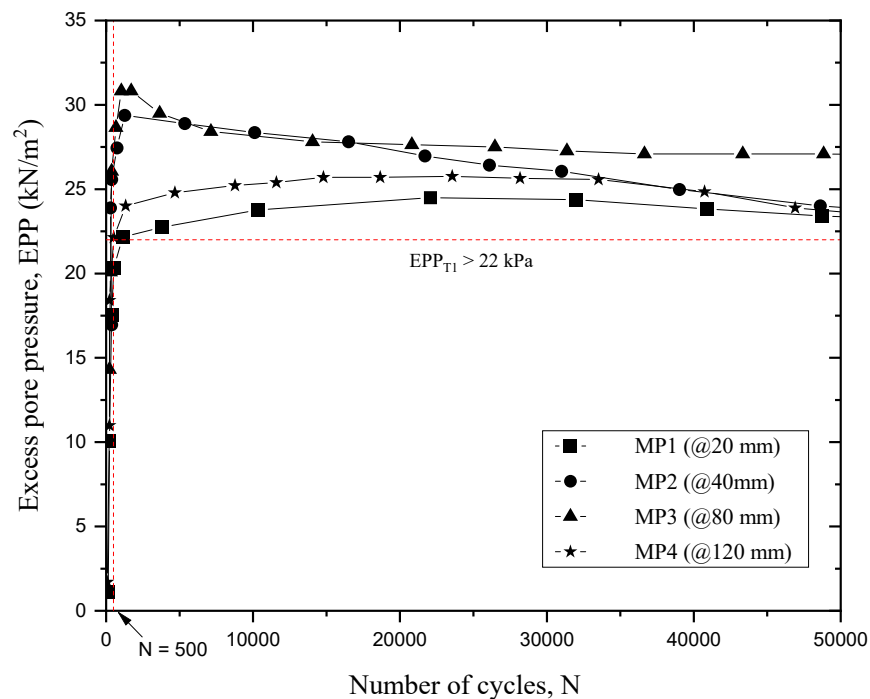
Figure 5. 2: Generation of EPWP and Axial strain (modified after Arivalagan et al. (2021)

Note: EPP $_{T1}$ – Excess pore pressure for Test T1 after 500 cycles (N>500)

Undoubtedly, the EPWP that develops inside the soil specimen without a significant reduction over time might cause subgrade instability. Furthermore, significant EPPG (Section 5.2.1.2) develops at various locations (inside the subgrade) can also induce instability by dislocating the fines from the original soil matrix. Similar observations were also reported in the past whereby the rapid generation of EPWP and development of local

hydraulic gradient under cyclic loading could lead to potential failures, including subgrade fluidisation (Singh et al. 2020b; Yu et al. 2016).

5.2.1.2 Excess Pore Pressure Gradient (EPPG)

The EPPG that developed with the increased number of cycles can be calculated using Equation 5.1. This time dependent EPPG that developed at different depths (Figure 5. 3) could induce enough hydraulic force to dislocate the fine particles from the coarser fraction of the soil matrix. The EPWPs measured at different locations by body transducers, as shown in Figure 5. 3, are used to calculate the EPPG. As Figure 5. 4 shows, the EPPGs developed in the top and middle layers (Layer (2-1), Layer (3-2) and Layer (4-3)) were above 35 within 15,000 cycles, but they decreased further as the number of cycles increased. Layer (5-4) had a maximum EPPG of 27, which was much lower than those developed at the top and middle layers. However, the EPPG that developed in the deep soil layer (Layer (6-5)) was always less than 15. This implies that the shallow part of subgrade soil subjected to cyclic loading is more prone to subgrade fluidisation.
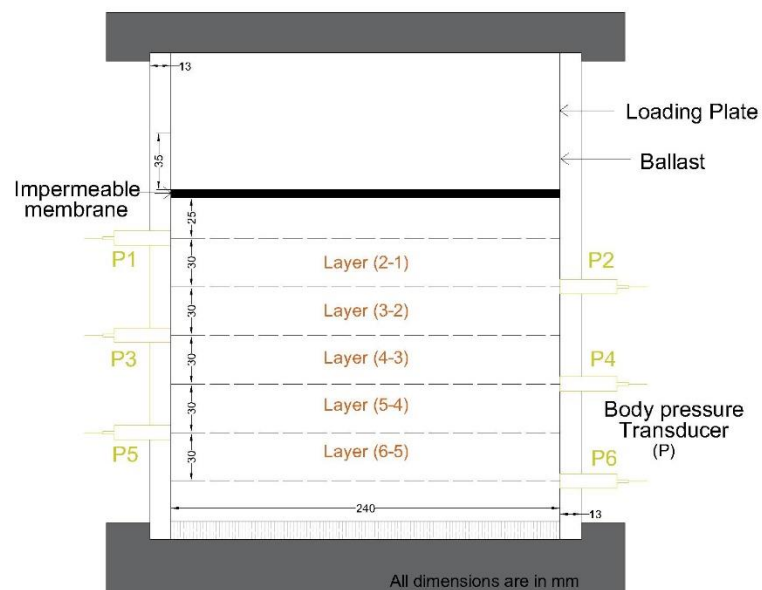
Figure 5. 3: Six layers of base soil profile (DFA)
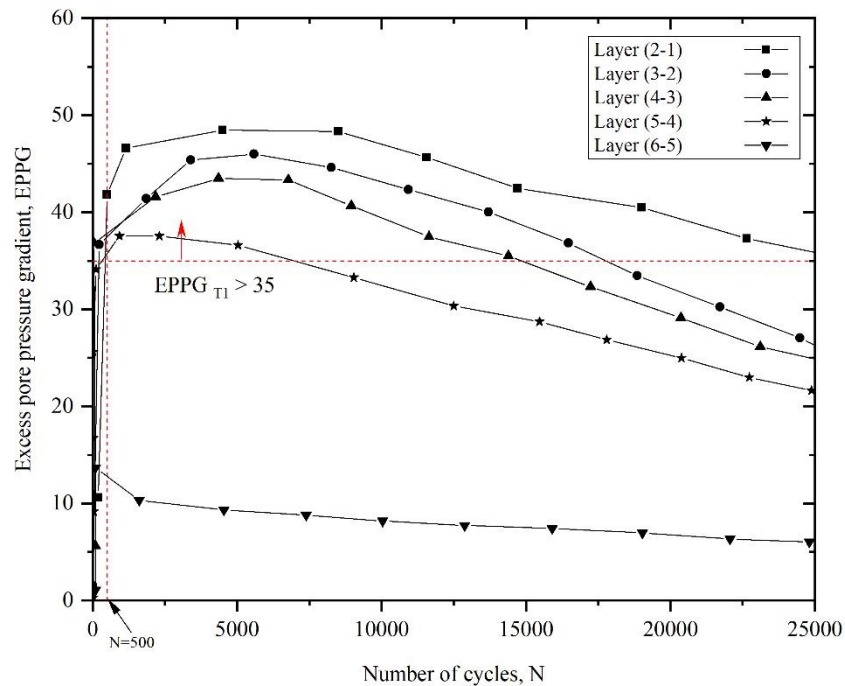
Figure 5. 4: Excess Pore Pressure Gradients for Test T1

Note: EPPG $_{T1}$ – Excess pore pressure gradients for undrained Tests (500 <N <15,000)

5.2.1.3 Variation in Particle Size Distribution (PSD) and Water Content

Three cyclic tests were carried out under undrained conditions and stopped at 500, 50,000, and 100,000 cycles; this roughly represents the duration of a continuous train passage of 1.7 min, 2.8 hr, and 5.6 hr, respectively. Fluidised particles were observed beneath the impermeable layer after less than two minutes of train loading (i.e., at 500 cycles). The PSD of the soil collected at three different locations at 0, 100, and 200 mm deep, were determined using the Malvern particle analyser. The PSDs of the soil at the top and middle are shown in Figure 5. 6 (a) and (b). Note here that a lot of fine particles of less than 75 microns, had accumulated on the top surface during repeated cyclic loading. Meanwhile, there is a significant loss of fines in the middle layers, as shown in Figure 5. 6. There was a rapid internal migration of very fine particles carrying moisture due to the high specific surfaces of the fines. This situation can be exacerbated by an increase in excess pore

120

pressure gradients under critical loading that can form slurry at the top surface under cyclic loading.
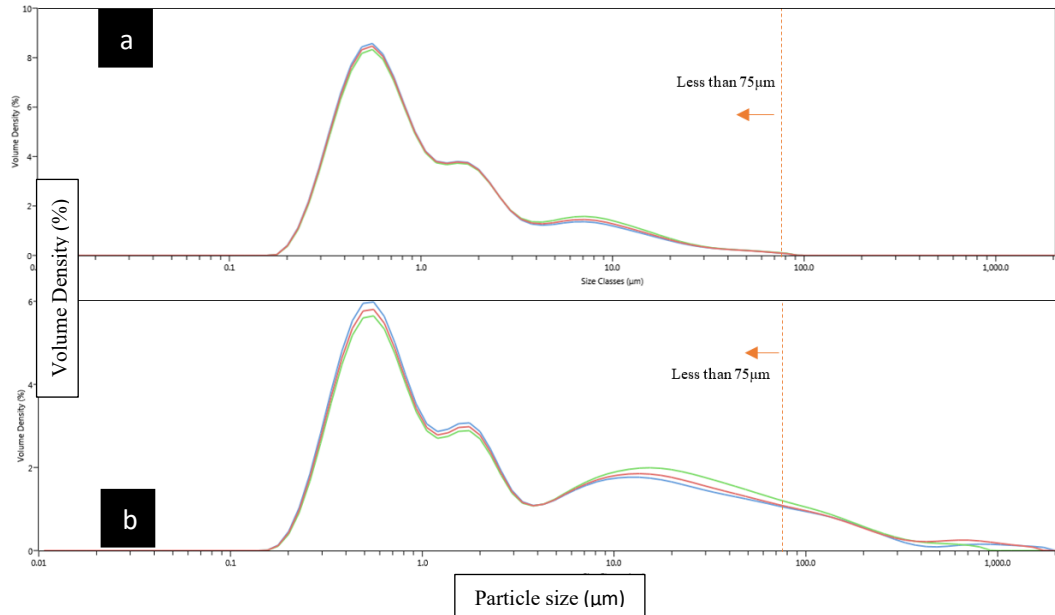
Figure 5. 5: Volume density of (a) collected slurry, and (b) Middle soil (at 100 mm from the interface) using Malvern particle analyser
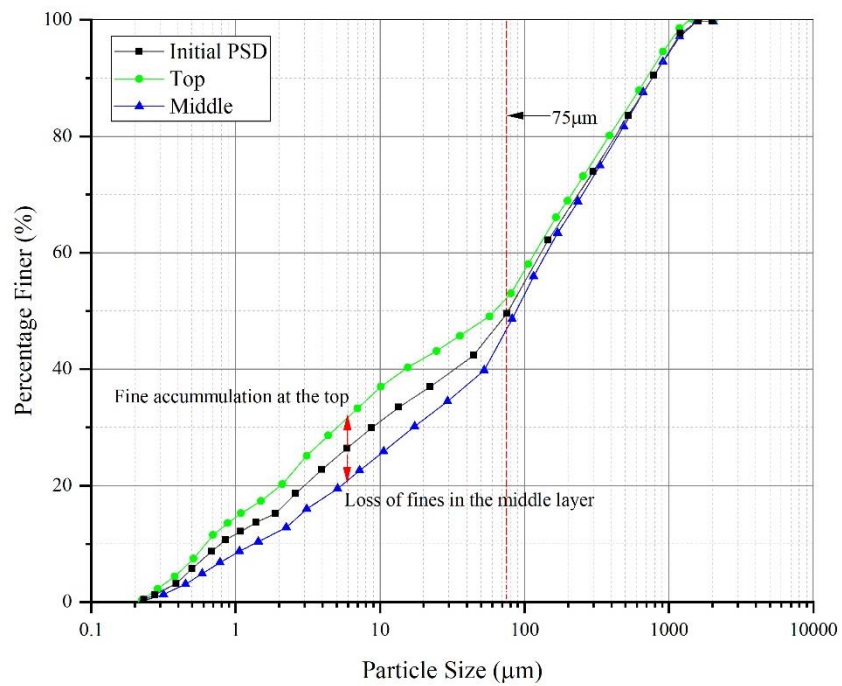
Figure 5. 6: Particle size distributions under undrained cyclic tests (modified after Arivalagan et al. (2021))

5.2.1.3.1 Fluidised Particles

The Liquidity Index (LI) indicates the consistency of soil in comparison to its liquid and plastic limits. As Figure 5. 7 shows, the water content of topsoil approached the LL. The LI of the tested specimen varied linearly from 1 at the top to 0.2 at the bottom in Test T1. The 30 mm of subgrade soil near the interface became slurry after just 500 cycles, and fines migrated upwards as the moisture increased in the middle layer. Subgrade soil can become a fluid, if its water content approaches the liquid limit. The undrained tests experienced an abrupt change in the moisture content, and a finer fraction of less than 75 μm was pumped up. These results imply that the migration of fine particles with a substantially increased water content can induce mud pumping under cyclic loading.
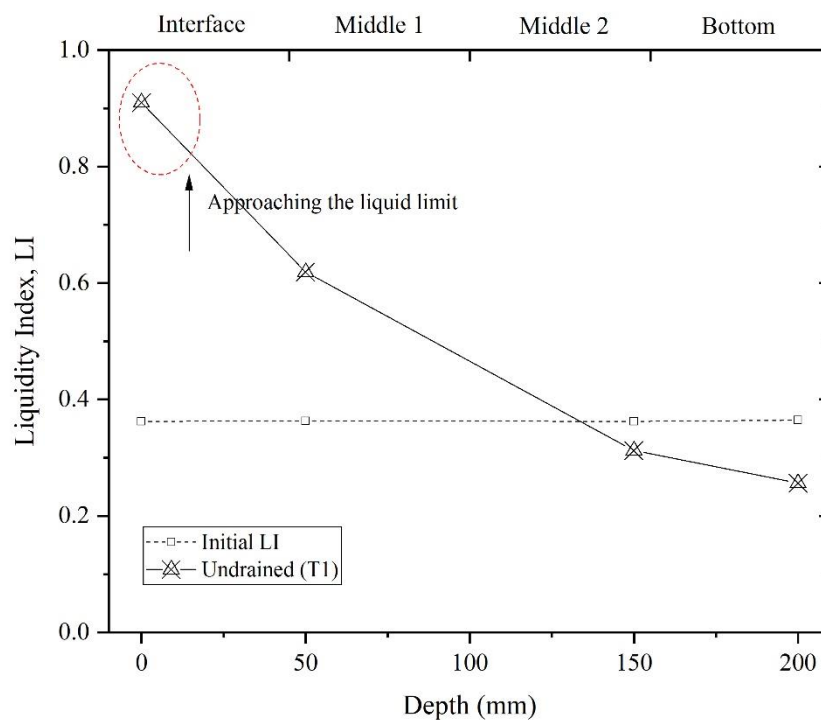
Figure 5. 7: Liquidity Index of the soil – Test T1 (after Arivalagan et al. (2021))

5.2.2 Fee Drainage Conditions (Test T2)

Cyclic tests under free drainage were carried out using the dynamic filtration apparatus (DFA). The ballast layer (35 mm thick) was placed directly onto the compacted subgrade soil (Figure 5. 8). Free drainage tests represent a railway track constructed without a capping layer. Subgrade without a capping layer may experience higher cyclic stress at the interface and have more potential for localised failures during the passage of heavy haul trains. Therefore, the primary objective of cyclic tests under free drainage conditions (Test T2) was to capture the 'interlayer creation' (i.e., the sinking of ballast particles inside the subgrade soil and fine migration into ballast) and measure the drainage capacity at the interface and middle regions of the subgrade. The test procedures for dynamic filtration tests are reported in Chapter 3.
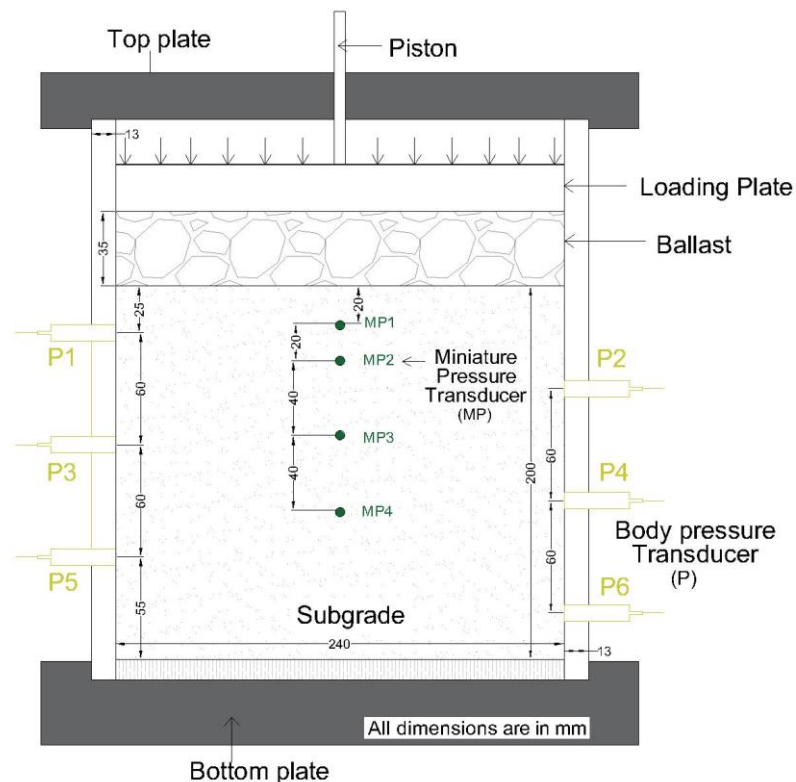
Figure 5. 8: Free drainage test – Dynamic filtration test setup
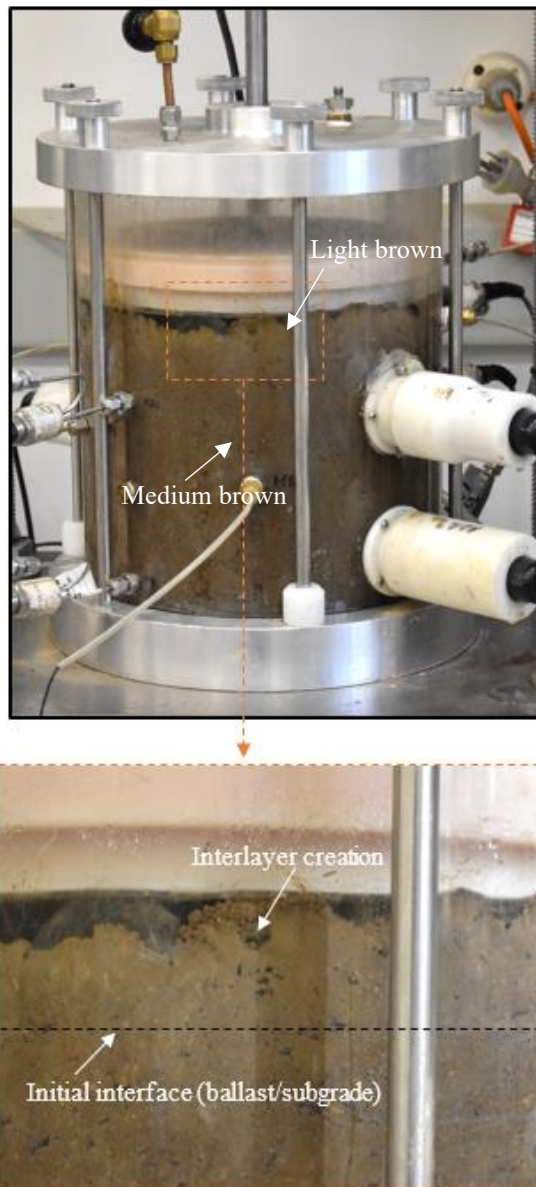
Figure 5. 9: 'Interlayer creation' due to penetration of ballast into subgrade in 'Free drainage test' (T2) at 500 cycles

5.2.2.1 Mid-test Observations – Interlayer Creation

Cyclic tests were also carried out at 500, 50,000 and 100,000 cycles to study the 'interlayer creation' (Figure 5. 9), changes in the moisture content, and the behaviour of subgrade soil near the interface. During Test T2, the 35 mm thick ballast completely immersed/sank into the subgrade soil after 100,000 cycles, as shown in Figure 5. 10(c). The interlayer mixed

with the ballast particles and there was a rapid increase in cyclic deformation due to the penetration of ballast particles into the subgrade soil (known as 'interlayer creation'); the top layer of subgrade soil also became a fluid (softening/fluidisation) under cyclic loading conditions, as shown in Figure 5. 10(b).
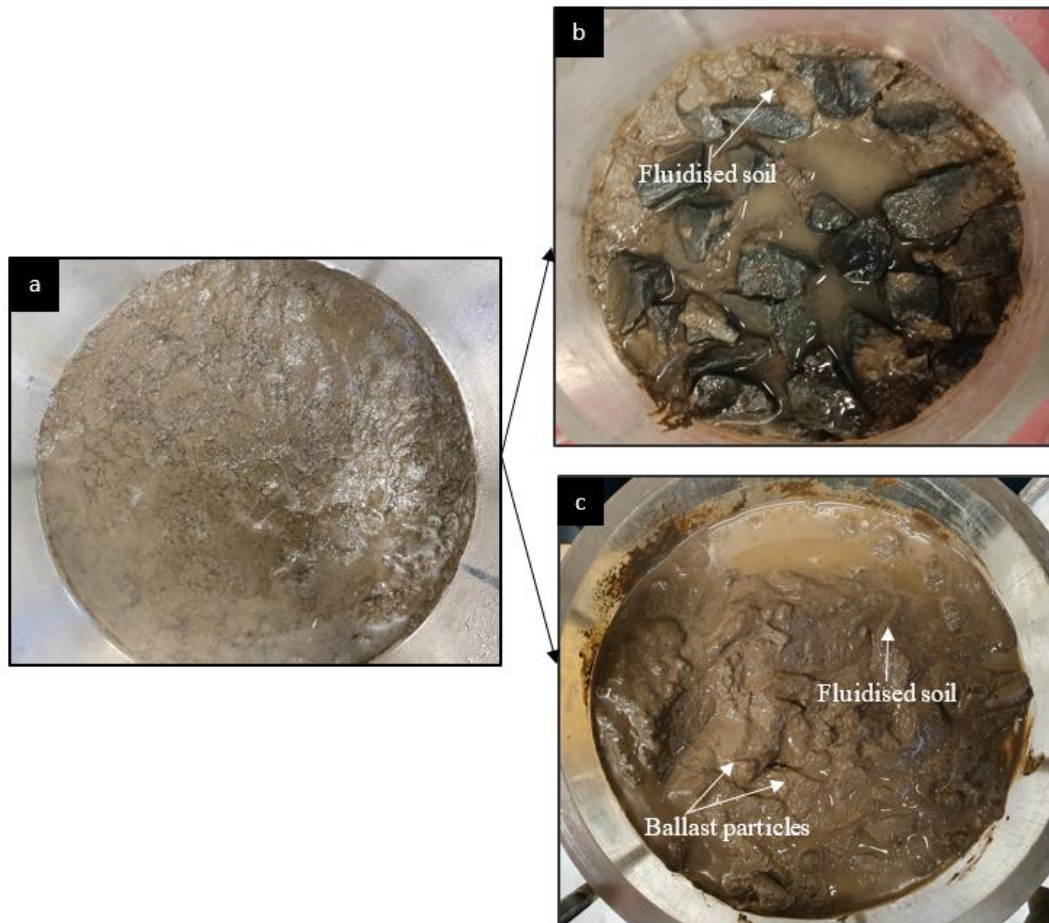
Figure 5. 10: Photos of (a) saturated specimen, fluidised specimen after (b) 500 cycles, and (c) 100,000 cycles under free drainage conditions (Test T2)

5.2.2.2 EPWPs and Axial Strains (ε)

The development of critical EPWP and axial strain was measured under free drainage conditions. As Figure 5. 11 shows, the EPWPs at depths of 40, 80, and 120 mm deep are more than 18 kPa at 500 cycles; this follows a decreasing trend as the number of cycles

increased. The readings from all the miniature pressure transducers were more than 8 kPa at 50,000 cycles. The EPWP measurements recorded near the interface (MP2 and MP3) are higher than those at a deeper depth (MP4). Since there was no capping layer at the ballast/subgrade, the EPWP developed at MP1 was lower than at MP2 (free drainage at the interface). The EPWP at MP2 (at 20 mm deep) was 3.5 kPa higher than that measured by MP1 at 50,000 cycles.
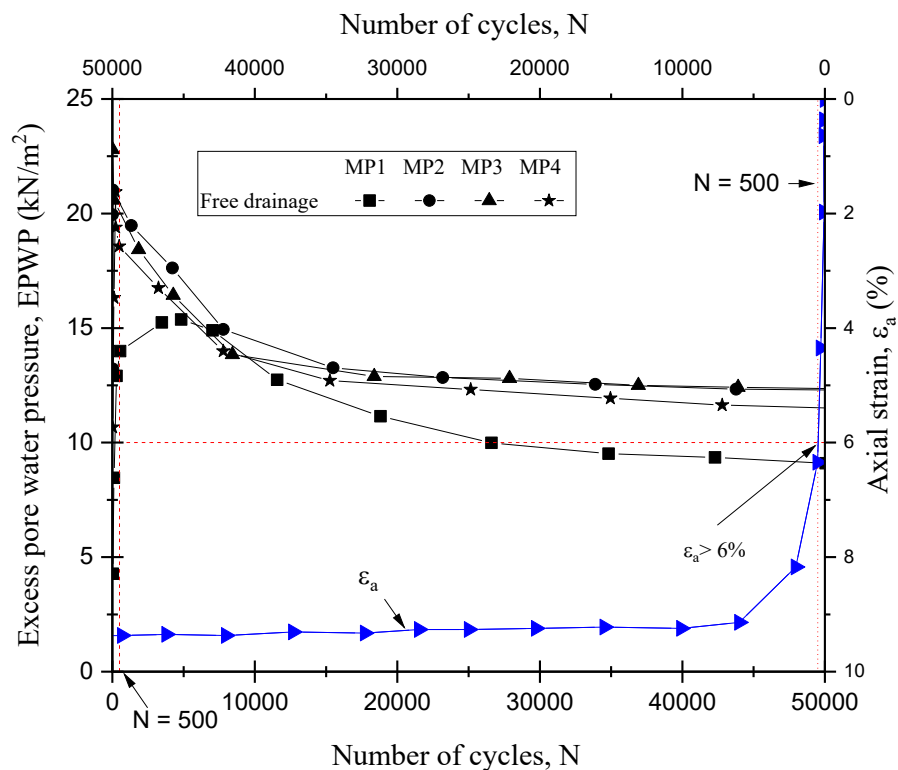
Figure 5. 11: Free drainage Tests (a) EPWP, and (b) Axial strain

As Figure 5. 11 shows, the development of axial strain is significant because there was no additional confinement at the interface (e.g., no capping or geosynthetics). There was a rapid increase in axial strain after less than 5000 cycles (Figure 5. 11). For instance, it increased up to 6% within 500 cycles, and was over 9% by the end of the test. This rapid increase was caused by the subgrade softening at the interface. Since confinement near the interface was minimum, finer particles can migrate towards the interface and ballast particles can penetrate the subgrade layer causing ballast fouling, as shown in Figure 5.

10(c). These tests were stopped after 500 cycles to observe the subgrade softening and measure the PSD and water content of the soil collected near the interface.

5.2.2.3 Excess Pore Pressure Gradients (EPPGs)

Six pressure transducers were installed (to measure the EPPG) at the opposite faces in an alternating pattern of polycarbonate cylinders and this can prevent any development of potentially weak hydraulic conditions under cyclic loads.

As Figure 5. 12 shows, the EPPGs that developed at critical layers (Layer 3-2 and Layer 2-1) are above 30 at 500 cycles and thus show the potential for inducing enough hydraulic force to dislocate the fines from the soil matrix. At the end of cyclic loading, the EPPG that developed at greater depths (Layer (5-4)) was 80% lower than the critical layers (Layer (3-2) and Layer (2-1)). This implies that the temporal variations in EPPG were significant at the shallow part of the subgrade soil and have an increased potential for pumping finer particles from the middle layers. This can be proven by carrying out particle size distribution tests at the top and middle of the soil specimen.

5.2.2.4 Change in Particle Size Distribution (PSD) and Moisture Content

A Malvern particle size analyser (Mastersizer) was used to measure the particle size distribution at the top and middle regions at the end. The PSDs of soil collected at the interface (Top) and the loss of fines in the middle region are shown in Figure 5. 13. As Figure 5. 13 shows, a lot more fines (< 75µm) accumulated near the interface (≈ 52%) than at the middle region (≈ 49%), which previously had approximately 50% of fines. This proves that finer particles are transported during cyclic loads, and a high-water content can facilitate the formation of a slurry at the interface. In both undrained and free drainage conditions, a finer fraction of less than 75 µm was pumped up from underneath soil and became slurry at the top during cyclic load.
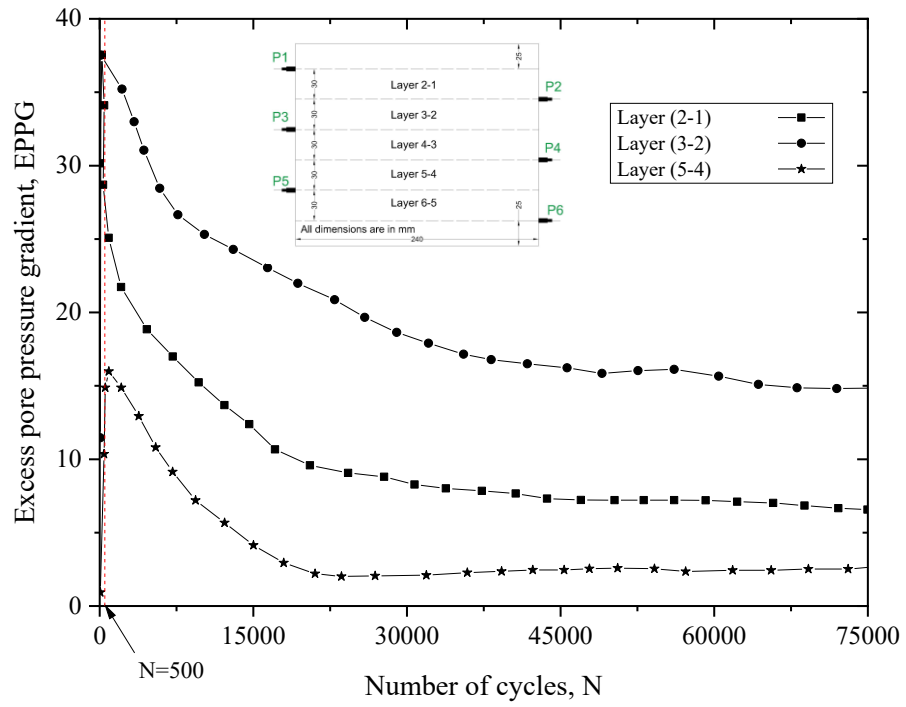
Figure 5. 12: Development of EPPG - Free drainage Test (T2)
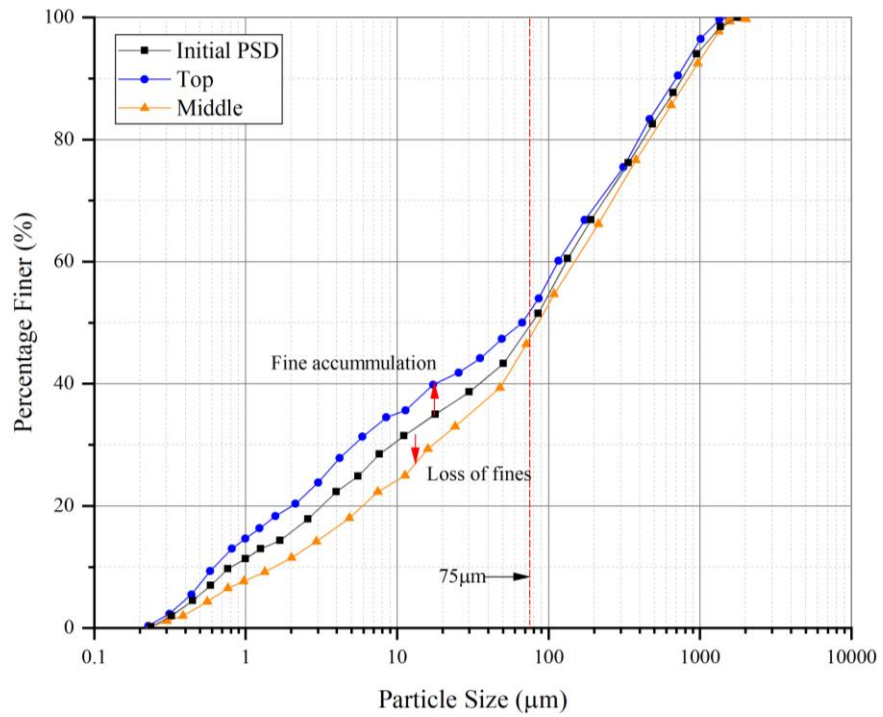
Figure 5. 13: Particle size distribution (Free drainage tests)

5.2.2.4.1 Variation in Water content

This change in the moisture content reveals the softening of the interface soil. As Figure 5. 14 shows, the soil close to the surface has a Liquidity Index (LI) approaching one. The soil becomes a liquid or slurry when the water content is equal to the Liquid Limit. The top and middle regions of the subgrade have an LI of around 0.94 and 0.56, respectively. The soil collected at the middle had a 3% increase in the water content, whereas the deeper subgrade soil remained the same until the test ended (at 100,000 cycles). In terms of water content, the maximum water content for T1 and T2 after 50,000 cycles was approximately 39 - 40% (at the interface). The water content near the interface and middle layers was higher than the initial water content in both undrained (T1) and free drainage (T2) conditions. This indicates that the selected subgrade soil has the potential for subgrade fluidisation because the water content approached the LL under critical hydraulic conditions.
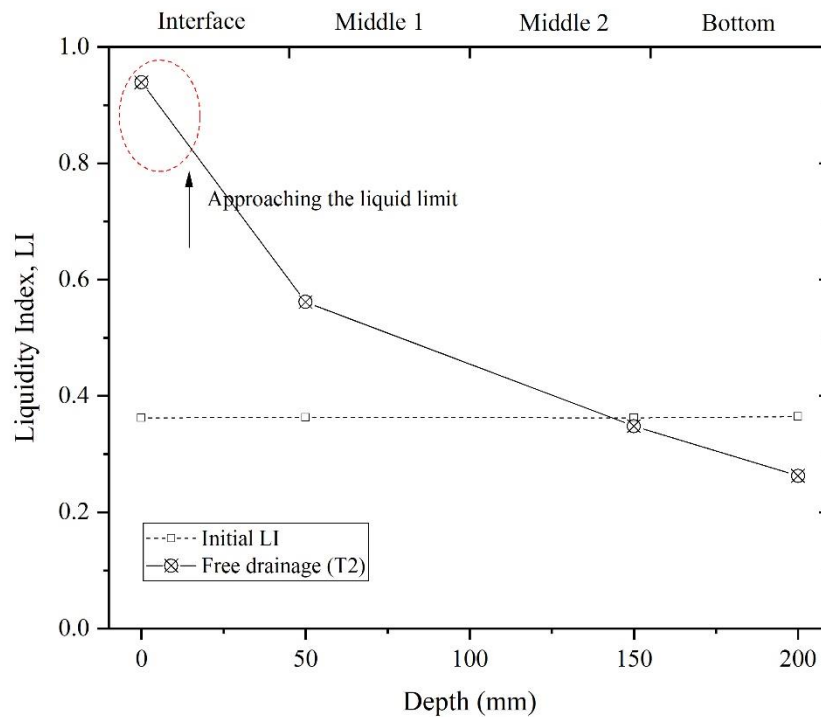
Figure 5. 14: Liquidity Index of the soil (modified after Arivalagan et al. (2021))

5.3 Chapter Summary

The free drainage and undrained cyclic tests could be used to explain the potential for subgrade fluidisation under cyclic loading conditions. The generation of EPWPs, EPPGs that developed at different locations, variations in the particle size distributions (PSD), and the rapid increase in axial strain and changes in the water content were used to assess the potential for subgrade fluidisation.

The undrained tests showed the rapid generation of EPWPs at the shallow part of the subgrade soil. The rapid increase in EPPG (i.e., the hydraulic force) within the layers of soil, could dislocate the fines towards the top layers. The particle size distribution curves indicated the migration of fines during cyclic loading from the middle layers towards the interface. The water content of the soil collected at the interface showed a significant increase because the fine particles and water migrated due to hydraulic uplift, up to the shallow part of the subgrade (subgrade fluidisation).

The free drainage tests indicated the potential failures due to a rapid increase in axial deformation and pumping of fines was observed as the number of cycles. An 'interlayer creation' was observed at the start of cyclic testing, and ballast particles had sunk completely into the subgrade soil. In summary, the test results under free drainage and undrained conditions can be used to analyse the behaviour of soft soil. These results indicated that subgrade soil subjected to continuous train loading can generate a higher EPWP without continual dissipation, and this can result in particle separation. A similar approach was carried out to measure the potential use of geosynthetics at preventing the risk of mud pumping, and the role of geosynthetics at reducing the potential for subgrade fluidisation, as reported in Chapter 6.

CHAPTER 6: THE ROLE OF GEOTEXTILES IN PREVENTING PARTICLE MIGRATION AND SUBGRADE FLUIDISATION

6.1 Introduction

The use of geotextiles to prevent particle migration and associated subgrade failures has been carried out by numerous researchers over the past few decades (Alobaidi & Hoare 1998a; Alobaidi & Hoare 1998b; Ayres 1986; Bhatia & Huang 1995; Chawla & Shahu 2016; Fatahi et al. 2011; Hameiri 2000; Kermani et al. 2020; Nithin et al. 2015; Raymond 1986; Zheng et al. 2021). Despite this intensive use of geotextiles, the measures and/or techniques used to prevent mud pumping and the primary function of geosynthetics to control the risk of subgrade fluidisation under heavy haul loading has not been understood very well in previous studies (Nguyen et al. 2019). The pore arrangement in geotextiles should be large enough to provide adequate seepage (drainage capacity) and yet small enough to prevent particle migration (filtration). Preventing particles from entering into the overlying layers can increase the permeability of the drainage layer and provide continuous performance under loads (Ai-Qadi & Appea 2003; Christopher et al. 2006). This chapter describes how well geotextiles/geocomposites help to control excessive particle migration towards the ballast layer and prevent the instability (soil softening) at the ballast/subgrade interface. In this study, geotextiles and geocomposites were placed between the subgrade surface and ballast layer; no sub-ballast layer (compacted sand layer) was placed over the geosynthetics. The filtration behaviour of subballast, the influence of cyclic load on the design of a combined geosynthetics and capping layer were not considered within the scope of this study.

6.2 Experimental Setup

A geotextile was placed on top of the subgrade soil, as shown in , and then the development of EPWP, axial strain, EPPG, and variations in the particle size distribution (PSD) and moisture content were measured under a cyclic load. The test procedures have already been described under Section 3.6 in Chapter 3.
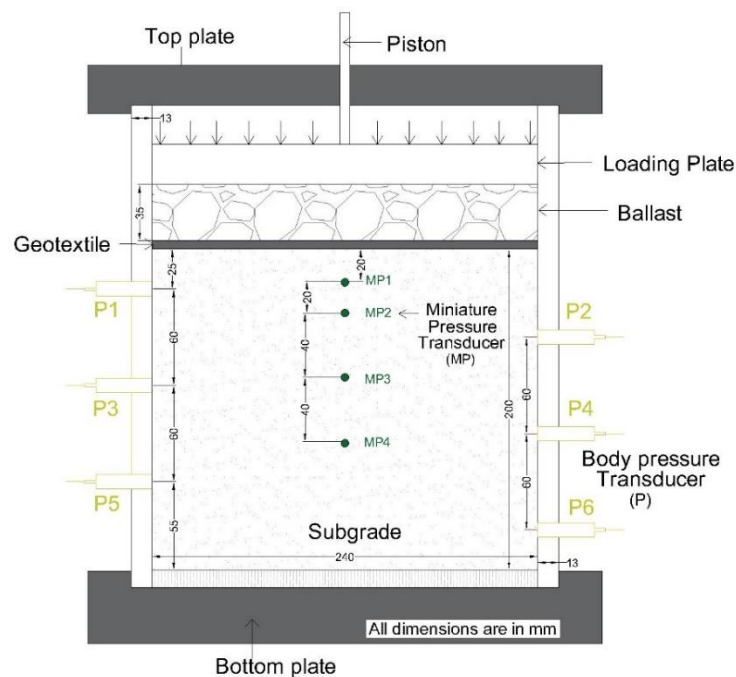
Figure 6. 1: The experimental setup with geotextile

Geotextiles with different aperture opening sizes were selected for the cyclic tests; the properties of the geotextiles are tabulated in Table 3. 1 (Chapter 3). Based on its ability to control subgrade fines and dissipate the EPWP, geocomposite G1 was used to perform the cyclic tests under varying axle loads and frequencies, as reported later in this chapter.

6.3 Experimental Results and Discussion (Different Geotextiles)

The role of geotextiles (G1, G2, G3, G4 and G5) in terms of EPWP, axial strain, and excess pore pressure gradient (EPPG) are assessed in this study. Table 6.1 shows the experimental

plan and loading conditions used to assess the effectiveness of different geotextiles under

partially drained conditions.

Table 6. 1: Experimental plan using different geotextiles

Test Name	Drainage condition at ballast subgrade interface	Tested Geosynthetics	σ_{min} (kPa)	σ_{max} (kPa)	Frequency (Hz)
G1*	Partially drained with G1	Geocomposite 1	30	70	5
G2	Partially drained with G2	Geotextile 2	30	70	5
G3	Partially drained with G3	Geotextile 3	30	70	5
G4	Partially drained with G4	Geotextile 4	30	70	5
G5*	Partially drained with G5	Geocomposite 2	30	70	5

6.3.1 Generation of Excess Pore Water Pressures (EPWP)

Although there was a rapid generation of EPWPs (>30 kPa) within 500 cycles in Test G1,

the EPWPs continued to decrease as the number of cycles increased. Figure 6. 2 shows that

all the readings from the miniature pressure transducers (MPs) are less than 22 kPa (EPP_{T1})

after 12,000 cycles. G1 could dissipate the EPWP to below 10 kPa at 100,000 cycles, which

indicates its ability to reduce the development of pore pressure for the next train loading.

As Figure 6. 2 shows, the pore pressure that developed in the middle layers (MP2 and MP3)

is higher than in the lower subgrade soils (MP4). This shows that the middle layers or the

shallower parts of subgrade soil have more potential for instability under undrained

conditions, and geocomposite G1 prevented the critical development of EPWP. There was

a 52% reduction in EPWP at MP3 after 50,000 cycles compared to the undrained tests

(Chapter 5). The pore development in MP1 (@20mm from the interface) decreased by 64%

with the inclusion of G1 at 50,000 cycles. This proves that geocomposite G1 can

continuously alleviate EPWPs that developed at critical layers under adverse hydraulic conditions.
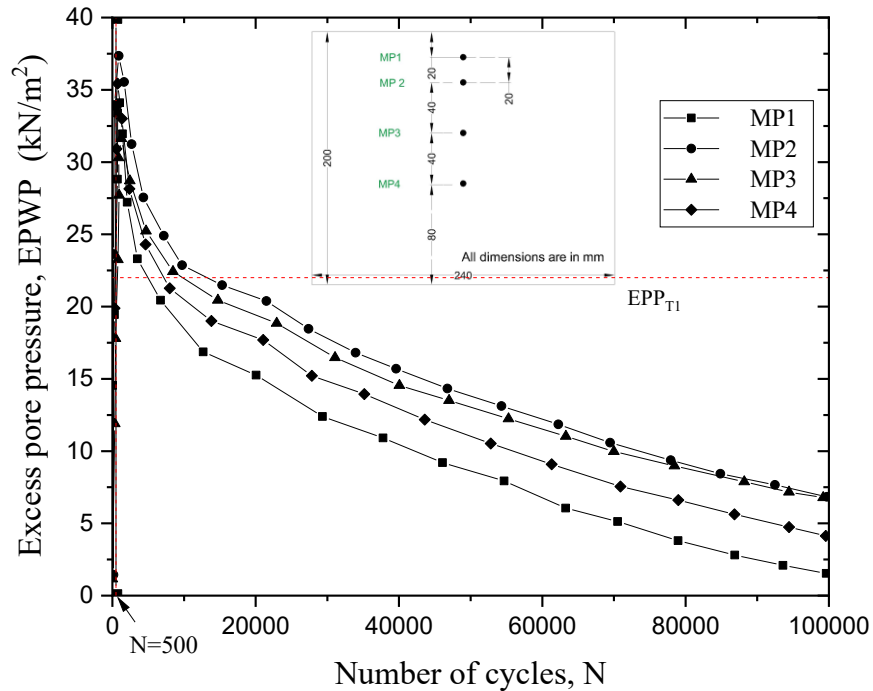
Figure 6. 2: Excess pore water pressure developed in Test G1

As Figure 6. 3 and 6.4 show, G1 dissipated EPWPs by more than 86% and 62%, at 20 and 40 mm below the interface, unlike geotextiles G2 and G3 (at 100,000 cycles). Until the test reached 65,000 cycles, the values from MP2 measured 40 mm below the interface were more than 22 kPa (EPP$_{T1}$) for G2 (Figure 6. 3) and G3 (Figure 6. 4), and with a very low rate of dissipation compared to G1. Unlike geotextile G3, G1 dissipated by more than 88% at 20 mm below the interface after 100,000 cycles. The miniature pressure transducer readings (MP2 and MP3) were more than 15 kPa over 50,000 cycles, and without any significant reduction during Tests G2 and G3. Therefore, the geocomposite (G1) inclusion dissipated the EPWP better than Test T1 (Undrained tests) and in comparison, to other geotextiles.
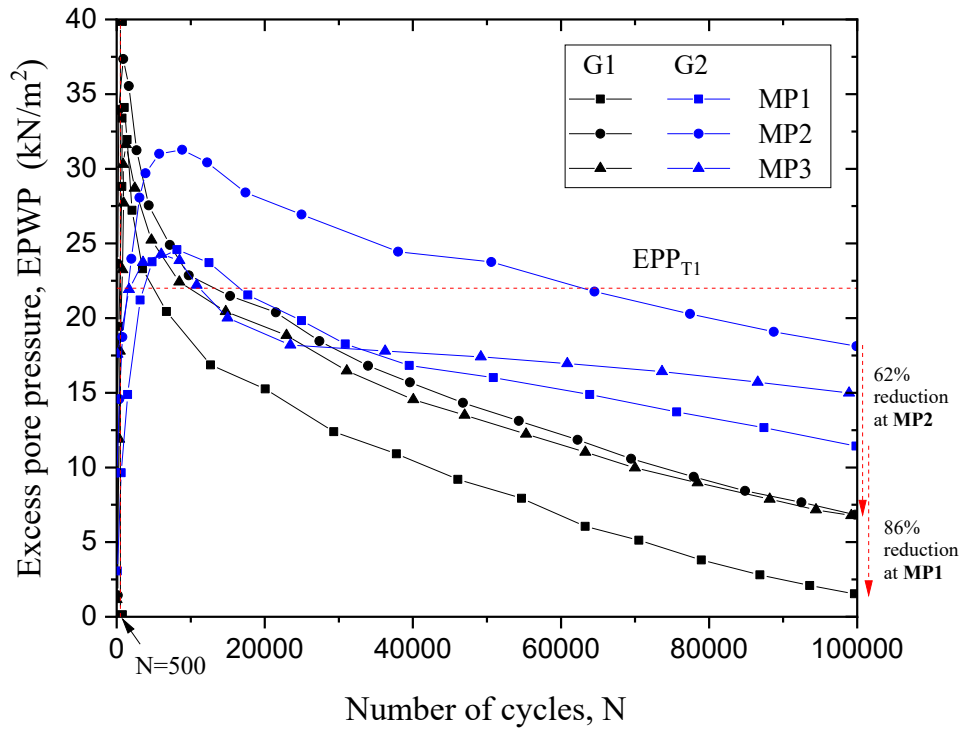
Figure 6. 3: Excess pore water pressure - Tests G2 and G1(after Arivalagan et al. (2021))
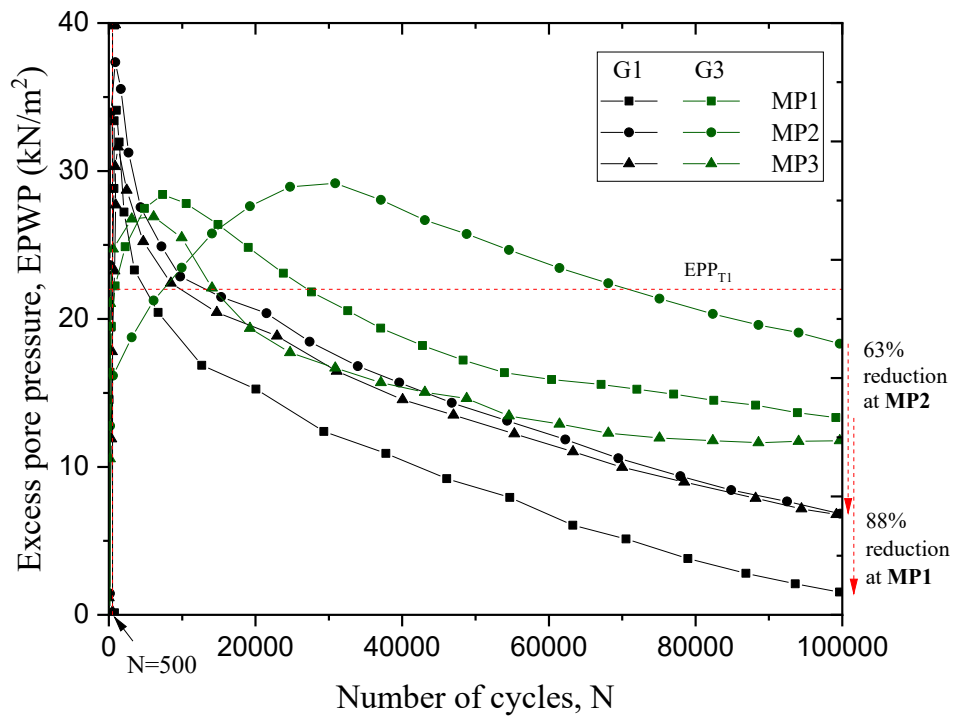
Figure 6. 4: Excess pore water pressure - Tests G3 and G1 (after Arivalagan et al. (2021))

Figure 6. 5 shows that both geocomposites G1 and G5 dissipated the EPWP quite significantly as the number of cycles increased, but the generation of EPWP at 20 mm from the interface was much lower in Test G1 than in Test G5. However, G5 controlled the EPWPs that developed within 500 cycles (i.e., they were less than 26 kPa in all three locations), as shown in Figure 6. 5.
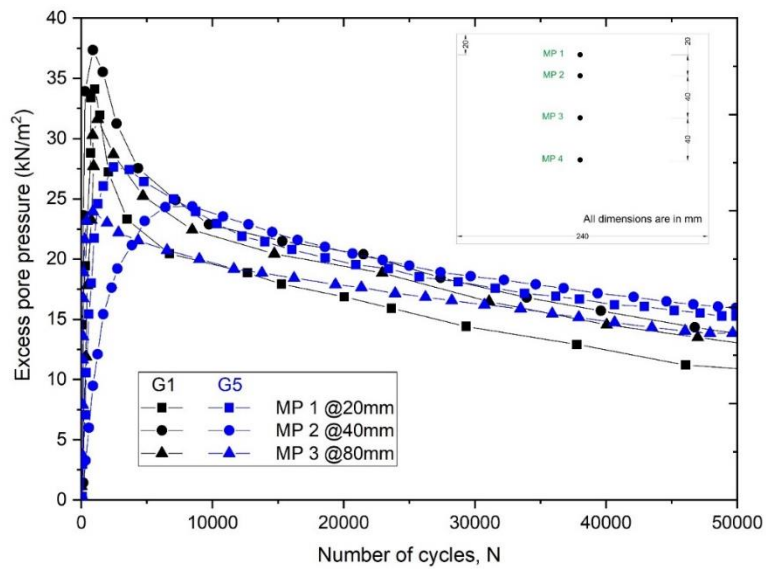
Figure 6. 5: Excess pore water pressure - Tests G1 and G5
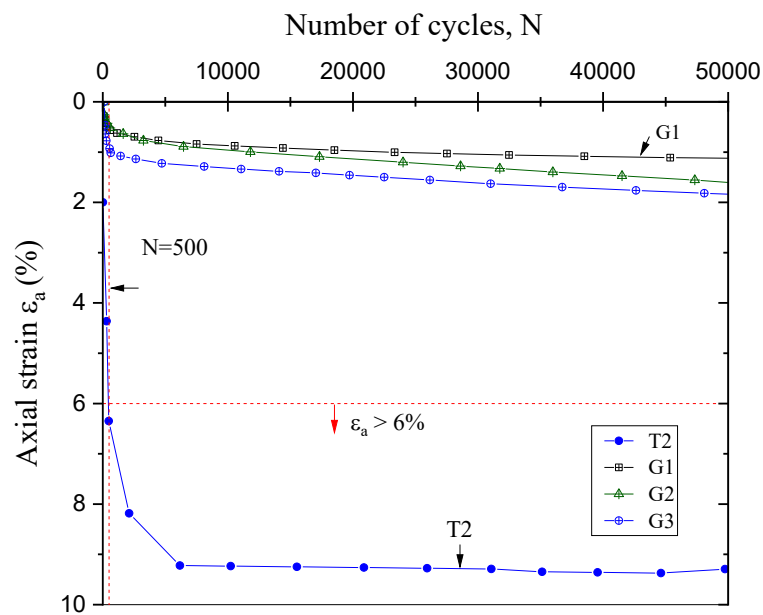
Figure 6. 6: Axial strain - Tests T1, T2, G1, G2 and G3 (after Arivalagan et al. (2021))

6.3.2 Development of Axial Strain

As Figure 6. 6 shows, the maximum axial strain at T2 (6%) only occurred after 500 cycles. Similar observations were reported by Indraratna et al. (2020b), who described the effect of increased axial strain during subgrade failure, including subgrade fluidisation. However, the development of axial strain was controlled due to the inclusion of geotextiles at the interface. The axial strain for G1 was less than 1.5% after 100,000 cycles, as shown in Figure 6. 6. Moreover, G1 prevented the formation of an 'interlayer creation' through additional confinement at the interface and thus prevented particle separation under cyclic loading conditions. The residual axial strain after 100,000 cycles remained above 2% for G2 and G3. There was a continual increase in axial deformation in G2, G3, and G4 because the drainage at the interface could not dissipate the pore pressure and prevent particles from migrating through the pore openings. This may lead to differential settlements in railway tracks under repeated cyclic loading conditions.

6.3.3 Development of Excess Pore Pressure Gradients (EPPG)

The drainage conditions at the interface and inside the soil are studied based on the generation of an excess pore pressure gradient (EPPG) at different depths. The EPWP measured at different locations by body transducers were used to calculate the EPPG. The EPPG that developed in Tests T1 rocketed above 40 after 500 cycles, and there was no significant reduction until 15,000 cycles. However, geocomposite G1 reduced the EPPG at the top three layers of the soil within 2500 cycles. The EPPGs that developed in Layers (2-1) and (3-2) decreased by 81% and 92% due to the inclusion of G1, as shown in Figure 6. 7. The EPPG that developed at the middle and lower regions (Layer (3-2) and Layer (4-3)) was less than five until the end of cyclic tests. As Figure 6. 8 shows, there was a 73% reduction in Layer (2-1) when using geocomposite G1 rather than G3. The EPPG that developed in G1 was 90% and 80% lower than G3 after 1000 and 100,000 cycles, respectively. This non-uniform development of EPPG (up to 75) in the middle and deeper

subgrade soil (the critical layers), i.e., Layers (2-1) and (3-2), created a significant upward

hydro-dynamic force that dislocated the finer particles towards the top layers.
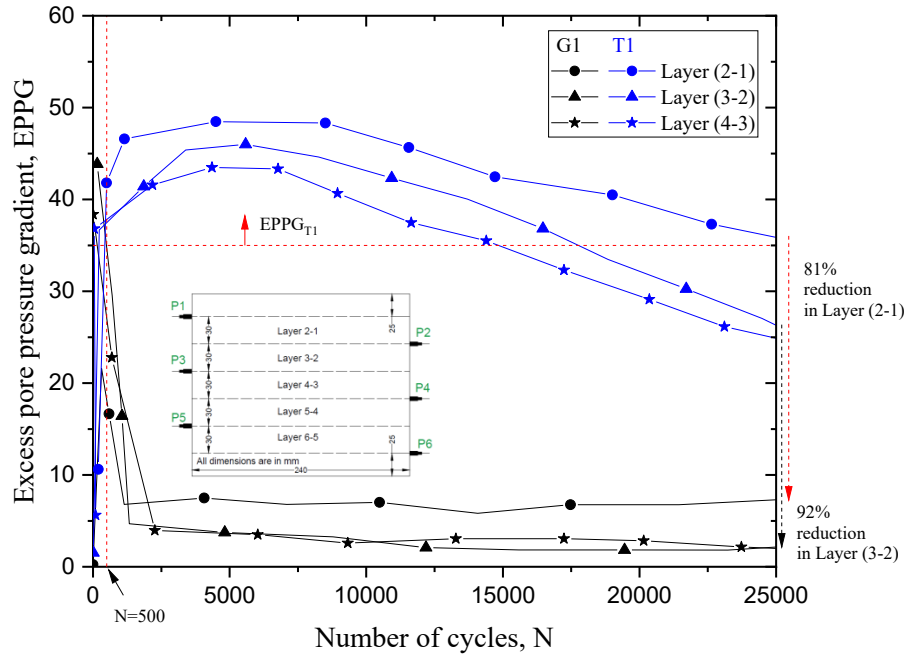
Figure 6. 7: EPPGs for Tests T1and G1 (after Arivalagan et al. (2021)
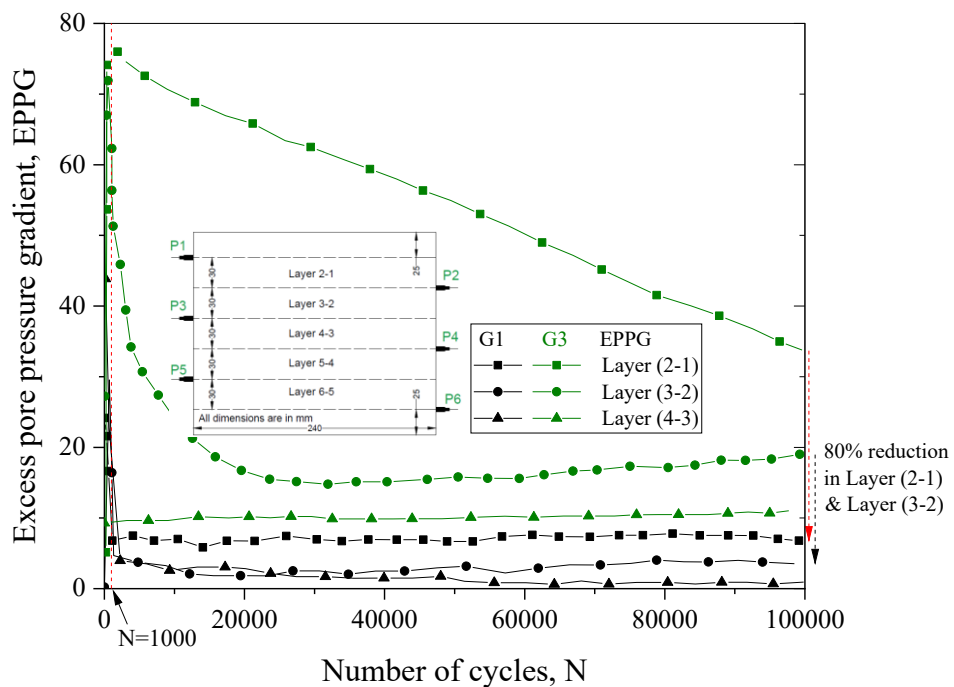
Figure 6. 8: EPPGs for Tests G1 and G3 (after Arivalagan et al. (2021))

6.3.4 Particle Size Distribution (PSD)

The test results obtained from undrained (T1) and free drainage (T2) conditions showed that the movement of finer particles with an increase in the moisture content caused subgrade fluidisation under critical loading conditions. A Malvern particle size analyser (Mastersizer – Figure 6. 9) was used to measure the particle size distributions at the top, middle, and bottom regions at the end of loading. As shown in Figure 6. 10(a), the inclusion of G1 prevented the migration of particles from the middle and lower regions. There were no significant variations in the particle size distribution, especially at the top and middle layers. This shows that geocomposite with an effective filter (G1) can prevent particle dislocation under critical hydro-dynamic conditions.

In Tests G2, fine particles of less the 75 μm had accumulated at the top surface, as shown in Figure 6. 10(b). Moreover, the percentage of coarser fractions larger than 30 μm in the middle layers was significant compared to Test G1. This proves there were significant changes in the void ratio and PSD due to the migration of fines under cyclic loading. As shown in Figure 6. 10(b), a lot more fines were lost in the middle layers (between 1 and 60 μm), compared to the initial PSD. Similarly, there was a large accumulation of fines (less than 1 μm) in the top and middle layers in Test G3.
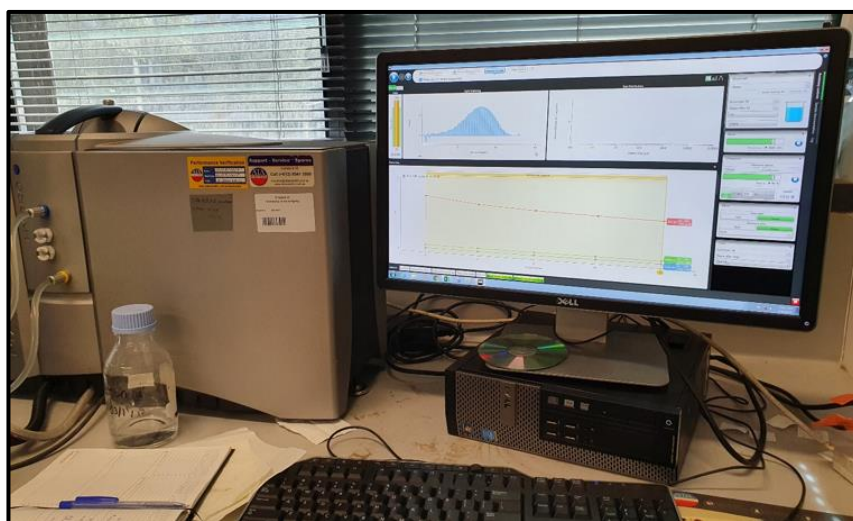
Figure 6. 9: PSD analysis using Malvern Particle Analyzer (Mastersizer)
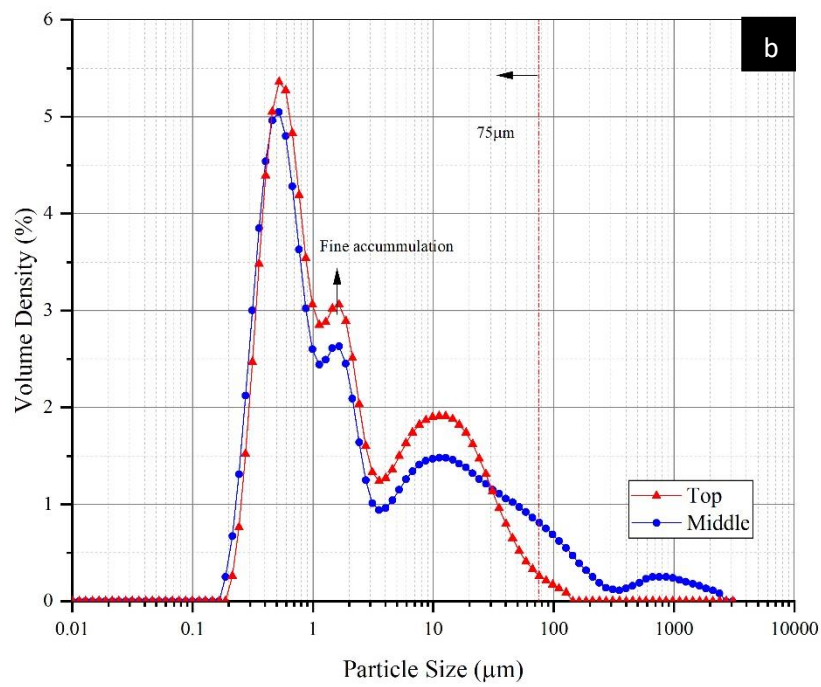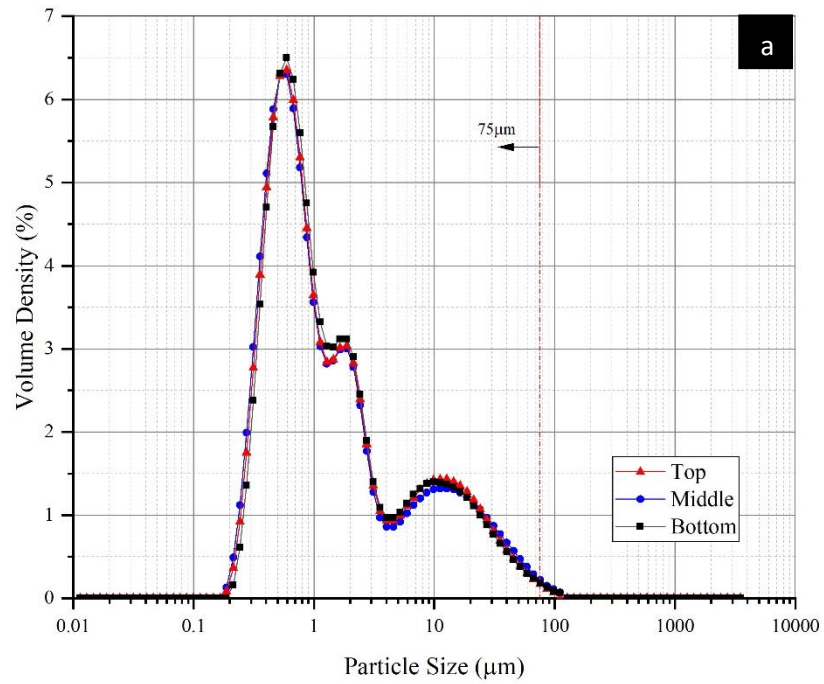
Figure 6. 10: Particle migration under cyclic load for (a) Test G1 and (b) Test G2 by Malvern Particle Analyzer

6.3.5 Water Content (w/c)

The ability of different geotextiles to curtail the water content of subgrade soil by providing adequate drainage is shown in Figure 6. 11. The water content for Tests T1 and T2 were close to the liquid limit at the top surface of the subgrade. The amount of high water near the interface causes softening and can induce fluidisation as finer particles accumulate below 500 cycles. However, geotextiles helped to reduce the water content of the soil specimen compared to the undrained (T1) and free drainage (T2) tests. G2 had a maximum water content of 32.5% near the interface which aggravated softening under cyclic loading. The water content of the interface soil was more than 30% closer to the interface when G3 and G4 were tested. The inclusion of G1 could further reduce the water content by approximately 5%, unlike the other geotextiles. The water content along the height of the specimen decreased significantly due to the inclusion of Geocomposite G1.

.
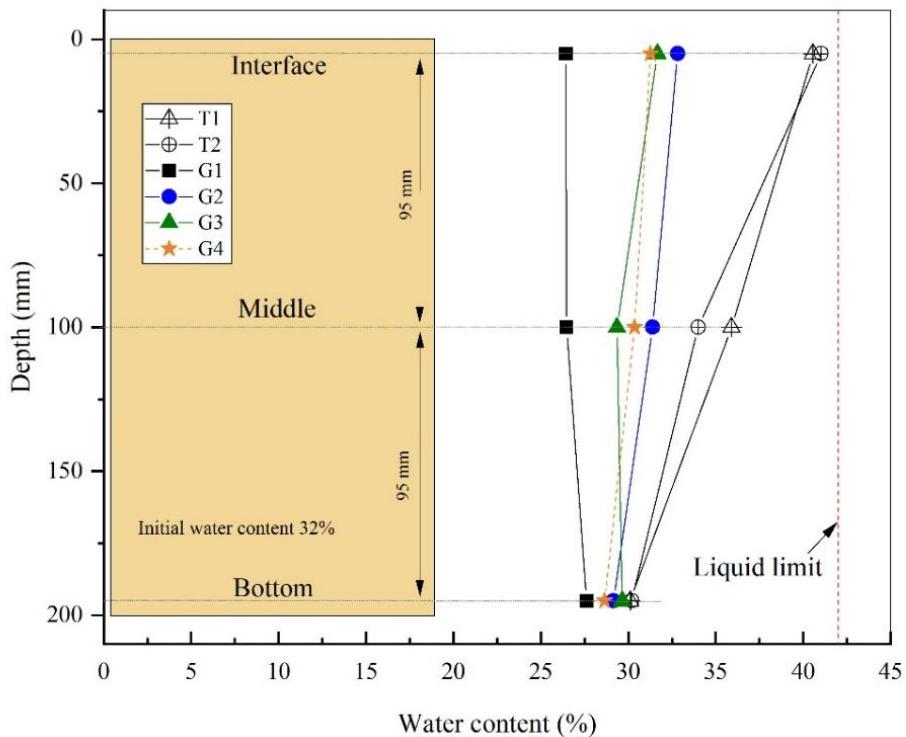
Figure 6. 11: Water contents after N = 100,000 cycles – Tests G1, G2, G3, G4, T1, and T1 (after Arivalagan et al. (2021))

6.3.6 Interface (Subgrade/Ballast)

The subgrade/ballast interface was monitored continuously during cyclic loading. The application of a geotextile on top of subgrade soil could prevent ballast particles from sinking into the subgrade (Interlayer creation) and softening the subgrade (Fluidisation), unlike Test T2 (Free drainage test). As shown in Figure 6. 12, geocomposite G1 prevented an 'interlayer creation' and the formation of slurry near the interface after more than 100,000 cycles. During test G2, finer particles were migrated near the interface and the thin layer of softened subgrade formed underneath the geotextile (Figure 6. 12(b)). There was no slurry or accumulation of fines in the interface soil in Test G1. In Test G4, slurry water (with fines of less than 75 microns) rose to the top because angular ballast particles had penetrated the fibres (geotextile G4) under repeated loading conditions.
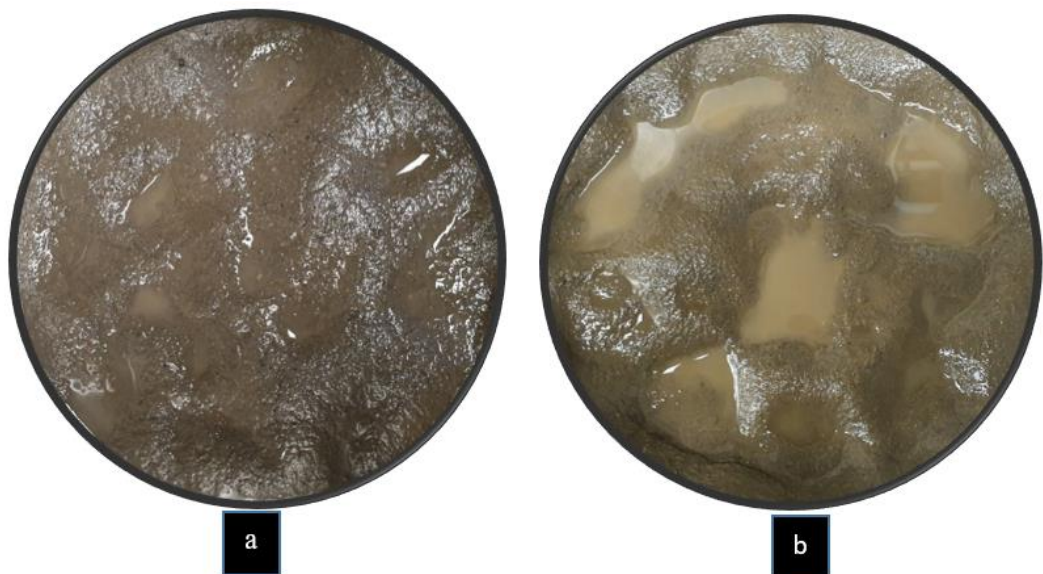
Figure 6. 12: Top surface of subgrade after cyclic loading (magnification = 0.273x) (a) Test G1 and (b) Test G2

6.3.7 Clogging, Permeability and Trapped Fines

Severe clogging occurred in geotextiles G2 and G4, as shown in Figure 6. 13. Finer particles were pumped up on top of the geotextiles during cyclic loading and hindered the

drainage capacity at the interface. This could lead to the rapid generation of EPWP in the middle layers, as described in the previous sections. As tabulated in Table 6. 2: Trapped fine particles, the mass of trapped fine particles was measured to analyse the clogging of the geotextile (the geotextile area was 4.15×10^{-2} m^2). The amount of fines trapped in G1 and G5 after 100,000 cycles were minimal (approximately 30 - 55% less than G3 and G4), which shows how effectively it prevented upward migration of fine particles. In other words, there was no particle migration through the pore openings of geocomposites (G1 and G5) as the number of cycles increased.

The permeability tests on geotextiles (subjected to cyclic loading) showed the reduction in hydraulic conductivity due to the trapping of fine particles inside the pores. The hydraulic conductivity of the geotextiles was determined by permittivity according to ASTM D4491-99 (1999). There was an almost 29% reduction in the permittivity of geocomposite G1 after the cyclic test (5.04×10^{-4} s^{-1}), however, the permittivity of G2 after the cyclic test was 6.21 s^{-1}, which was an almost 58% reduction. The geotextiles G3 and G4 showed a 41% and 61% reduction in permittivity due to the trapping of fine particles, respectively. Moreover, there was also pumped-up slurry near the subgrade surface, which indicated that G2, G3, and G4 failed to prevent the fine particles from migrating under cyclic loading.

Table 6. 2: Trapped fine particles

Geotextiles	Trapped Fine particles (g)
G1*	5.92
G2	8.12
G3	9.16
G4	11.62
G5*	5.29
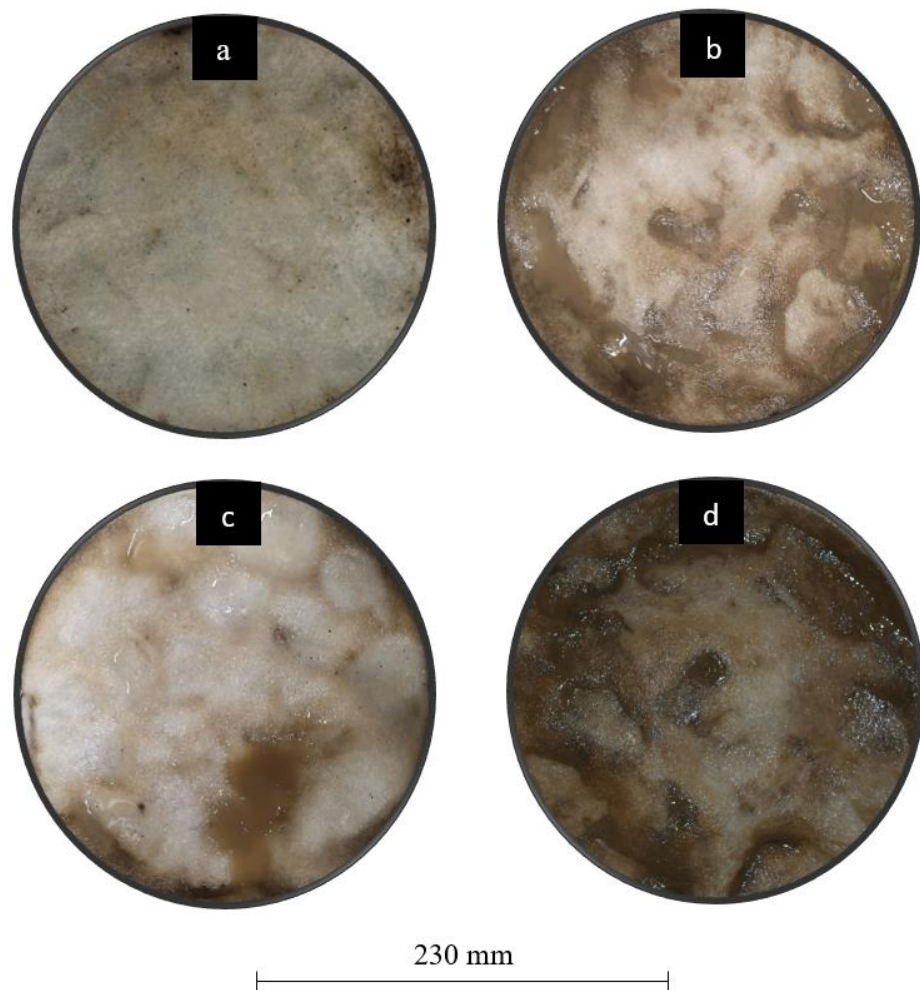
Figure 6. 13: Photos of tested geotextiles (magnification = 0.209x) after 100,000 cycles (a) Test G1 (b) Test G2 (c) Test G3 and (d) Test G4

6.3.8 Results of Micro CT scan

A micro CT scanner was used to study the pore arrangement of soil specimens tested under cyclic loading. The 20 mm x 50 mm specimens were cored using a 1.5mm thick glass tube at different locations (0-50mm, 50-100mm) after cyclic loading, as shown in Figure 6.14(a). The cored specimens were oven-dried before X-Ray diffraction analysis. As Figure 6. 15 shows, the CT scan images of the extruded soil samples could capture the particle arrangements at the interface soil. The accumulation of fine particles and the formation of slurry are shown in Figure 6. 15(b) and (c), respectively. The CT-Scan only captures finer

fractions larger than 4µm, as described in Chapters 3_ Section 3.3.2.8 (4-µm voxel size resolution).
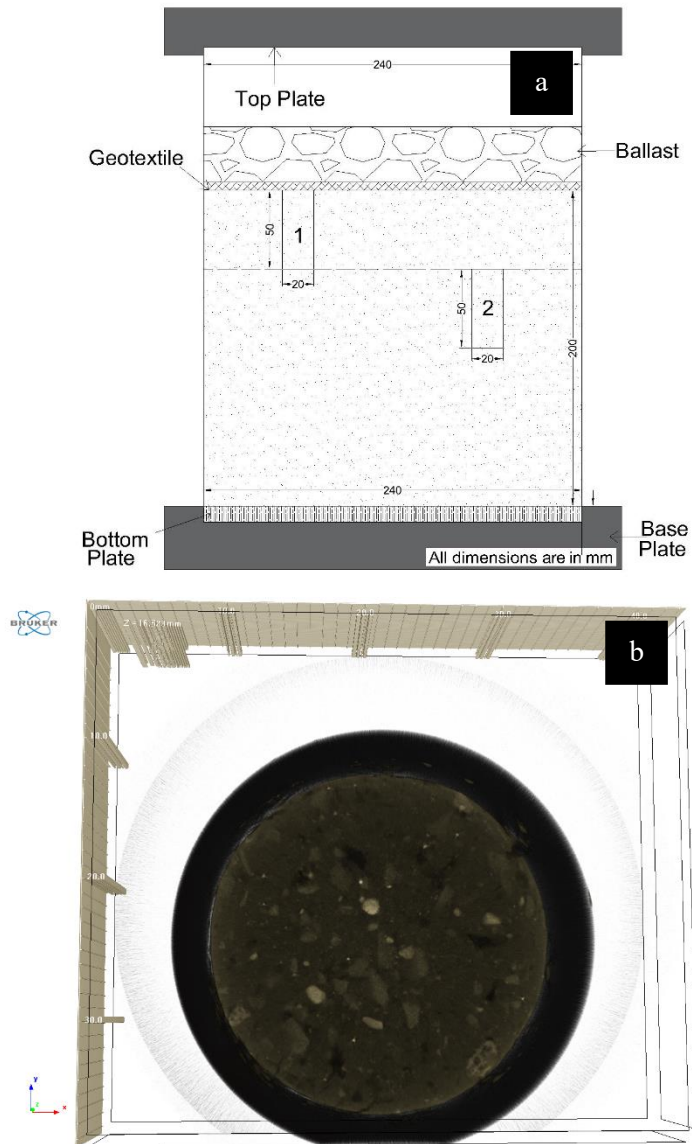
Figure 6. 14: (a) Core sample locations, and (b) Images of cross-sections captured using a micro CT scanner

Since the PSD of the soil specimen had approximately 51 per cent of finer content (the percentage that passed through 75 microns), it was challenging to capture the porosity at specific depths (cross-sections). As a result, the finer particles are blurred at the interface,

as shown in Figure 6. 15(c). However, the coarser fractions can be seen in the middle layers (Figure 6. 16). The loss of fines can be seen in Tests G3 and G4 at the middle layers (Figure 6. 15(b) and (c)). Dislocated particles can be transported towards the top layers under the influence of a hydraulic gradient developed by EPWP. The top and middle layers have almost the same pore arrangements as in Test G1, as shown in Figure 6. 15 (a) and 6.16(a). It is clear that G1 could prevent particle separation better than the other geotextiles under cyclic loading conditions.
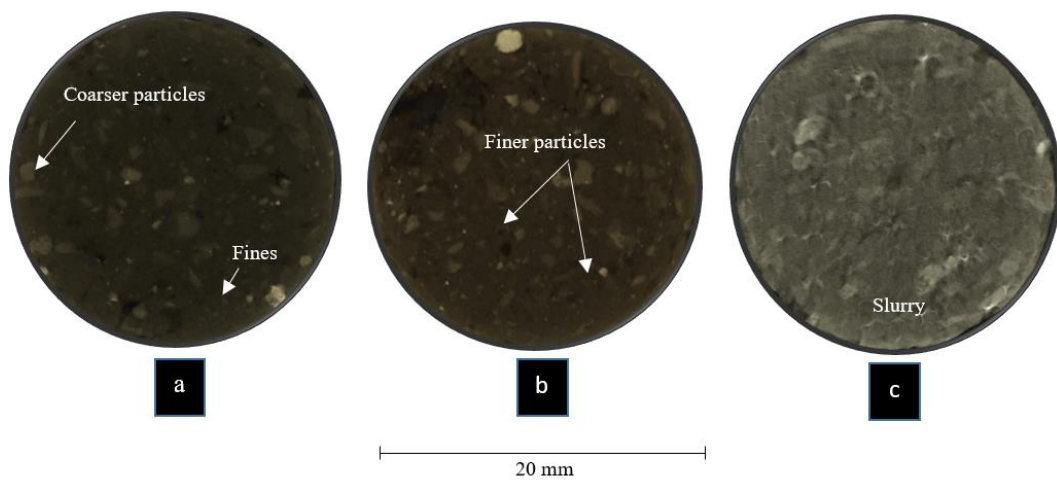
Figure 6. 15: CT scan images of cored samples (magnification = 2.1x) at the interface (a) Test G1, (b) Test G3, and (c) Test G4
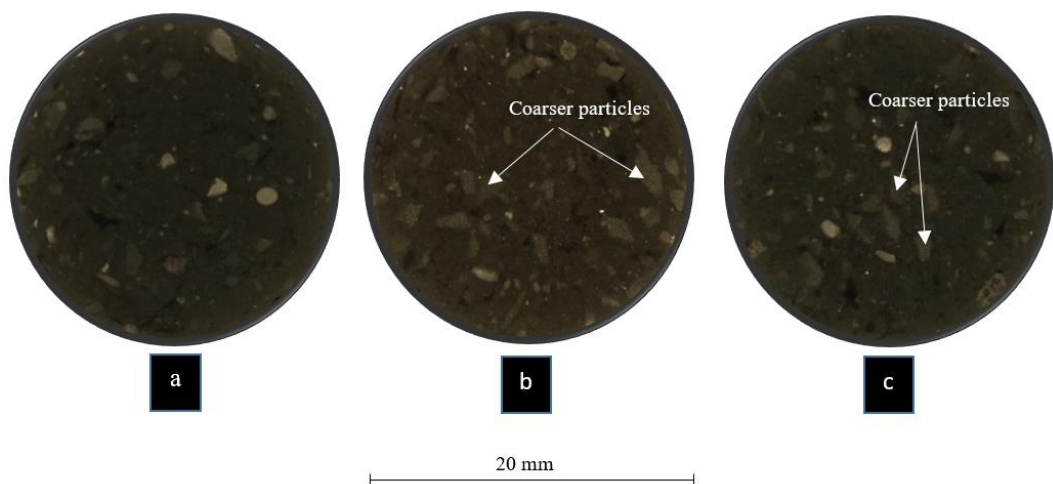
Figure 6. 16: CT scan images of cored samples (magnification = 2.1x) at 50 mm from the interface (a) Test G1, (b) Test G3, and (c) Test G4

6.4 Effects of Cyclic Stress and Frequency

6.4.1 Introduction

The performance of three geotextiles (G2, G3, and G4) and two geocomposites (G1 and G5) was discussed in the previous section 6.3. geocomposite G1 performed well because it dissipated the EPWP and prevented particles from migrating through the pore openings. An axle load of 25 tonnes (5 Hz frequency) was considered in Section 6.3. However, the geotextiles with larger pore openings could not prevent pumping and severe clogging under cyclic loading conditions, and there was a continual increase in axial strain and soil softening after 100,000 cycles when geotextiles G4 and G2 were used. This shows their inability to prevent particles from passing through the pore openings of geotextiles under critical hydro-dynamic conditions. Although geocomposite G1 could dissipate the EPWP that developed under 25-tonne axle loads, their effectiveness must be assessed by simulating different axle loads and the speed of heavy haul trains. On this basis, 25 – 35 tonnes axle loads and 1-5 Hz frequencies were used to simulate typical railway track conditions. Geocomposite G1 was used in all six cyclic tests as tabulated in Table 6. 3: Experimental plan under different cyclic loading conditions, and the ability of geotextiles to prevent subgrade fluidisation is discussed in the following sections.

Table 6. 3: Experimental plan under different cyclic loading conditions

Test Name	Drainage condition at ballast subgrade interface	Tested Geocomposite	σ_{min} (kPa)	σ_{max} (kPa)	Frequency (Hz)
G-70-5	Partially drained with G1	G1	30	70	5
G-85-5	Partially drained with G1	G1	30	85	5
G-100-5	Partially drained with G1	G1	30	100	5
G-70-1	Partially drained with G1	G1	30	70	1
G-70-3	Partially drained with G1	G1	30	70	3
G-70-5	Partially drained with G1	G1	30	70	5

6.4.2 Effects of Cyclic Stress

6.4.2.1 Generation of EPWP

Three different deviatoric stresses, i.e., σ_{max} of 70, 85 and 100 kPa, were used to demonstrate how an increased axle load affects the cyclic behaviour of subgrade soil, and to assess the effectiveness of G1 under increased cyclic stress. As predicted, there was an expeditious development in EPWP when the cyclic deviator stress increased up to 100 kPa. As shown in Figure 6. 17, geocomposite G1 could not reduce the cyclic EPWP effectively at the middle to the lower region (i.e., the critical layers) when the cyclic stress increased to 100 kPa. The readings from miniature pressure transducers MP2, MP3, and MP4 remained above 40 kPa until the test ended. All the miniature readings were higher than 16 kPa at 100,000 cycles in Test G-85-5.
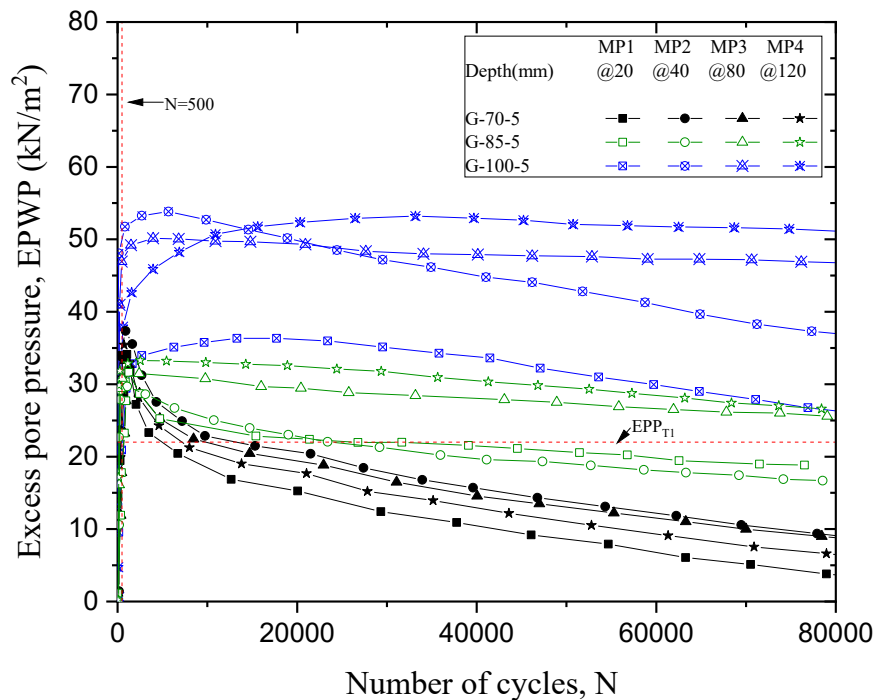
Figure 6. 17: EPWPs - Tests G-70-5, G-85-5, and G-100-5 (Arivalagan et al. 2021)

The EPWPs developed at MP3 and MP4 for Test G-85-5 are higher than EPP_{T1} (22kPa), which can cause instability in subgrade soil under repeated train loading. Figure 6. 17

shows an approximately 85% lower EPWP at 120 mm below the interface in Test G-70-5 compared to Test G-100-5 after 80,000 cycles. These results imply that an increased axle load in railway tracks (35-40 tonnes) generates a rapid increase in EPWPs, and the inclusion of geotextiles cannot dissipate them quickly under adverse hydraulic conditions.

6.4.2.2 Axial Strain

The increasing trend in axial strain was reported in previous studies when subgrade soil is subjected to a higher CSR (Indraratna et al. 2020a; Indraratna et al. 2020b). A similar increasing trend in Test G-100-5 reached 5% before 75,000 cycles, as shown in Figure 6. 18. The axial strain for G-70-5 was less than 1.5% until the test ended, but it rocketed up to 2.2 and 5.3% at 80,000 cycles in Tests G-85-5 and G-100-5, respectively. There was a continual increase in axial strain (in Tests G-85-5 and G-100-5) until the test ended, which may induce instability due to excessive deformation in railway tracks.
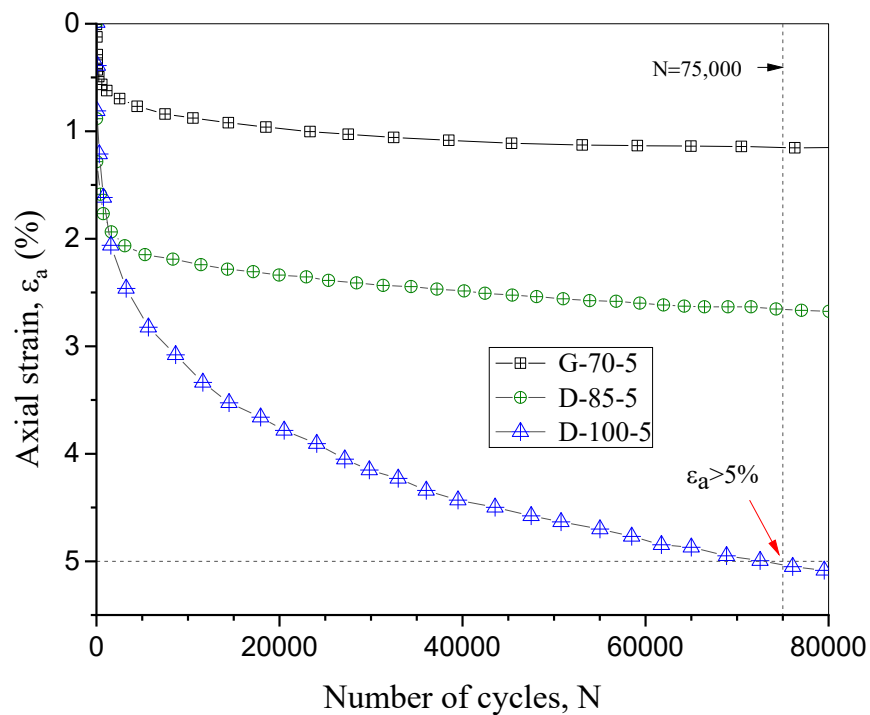
Figure 6. 18: Axial strains under different cyclic deviatoric stresses (Tests G-70-5, G-85-5, and G-100-5: after Arivalagan et al. (2021))

6.4.2.3 Development of EPPG

Figure 6. 19 shows that the maximum EPPG of 120 and 225 in Tests G-85-5 and G-100-5 occurred in less than 1000 cycles in Layers (2-1) and (3-2), respectively. However, in Test G-70-5, the EPPGs in the top and middle layers (i.e., Layers (2-1), (3-2), and (4-3)) dropped to 10 immediately after 1000 cycles, and remained constant until the tests ended. The rate of dissipation in EPPG after 1000 cycles in the critical layers (Layers (3-2) and (4-3)) of soil was minimal when the cyclic stress increased, unlike in Test G-70-5. The rapid development of EPPG within 1000 cycles could create enough hydraulic pressure to dislocate the fines.
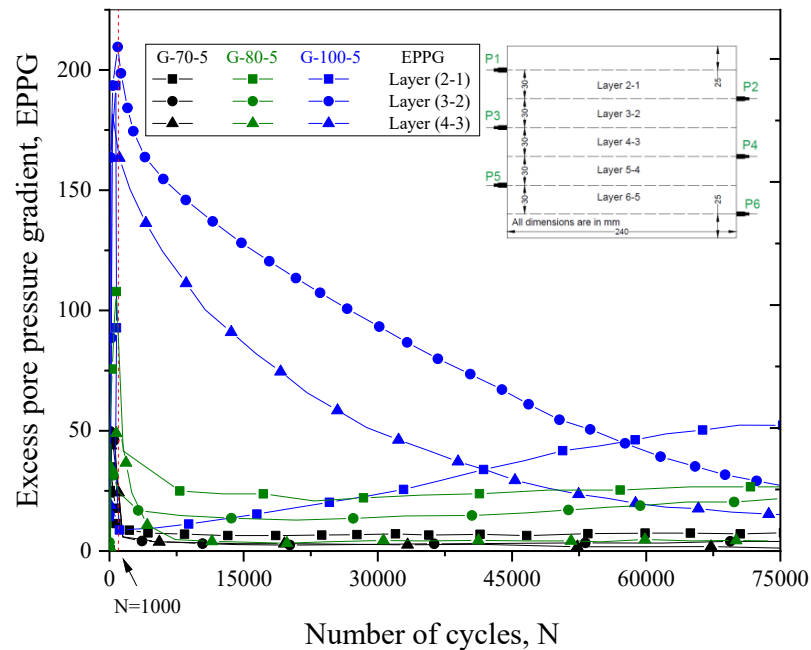
Figure 6. 19: Development of EPPGs (Tests G-70-5, G-85-5, and G-100-5)

6.4.2.4 Particle Size Distribution (PSD)

As Figure 6. 20 shows, there were no significant changes in the PSD of the topsoil in Test G-85-5, but there was a small increase in finer content in the middle layers in Test G-85-5. However, a lot of fine particles accumulated during Test G-100-5, as shown in Figure 6. 21. There was a significant loss of fines in the middle layers (between 3 and 100 μm) in

Test G-100-5, which proved that particle migration occurred under cyclic loading from the middle layers towards the top. This influence at the subgrade interface could become slurry due to the increase in moisture mixed up with pumped up finer particles.
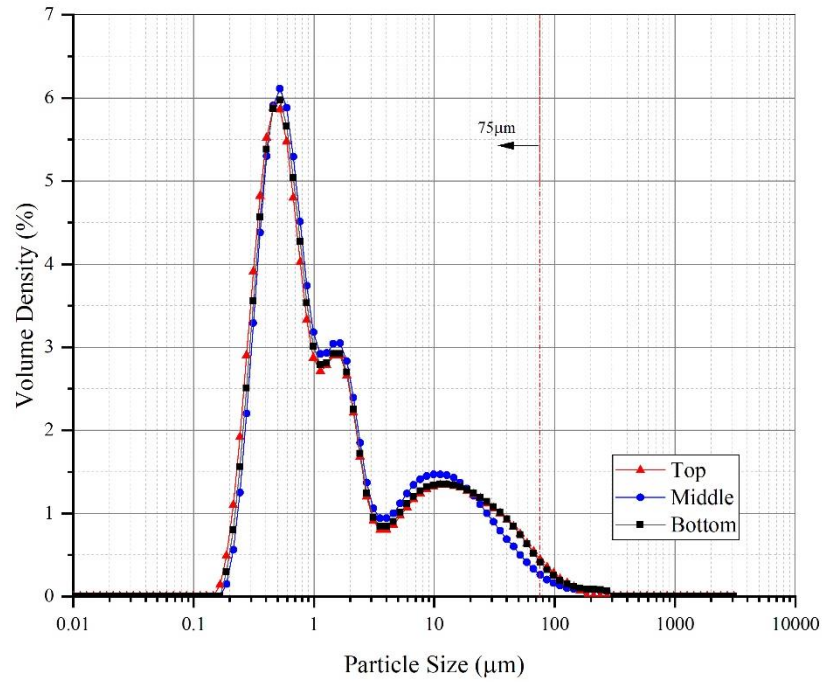
Figure 6. 20: Variations in PSD after cyclic load for Test G-85-5
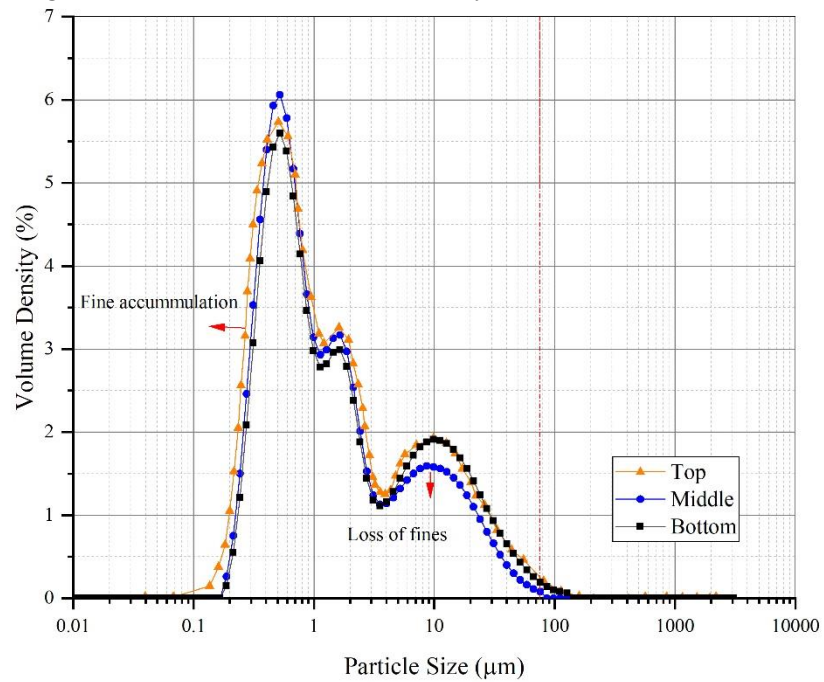
Figure 6. 21: Variation in PSD after cyclic load for Test G-100-5

6.4.2.5 Water Content

The water contents near the interface in Tests T1 and T2 were close to the liquid limit of the soil. The inclusion of geocomposite G1 could reduce the water content of the interface soil in Tests G-70-5 and G-85-5. The water content in the top and middle layers decreased significantly due to the inclusion of geocomposite G1 under lower cyclic stress, but there was an approximately 5% increase in the water content at the interface in Test G-100-5, as shown in Figure 6. 22. This proves that G1 could not effectively prevent an increase in the water content and subsequent fine migration with increased moisture from the middle layers as the cyclic stress increased. (σ_{max} of 100 kPa represents approximately 35 tonnes of axle loading).
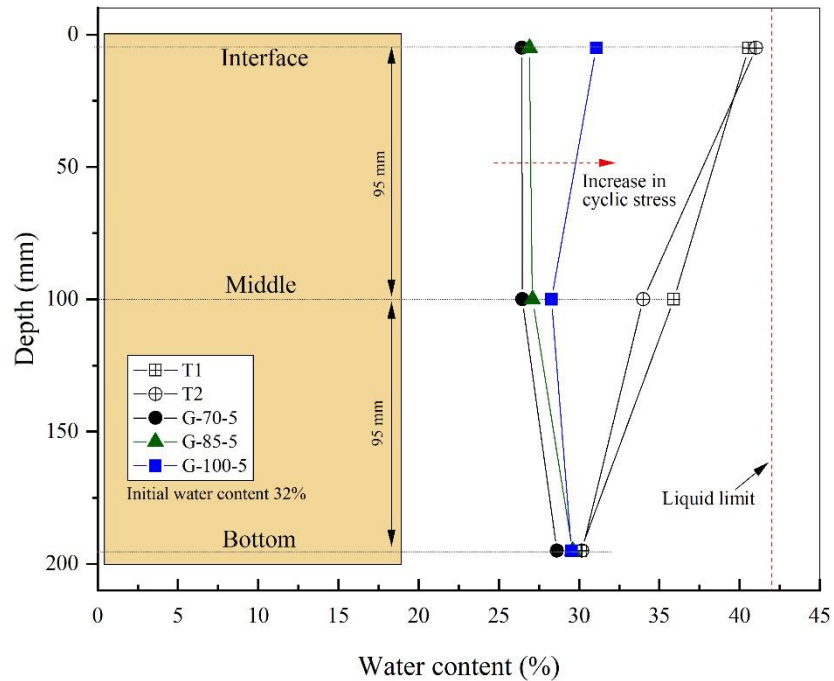
Figure 6. 22: Water content after 100,000 cycles (Tests T1, T2, G-70-5, G-85-5, and G-100-5 after Arivalagan et al. (2021))

6.4.2.6 Clogging and Interface (subgrade/geotextile) Confinement

Finer particles did not migrate continuously through the pores of the geocomposite at the top in Tests G-70-5 and G-85-5, but there was severe clogging and pumped-up fines at the interface in Test G-100-5 due to cyclic loading, as shown in Figure 6. 23. As described in the previous sections, G1 alleviated the EPWP, reduced the generation of EPPG, and reduced the water content at the interface. However, significant EPWP and EPPG developed in Test G-100-5 and geocomposite G1 could not prevent particles from migrating or the subsequent pumping through the pore openings. As Figure 6. 23(b) shows, the subgrade interface in Test G-100-5 turned to slurry, and the pumped-up fines severely clogged the geotextile. This implies that accumulated fines (G-100-5) may clog the pores of geotextiles and hinder its performance in terms of filtration and drainage.
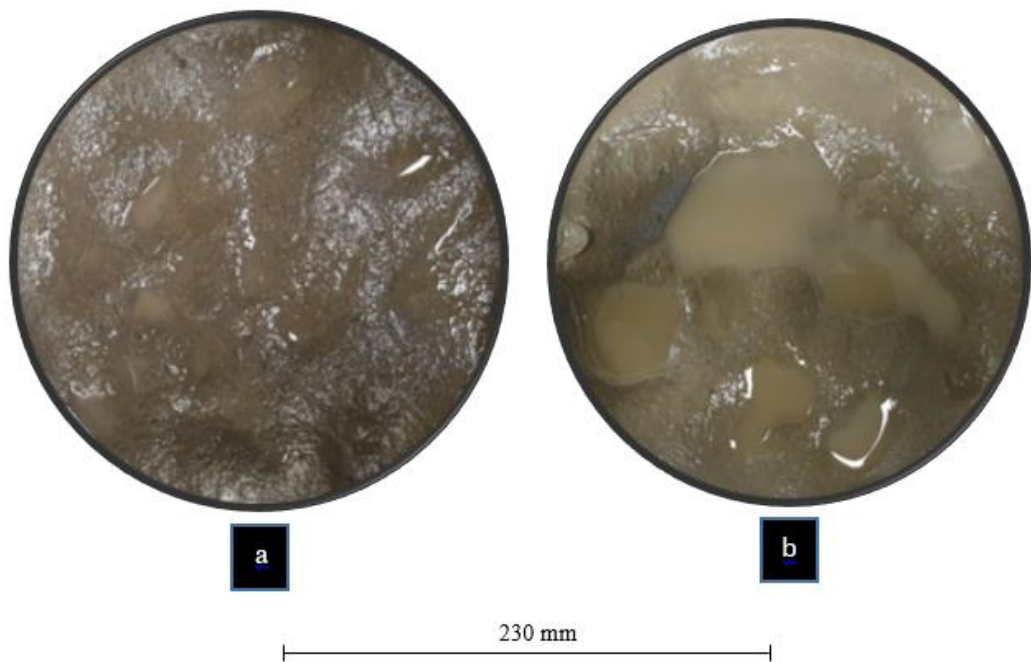
Figure 6. 23: Top surface of subgrade after 100,000 cycles (a) G-70-5 and (b) G-100-5
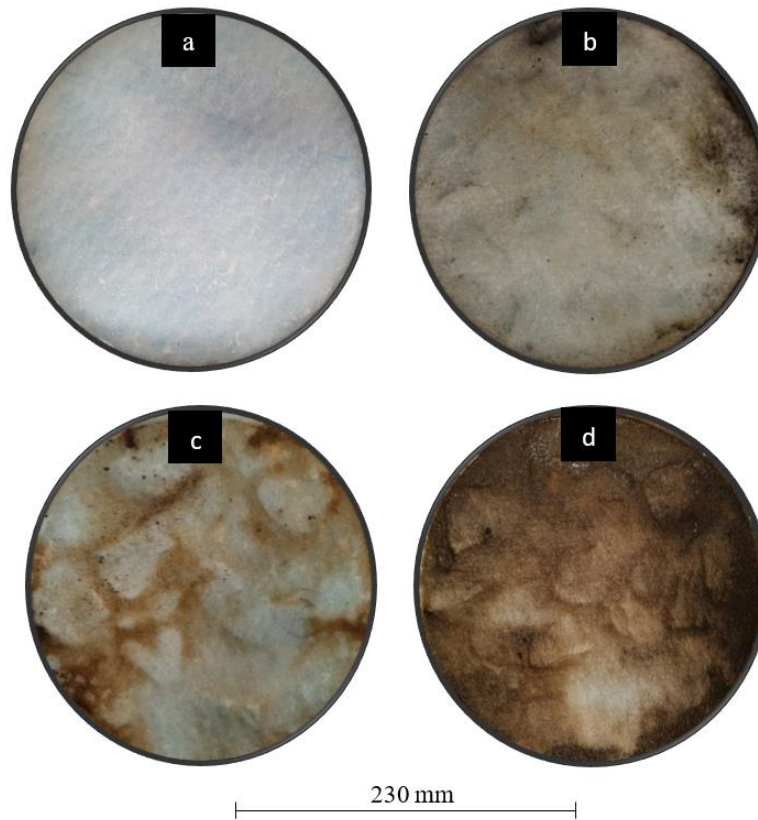
Figure 6. 24: (a) Photo of saturated geotextile, Photos of tested geotextiles after 100,000 cycles (b) Test G-70-5 (c) Test G-85-5, and (d) Test G-100-5 (after Arivalagan et al. (2021))

6.4.3 Effects of Loading Frequency

In this study, frequencies of 1, 3, and 5 Hz, were used to compare and highlight their effect on soil behaviour and the performance of geocomposite G1. These frequencies correspond to train speeds of 45-225 km/h (Indraratna et al. 2020b; Mamou et al. 2017; Powrie et al. 2007).

6.4.3.1 Generation of EPWP

Figure 6. 25 shows the evolution in EPWP corresponding to the load applied at different frequencies. The cyclic test at a lower frequency (G-70-3) developed a rapid increase in EPWPs, unlike the higher frequency (G-70-5). As shown in Figure 6. 25, the higher

frequency (f = 5 Hz) led to a more than 50% reduction in EPWP 120 mm below the interface at 50,000 cycles compared to Test G-70-3 (f = 3 Hz). Moreover, the residual EPWP for f = 3 Hz was more than 22 kPa (EPP_{T1}) after 50,000 cycles, and EPP_{T1} was the minimum EPWP that developed at 500 cycles under undrained conditions. This implies that soil subjected to smaller frequencies experienced a rapid generation in EPWP. The smaller frequency implies a more extended period for the load to make contact with the soil before unloading in each cycle, which led to a larger residual excess pore water pressure (EPWP) and axial strain in the test specimens. These observations support that train loading with a smaller frequency can initiate earlier fluidisation under the same loading conditions.
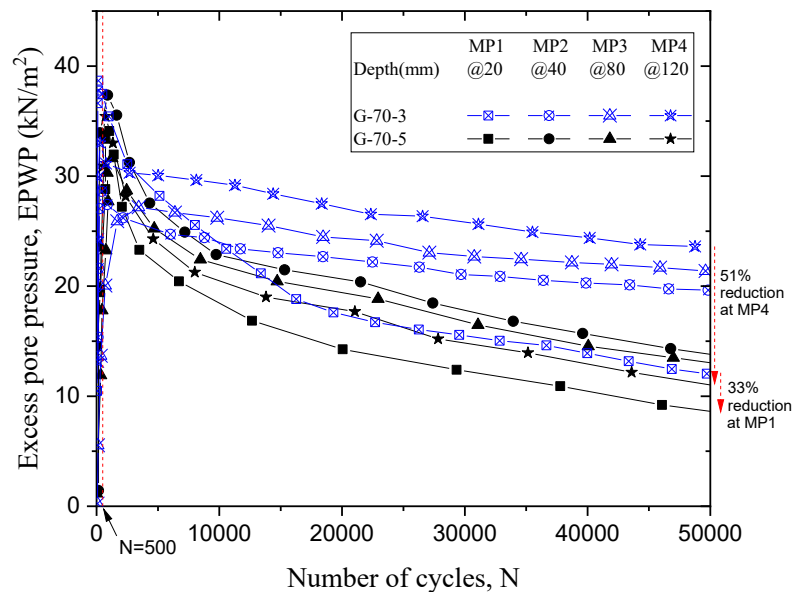
Figure 6. 25: Excess pore water pressure (Tests G-70-3 and G-70-5: after Arivalagan et al. (2021))

6.4.3.2 Axial strain

The time-dependent axial strains were recorded under different frequencies; they showed a larger accumulation of residual axial strain (2.5% at 50,000 cycles) under a lower

frequency (f = 3 Hz). Similar observations for specimens under cyclic loading were reported by Indraratna et al. (2020b) and Abeywikrama (2020) after they carried out undrained dynamic triaxial experiments. The axial strain was over 2% in less than 10,000 cycles in G-70-1 and G-70-3; this may cause instability/failures due to differential settlement in railway tracks.

6.4.3.3 Development of Excess Pore Pressure Gradients (EPPG)

The EPPG plotted in Figure 6. 26 shows the significant development in EPPG after 500 cycles in the middle and deeper layers of soil (i.e., Layer (3-2) and Layer (4-3)). As Figure 6. 26 shows, the EPPG was above 55 and 30 in Layers (4-3) and (3-2) only after 10,000 cycles in Test G-70-3. Therefore, the cyclic tests under smaller frequencies can dislocate the fines due to the local development of hydraulic forces because there was no significant reduction in EPPG until it reached 50,000 cycles. Moreover, due to this increased EPPG, the void ratio of the soil layers, especially in the middle and lower regions, changed due to fines being pumped up from the middle to the lower region of subgrade soil, and towards the top.

6.4.3.4 Particle Size Distribution

There was no accumulation of fines on the top surface in Test G-70-5, and there was no significant variation in the PSD at the top, middle, and bottom layers of the soil specimen. However, finer particles of less than 1 μm were pumped up over the top layer in Test G-70-3 from the middle layer, as shown in

Figure 6. 27. The percentage of coarser fraction (3 to 2000 μm) in the top layer was less than in the middle layer in Test G-70-3, unlike test G-70-5. In summary, the fines that accumulated at the interface due to the cyclic loading and at lower frequencies can cause instability under adverse hydraulic conditions.
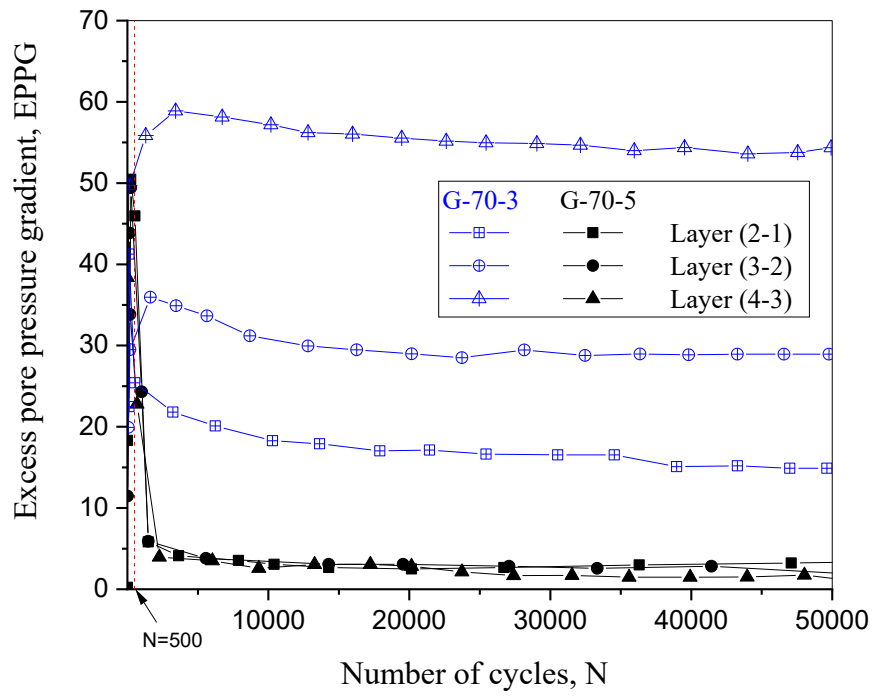
Figure 6. 26: Excess pore pressure gradient (Tests G-70-3 and G-70-5)
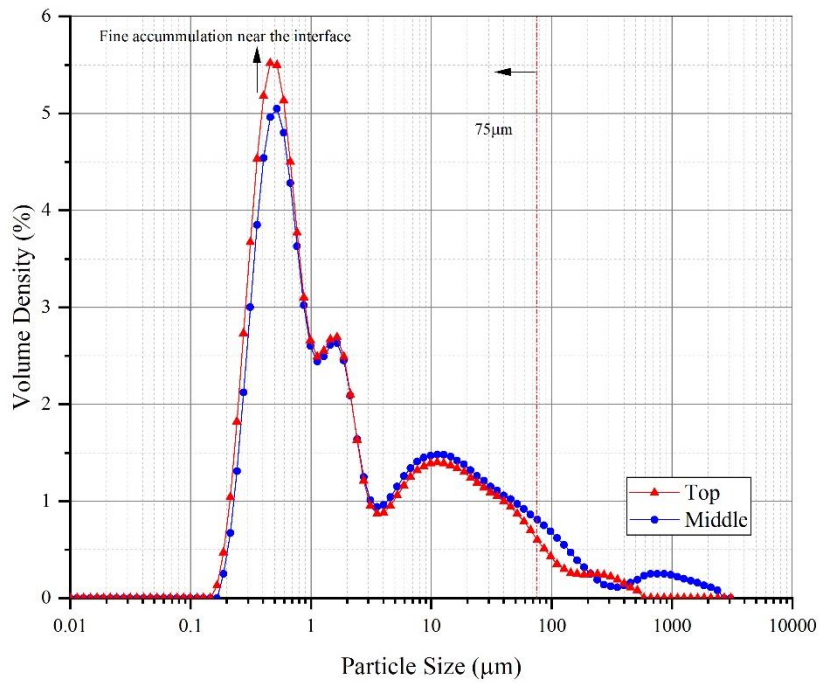
Figure 6. 27: Fine particle accumulation under cyclic load for Test G-70-3

6.4.3.5 Clogging and Interface (subgrade/geotextile) Confinement

Photos of the geotextiles tested under different frequencies are shown in Figure 6. 28 and 6.29.
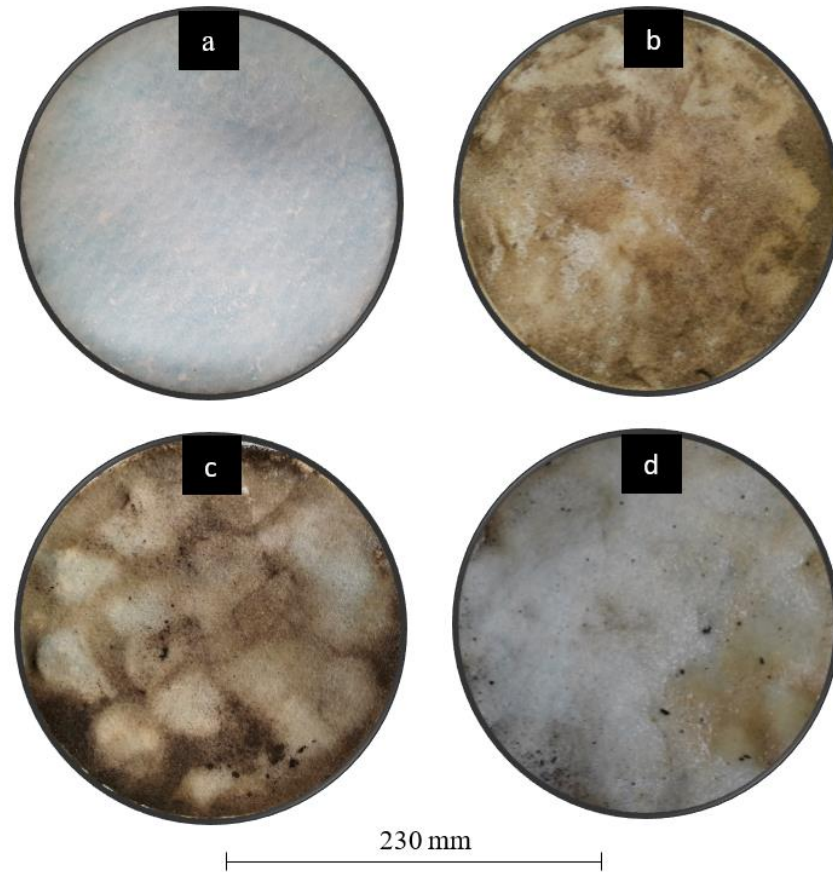
Figure 6. 28: Photos of (a) saturated geotextile and tested geotextiles after 100,000 cycles (b) Test G-70-1 (c) Test G-70-3, and (d) Test G-70-5
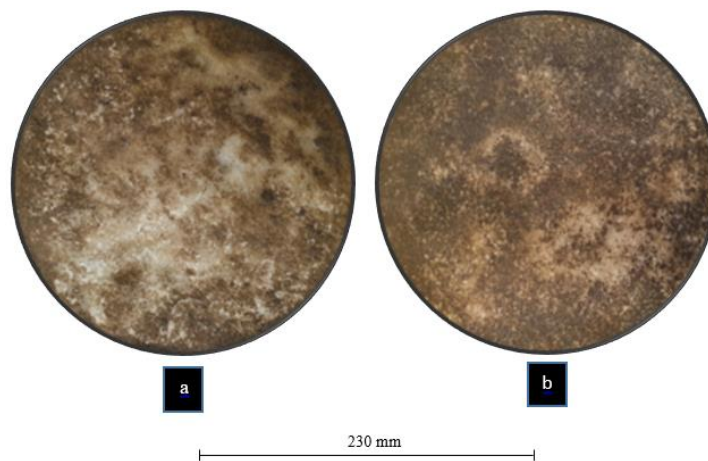
Figure 6. 29: Bottom surface of tested geotextiles (a) Test G-70-5 and (b) Test G-70-3

As shown in Figure 6. 28 and 29, severe clogging and migrated fine particles were observed at the interface in Tests G-70-1 and G-70-3, unlike G-70-5, due to cyclic loading.

6.4.3.6 Water Content

The soil had a water content close to the LL, thus creating more potential for the subgrade fluidisation described under Tests T1 and T2. However, the water content near the subgrade/ballast interface can be reduced by the inclusion of geocomposites. As Figure 6. 30 shows, the water content of the top and middle soil was greatly reduced in Test G-70-5. However, there was a considerable increase in the water content (around 3%) under lower frequencies, which shows that geotextiles could not maintain a lower water content/almost dry conditions at the interface.
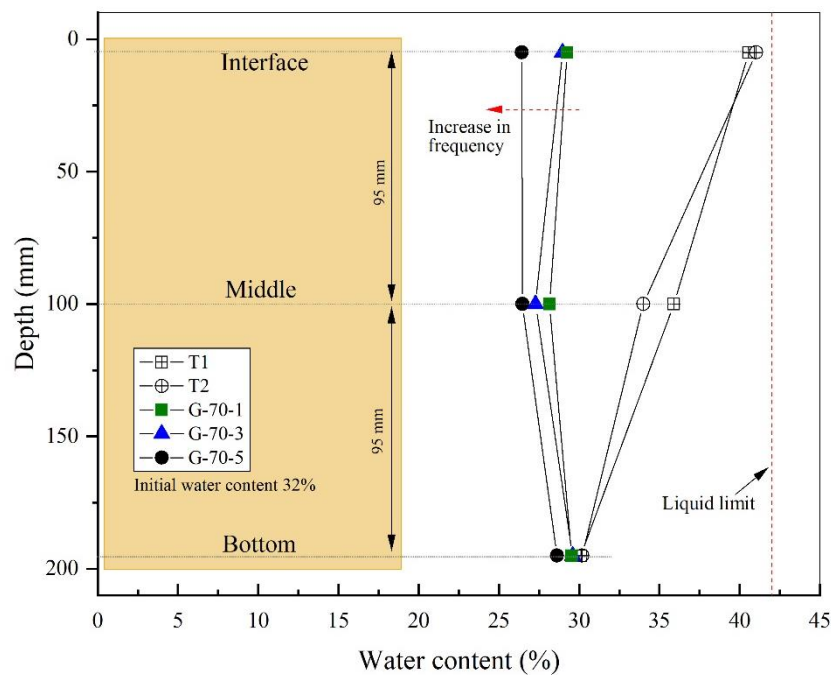
Figure 6. 30: Water contents after N = 100,000 cycles (Tests T1, T2, G-70-1, G-70-3, and G-70-5: after Arivalagan et al. (2021))

6.5 Chapter Summary

This chapter discussed the role of geotextiles as a drainage medium and filter in railway tracks to prevent particle migration and associated subgrade fluidisation under different axle loads and speeds by simulating typical railway track conditions. Unlike in undrained and free drainage conditions, the inclusion of geocomposites (G1 and G5) could dissipate the EPWP, reduce overall deformation, and prevent fine particles from migrating in the middle or lower regions under the same loading conditions (σ_{max} = 70 kPa). However, the EPWP that developed in the critical layers for G2 and G3 were higher than EPP_{T1} (22 kPa) at 10,000 cycles, and the rate of dissipation was not significant as the number of cycles increased. Furthermore, geotextiles G2, G3, and G4 could not prevent particle migration, and they became severely clogged with fine particles trapped inside the fibres. Although the aperture size of the filter (G1 and G5) was less than 10μm, it still provided enough drainage to alleviate the EPWPs that developed near the interface and prevent particle separation/migration under cyclic loading.

The EPPGs generated by cyclic excess pore water pressure were measured at different soil layers; this showed the temporal variation in local hydraulic force that developed within the subgrade soil, which can transport fines from the middle region towards the top. The variations in the particle size distributions and changes in the moisture content of the soil explain the phenomenon of subgrade fluidisation under train loading. The abrupt change in the moisture content and the migration of finer fractions (less than 75 μm) were captured as the cyclic deviatoric stress increased. A micro CT Scan was also used to examine the cross-sections of cored soil specimens after cyclic loading at the top and middle layers. The laboratory results from the 'dynamic filtration apparatus', proved that the potential for fines to migrate can become less as the cyclic stress decreases, and subgrade fluidisation can also be triggered at lower frequencies in tracks under critical hydraulic conditions.

CHAPTER 7: DESIGN GUIDELINES

USE OF GEOSYNTHETICS IN RAIL TRACKS VULNERABLE TO MUD PUMPING

This chapter provides practical guidelines and design criteria to select the geotextiles/filters to control the risk of mud pumping in soft soils, based on the research findings described in the previous chapters.

7.1 Track Substructure

Rail track substructure includes ballast, subballast, and subgrade. Ballast is the uppermost layer, it is about 250 - 350 mm thick and acts as a load-bearing platform which facilitates the drainage of water, and uniformly distributes the load towards subballast and subgrade. The subballast or compacted sand blanket is a granular layer between the ballast and the subgrade. The subbalast consists of well-graded crushed rock with a thickness that varies from 100 – 150 mm and this prevents ballast from penetrating into the soft soil and also reduces the upward migration of fines during the passage of trains. Subgrade can be a treated soil or fill material when natural soil does not have enough bearing capacity to withstand train loads. The subgrade should support the track structure, accommodate the stresses transferred by repetitive cyclic loads, and also prevent failure or excessive deformation. The deterioration of subgrade soil due to mud pumping dramatically affects the performance of railway tracks.

7.2 Mud Pumping Mechanisms

Saturated subgrade is more prone to instability under repetitive cyclic loads due to the accumulation of excess pore water pressure and extreme upward hydraulic gradients. The

process whereby fine particles in the form of slurry, infiltrate into ballast is commonly known as mud pumping (Singh et al. 2020; Yu et al. 2016). The subgrade mud pumping site near Wollongong city in New South Wales is shown in Figure 7. 1. The fouled ballast (i.e. coarser ballast particles coated by fines/slurry) will immediately lose its shear strength and drainage capacity and can no longer withstand greater axle loads. The adverse effects of mud pumping result in ballast degradation and differential settlements, and thus lead to frequent maintenance activities in railway tracks.

7.3 Characteristics of Vulnerable Subgrade Soils

Apart from adverse drainage conditions and train loading, the properties of subgrade soil can influence the occurrence of mud pumping. Table 7. 1 and 7.2 summarise the characteristics of subgrades and subsoils (from previous studies) collected from mud pumping sites. The liquid limit (LL) of the subgrade varies between 20 and 50, whereas the plasticity index (PI) is below 30. According to the Unified Soil Classification System, most of the soils can be classified as low to medium plasticity of inorganic clay. These soils are more prone to dislodge fines into the upper coarse layers under an excessive hydraulic gradient induced by cyclic loads (Nguyen et al. 2019).

Figure 7. 1: Subgrade mud pumping and loss of contact between sleeper and ballast (Courtesy: Prof Buddhima Indraratna)

Table 7. 1: Characteristics of soil subjected to mud pumping reported in previous studies

Mud pumping sites/References	Soil description	Country/location	LL	PI	Particle size
Ayres (1986)	Marine deposited calcareous clay	Lower Lias, UK	44	24	95% finer than 63 μm
Raymond (1986)	El Dorado Fill plastic clay	Kansas, USA	48	30	99% finer than 60 μm
Boomintahan & Srinivasan (1988)	Attipattu Clayed silt	Attipattu, India	45	27	67% silt and 12% clay
Rollin et al. (1990)	Non-plastic silt (S1 & S2) & plastic clay (C3)	Canada			75% finer than 75 μm
Alobaidi & Hoare (1994),(1999)	Silty clay with medium plasticity (Keuper Marl)	Birmingham, UK	49	26	
Hayashi & Shahu (2000)	Shirasu soil (SW)	Kagoshima, Japan			10% silt and 82% sand
Voottipruex & Roongthanee (2003)	Inorganic clay with low to medium plasticity	Thailand	43	21	77% finer than 75 μm
Muramoto et al. (2006) & Muramoto & Nakamura (2011)	Arakida clay	Japan	49.9	22	50.6% silt and 46.6% clay
Trinh et al. (2012)	Finely grained soil (CH)	Lyon, France	57.8	24.1	98% finer than 100 μm
Liu et al. (2013)		China	23	12	
Duong et al. (2014)	70% crushed sand & 30% kaolin	France	27	11	95% finer than 80 μm
Chawla & Shahu (2016)	Dhanaury clay (CI)	India	36	15	99% finer than 60 μm
Chawla & Shahu (2016)	Delhi Silt (ML)	India	25.5	5	40% finer than 70 μm
Hudson et al. (2016)	Alluvial clay, silt and sand	UK			
Kuo et al. (2017)	Out of 30 sites 50% are ML (mud)	Hsinchu, Taiwan			25-80% finer than 75 μm
Wheeler et al. (2017)	Peat subgrade	Canada			
Indraratna et al. (2020)	Low plasticity clay (CL)	Australia	26	11	30% finer than 75 μm

Table 7. 2: Properties of subgrade at South Coast (SC) rail line, NSW, Australia (Nguyen & Indraratna 2021)

Location	Liquid Limit (LL)	Plastic Limit (PL)	Specific gravity (Gs)	Hydraulic conductivity (m/s)	Fine percentage (%) (< 0.075 mm)
Helensburgh A	30	23	2.56	4.3×10^{-6}	26.3
Helensburgh B	23	18	2.51	9.1×10^{-6}	28.9
Otford A	21	16	2.51	1.1×10^{-5}	19.8
Otford B	23	17	2.50	7.8×10^{-6}	36.7
Clifton	38	18	2.69	6.1×10^{-7}	51.7
Austinmer	24	19	2.53	6.5×10^{-6}	45.3
North Wollongong	27	20	2.43	2.8×10^{-6}	54.5
Coniston A	44	22	2.65	1.7×10^{-7}	78.9
Coniston B	40	20	2.66	2.3×10^{-7}	72.2
Dapto A	39	22	2.62	7.2×10^{-7}	58.4
Dapto B	38	20	2.67	6.8×10^{-7}	58.6
Croom	37	19	2.69	6.6×10^{-7}	59.5

7.4 Functions of Geotextiles

Subgrade instability, including mud pumping in railway tracks, are associated with high in-situ water content and poor drainage conditions, especially after heavy rainfall. The migrated fines can clog the pores of subbase (road) or subballast (railway tracks), and thus impede the drainage capacity. As the drainage capability of tracks decreases (i.e., poor drainage/undrained conditions), the pore water pressure cannot be dissipated swiftly enough, which leads to softening and pumping failure.

An effective filter must withstand the pressure applied by the soil and the water by retaining the soil particles within the subgrade in order to prevent piping and excessive clogging. There can be an initial migration of particles through geotextiles that follow a stable bridging network at the geotextile/subgrade soil interface. Several studies that have proposed geotextile retention criteria are listed in Table 7. 3 (Giroud 1982; Holtz et al. 1997; Lafleur et al. 1996; Luettich et al. 1992).

The primary functions of a geotextile in railway tracks can be summarised as follows:

- o Separation: to maintain the integrity of subgrade and the functionality of ballast, i.e., to prevent the intrusion of ballast into fine particles and the pumping of fine particles into ballast

- o Filtration: to retain fine-grained subgrade soil from migrating to geotextiles or ballast

- o Drainage: to provide enough drainage of water to minimise the build-up of EPWPs during train loading

The aperture opening size (O_{95}) in combination with the constriction size distribution curve (pore structure) of a geotextile primarily controls the filtering performance of soft vulnerable soils. It is noted that satisfying these design criteria enables stable filtration and appropriate drainage capacity while it controls excessive amount of fine particles from

being pumped through the geotextiles (Bhatia & Huang 1995). There can be initial migration of particles through the geotextiles that follow a stable bridging network at the geotextile/subgrade soil interface. However, internally unstable soils are more prone to excessive particle migration (fines) through the pore opening of geotextiles. Based on laboratory observations, the uniformity coefficient of soil was considered to propose the retention criteria listed in Table 7. 3.

Table 7. 3: Retention criteria of a soil/geotextile filtration system

Criterion	Conditions	References
$\dfrac{O_{95}}{d_{85}} \leq 1-2$ $\dfrac{O_{95}}{d_{15}} < 1 \ or \ \dfrac{O_{50}}{d_{85}} \leq 0.5$	Dependent on subgrade soil type and C_u Dynamic, cyclic flow	Christopher & Holtz (1985)
$\dfrac{O_{95}}{d'_{50}} \leq 9/C'_u$ $\dfrac{O_{95}}{d_{10}} < 2.5 \ and \ O_{95} < d_{90}$	$C_u' > 3$ loose soil $C_u > 5$, dynamic flow with mild water currents	Luettich et al. (1992)
$\dfrac{O_{95}}{d'_{50}} < \dfrac{9}{C'_u} \ for \ C'_u > 3$	Soil retention criteria	Giroud (1982)
$\dfrac{O_{95}}{d_{85}} < 0.65 - (0.05C_c) \ C_c > 7$ $\dfrac{O_{95}}{d_{85}} < 2.71 - (0.36C_c) \ C_c < 7$	$n < 60\%$	Bhatia & Huang (1995)
$O_{95} < d_{85}$	$n > 60\%$	Bhatia & Huang (1995)
$\dfrac{O_{50}}{d_{85}} < 0.5$	O_{50} of a geotextile	Christopher & Holtz (1985)

$$AOS < \frac{18}{C_u} d_{50}$$ $$AOS \leq 0.5 d_{85}$$	non-woven geotextiles on non-cohesive silty soil	Koerner (2012), Narejo (2003), Kermani et al. (2019)
$$O_{95} < (2.71 - 0.36 C_c) d_{85}$$ $$C_c < 7 \text{ and} < O_{95} < (0.65 - 0.05 C_c) d_{85}$$ $$C_c > 7; \text{ and } O_{95} < (9 * d'_{50}) C'_u$$	Internally unstable soils	Luettich et al. (1992)

Notes: AOS is the Aperture opening size; n is the porosity of the geotextile; O_y is the pore opening size such that Y% of the pores are smaller than that size; d_x is the fine soil particle size in mm for which X% of the soil is finer; C_c is the Coefficient of Curvature; C_u' is the linear coefficient of uniformity; C_u is the coefficient of uniformity of the subgrade soil, and d'_{50}, d'_{100} and d'_0 are equivalent to the d_{50}, d_{100} and d_0 that obtained from the straight line approximation of the PSD.

Table 7. 4: Geotextile specifications

	Tests	Standard	Unit	Geocomposite with a filter membrane G1	Track bed separator G2	Robust separator G3	Track bed Separator G4
Mechanical	Tensile strength	EN ISO 10319	kN/m	50	52.5	30	22
	Tensile Elongation	EN ISO 10319	%	75	60	80	60
	CBR Puncture Resistance	EN ISO 12236	kN	10	9	5	4.3
	Cone drop test	EN ISO 13433	mm	<1	2	5	22
Hydraulic	Aperture Opening Size (AOS)	EN ISO 12956	μm	<10 (membrane filter) 75 (non-woven geotextile)	60	75	60
	Permeability	EN ISO 11058	m/s	0.03	45	40	30
Durability	Microbiological resistance	EN 12225	%	No loss	No loss	No loss	No Loss
	Resistance to acids and alkalis	EN 14030	%	No loss	No loss	No loss	No Loss
	Oxidation at 85 days (100 years)	EN 12226	%	>90	>90	>90	>90
	Weathering (UV Exposure)	EN 12224	%	>90	>90	>90	>90
Physical	Thickness (nominal)	EN ISO 9863	mm	4.5	2.5	3.5	2

7.5 Performance of Geotextiles

The specifications for different geotextiles and geocomposite are listed in Table 7. 4. Based on the dynamic filtration test reported by Arivalagan et al. (2021), the performance of different geotextiles (G1, G2, and G3) under cyclic loading can be summarised as shown in Tables 7. 5 and 7.6. The selected geotextiles and geocomposites are based on the retention criteria proposed in previous studies (Table 7. 3). Cyclic tests were carried out using different nonwoven geotextiles and geocomposites under a typical train loading. Later, the effectiveness of geocomposite G1 with a filter membrane was assessed under typical axle loads and the speeds of heavy haul trains.

7.5.1 Cyclic load and frequency

A uniform normal stress was applied as a minimum vertical stress, while the sinusoidal vertical cyclic stress (σ_{min} = 30 kPa and σ_{max} = 70-100 kPa) simulates a maximum axle load of up to 35 tonnes. The frequency varied between 1 Hz and 5 Hz, corresponding to a train speed of 45- 225 km/h (Indraratna et al. 2020c; Mamou et al. 2017; Powrie et al. 2007).

Table 7. 5: Effectiveness of different geotextiles (Arivalagan et al. 2021)

Geosynthetics	G1	G2	G3
Separation	✓	✓	✓
Filtration	✓	✗	✗
Drainage	✓	✗	✓
Clogging	✓	✗	✗

✓ effective
✗ ineffective

Notes: If a geotextile/geocomposite fails to provide one of the primary functions (retention, permeability, and clogging criteria) under cyclic loading, it is considered as an ineffective filter/separator at the subgrade surface. The selected geotextile/geocomposite could no longer provide track stability and did not satisfy the design requirements of effective geosynthetic filters.

7.5.2 Dynamic Filtration Tests

The tests showed that geotextiles with larger pore openings such as G2 and G3 could not prevent particle migration and became clogged with fines. The dissipation rate of excess pore water pressure was also lower than G1, thus showing its inability to provide sufficient drainage at the interface. Geocomposites with fliter membrane effectively reduced the accumulation of excess pore water pressure with time and prevents particle migration through the interface.

Table 7. 6: Performance of Geocomposite (G1) under different axle loads and speeds (Arivalagan et al. 2021)

The mean cyclic stress (kPa)	Frequency of loading (Hz)	Separation	Filtration	Drainage
50	5	✓	✓	✓
57.5	5	✓	✓	✗
65	5	✓	✗	✗
50	1	✓	✗	✗
50	3	✓	✓	✓
50	5	✓	✓	✓

✓ effective
✗ ineffective

The loading frequency on subgrade soil is mainly affected by the train speed, the carriage length, the bogies, and the distance between axles. Larger axial strains and EPWPs can develop at lower frequencies with increasing loading cycles (Indraratna et al. 2020; Konrad & Wagg 1993; Procter & Khaffaf 1984; Wichtmann et al. 2013; Zhou & Gong 2001). Wheeler et al. (2017) reported that a single train passing at approximately 40 km/h (25 miles/h) could pump fluid and fines upwards.

G1 could prevent the migration of particles and provide adequate drainage to the subgrade surface at lower axle loads (25-30 tonne axle load), but during the passage of heavy haul trains with an axle load up to 35 - 40 tonnes, the ability of G1 to prevent subgrade fluidisation and associated mud pumping diminished.

7.6 Critical Factors that Affect the Performance of Geotextiles

Conventional methods such as the removal of fouled ballast, maintaining the ballast shoulders, side ditches, and drainage system, will improve the overall drainage capacity of a track, however, the inclusion of geosynthetics is an effective way of stabilising vulnerable subgrade soils under poor drainage conditions. If the cyclic stress that is transferred to a subgrade is within an acceptable level, geocomposite with an effective membrane can be a substitute for a compacted capping layer in railway tracks. Furthermore, geosynthetics can also prevent severe particle migration and soil softening and provide additional confinement at the interface (Arivalagan et al. 2021; Kermani et al. 2019). However, over the long term, the unacceptable performance of geotextiles can be observed under adverse hydro-dynamic conditions (i.e., critical loading exceeds 40 tonnes or severely clogged geotextiles create undrained conditions or wheel imperfections). Field investigations shows large dynamic impact stresses (over 400 kPa) can be developed due to wheel imperfections (wheel-flats) and should be assessed in track designs (Indraratna et al. 2010a). In fact, a series of cyclic tests would be required to assess the following functions of other geotextiles in relation to subgrade soil.

- Characteristics of the geotextiles: porosity, thickness, primary and secondary bonding mechanism, pore size distribution, constriction size distribution

- Properties of the soils: water content, plasticity, porosity, degree of compaction, state of stress, specific gravity, constriction size distribution, grain size analysis

- Filtration performance and drainage capacity at the interface of ballast and subgrade under critical dynamic loading

- Drainage conditions: Rainfall intensity, rise in the water table, degree of saturation of subgrade soil, slopes of formation, side ditches, cess drain (ag-pipes).

7.7 Geotextile Filter Design

An effective filter must withstand the pressure applied by the soil and the water by retaining the soil particles within the subgrade in order to prevent piping and excessive clogging. There can be an initial migration of particles through geotextiles that follow a stable bridging network at the geotextile/subgrade soil interface. Geotextile filters should have a significant number of pore openings, even if soil particles block/clog a few openings. Adequate drainage at the interface can only prevent subgrade instability. To select an effective geotextile filter, the material properties should satisfy the required properties;

a.   maximum allowable apparent opening size (O_{95}) of the geotextile

b.   allowable constriction size distribution curve of the geotextile filter

c.   minimum allowable permeability or permittivity of the geotextile

d.   minimum allowable porosity (n), or percent open area (POA) of the geotextile

e.   minimum allowable physical strength requirements of the geotextile

f.   adequate durability of the geotextile

Critical applications such as subgrade fluidisation may result in retention failure and thus may require additional laboratory and/or field tests prior to the field application. Luettich et al. (1992) reported that retention, lower bound retention, clogging, survivability, durability and abrasion testings are required to perform complete geotextile filter design, more than rely on retention and permeability criteria. Other design considerations, such as boundary conditions and the internal stability of the soft soil, must be included in the design process. Dynamic flow conditions in soft soil foundations have the potential to disturb the internal stability of the base soil and/or the geosynthetic interface. Furthermore, a stable soil/geotextile interface cannot be reached under adverse hydro-dynamic conditions (Hameiri 2000). Arivalagan et al. (2021) reported that geotextiles/geocomposites might perform well at lower axle loads, however, their ability to prevent particle migration and mitigate subgrade fluidisation or associated mud pumping can diminish under increased cyclic stress. In this instance, the existing design criteria proposed in common design

practice, which have not been explicitly validated from laboratory results, cannot be used.

Additional large-scale tests are required before the field application.

CHAPTER 8: EFFECTIVENESS OF A COMBINED PREFABRICATED VERTICAL DRAIN-GEOCOMPOSITE SYSTEM IN PREVENTING SUBGRADE INSTABILITY

8.1 Introduction

Over the past few decades, numerous investigators have reported the use of Prefabricated Vertical Drains (PVDs) in weak soils (Gao & Zhang 2020; Guo et al. 2018; Hansbo 1981; Holtz et al. 1991; Indraratna et al. 2009; Indraratna et al. 2011b; Lorenzo et al. 2004). The installation of PVDs is one of the most cost-effective methods for improving soft clays compared to other ground improvement techniques. PVDs can continuously dissipate the EPWPs that can develop in subgrade, even after the passage of trains, making the tracks more stable for the next train loading. Indraratna et al. (2009) reported that installing PVDs at shallow depths (within 6-8 m) can prevent the generation of critical EPWPs during cyclic loading, but there is no specific study into using a combined PVD-geocomposite system that would prevent subgrade fluidisation by simulating typical railway track conditions.

This chapter examines a combination of a geocomposite and PVDs to alleviate the occurrence of mud pumping. It describes how effectively a combined PVD-geocomposite system can prevent finer particles from migrating towards the ballast layer and reduce instability at the ballast/subgrade interface. Dynamic filtration tests (DFTs) were carried out to assess the fluidisation potential of soft soil by measuring the vertical and horizontal excess pore pressure gradients (i_V and i_H) that can develop as the number of cycles increases. The role that prefabricated vertical drains play in dissipating the EPWP

developed at greater depths was studied, and interfacial behaviour due to the inclusion of a PVD-geocomposite system (i.e., enhanced drainage capacity to prevent particle dislocation and pumping) were also discussed.

8.2 Experimental Setup

8.2.1 Prefabricated Vertical Drains (PVDs)

In this study, four miniature pressure transducers (MPs) were installed close to the vertical drain, as shown in Figure 8. 1, at 20, 40, 80, 120 mm from the interface. A 35-mm thick layer of ballast was placed onto the subgrade to evaluate the performance of a sole PVD under cyclic loading conditions. Details of the test procedures are given elsewhere in Chapter 3.
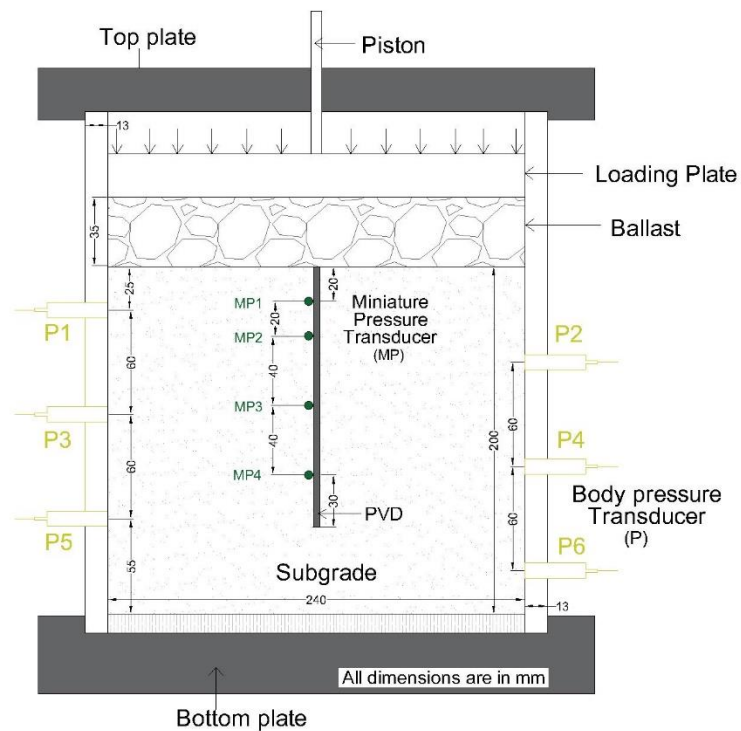
Figure 8. 1: Cyclic Tests using PVDs

8.2.2 A combined PVD-Geocomposite System

The appropriate use of geotextiles/geocomposites in railway tracks as a filter and a separator undoubtedly increases the stability of the substructure by dissipating the EPWP

at the ballast/subgrade interface, thus preventing the fine soils from infiltrating into the ballast layer with increased moisture content (Kermani et al. 2020; Singh et al. 2019). Geotextiles designed with a filter membrane can provide adequate drainage at the interface, but they cannot dissipate EPWP that develops at greater depths (Chapter 6). Geotextiles were generally effective at the subgrade/ballast interface, and they could dissipate the EPWP that developed near the interface when the soil was subjected to cyclic stress (Alobaidi & Hoare 1996; Arivalagan et al. 2021). In contrast, a short drain can dissipate the EPWP that develops deeper in the subgrade (up to 6 – 8 m in the field), and provide drainage in vertical and horizontal (radial drainage) directions. On this basis, a combined PVD-geocomposite system was selected for this study. Based on the results in Chapter 6, geocomposite G1 was chosen. The experimental setup for a combined PVD-geocomposite system is shown in Figure 8. 2.
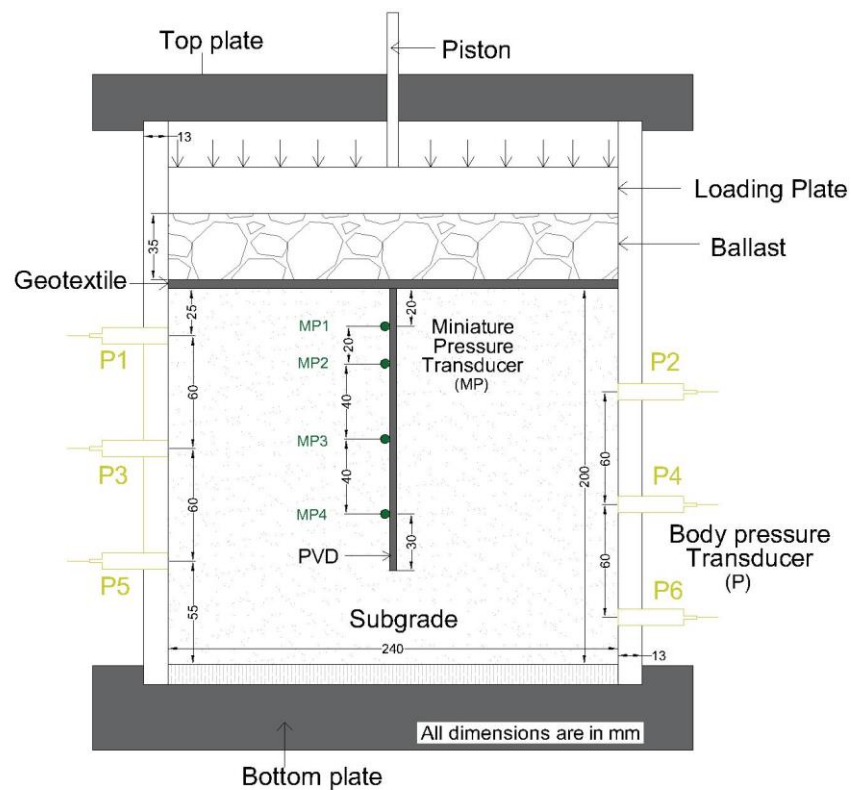
Figure 8. 2: A combined PVD and Geocomposite system

8.2.3 Preparation of PVDs

In practice, the vertical drains can be installed in a square or a triangular pattern, and the drain spacing (S) can be around 1 to 1.5. m. Furthermore, the corresponding equivalent radius of the influence zone (r_e) is 0.546S and 0.525S for drains installed in a square and triangular pattern, respectively. The available dynamic filtration setup was 240 mm in diameter and if a single drain is installed at the centre, the drain spacing (0.24 m) will be much smaller than the actual drain spacing. Therefore, PVDs with a modified size were adopted in this study. Additionally, this modification was based on the concept of the given time factor (T_h) and the average degrees of soil consolidation in the field and in the laboratory tests (Ni 2012).

For a given time factor (T_h), the average degree of consolidation in the field and the laboratory will be the same. For simplicity, an ideal drain was used to calculate the average degree of consolidation for the soil cylinder in the field as follows:

$$U_h = 1 - \exp\left(-\frac{8T_h}{\mu_I}\right) \qquad \text{Equation 7.1}$$

where $\mu_I = ln\left(\frac{r_{e,re}}{r_{w,re}}\right) - 0.75 \ and \ r_{e,re} = 600 \ mm$ which represents the radius of influence zone in the field.

According to Hansbo (1979) the equivalent radius of PVDs ($r_{w,e}$) can be calculated using Equation 7.2:

$$r_{w,re} = 2\left(\frac{a_{re} + b_{re}}{\pi}\right) \qquad \text{Equation 7.2}$$

where $a_{re} = 100 \ mm \ and \ b_{re} = 3.4 \ mm$, width and thickness of selected PVD

The average degree of consolidation for the soil cylinder in the field can be calculates using

Equation 7.1, where $\mu_{I,ex} = ln\left(\frac{r_{e,ex}}{r_{w,ex}}\right) - 0.75$ and $r_{e,ex} = 120$ mm which represents the

radius of influence zone of soil cylinder in laboratory.

$r_{w,ex}$ can be calculated using Equation 7.3:

$$r_{w,ex} = 2\left(\frac{a_{ex}+b_{ex}}{\pi}\right) \qquad\qquad \text{Equation 7.3}$$

Where $b_{ex} = 3.4$ mm and a_{ex} is the modified width that need to be calculated.

For any given time factor (T_h) the relationship between the average degree of consolidation of field $(U_{h,re})$ and laboratory $(U_{h,ex})$ conditions can be expressed as follows:

$$U_{h,re} = U_{h,ex} \qquad\qquad \text{Equation 7.4}$$

Therefore,

$$1 - \exp\left(-\frac{8T_h}{\mu_{I,re}}\right) = 1 - \exp\left(-\frac{8T_h}{\mu_{I,ex}}\right) \qquad \text{Equation 7.5}$$

$$\mu_{I,re} = \mu_{I,ex}$$

$$ln\left(\frac{r_{e,re}}{r_{w,re}}\right) = ln\left(\frac{r_{e,ex}}{r_{w,ex}}\right)$$

$$\left(\frac{r_{e,re}}{r_{w,re}}\right) = \left(\frac{r_{e,ex}}{r_{w,ex}}\right)$$

$$r_{w,ex} = r_{e,ex}/\left(\frac{r_{e,re}}{r_{w,re}}\right) \qquad\qquad \text{Equation 7.6}$$

From Equation 7.6: $r_{w,ex} = 13.17$ mm

From Equation 7.3: $r_{w,ex} = 2\left(\frac{a_{ex}+b_{ex}}{\pi}\right), a_{ex} = 17.3$ mm

The size of the modified PVDs used in the dynamic test was 17.3 mm x 3.4 mm.

8.3 Experimental Results and Discussion

The effectiveness of PVDs (**Test P**), Geocomposite (**Test G**), and PVDs combined with the geocomposite (**Test P+G**) were evaluated and then the results were compared to the undrained (**Test U**) and free drainage (**Test F**) tests.

8.3.1 Excess pore water pressures (EPWPs)

Figure 8. 3 shows that the EPWP developed in Test P is much lower than Test G, even from the beginning of the cyclic test. For example, the rapid generation of EPWP in Test G is more than 37 kPa at MP2 (@40 mm) after only 500 cycles, but it remains well below 22 kPa while using PVDs. Furthermore, the geocomposite in Test G could not dissipate the EPWP in the middle region of soil sample (i.e., at 40 and 80 mm from the interface) below 15 kPa until 30,000 cycles.
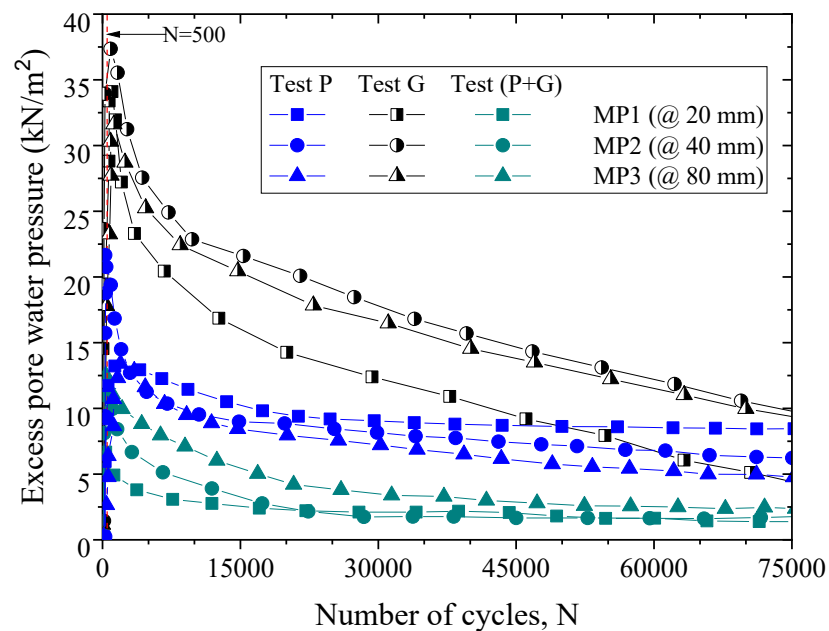
Figure 8. 3: Development of excess pore water pressure – Tests P, G and P+G (Arivalagan et al. 2022)

It is clear that when only using a geocomposite, the rate of excess pore water dissipation in Test G was higher near the ballast/subgrade interface (MP1) than the middle/shallow part

of the subgrade (MP2 and MP3). In contrast, the prefabricated vertical drain (Test P) dissipates the EPWP developed at greater depths, whereas the EPWP at MP3 remains less than 4 kPa after 75,000 cycles. Prefabricated vertical drains (Test P) could dissipate the EPWP to less than 15 kPa at all three depths after 2000 loading cycles, whereas the residual EPWPs near the interface are higher than those beneath because there is no more confinement at the ballast/subgrade interface in Test P (i.e., no capping).
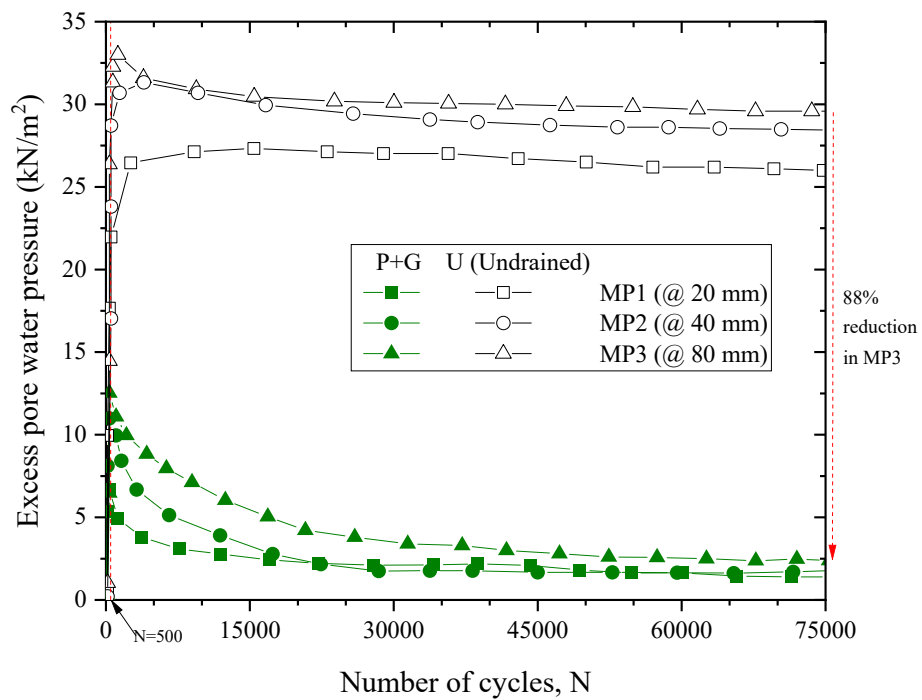
Figure 8. 4: Developed EPWPs – Tests U and P+G

As shown in Figure 8. 3, the magnitudes of EPWP that developed in Test G are more than 30 kPa at 500 cycles at all three depths; however, the presence of PVD (Test P) certainly dissipates the EPWPs, especially in the deeper layers of soil. Therefore, the values of EPWPs from Test P+G are less than 15 kPa within 500 cycles and less than 4 kPa after 75,000 cycles. On the other hand, although the undrained test (Test U) shows a maximum EPWP of more than 25 kPa at 75,000 cycles, there is approximately 88% reduction in EPWPs 80 mm under the interface due to the inclusion of the PVD-geocomposite system

shown in Figure 8. 4 (i.e., the EPWPs at MP2 and MP3 remain below 5 kPa). This proves

that a combined PVD and geocomposite (P+G) system can reduce the potential for

subgrade fluidisation during cyclic loading due to the continuous dissipation in EPWPs,

unlike in the undrained or free drainage tests.
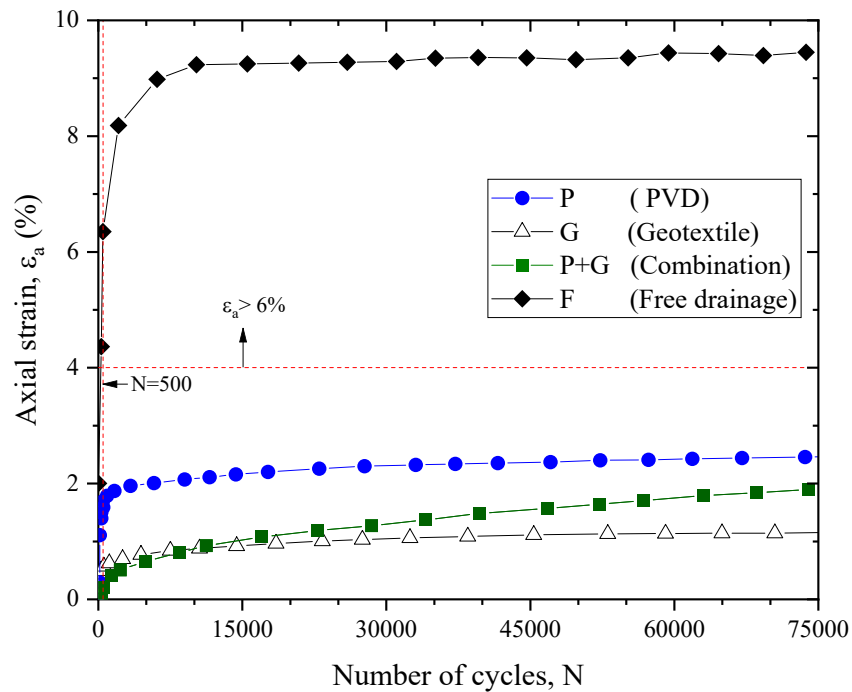
Figure 8. 5: Axial strain – Tests P, G, F, and P+G (Arivalagan et al. 2022)

8.3.2 Axial Strain

Figure 8. 5 shows that the axial strain developed in Test F reaches 6% before 500 cycles.

There was excessive axial deformation due to ballast penetrating into softened subgrade

soil, as well as a significant generation of EPWP at the interface in the free drainage test

(Test F). However, geosynthetic inclusions significantly reduce the rapid increase in axial

strain as the number of cycles increase. For instance, the axial strain in Test G is 56% less

than in Test P, while the axial strain in Test G is 1.2% at 75,000 cycles (Figure 8. 5). This

implies that a geocomposite (G) inclusion can prevent ballast fouling caused by interlayer mixing, and thus control axial development under cyclic loads.

8.3.3 Generation of excess pore pressure gradients (EPPG)

The body pressure transducers installed at six locations were used to calculate the EPPGs, as defined in Equation 5.1 (Chapter 5). Figure 8. 6 shows that the EPPGs in the middle and lower regions (i.e., Layers (3-2) and (4-3)) decrease significantly over time when both PVD and geocomposite are installed.
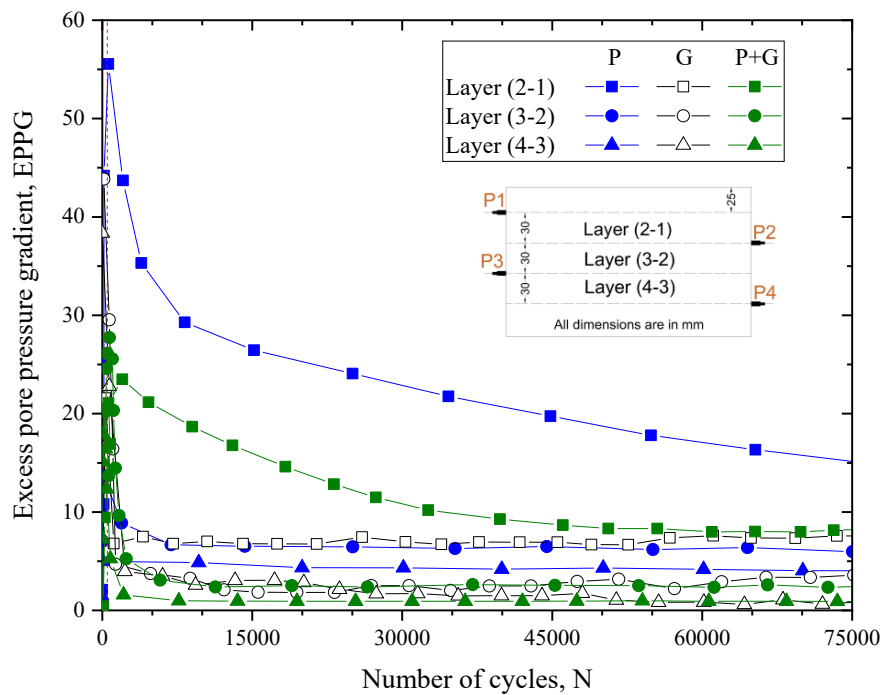
Figure 8. 6: Excess pore pressure gradient – Tests p, G, and P+G

The EPPG developed in Layer (4-3) approaches zero after 5000 cycles, thus confirming the ability of geosynthetics (P+G) to prevent the EPPGs from reaching a critical level. In Test G, the EPPG that developed close to the interface is much lower than Test P. A lower and vertical (upward) EPPG cannot create enough hydraulic force to dislocate the fines from the coarser fraction of the soil matrix, but the topmost layer (i.e., Layer (2-1)) has a higher EPPG (25 at 1000 cycles) because the increased local hydraulic gradient facilitates

182

surficial drainage through the pores of the geocomposite. In this case, a rapid increase in EPPG near the interface without further continual reduction may pump the fines up through the geocomposite. For instance, the critical EPPGs in Layers (3-2) and (4-3) exceed 40 in Test U, which shows the increased potential for the subgrade fluidisation described in Chapter 5.

8.3.4 PSD and Clogging

The increase in the fine percentage and the formation of slurry near the subgrade surface (abrupt change in the water of soil) were used to assess the potential for subgrade fluidisation in several studies (Arivalagan et al. 2021; Indraratna et al. 2020a; Indraratna et al. 2020b). Therefore, PSD and moisture content tests were carried out to measure variations in the particle size distribution and water content at the end of cyclic tests.
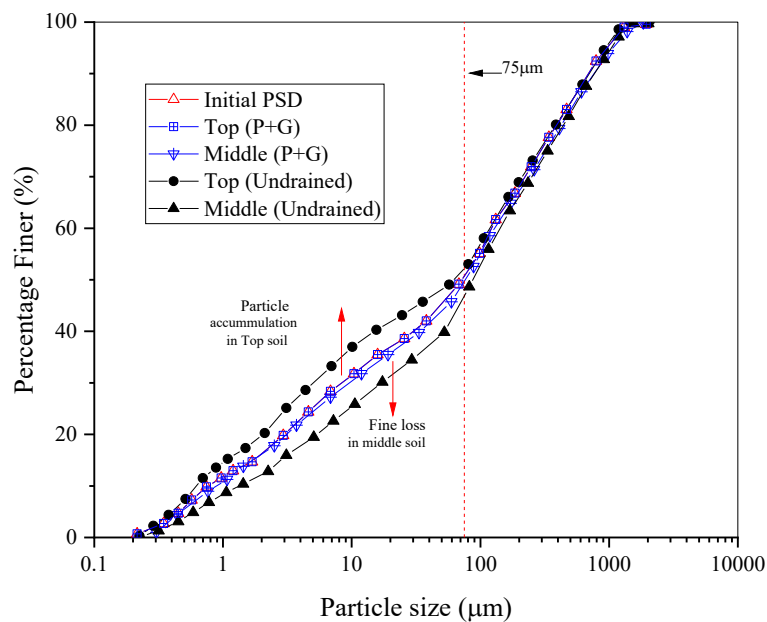
Figure 8. 7: Particle size distribution – Tests U and P+G

Figure 8. 7 shows a high particle migration from the middle of the soil towards the top in Test U, whereas particle migration is controlled better in Test P+G. The PSD of the top and middle specimens remains the same in Test P+G, and there is no sign of particle migration

during cyclic loading. This proves how effectively geocomposite and PVDs could prevent
particles from migrating towards the upper layers.
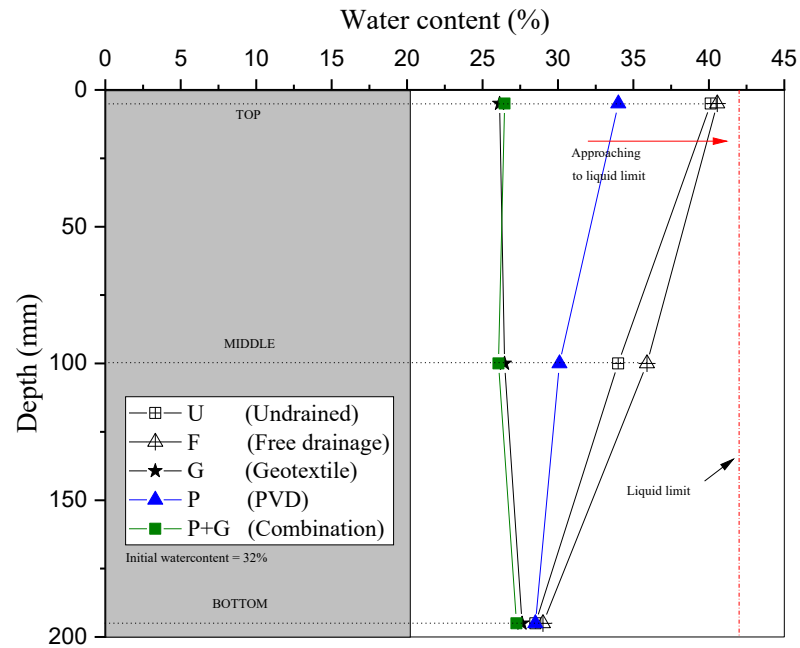
Figure 8. 8: Water content at 100,000 cycles – Tests U, F, G, P, and P+G (Arivalagan et al. 2022)

8.3.5 Water content

As shown in Figure 8. 8, PVD installed alone within subgrade soil cannot reduce the water content near the top surface; the water content in Test P is almost 35% at the interface (subgrade surface). During the test, fine particles with increased moisture accumulated near the interface due to ballast penetrating into the subgrade surface. However, the inclusion of geocomposite (in Test P+G) significantly reduces the water content and prevents the accumulation of fines from the middle layers. Since the variations in the water content in Tests G and P+G are similar, geocomposite on the top soil can help reduce the water content by providing adequate confinement and drainage capacity at the interface.

8.4 Radial Drainage

8.4.1 Experimental Setup

Miniature pressure transducers were installed at different locations from the centre (in radial direction 0,30, and 60 mm from the centre) to measure how much the prefabricated vertical drains could alleviate the EPWPs, as shown in Figure 8. 9.
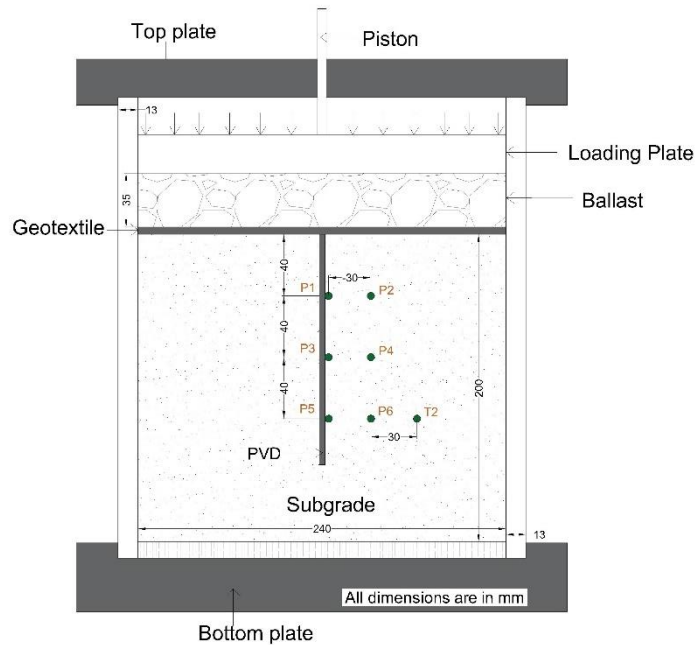
Figure 8. 9: MPs installed at different locations from the centreline

8.4.2 Results and Discussions

As Figure 8. 10 shows, six pressure transducers were installed at different depths and radial distances to evaluate the effect of the drainage path. As expected, the EPWPs measured at P1, P3, and P5 are the lowest because they have the shortest drainage paths at these locations, whereas the highest EPWP occurred at P6, which is further away from the centreline. Furthermore, the EPWPs that developed at P1, P2, and P5 approached zero after 180 minutes of cyclic loading, whereas the EPWPs measured at P2, P4, and P6 decreased continuously as the number of cycles increased; they were less than 12 kPa at the end of the cyclic test. This shows that PVDs can continually dissipate EPWPs during cyclic loading, and even during the rest period after each train passes by.
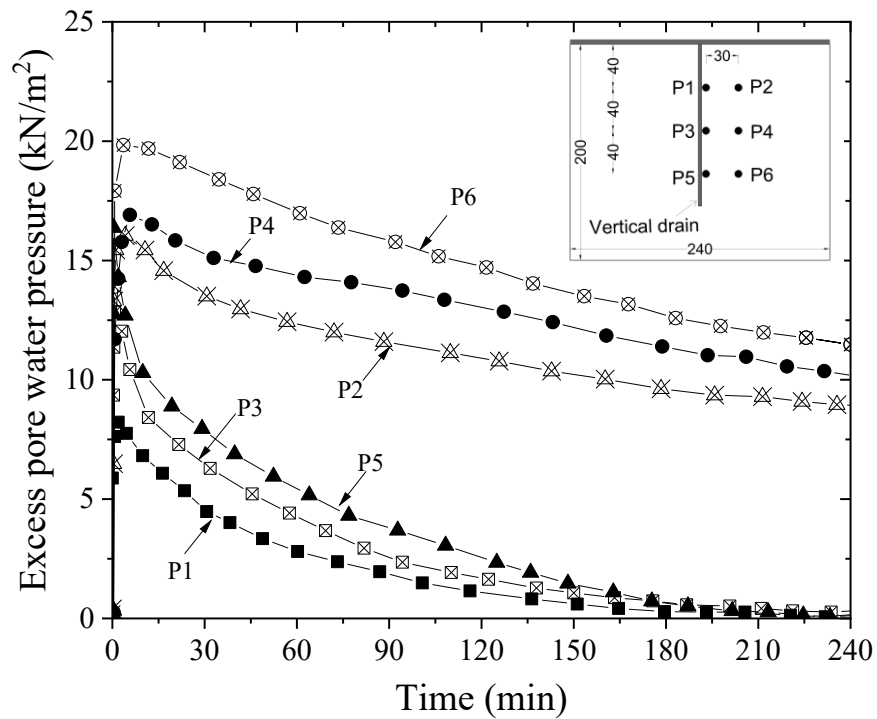
Figure 8. 10: Excess pore water pressure developed inside the subgrade soil (Arivalagan et al. 2022)

As Figure 8. 11 shows, the miniature pressure transducers were installed at 0 mm (Test T1) and 90 mm (Test T2) from the PVD to measure the generation of EPWPs. The EPWP measured at T1 (i.e., the shortest drainage path) is lower than at T2. Although the EPWP at location T2 may take much longer to dissipate than T1, the PVDs successfully dissipate them before reaching their critical values. Previous studies reported that soft clays with PVDs could not experience undrained failure even if the cyclic stress levels were higher than the critical cyclic stress levels (Indraratna et al. 2011a). The observations of cyclic loading in this study confirmed the fact that prefabricated vertical drains combined with a drainage filter (geocomposite at the interface) further reduce the development of EPWP, which suggests that a combined P+G system can increase track stability by preventing soil softening and subgrade fluidisation.
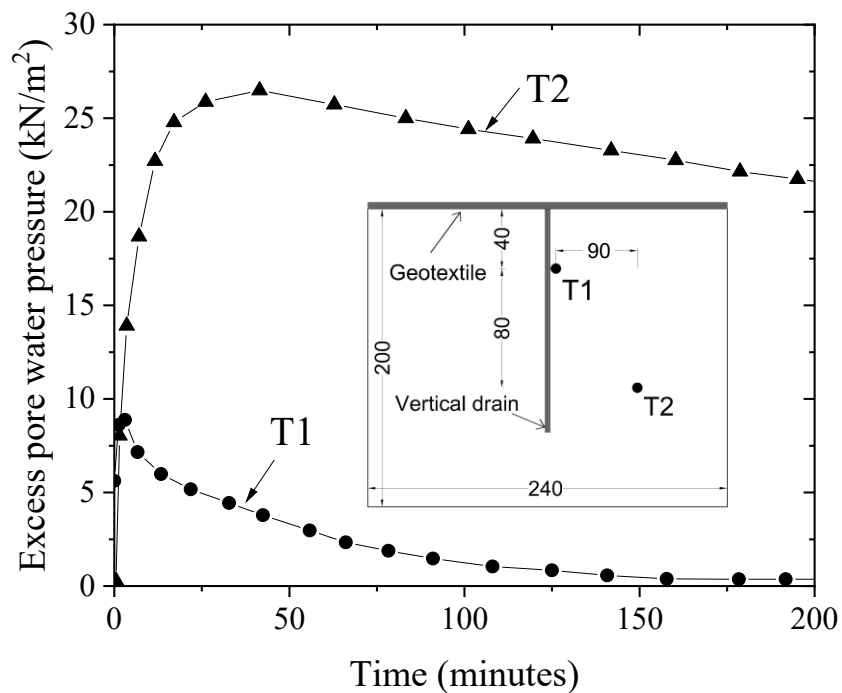
Figure 8. 11: Excess pore water pressure (T1 and T2)

8.4.3 Horizontal EPPG developed at Critical Layers of Subgrade

The miniature pressure transducers (P1 - P6) installed at various locations were also used to determine the time-dependent EPPGs in vertical and horizontal directions. Figure 8. 12 shows the disparity between vertical (i_V) and horizontal (i_H) EPPGs that developed with geosynthetic inclusions (i.e., a PVD-geocomposite system). In this case, radial drainage became predominant because the lateral EPPGs rapidly increased to more than 20 within 5 minutes of cyclic loading. The horizontal EPPGs in deeper soil ($i_{H(6-5)}$) developed to higher values than those at the top soil ($i_{H(2-1)}$) as the number of cycles increased. Moreover, the horizontal EPPGs remained above 30 until the end of testing, in fact they were approximately ten to twelve times greater than the vertical EPPGs (after 240 minutes of cyclic loading). This indicates that prefabricated vertical drains provide radial drainage and can thus minimise the development of EPWPs. This scenario was more visible in the deeper

layers; this continuous dissipation in EPWPs will make the track more stable for the next train loading.
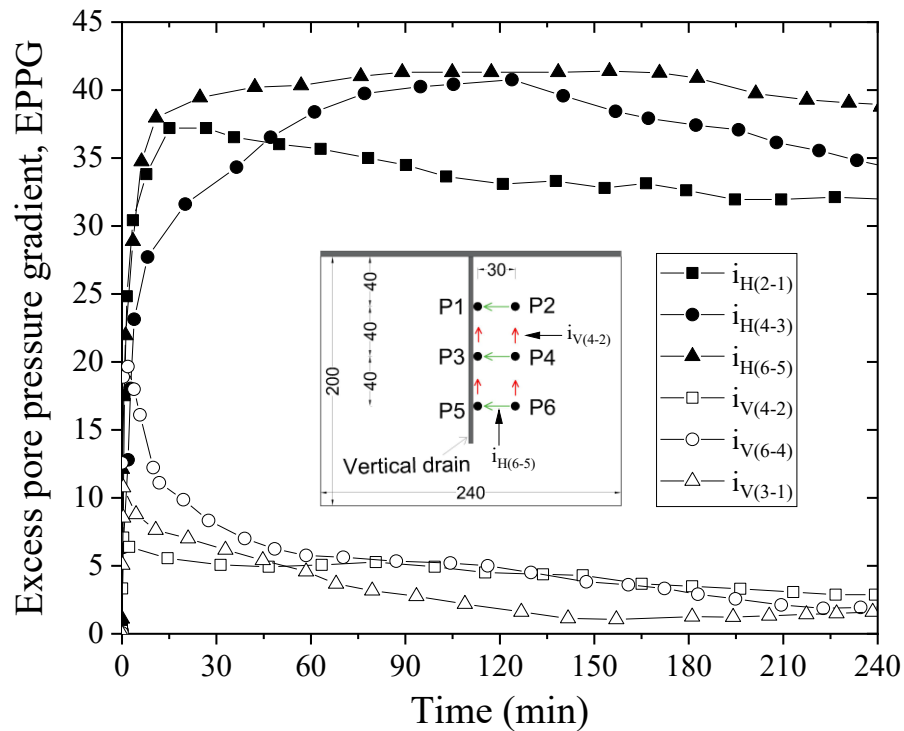
Figure 8. 12: Excess pore pressure gradient (Arivalagan et al. 2022)

8.5 Effects of Cyclic Stress and Frequency

8.5.1 Introduction

A combined PVD and geocomposite system quickly dissipated the EPWP and prevented particle migration through the pore openings under smaller axle loads (i.e., an axle load of 25 tonnes (5 Hz frequency) was considered in Section 7.3). Therefore, their effectiveness must be assessed by simulating different axle loads and speeds under a typical railway track environment (25 – 35 tonnes of axle load and 1-5 Hz frequencies were chosen). Geocomposite G1 was used in all six cyclic tests, as tabulated in Table 8. 1, and the role of a PVD-geocomposite system at preventing subgrade fluidisation is discussed in the following sections. In this case, Miniature Pressure Transducers (MPs) were installed 60 mm from the centreline/edge of the cylinder, as shown in Figure 8. 13.
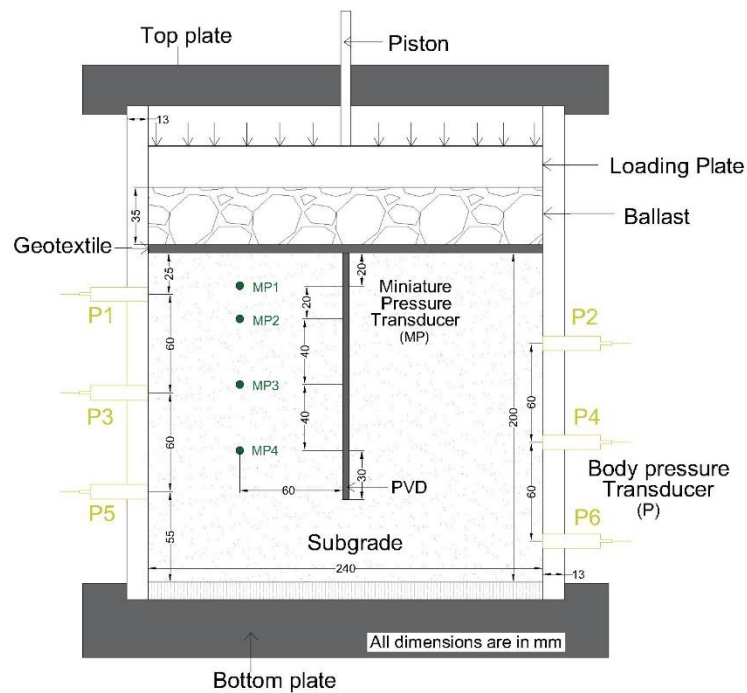
Figure 8. 13: Experimental setup under different cyclic stress and frequency

8.5.2 Effect of Cyclic Stress

This section examines the ability of a PVD and geocomposite system under three different

cyclic stresses (amplitude of 20, 27.5, and 35 kPa).

Table 8. 1: Effects of cyclic stress and frequency (Phase 6_Chapter 3)

Test Name	Drainage condition at the ballast subgrade interface	Testes Geosynthetics	σ_{min}	σ_{max}	Frequency (Hz)
PG-70-5	With P1+G1	PVD+Geocomposite (G1)	30	70	5
PG-85-5	With P1+G2	PVD+Geocomposite (G1)	30	85	5
PG-100-5	With P1+G3	PVD+Geocomposite (G1)	30	100	5
PG-70-1	With P1+G4	PVD+Geocomposite (G1)	30	70	1
PG-70-3	With P1+G5	PVD+Geocomposite (G1)	30	70	3
PG-70-5	With P1+G6	PVD+Geocomposite (G1)	30	70	5

8.5.2.1 Excess Pore Water Pressure

Figure 8. 14 shows that the rapid generation of EPWP in Test C100 at MP2 (@40 mm) approached 50 kPa prior to reaching 5000 cycles. However, the EPWPs in the top and middle layers (MP1 and MP3) continued to decrease due to the inclusion of PVD and geocomposite. For instance, the EPWPs that developed at MP1 and MP3 were less than 25 kPa under all three different cyclic stresses at 100,000 cycles. In essence, the rapid axial development was controlled using geosynthetics because the axial strain was only 3% and 2.2% after 100,000 cycles in Test C100 and Test C85, respectively. During cyclic loading, there was no continual particle migration through the pores of the geocomposite at the interface (under increased cyclic stress). This proves that the PVD-geocomposite system controlled the axial strain of the test specimen from the outset.
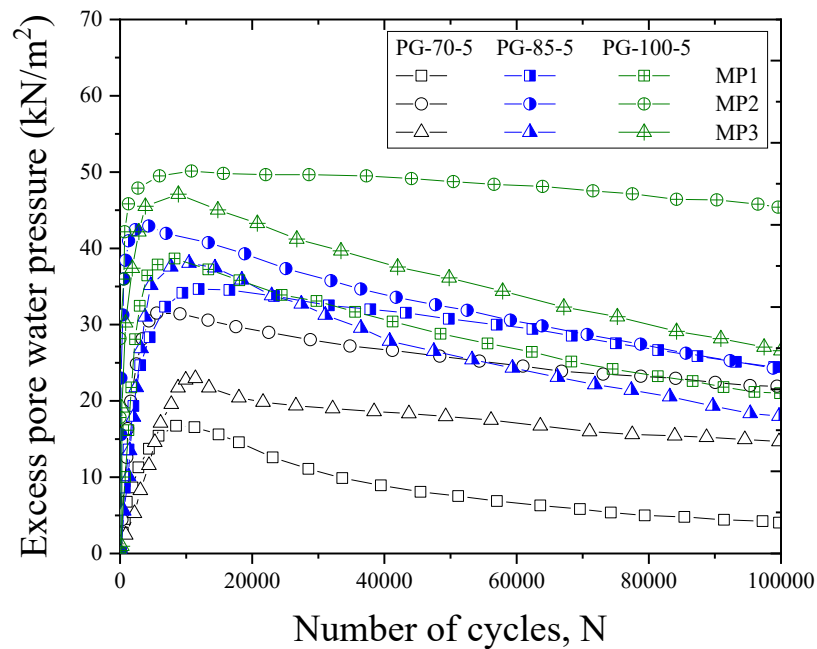
Figure 8. 14: Generation of excess pore water pressure under different cyclic stresses

8.5.2.2 Excess Pore Pressure Gradient

As shown in Figure 8. 15, the EPPGs in Layers (3-2) and (4-3) decrease to 13 and 3 respectively at 75,000 cycles in Test C85. Although the increase in EPPGs observed at the initial stage (<10,000 cycles) is significant, the combination of geocomposite and PVD reduces them at 75,000 cycles. For instance, the EPPGs developed at 75,000 cycles are less than 30. The lower the EPPG means there is less potential for an upward hydraulic force to dislocate particles inside the layers of soil.
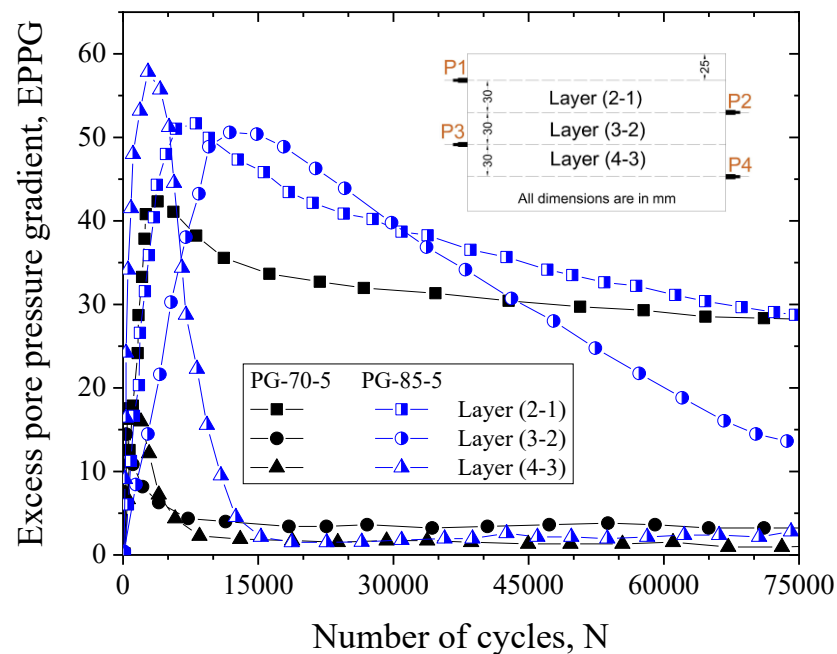
Figure 8. 15: Excess pore pressure gradient – Tests PG-70-5 and PG-85-5 (Arivalagan et al. 2022)

8.5.2.3 Water content and Particle Migration

The inclusion of PVD and geocomposite could prevent the water content close to the top and in the middle from approaching its liquid limit, by increasing the drainage capacity. For example, the soil at the top and middle layers contain less than 27% of water content in Tests PG-70-5 and PG-85-5, and there is only a 2% increase when the maximum cyclic stress increases to 100 kPa, as shown in Figure 8. 16.

191
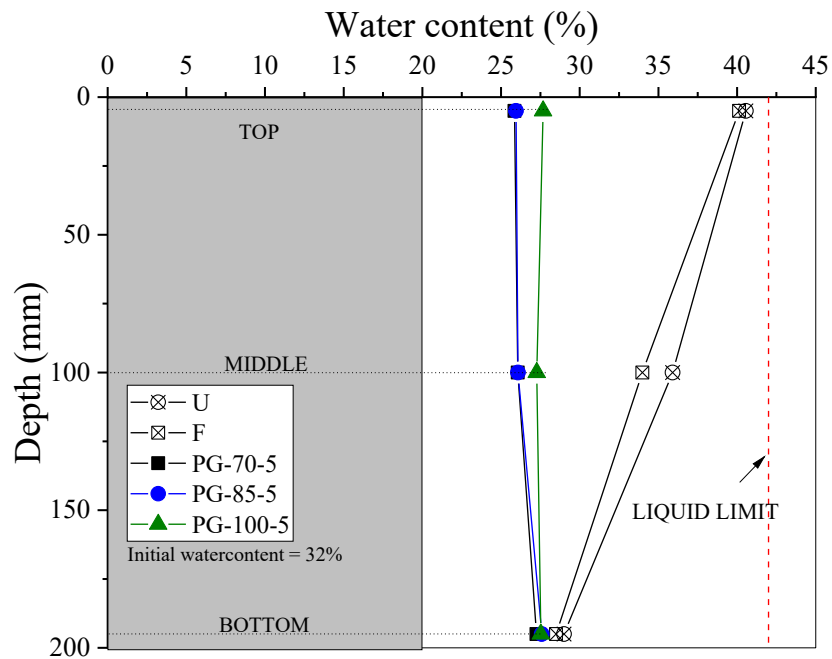
Figure 8. 16: Water content at 100,000 cycles
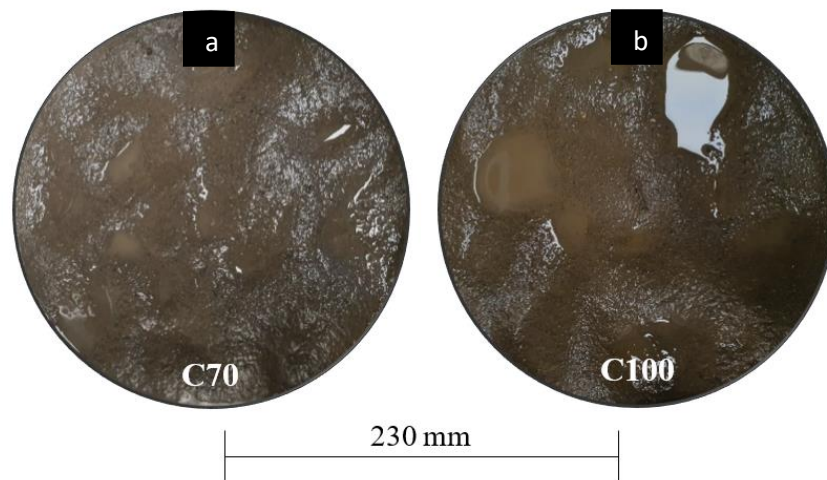
Figure 8. 17: Photos of the subgrade surface (a) PG-70-5 and PG-100-5

There is no sign of particle pumping at the subgrade surface, as shown in Figure 8. 17. Furthermore, the finer particles that accumulated at the top (below the geocomposite) and the top surface of the subgrade soil are insignificant in Test PG-85-5. Figure 8. 18 shows the PSD curves in the top and middle specimens (Test PG-85-5). In essence, the percentage

of fines trapped in the pores of the tested geocomposites are 5.83, 6.12 and 6.46 g in Tests PG-70-5, PG-85-5 and PG-100-5, and where the area of geocomposite is 4.15×10^{-2} m^2. Moreover, a visual inspection shows insignificant changes in the particle size distribution and water content in the middle and top layers (Figure 8. 17 and 8.19). This confirms that this combination will prevent the formation of slurry under cyclic loading.
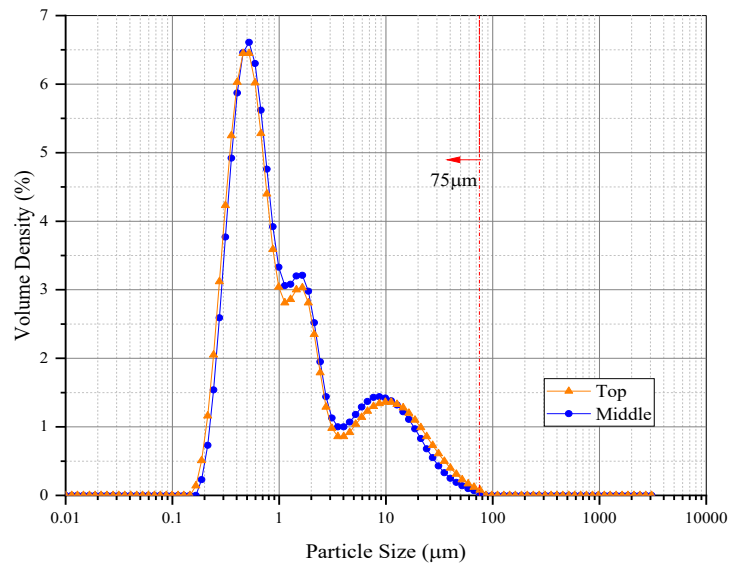
Figure 8. 18: PSD of Top and Middle Soil after 100,000 cycles – PG-85-5
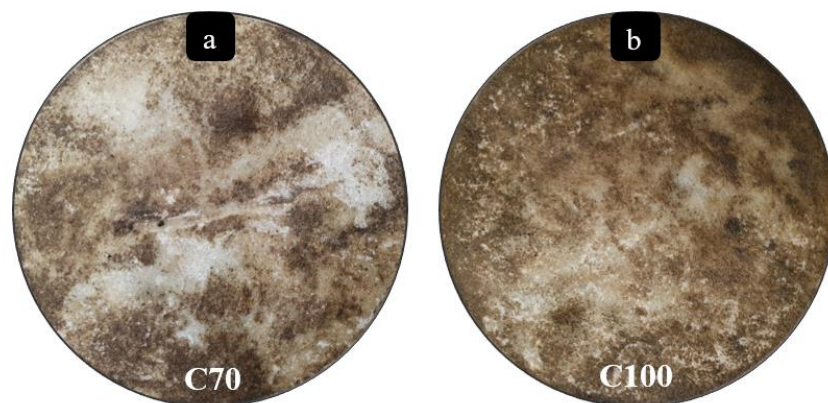
Figure 8. 19: Fine particles that accumulated at the bottom of the geocomposites (a) Tests PG-70-5 and Test PG-100-5

8.5.3 Effect of Frequency

8.5.3.1 Excess Pore Water Pressure and Axial Strain

Figure 8. 20(a) shows the effects of two different frequencies (3 and 5 Hz) with the combination of PVD and geocomposite system. The EPWPs that developed in all three miniature pressure transducers decreased at a lower frequency. An increase in frequency (f=5 Hz) causes a significant increase in EPWPs at MP1 compared to Test PG-70-3, as shown in Figure 8. 20(a). In essence, the rate of dissipation of EPWP is slightly higher in the test carried out at a lower frequency. The EPWPs that developed at MP1 are 4 kPa and 5.1 kPa for Tests C3 and C5 at the end of the cyclic tests; these results confirmed that PVD combined with geocomposite can still dissipate the EPWP even under higher frequencies. Figure 8. 20(b) shows that the axial deformations for Tests PG-70-3 and PG-70-5 are less than 2% at 75,000 cycles. As expected, there is no 'interlayer creation' or particle migration during cyclic loading.

8.5.3.2 Excess Pore Pressure Gradient

Figure 8. 20(c) shows the non-uniform development of EPPGs under different frequencies. It is clear that subgrade soil under higher frequencies is more likely to become unstable than at very low frequencies. However, the results in Figure 8. 20(c) show that the EPPGs that developed in Layers (3-2) and (4-3) under f=5 and 3 Hz, decrease significantly (i.e., EPPGs are less than five after 25,000 cycles) as the number of cycles increase.

8.5.3.3 Water content and Trapped Fines

Figure 8. 20(d) further shows that the water content approaches the liquid limit of the soil specimen under undrained and free drainage conditions before slurry begins to form at the subgrade interface. However, in both tests (f = 3 and 5 Hz), the water content at the subgrade surface decreased, and there was no slurry or accumulated fines near the interface.
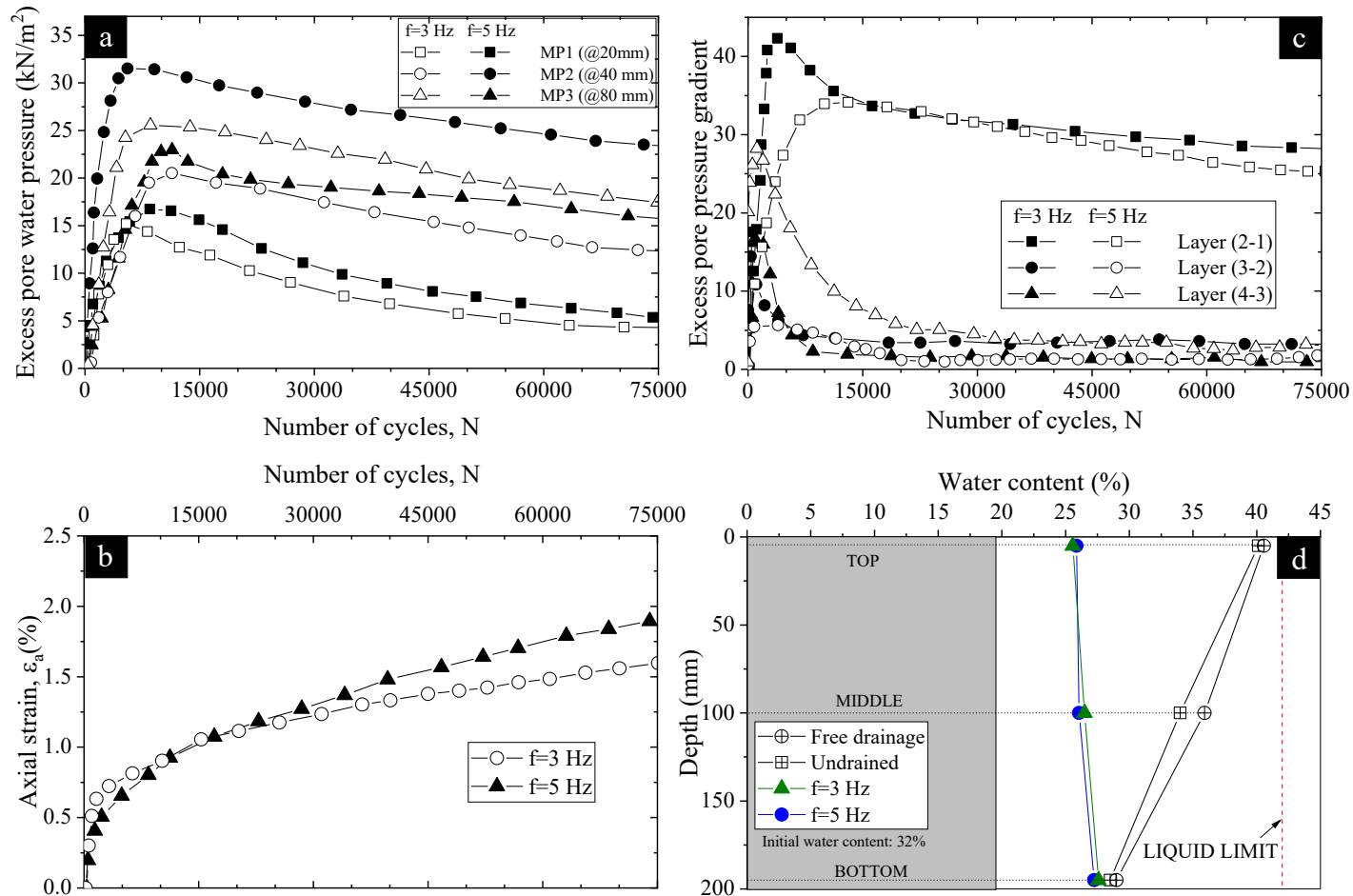
Figure 8. 20: Generation of (a) EPWPs, (b) Axial strains, (c) time-dependent EPPGs, and (d) measured water content at the end of cyclic loading (after 100,000 cycles) (Arivalagan et al. 2022).

Figure 8. 20(d) also shows that the water content in the middle and topsoil layers are less than 27%. This indicates that the combination of PVD and geocomposite significantly reduces the water content at greater depths, thus enhancing the drainage capacity of the substructure.

8.6 Chapter Summary

This chapter summarises the effectiveness of PVD combined with geocomposite to enhance the stability of soft subgrade soils under cyclic loading. The laboratory tests indicated that this approach is an effective way to stabilise soft soils under adverse hydro-dynamic conditions, and a PVD-geocomposite system will alleviate track instability and subgrade fluidisation by controlling the EPWP, even under higher axle loads.

On the one hand, geocomposite could alleviate the EPWPs that developed at or close to the interface as the number of loading cycles increased. In essence, there was a dramatic decrease in the water content (26% at the subgrade surface) when geocomposite was included, and the subsequent penetration of particles into the geocomposite was insignificant. On the other hand, the inclusion of PVDs also led to a rapid increase in horizontal EPPG which facilitated radial drainage and decelerated the critical build-up of EPWP in the subgrade. Furthermore, the combined PVD-geocomposite system significantly reduced the EPWP from the outset of cyclic loading. This led to the conclusion that a PVD-geocomposite system could further reduce the generation of EPWP (i.e., increase its dissipation rate), especially in the middle and lower regions of the specimen, and also prevent the separation of fine particles and soil softening at the ballast/subgrade interface.

CHAPTER 9: NUMERICAL STUDY OF GEOSYNTHETICS IN SOFT SOILS

9.1 Introduction

Undoubtedly, a rapid generation of EPWP plays a key role in inducing soil softening and associated mud pumping at the subgrade surface. This chapter primarily discusses the numerical simulations carried out using PLAXIS 2D to model the EPWPs generated under train loading. A plane strain finite element analysis in PLAXIS 2D was used to investigate the cyclic behaviour of soil improved by geotextiles and PVDs under a typical train loading. A set of numerical simulations were used to assess (1) the generation of EPWPs in a conventional railway track, (2) the role of geotextiles in alleviating EPWPs at the subgrade surface, and (3) the ability of PVDs to delay the build-up of EPWPs at shallow depths under different axle loads and freight trains travelling at varying speeds.

9.2. 2D Finite Element (FE) Model

Vertical cross sections of track were modelled under plane strain conditions using PLAXIS 2D. The 'equivalent 2D plane strain model' for PVDs was used for the numerical simulations. Indraratna & Redana (1997) and Indraratna & Redana (2000) clearly explained that an equivalent 2D plane strain model for multi-drain FE analysis could predict acceptable pore water pressures, settlements, and lateral displacements. Furthermore, the 2D FE analysis could provide accurate results, albeit with some adjustments, to simulate the 3D loads and lateral spreading of granular layers along a track in an transverse direction. Furthermore, transforming 3D into 2D finite element method

can successfully reduce the complexity, time of computation and effort and can yield comparable results with 3D analysis (Brinkgreve et al. 2012; Georgiannou et al. 2017).

9.3 FE Model to Simulate Railway Tracks

This section reports the innovative approaches using dynamic load multipliers in PLAXIS 2D. The performance of conventional railway tracks with extremely poor drainage conditions and the ability of geotextiles, short vertical drains, and a combined vertical drains-geocomposite system to mitigate the rapid generation of EPWPs under cyclic train loading were discussed. The performance of ballasted railway tracks with and without geosynthetics was assessed by considering two different cases. Firstly, the cyclic soil response of a soft soil model was analysed under the cyclic loading conditions (Sandgate Project). Secondly, a conventional railway track was modelled with and without PVDs to evaluate the use of PVDs as subsurface drainage under various speeds and axle loads. The numerical results were compared with previous studies (Abeywikrama 2020; Indraratna et al. 2010; Singh et al. 2020), and this Chapter critically defines the effectiveness of geosynthetics under cyclic loading conditions.

9.3.1 Case 1: Modelling Track Behaviour at Sandgate Project

The Sandgate project is located at Sandgate, a town in the Hunter Region, NSW, Australia. An FE analysis undertaken utilising an equivalent static approach has already been published with Class A predictions (Indraratna et al. 2010b). In this study, the use of short PVDs and geotextiles in soft soils to stabilise track foundations subjected to dynamic loading was simulated. A dynamic load (20t axle load and 110 km/h train speed) was generated to capture the development of EPWPs with and without geosynthetics, where PVDs were installed at intervals of 1.5 m. The effectiveness of these geosynthetics can be analysed by covering three distinct numerical phases.

- Phase 1 (effect of poor drainage conditions): To measure the effectiveness of a capping layer, an impermeable boundary was created at the surface of the soft subgrade.

- Phase 2 (influence of drainage medium at the subgrade interface): The main objective of phase 2 was to assess the ability of geotextiles to control the development of EPWPs at the subgrade surface using a drainage layer (geotextile) at the interface.

- Phase 3 (effectiveness of PVDs and geotextiles): An FE analysis under phase 3 was undertaken to investigate the rate of dissipation of EPWPs at shallow depths induced by the installation of a combined PVD-geotextile system (influence of radial drainage by PVDs).

A vertical cross-section of the Sandgate rail track and the discretization of FE mesh is shown in Figure 9. 1. In this case, the top layer of compacted crust was modelled by utilising the Mohr-Coulomb theory and the normally consolidated clays were modelled utilising the Soft Soil Model. The soft soil characteristics based on the field and laboratory tests are listed in Table 9. 1. The properties of the ballast and fill layer of the Sandgate model are taken from Indraratna et al. (2010b). The 1.68 m gauge length of a concrete sleeper with a nominal length of 2.5 m was simulated.
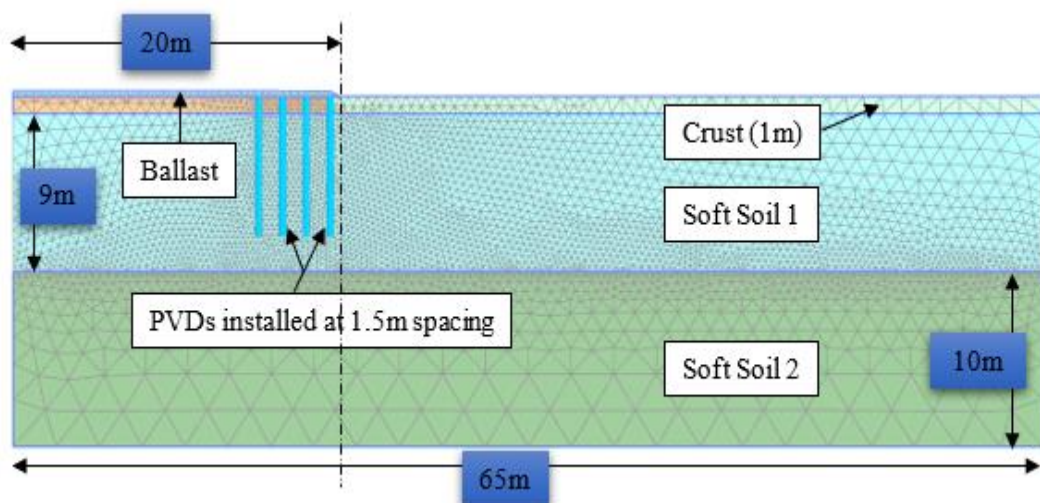
Figure 9. 1: Sandgate rai track and foundation (Indraratna et al. 2010b)

9.3.2 Case 2: Conventional Railway Track

This model proposed a composite multi-layer railway track (Figure 9. 2) which included rails, sleepers, ballast, subballast, and subgrade. The main objective was to assess the use of short vertical drains as subsurface drainage under various speeds and axle loads (20-40t axle load and 60-140 km/h speed). In this case, short vertical drains (up to 8 m) were installed within the subgrade soil at spacings of 1.5 and 2 m. The FE results were also compared with rail tracks under undrained conditions.

Figure 9. 2 shows the superstructure and substructure of a typical plain strain track model where in this case the material properties have been taken from Indraratna et al. (2012b). The layer of subgrade was 20 m wide by 15 m deep. The thickness of subballast, ballast and concrete sleeper were 150, 300 and 200 mm respectively, all of which were modelled over the soft subgrade. The side slope was maintained at 1V:2H. The rail was considered as a 160 mm wide structural plate element. The boundary conditions were modified where the lateral boundaries restrained horizontally, and the bottom was fixed in both direction (i.e. no horizontal and vertical movements were allowed at the bottom boundary). In FE analysis, various seepage conditions were also used to model impervious and drain boundaries. All the material properties used for different tracks are discussed in Section 9.4. During the mesh generation, the clusters were discretised using 6-noded triangular elements. The model had a medium/fine mesh with refinements (i.e. increasing the mesh density) that were based on the sensitivity analysis. Local mesh refinement was also used near the interfaces to improve the accuracy of numerical analysis.
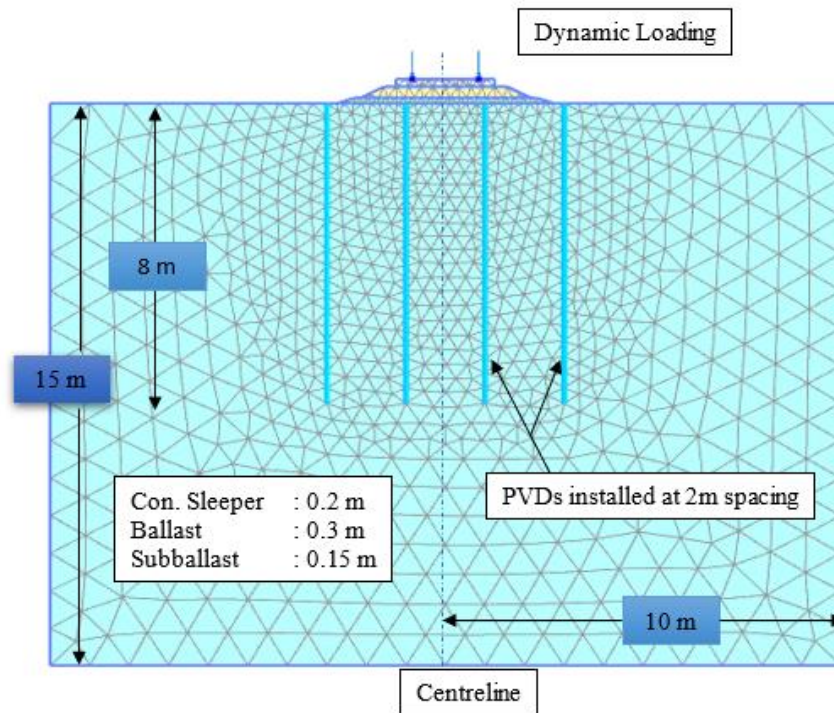
Figure 9. 2: FE Mesh for railway foundation with PVDs installed at 2 m spacing

9.4 Material Parameters

The dynamic wheel loads, moduli of granular materials, and characteristics of subgrade soil (subgrade soil type and compressive strength, and other properties) are typical input parameters for this track design (Indraratna et al. 2012a; Indraratna et al. 2010b; Powrie et al. 2007; Punetha et al. 2021; Singh et al. 2020). The soft soil characteristics used in the Sandgate model (Case 1) are listed in Table 9. 1 (Indraratna et al. 2010b).

Table 9. 1: Sandgate Soft soil parameters (adapted from Indraratna et al. (2010b))

Parameters	Soil 1	Soil 2
Material model	SS	SS
Material type	Undrained	Undrained
γ_{dry} (kN/m³)	8.46	8.46
γ_{wet} (kN/m³)	14.80	14.86

k_h (m/day)	3.5×10^{-5}	1.53×10^{-4}
k_v (m/day)	7.0×10^{-5}	7.5×10^{-5}
λ^*	0.111	0.990
κ^*	0.011	0.015
e_0	2.06	2.04
c (kPa)	10	10
φ (°)	25	20
ψ (°)	0	0

Other input parameters such as the static wheel load (Ps), wheel diameter (D), sleeper spacing (a), and train velocity (V), were used to determine the static and dynamic stresses exerted on the ballast-sleeper interface (Section 9.5).

Table 9. 2: Model parameters used in Case 2 (adopted from Indraratna et al. (2012b))

Parameter	Subgrade	Subballast	Ballast	Concrete	Rail
Model	MC	MC	HS	LE	LE
γ (kN/m^3)	17.3	16.67	15.98	24	78
E (kPa)	25.5×10^3	80×10^3		30×10^6	210×10^6
E_{50}^{ref} (kPa)	-	-	21.34×10^3	-	-
E_{oed}^{ref} (kPa)	-	-	21.34×10^3	-	-
E_{ur}^{ref} (kPa)	-	-	64.02×10^3	-	-
ν	0.3	0.35	-	0.15	0.3
ν_{ur}	-	-	0.2	-	-

m	-	1	0.5	-	-
c' (kPa)	10	1	0	-	-
φ (°)	20	35	58.47	-	-
ψ (°)	-	5	12.95	-	-
P^{ref} (kPa)			50		
K_o^{nc}			0.3		
R_f			0.9		
Groundwater parameters					
Data set	USDA	USDA	-	-	-
Model	Van Genuchten	Van Genuchten	-	-	-
Type	Silty clay	Sand	-	-	-
c_k	0.05	1×10^{15}	1×10^{15}		

where γ = unit weight, E = modulus of elasticity, E_{50}^{ref} = secant modulus at 50% strength for loading conditions, E_{oed}^{ref} = tangent stiffness for primary oedometer loading, E_{ur}^{ref} = triaxial unloading/reloading stiffness, ν = Poisson's ratio, ν_{ur} = Poisson's ratio for unloading/reloading, c' = effective cohesion, φ = effective friction angle, ψ = dilatancy angle, c_k = change of permeability, m = power for stress level dependency of stiffness, K_o^{nc} = coefficient of earth pressure at rest for normal consolidation, R_f = failure ratio, P^{ref} = reference confining pressure

Note: MC - Mohr-Coulomb, Hardening Soil (HS), Linear Elastic (LE), Soft Soil (SS) and USDA series is a international soil classification system (Plaxis_Manual 2021)

Table 9. 3: Material parameters for different subgrades (adapted from Punetha et al. (2021))

Parameters	Poor (soft clay)	Fair (medium clay)	Good (dense sand)	Hard rock
Material model	MC	MC	MC	MC
E (kPa)	12.5×10^3	25.5×10^3	80×10^3	3×10^6
γ (kPa)	16	17	18	19
ν	0.4	0.3	0.3	0.2
c (kPa)	15	10	0	15000
φ (°)	12	20	30	20
ψ (°)	0	0	0	0

Table 9. 2 summarises the material properties used in a conventional rail track (Case 2). The material properties and constitutive models for different subgrades are also listed in Table 9. 3. The steel rails had a Young's modulus of 210×10^6 kPa and an average cross-sectional area (A) of 7.6125×10^{-3} m^2. The moment of inertia (I) was 2.7×10^{-5} m^4 (Priest et al. 2010). The sleeper was simulated as a linear elastic material. As reported in Indraratna & Nimbalkar (2013), a HS model was used for the ballast layer under repeated dynamic loads. The subballast and subgrade layers was modelled using the Mohr-Coulomb (MC) elastic-perfectly plastic model in Case 2. The limitations of this study are discussed in Section 9.8.

9.5 Dynamic Load Calculations

In previous studies the FE analysis was carried out using a static load with an impact factor to represent the dynamic forces (Attya et al. 2007). In general, the static wheel load is the average wheel load of all the wagons over a design period, and it is determined when the wagon and wheel carriage are under static equilibrium in a vertical direction (Indraratna &

Ngo 2018). In other words, the static wheel load can be taken as the weight of a stationary train divided by the number of wheels. The dynamic component of train load is more complex and primarily varies with track geometry, train configuration, speed, etc.

Based on the AREA (American Railway Engineering Association) method, the computation of the design wheel load can be expressed as follows (Li & Selig 1998):

$$P_d = \emptyset P_s \qquad \text{Equation 9.1}$$

where P_d =design wheel load that incorporates dynamic effects, P_s = static wheel load, and $\emptyset$ = dimensionless impact factor (>1.0).

$$\emptyset = \left(1 + \frac{0.0052V}{D_w}\right) \qquad \text{Equation 9.2}$$

where, D_w =diameter of the wheel (m), and V =velocity of the train (km/h).

The sleeper/ballast contact pressure was assumed to be uniform in the analysis, and the average contact pressure (P_a') at the sleeper and the ballast interface can be expressed as follows (Indraratna et al. 2011):

$$P_a' = \left(\frac{3P}{Bl}\right)F \qquad \text{Equation 9.3}$$

where P =maximum rail seat load; B = width of the sleeper (0.26 m); l = nominal length of the sleeper (2.5 m); and F = factor that depends on the type of sleeper/tie and rail way track maintenance.

9.5.1 Sleeper/Ballast Contact Pressure

Axle loads of 20, 30, and 40 tonnes were selected for FEM analysis. The calculation of the rail seat load corresponding to a 40t axle load is given in this section. The USACE (2000) railroad design manual by the U.S. Army Corps of Engineers reported that the average wheel point load was distributed between five sleepers, and the maximum load was

generated under the wheels. Therefore, the contact pressure developed at the sleeper and ballast interface can be obtained by the elastic theory (Indraratna et al. 2018).

From Equation 9.3, for a typical 40-tonne axle load:

$$P'_a = \left(\frac{3x78000}{0.26x2.5}\right) x 1/1000 \approx 360 \text{ kPa}$$

where P = maximum rail seat load (e.g., for a 40t axle load, P = 0.4 × 40,000/2 × 9.81 ≈ 78 kN; B = width of the sleeper (0.26 m); l = length of the sleeper (2.5 m); and F = factor depending on the type of sleeper/tie and the track maintenance (F = 1).

The sleeper/ballast contact pressure (P'_a) are around 360, 318, 272, 226 and 180 kPa for axle loads of 40, 35, 30, 25 and 20 tonnes, respectively. However, high impact loads can be developed by wheel imperfections or flat spots, both of which were carefully accounted in this design. According to Indraratna et al. (2010a), a 25t axle load generated the maximum vertical cyclic stresses (sleeper/ballast) of up to 230 kPa, while one peak was observed at 415 kPa (around 2 times the P'_a) due to the arrival of a wheel flat. Several field studies and laboratory tests often represented an efficient strategy and assessment that would prevent track degradation due to impact loads. Furthermore, the laboratory measurements reported that the maximum sleeper/ballast contact stress for a typical train speed varies between 300-450 kPa (Indraratna et al. 2011).

9.5.2 Dynamic Load Used in FEM

PLAXIS 2D can generate a sinusoidal load using the 'dynamic mode'. For instance, a 40-tonne axle load corresponds to a static wheel load of around 240 kN (length and width of sleeper are 2.5 and 0.26 m, respectively). As proposed by Singh et al. (2020), the finite element analysis was carried out using a 'harmonic load multiplier' and a 'static load'. The amplitude for the load multiplier is listed in Table 9. 4. In this case the applied load (40t)

can simulate the sinusoidal wave load on top of the ballast from zero to 480 kN. The maximum number of cycles was restricted to 1500 due to the computational time required to run PLAXIS 2D models under dynamic mode. The staged loading application for a rail track subjected to a 15 Hz frequency is given in Table 9. 5. The selected range roughly represents the passage of a 4-6 km long train.

9.5.3 Train Speed and Frequency

The frequency of train load depends mainly on train speed, vehicle geometry, and the target depth (attenuation). The frequency can be determined by $f = v/L$, where v is the train speed, and L can be either the bogie spacing or the characteristic length between the closest sets of axles (Indraratna et al. 2018). Since the total distance between two axles is much smaller than the distance between the two bogies, the two rear axles (of a front wagon) and two front axles (of a trailing wagon) can induce maximum frequency (Indraratna et al. 2014). For instance, f=15 Hz can represent a train speed of approximately 110 km/h with an axle distance of 2.2 m. Moreover, a 25-tonne axle load and frequency of 8.25 Hz would generate an average train speed of 60 km/h, where the distance between two axles is 2.02 m (Indraratna et al. 2010a).

Table 9. 4: Selected axle load and speed of trains (Indraratna et al. 2010a; Indraratna et al. 2018; Israr 2016)

Axle load (tonne)	Selected Amplitude of Load (kN)	Train speed (km/h)	Corresponding Frequency (Hz)
20	120	60	8.25
30	180	110	15
40	240	140	20

Table 9. 5: Staged loading application (Dynamic analysis in the time domain, f=15Hz)

Phase No	Number of cycles	Dynamic time interval (s) – From previous phases
Phase 1	1	0.07
Phase 2	10	0.60
Phase 3	50	2.67
Phase 4	100	3.34
Phase 5	200	6.67
Phase 6	500	20.01
Phase 7	1000	33.33
Phase 8	1500	33.33

9.6 Geosynthetic Inclusions in Railway Tracks

9.6.1 Prefabricated Vertical Drains

PVDs can increase the stability of clayey foundations and they can also be used to alleviate the problems of drainage often associated with low-permeability soft soil. However, most studies that used PVDs have only been investigated under static loading conditions (Chu et al. 2004; Indraratna et al. 2005). Although previous studies reported how PVDs could stabilise railway track foundations, FE analyses were generated using a static or an equivalent static load, which severely limited their model (Indraratna et al. 2010b; Indraratna et al. 2005). The relatively short PVDs (6 to 8 m long) can still alleviate cyclic pore pressures, reduce the lateral movements, and improve the stability of a soft soil formation beneath the subballast. Short vertical drains with a spacing of 1.5 and 2 m can be simulated in PLAXIS 2D. In this instance, an 8 m length of PVD was used for the FE analysis. Prefabricated vertical drains (PVDs) were modelled in PLAXIS 2D by creating a

drain element set to a hydraulic head of 0.0 m to simulate an ideal zero pore pressure boundary. The present model had an array of 8.0 m long PVDs at 1.5 m and 2 m spacing.

9.6.2 Drainage Layer at the Subgrade Surface (Geotextiles)

The laboratory results proved that geotextiles with an effective filter membrane could dissipate the EPWPs and increase track stability under cyclic loading. The drain available in Plaxis 2D models can display the nodes representing the drain and their location, the total discharge, and the defined groundwater head of the drain (Plaxis_Manual 2021). In the FE model, a drainage medium at the subgrade surface was modelled using an array of short drain elements at relatively close spacings (0.05 m long drains at 0.1 m intervals), as shown in Figure 9. 3. This can typically represent a thin drainage medium and the effective use of a geotextile filter at the subgrade/subballast interface can be captured. The numerical results are discussed in the following sections
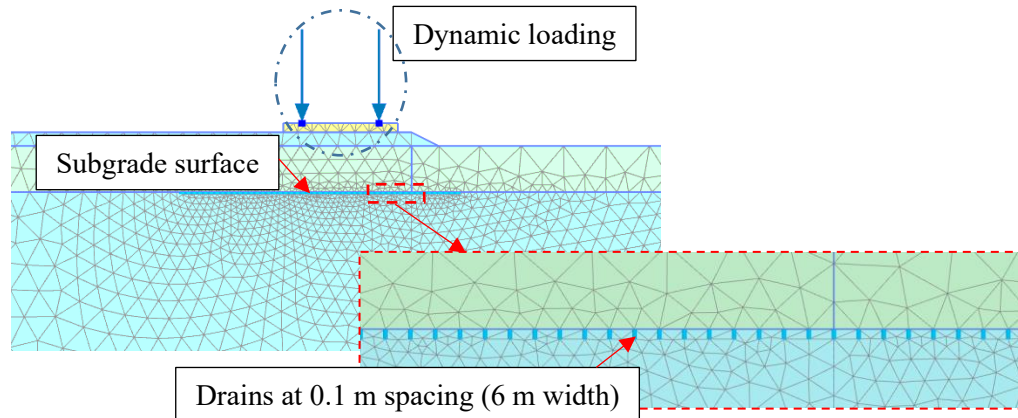
Figure 9. 3: Drainage medium at the subgrade surface

9.7 Results and Discussions

The numerical results from two different projects are discussed in this section, which highlights the effectiveness of geosynthetics at dissipating EPWPs under cyclic loading conditions.

9.7.1 Case 1: Modelling Track Behaviour at Sandgate Project

9.7.1.1 Influence of Geotextile

The impermeable boundary (represents extremely poor drainage conditions by a capping layer) and a drainage medium (represents an effective geotextile filter) were simulated at the subgrade interface to measure the effectiveness of geotextiles under dynamic loading conditions.
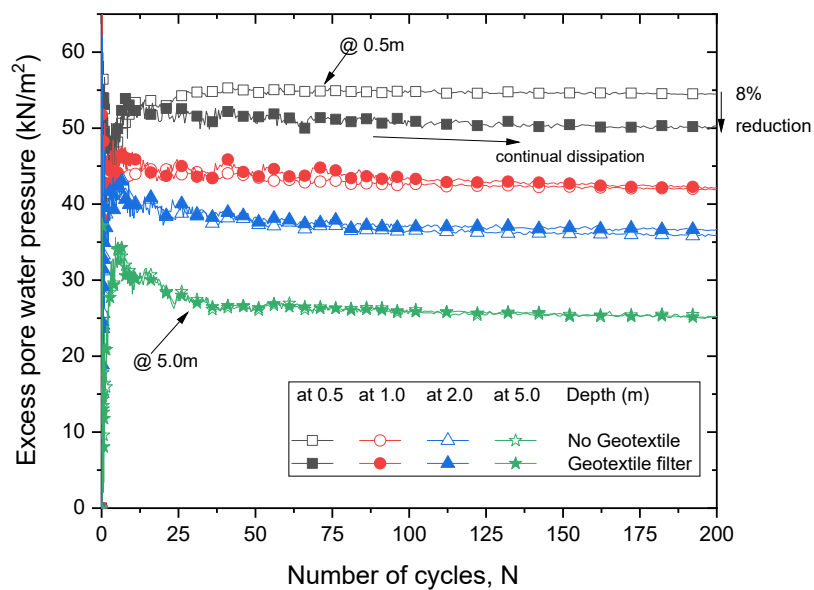
Figure 9. 4: Generation of EPWPs with and without geotextiles

Figure 9. 4 shows the rapid generation of EPWPs under poor drainage conditions. For example, the EPWPs that developed at 0.5 m from the subgrade surface rapidly increase to more than 50 kPa after only ten cycles, and remain over 54 kPa at the end of 200 cycles. Furthermore, there is no significant reduction in EPWPs after 50 cycles, and this may cause subgrade instability. However, the inclusion of a geotextile filter in soft soils can reduce the critical pore water pressure that develops at the subgrade surface. For instance, the generation of EPWPs at 0.5 m decrease by 8% compared to undrained conditions. However, there is no significant reduction in EPWPs at 1 to 5 m depth within the subgrade.

This shows that geotextile filters that can provide adequate drainage at the subgrade interface and their ability to reduce the fluidisation potential can diminish with increasing depth.
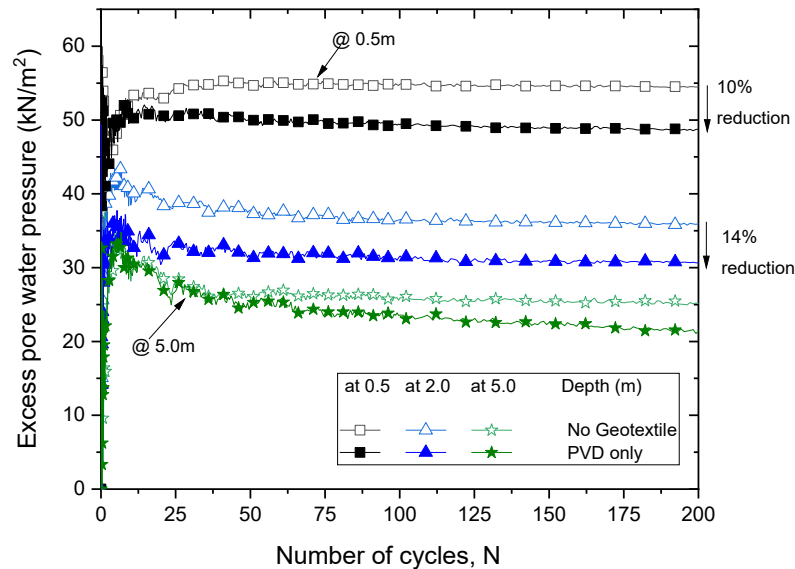
Figure 9. 5: Generation of EPWPs with and without PVDs (20t and 15Hz, PVD at 1.5 m spacing)

9.7.1.2 Effectiveness of PVDs

PVDs can activate the radial drainage paths and accelerate the pore pressure dissipation under cyclic loading conditions. Figure 9. 5 shows the EPWP dissipation at shallow depths due to the inclusion of PVDs. For example, the cyclic pore water pressures that developed at 200 cycles are more than 14% at depths of 2 m and 5 m from the subgrade interface; these results verify that PVDs can significantly dissipate the EPWP that can develop at greater depths (compared to a sole geotextile). In addition, the simulations show that the model with the PVDs (at 1.5 m spacing) can dissipate the EPWPs at 1500 cycles by around 15 -25% at shallower depths compared to the model without PVDs.

Under a cyclic load, the generation of EPWPs at the subgrade interface ishigher than those at the greater depths because of the attenuation of cyclic stress. However, the activation of radial drainage paths by PVDs is proven to be effective at shallow depths.

Prefabricated vertical drains can facilitate the dissipation of EPWPs during and after dynamic loading, as shown in Figure 9. 6. During the rest period, the accumulated EPWPs begin to decrease dramatically with increased cycles, and then remain less than 10 kPa until the next train loading. This indicates there is no substantial increase in EPWPs when there are more trains passing. Figure 9. 7 shows the total displacement contours for the model (PVD only) at 1000 cycles. Due to consolidation by the installation of PVD, there is a a substantial increase in maximum displacement (up to 0.2 m) near the top surface of the subgrade (clay), but then it decreases with increasing depth, as shown in Figure 9. 7. Furthermore, the rate of cyclic consolidation is minimal in undrained tests since there is no significant EPWP dissipation over time.
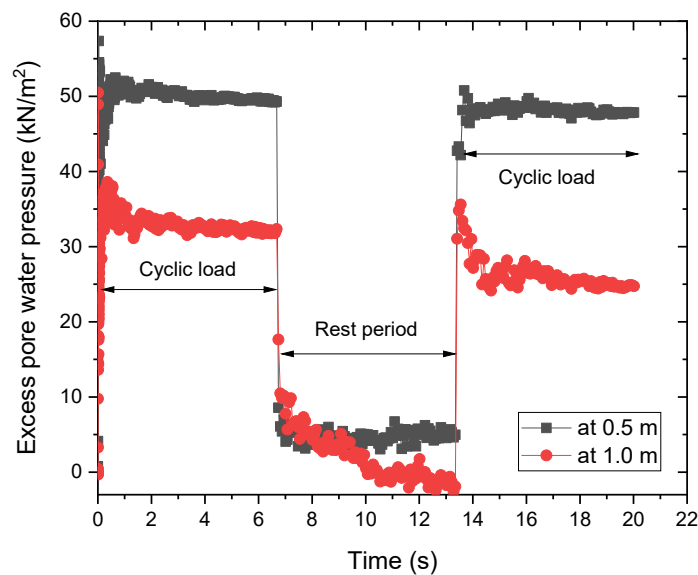
Figure 9. 6: Generation and dissipation of EPWPs with a rest period
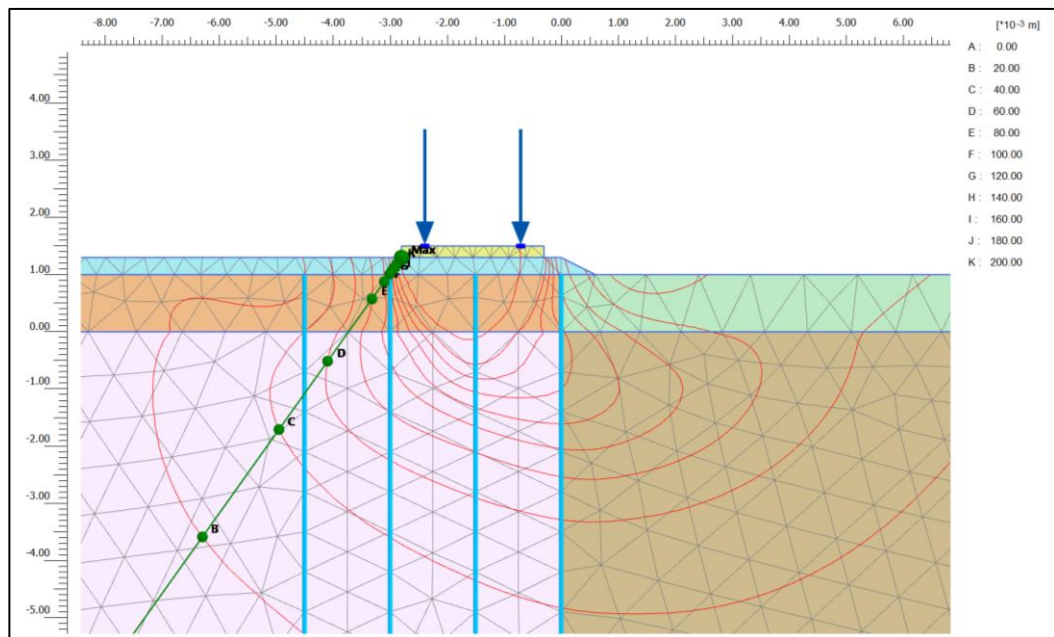
Figure 9. 7: Displacement contours after 1000 cycles using PVDs (20t and 15 Hz)

9.7.1.3 The combined PVD-Geotextile System

Laboratory experiments proved that a combined PVD-geotextile system could further reduce the accumulation of EPWPs and prevent the occurrence of subgrade instability by providing additional confinement at the interface; where geotextiles could reduce the water content of subgrade surface. Therefore, a 'T section' was created at the subgrade interface by modelling an array of 8 m long short vertical drains with 1.5 m spacing, and a geotextile filter. A combined PVD-geotextile system was used in this analysis because PVD installed alone within subgrade soil could not substantially reduce the EPWPs at the middle of two adjacent PVDs, where a sole geotextile that had been installed could not dissipate the EPWPs at deeper layers.

As shown in Figure 9. 8, the combined PVD-geotextile system alleviates the EPWPs at the critical soil layers (i.e. 0.5 – 5 m depth). For instance, the EPWPs that developed at 0.5 m, and 5 m from the subgrade interface decrease by 19% and 12% compared to the results with a sole geotextile. This combination (PVDs and geotextiles) may become ineffective

over depths of 10 m. Since mud pumping is a shallow layer phenomenon, a PVD-geotextile system can dissipate the critical accumulation of EPWPs in vulnerable layers of soil (i.e., more prone to subgrade fluidisation) during and after train passings.
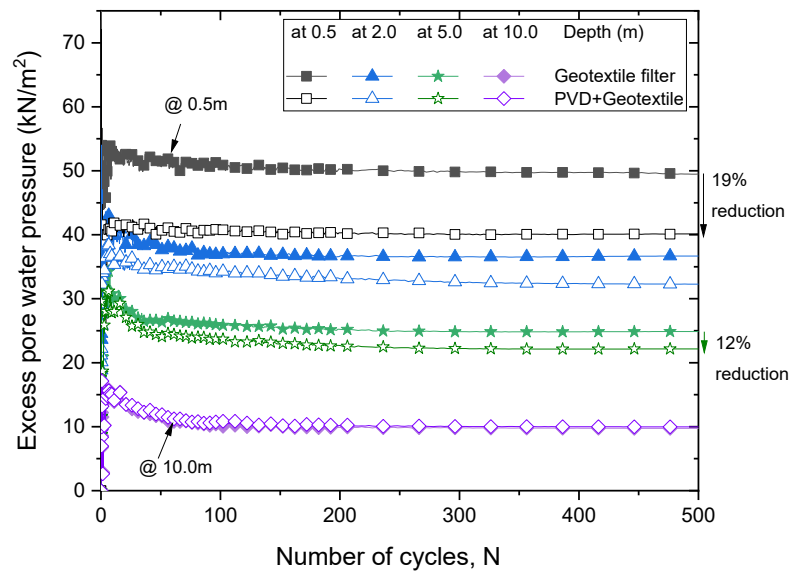
Figure 9. 8: Generation of EPWPs with a combination of PVD and geotextile filter

9.7.2 Case 2: Modelling Railway Tracks with and without PVDs

The numerical and laboratory results proved that subgrade was susceptible to fluidisation when the EPWPs reached its threshold value, and also become vulnerable to mud pumping under repeated cyclic loading. Therefore, the generation of EPWPs at the subgrade interface was considered (i.e., 0.5 m from the subgrade surface) in the following sections, whereas the interface behaviour can be assessed using the rate of dissipation of EPWPs.
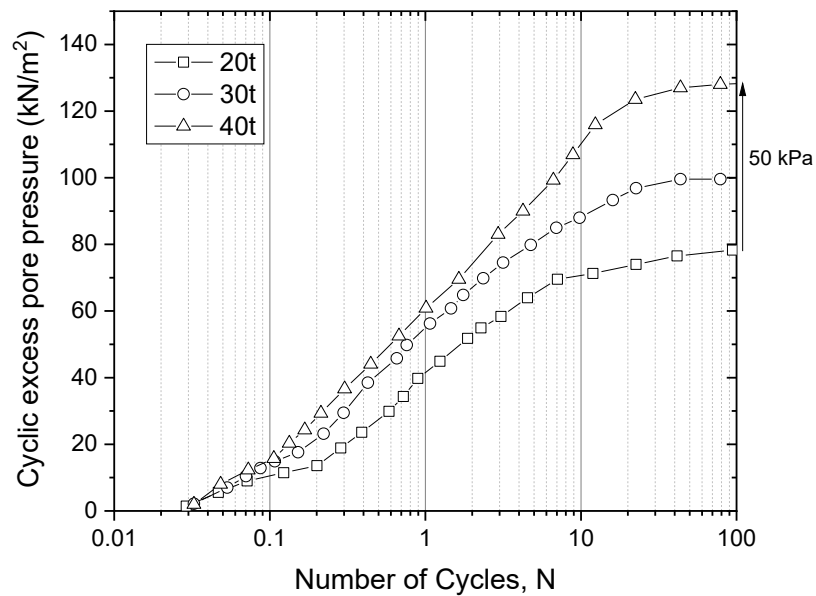
Figure 9. 9: Generation of EPWPs under different axle loads (No PVDs)

Figure 9. 9 shows the EPWPs that developed 0.5 m away from the interface with varying axle loads under critical drainage conditions (impermeable). As expected, there is a rapid increase in EPWP as the axle load increases. For instance, the EPWP that developed 0.5 m below the interface rapidly increase to more than 100 kPa at ten cycles when the axle load increases to 40 tonnes; it is around 70 kPa with 20t axle loading. Furthermore, the EPWPs that developed under 40t loading are more than 50 kPa at 100 cycles compared to 20t cyclic loading.
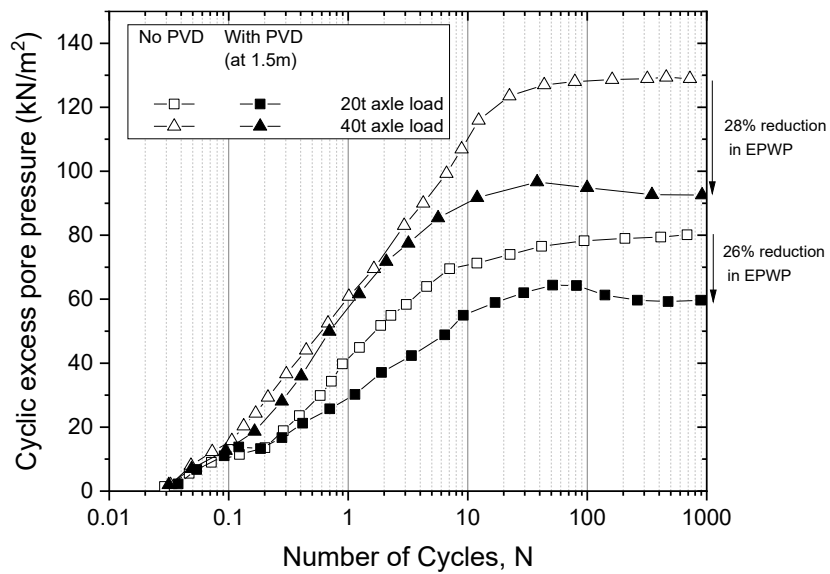
Figure 9. 10: Generation of EPWPs under increased axle loads (with PVDs)
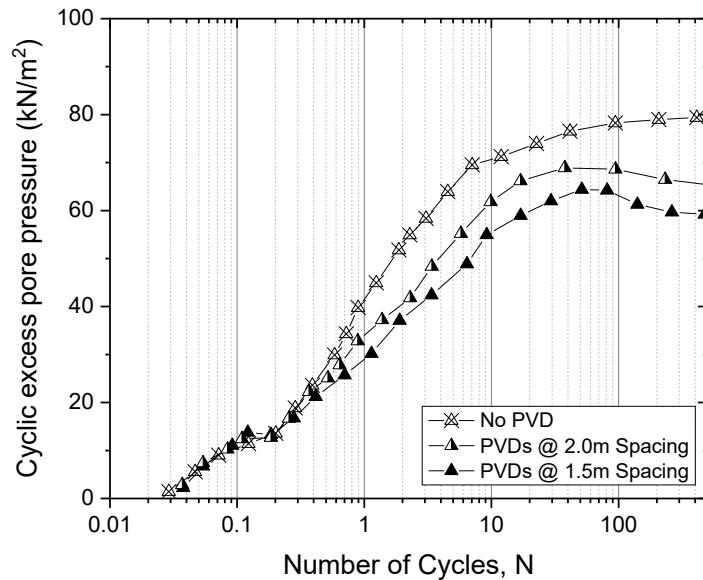
Figure 9. 11: The rate of dissipation of EPWPs at 0.5m depth

A set of FE simulations were used to study how PVDs can dissipate the generation of

EPWPs in a railway subgrade by activating radial/shorter drainage paths. Figure 9. 10

shows that the EPWPs that accumulated after 1000 cycles decreased by more than 25%

(compared to the conventional track) with PVDs even though cyclic load increased to 40

tonnes. This shows that PVDs can alleviate the rapid generation of EPWPs, which is the primary causative factor in dislocating/pumping fine particles upwards. Drain spacings of 2.0 and 1.5 m were selected, and Figure 9. 11 shows the effect of drain spacing on a railway structure under a typical train load. Although the maximum EPWPs reached around 70 kPa after 500 cycles (No PVDs), PVDs could still dissipate them effectively because they were 60 and 66 kPa for 1.5 and 2.0 m drain spacings, respectively. This shows that when the drain spacing is smaller, the rate of dissipation increases due to shorter drainage paths. The effect of loading frequency was also examined (varied from 8 Hz to 20.0 Hz) to simulate train speeds of roughly 60 km/h to 140 km/h.
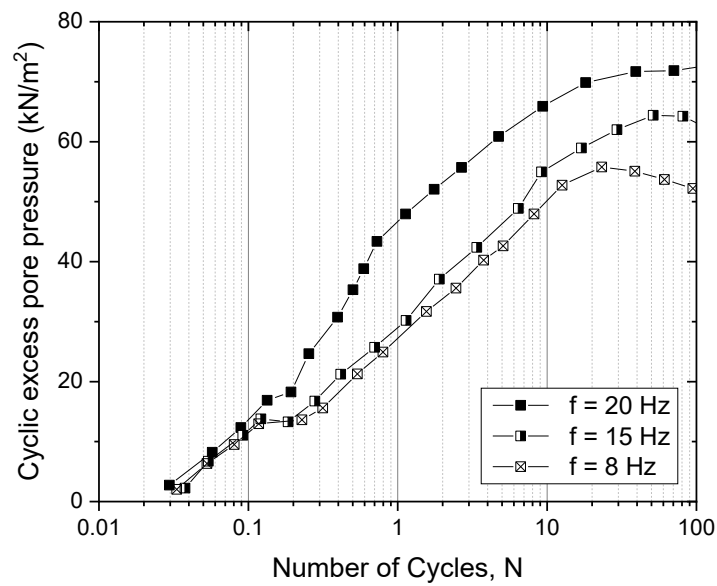
Figure 9. 12: Variation in the cyclic EPWPs at different frequencies (f=8, 15 and 20 Hz)

Figure 9. 12 shows the EPWPs that developed inside the subgrade had dissipated rapidly with smaller frequencies. For instance, at a depth of 0.5 m, the EPWPs rocketed to 72 kPa at 100 cycles under 20 Hz and were around 50 kPa at 8 Hz. Similar observations were reported in previous studies (Arivalagan et al. 2022; Singh 2021). In addition, PVDs also mitigated lateral deformation when the cyclic load increased to 240 kN (40 tonnes) or the train speed increased to more than 140 km/h (20 Hz). It was observed that under a frequency

of 15 Hz, the short vertical drains reduced lateral deformation from 60 mm to less than 15 mm. This indicates that PVDs can be used to stabilise railway embankments by reducing lateral deformation and rapid EPWP generation.

9.8 Limitations of this Study

- The primary objective of this numerical study was to determine the generation of EPWPs under cyclic loading by using a plane strain 2D model of a whole embankment to represent various drainage conditions. The effect of geosynthetics in controlling the vertical and lateral displacement were not studied in detail.

- The current FE analysis will need to be verified further to more extensive field monitoring of potential mud pumping sites in order to study the rate of dissipation in EPWPs under cyclic loading. Such information will be required to validate the numerical analysis and also extend existing track design guides.

- The characteristics of subgrade used in the simulations were mostly obtained from field studies. The variations in the characteristics of subgrade revealed the key role of subgrade in reinforcement. Therefore, the effect of the shear strength parameters and the constitutive models of ballast and sub-ballast must be included in future studies to simulate different track conditions.

- The linear elastic perfectly plastic Mohr-Coulomb (MC) model is a first-order model that only includes a limited number of features, as illustrated in Plaxis_Manual (2021). The increment of stiffness and depth can be considered but the MC model does not include stress-path dependency, the strain dependency of stiffness, or anisotropic stiffness (Plaxis_Manual 2021).

- The well resistance was ignored due to the installation of short PVDs. However, the extent of the smear zone was not considered in this FE model by measuring the k_h/k_v of soil surrounding the drains.

9.9 Chapter Summary

This chapter reports an innovative approach using dynamic load multipliers in PLAXIS 2D. The performance of conventional railway tracks with extremely poor drainage conditions and the ability of geotextiles, PVDs, and PVD-geotextile systems to mitigate the rapid generation of EPWPs under cyclic train loading were studied. The rapid generation of EPWPs was observed under adverse hydro-dynamic conditions. It was found that PVD can alleviate the EPWPs at a shallow depth of subgrade and the rate of dissipation of EPWPs was minimal near the subgrade surface (between two adjacent PVDs). Geotextiles could reduce the build-up of EPWPs only at the subgrade interface. The test results indicated that a combination of PVD and geotextile could reduce the critical generation of EPWP in shallow subgrade more uniformly, even after train loading, thus increasing the stability of railway foundations.

CHAPTER 10: CHULLORA FIELD TRIAL

10.1 Introduction

This chapter primarily investigates the practical application of geosynthetics (geocomposite G1 with a filter membrane and robust geotextiles) to prevent mud pumping under typical train loading conditions. Although there are four different sections; namely (1) Rubber Intermixed Ballast System (RIBS), (2) EcoFlex, (3) Energy Absorbing Rubber Seam (EARS), and (4) Instrumented Control Section (ICS) with geocomposite, in the Chullora field trial, the design and construction stages of the "Instrumented Control Section" (ICS) are mainly discussed in this chapter (Figure 10. 1).
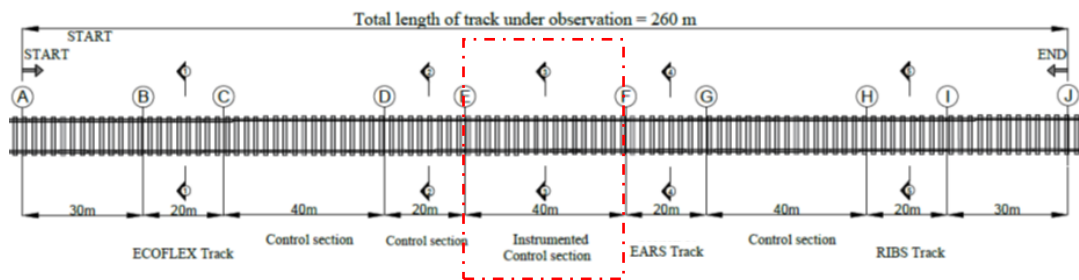
Figure 10. 1: Plan view of all the sections in Chullora Track

The trial track constructed at the Chullora technology precinct contains a section of track with geocomposites. The primary objective of this 40 m long instrumented control section is to compare the performance of geocomposite and filter membrane with other sections such as EARs, EcoFlex and RIBS. As Figure 10. 1 shows, two control sections with a minimum length of 20 m were also constructed between two instrumented sections to avoid boundary conditions influenced by neighbour sections; this means that each section can perform independently during the passage of trains. Furthermore, around 30 m of conventional track was constructed at both ends (left and right hand side of the trial track) in order to achieve the desired train speeds in all sections.

10.2 Chullora Site Investigation

A site investigation was carried out to obtain the soil profile underneath the track and the overall depth of the hard stratum from the ground level. The Cone Penetration Tests (CPT) and Standard Penetration Tests (SPT) carried out at five different locations along the tracks reveal that the ICS had the thin surficial strata of silty clay and clayey sands underlain by weathered shale and relatively stiff clay stratum existing at greater depths (Table 10.1). The SPT soil sample from the ICS section is shown in Figure 10. 2. After the site investigation, the sleepers and rails were removed from the existing track (Figure 10. 3(a)), and the area was excavated to the bottom of the track foundation (Figure 10. 3(b)).

Figure 10. 2: Soil sampling at the instrumented control section (SPT 0-0.5 m)

Figure 10. 3: (a) Existing track in Chullora, and (b) Excavation at the instrumented control section (ICS)

Table 10. 1: Standard Penetration Test at ICS

Depth	SPT Number of blows		
	1st 150 mm	2nd 150mm	3rd 150mm
0.5-1m	5	7	11
1-1.5m	5	6	7
1.5-2m	5	12	21
2-2.5m	29	50 refusal weathered shale	

10.3 Railway Track Design

The design criteria considered for the Chullora track was for 25 tonnes of axle loading at a maximum speed of 80 km/h for a design life of 20 years; i.e., with total traffic of 5 MGT/year. The dimensions of the track are in accordance with the code of practices, track guidelines, and ballast specification, issued by Transport for NSW (ARTC 2018, 2019). The design of each section was to satisfy several criteria for the strength of individual track components such as rail and sleeper stresses, pressure between the sleeper/ballast interface, and the pressure exerted onto the subgrade due to train loading. According to the methodology proposed in "Ballast railroad design: SMART-UOW approach", track design calculations were carried out (Indraratna & Ngo 2018). Table 10. 2 summarises the design parameters used to design the track structure based on field measurements and extensive laboratory testing and computational modelling. Based on the design criteria, typical ballast and capping thickness for the Chullora field trial were approximately 250-300 mm and 150-200 mm, respectively. Since the train speed permitted at this site (Chullora) is approximately 15 km/h, the thickness of the ballast was reduced to 250 mm and placed over a 150mm thick compacted capping layer. The thickness of the ballast and capping remained the same for all the sections. A 100 mm thick granular drainage layer was introduced (not included in the design) at the bottom of the excavated track to improve the drainage capacity of the track, as detailed in Section 10.4.

Table 10. 2: Design parameters used for track design calculation

Track components	Design Parameters
Sleepers	Width=0.25m, Length=2.5m, Height=0.23m Spacing (S)=0.6m
Ballast	Density=1560kg/m^3, Friction angle=48°, $E_{Ballast}$=250MPa, Resilient modulus=275MPa, Layer thickness=0.25m
Subbalast/capping	Density=1670kg/m^3, Friction angle=35°, $E_{subballast}$=115MPa, Layer thickness = 0.2m,
Subgrade	Density=1730kg/m^3, Friction angle=20°, $E_{subgrade}$=25MPa, c=10kPa, Layer thickness=1.5m, Subgrade soil compressive strength=85kPa, Allowable subgrade plastic strain, ε_p=2%, Allowable settlement =0.025m,
Load	Wheel diameter (D) =1.016 m, Axle load = 25ton, Train speed (V)=80 Km/h, Number of cycles used for the design=N=4,000,000, Axle spacing=1.9m

10.4 Improved Drainage at Chullora Field Trial

Laboratory investigations (Chapter 5) reveal that mud pumping or subgrade failures would happen with low to medium plasticity soils under adverse hydraulic conditions. Therefore, drainage capacity of the subgrade/capping interface had to be improved prior to constructing the track at Chullora. Although the water table was below the track, the entire site was flooded due to heavy rainfall and was filled up/inundated with surface runoff water from the surrounding areas. A granular drainage layer (100 mm) combined with a filter geotextile (Figure 10. 5) could be the best way to enhance the drainage capacity of railway tracks. Geocomposites with filter membranes and appropriate drainage characteristics can also control the upward migration of fines by dissipating the EPWP (Chapter 8). As Figure 10. 4 shows, sumps were constructed along the track to collect water that had built up underground before construction. Cess drains (150-300 mm diameter pipe) were placed at formation level at the side of the track to collect the water that continuously percolated through the ballast, and send it to a nearby culvert (Figure 10. 6).
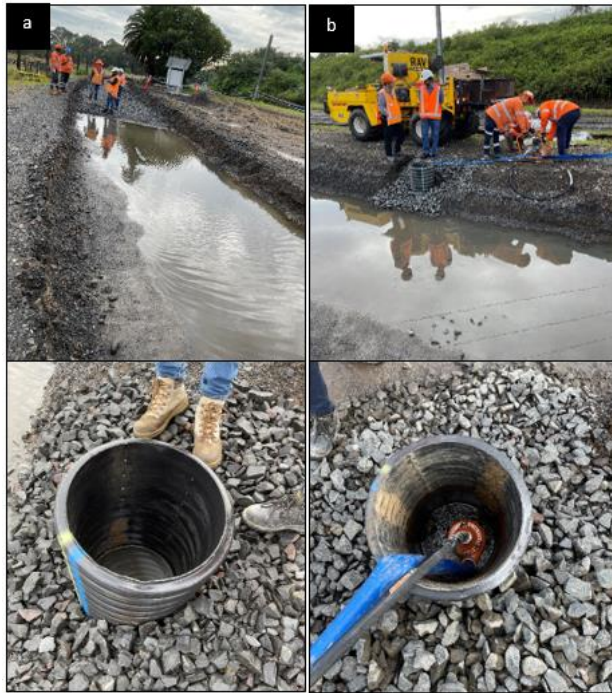
Figure 10. 4: (a) Chullora track after heavy rainfall - Construction of sumps, and (b) Dewatering system

Figure 10. 5: Drainage layer at subgrade level

Figure 10. 6: Cess drain construction – 300 mm diameter ag-pipe installation

10.5 Geosynthetic Inclusions

The subgrade soil in the ICS (Figure 10. 7) had a high fine content and was more prone to mud pumping under heavy haul train loading. As recommended in Chapter 8, geocomposite with a filter membrane was used for the instrumented railway track because it could prevent particle separation and the migration of fines through the pore openings of the geocomposite (Arivalagan et al. 2021). The geocomposite was placed at the subgrade level, over which a 100 mm thick drainage layer was placed to provide adequate drainage during heavy rainfall and prevent soil fluidisation (Figure 10. 8). According to the literature, anti-pumping geosynthetics should consist of a high compression modulus which can reduce the excessive cyclic deformation and provide sufficient permeability (Alobaidi & Hoare 1998; Alobaidi 1991). They can also prevent pore water pressure from being generated under the subgrade interface, and this can reduce the potential for mud pumping due to moving loads.

Bidim A44 nonwoven geotextile was used to separate the ballast and capping layer because it could also act as a drainage medium (Figure 10. 9). It can also be a reinforcing separator to protect the capping surface from undue damage from ballast tamping. MastaTEX F

225

Range nonwoven needle-punched geotextile was used to cover the ag pipe during the construction of the cess drain. Due to high levels of elongation, mastaTEX can withstand being damaged during installation and will prevent the ingress of fines into the drainage media (Figure 10. 10(c))

A robust nonwoven geotextile (Profab Ultra) was used in all the other sections (at the subgrade/capping interface) to compare the performance/effectiveness with the geocomposite G1 used in ICS. All the material properties of the selected geosynthetics are listed in Table 10. 3. In addition, as Figure 10. 10(a) and (b) show, a woven geotextile was used in the EcoFlex section to separate the ballast and recycled rubber energy absorbing layer, and Rubber geogrids were also installed in the EARS section.

Table 10. 3: Properties of selected Geosynthetics

Geotextile Properties	Bidim A44	Hydrotex 3	Profab Ultra	mastaTEX
Peak Tensile Strength (kN/m)	26.5	50	50	35
CBR Burst Strength (kN)	4.7	10	9.2	5.6
AOS Size (um)	75	<1	<75	<110
Permeability (l/m^2/s)	4.3	0.03	40	90
Cone drop diameter (mm)	<1	<1	<1	<5

Figure 10. 7: Subgrade soil at Instrumented control section

Figure 10. 8: Installation of Terram Hydrotex on subgrade soil – Geocomposite G1

Figure 10. 9: Installation of Bidim A44 on compacted capping layer
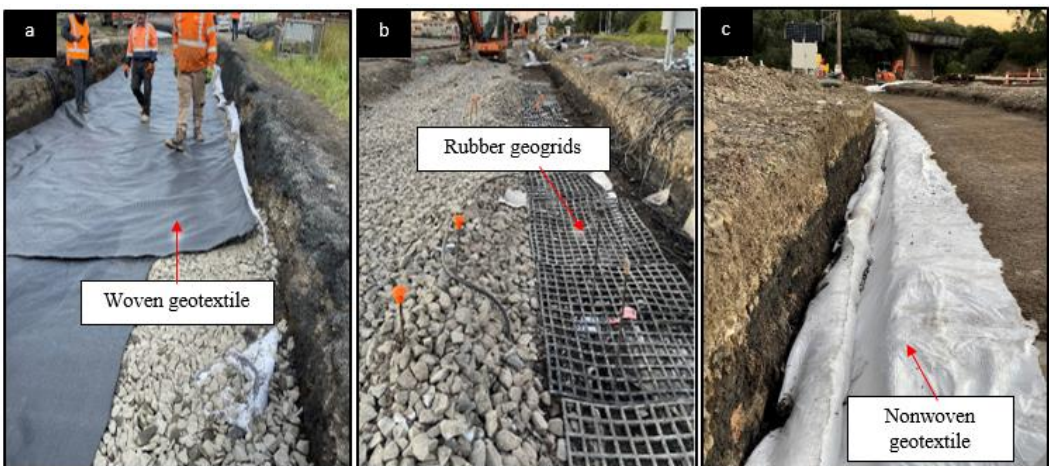
Figure 10. 10: (a) Woven geotextile at capping/ballast interface (ECOFLEX), (b) Rubber geogrids at capping/ballast interface (EARS), and (c) MastaTEX nonwoven geotextile to protect ag-pipes

10.6 Instrumentation

Figure 10. 11 shows a suite of instruments laid on the subgrade, capping, ballast, sleeper and rail interfaces to measure the distribution of stress, the generation of pore pressure, differential settlement, and the acceleration of motion of a structure. To evaluate the performance of each layer by measuring the deformation, stress transformation (energy absorption), and vibration, different types of instruments were proposed, as shown in Table 10. 4. The symbols set for the identification and placement level are also given in Table 10. 5. The pressure cells, extensometers, and accelerometers were connected to the data acquisition; i.e. DAQ ICS for the instrumented control section. As Figure 10. 12 and Figure 10. 13 show, the settlement pegs were designed to measure the vertical track deformation (settlement); the level of the settlement peg can be taken manually or by a camera. A set of settlement pegs were proposed for manual reading, and a wide-angle Pan-Tilt-Zoom (PTZ) camera was also used to monitor the settlement in tracks (Figure 10. 14).
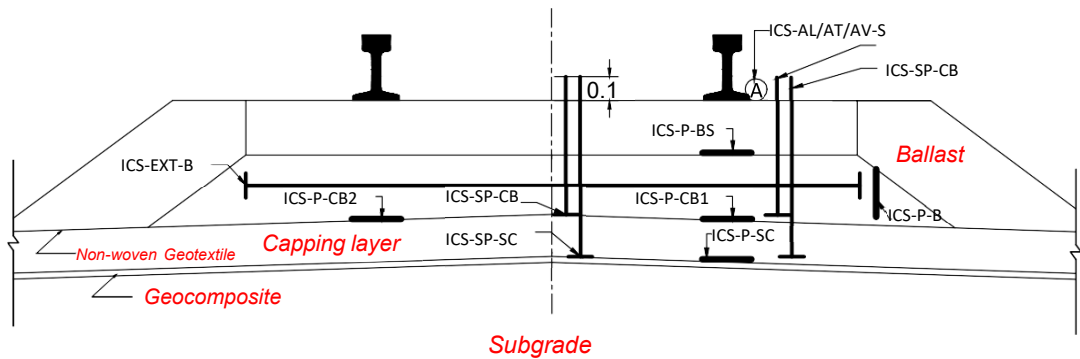
Figure 10. 11: Instrumentation of ICS section (scale: 1:20)
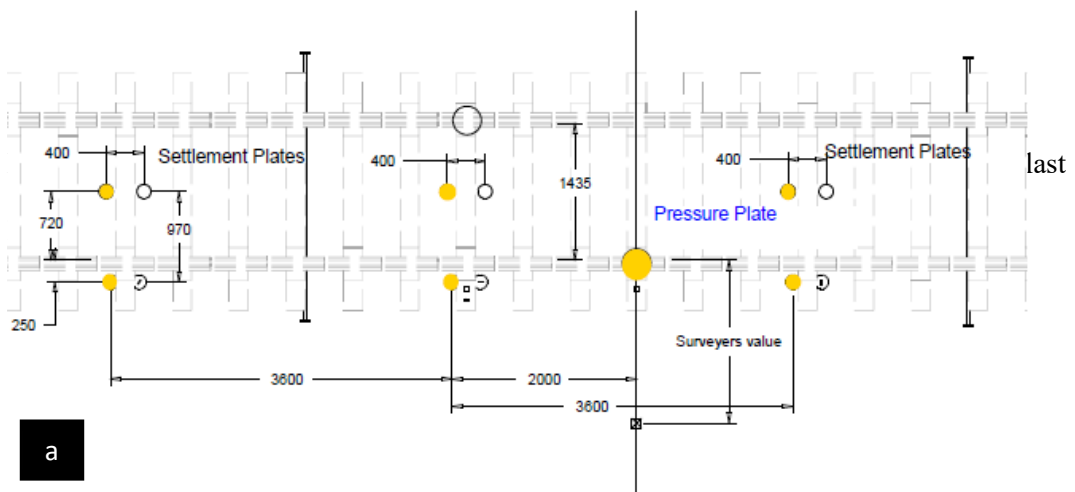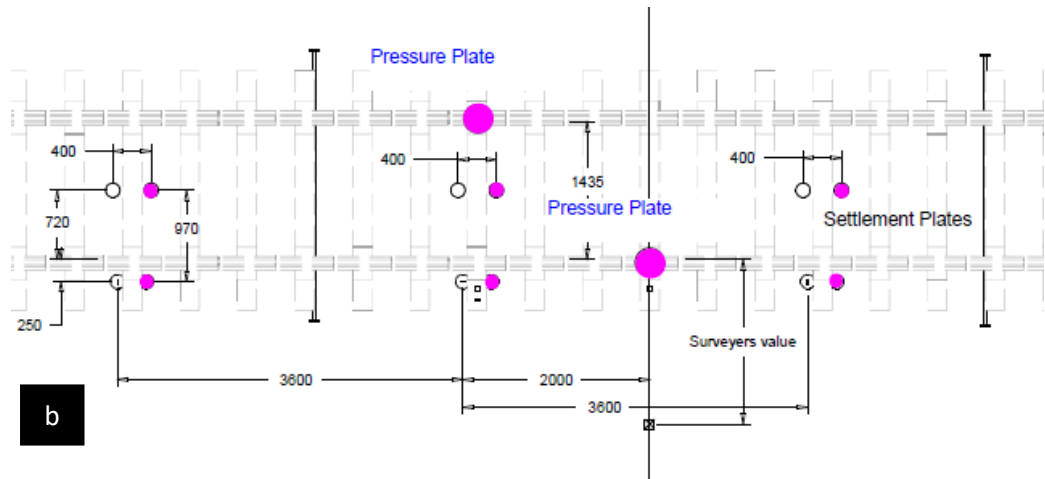
Figure 10. 12: Plan view of ICS instrumentation (a) subgrade/capping interface and (b)

Capping/ballast interface (Eng.Analysis)

Figure 10. 13: (a) Instrumentation at the capping/ballast interface, (b) Settlement Plates and

(c) Pressure cell
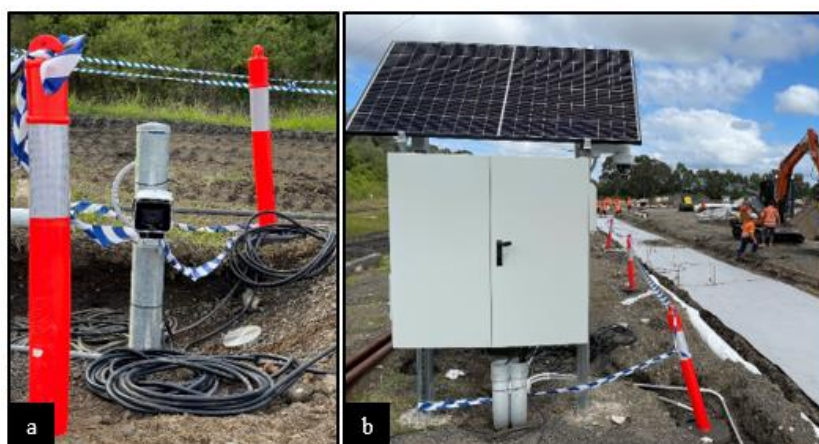
Figure 10. 14: (a) Wide angle PTZ camera and (b) Data Acquisition System (DAQ)

Table 10. 4: Type of sensors used in Instrumented control section (40 m section)

Location of the Instrument	Sensor Name	Sensor type
Subgrade	ICS-MS-G-17.810	Moisture sensor
	ICS-PP-G-17.810	Pore pressure Transducer
Subgrade-Capping Interface	ICS-SP-SC-17.806	Settlement plate ©
	ICS-SP-SC-17.810	Settlement plate (M)
	ICS-SP-SC-17.814	Settlement plate (M)
	ICS-P-SC-17.808	Pressure plate - 1 MPa
Capping-Ballast Interface	ICS-SP-CB-17.806	Settlement plate ©
	ICS-SP-CB-17.810	Settlement plate (M)
	ICS-SP-CB-17.814	Settlement plate (M)
	ICS-P-CB-17.808	Pressure plate - 1 MPa
	ICS-P-CB-17.810	Pressure plate - 1 MPa
Ballast	ICS-EXT-B-17.804	In ballast extensometer
Ballast/Sleeper Interface	ICS-P-BS-17.808	Pressure plate - 1 MPa
	ICS-P-BS-17.810	Pressure plate - 1 MPa
Sleeper and Rail	ICS-SP-S-17.810	Settlement target on sleeper ©
	ICS-AL-S-17.808	Accelerometer - X
	ICS-AT-S-17.808	Accelerometer - Y
	ICS-AV-S-17.808	Accelerometer - Z

Table 10. 5: Notations used for instrumentation of the track

Notations	Description
ICS	Instrumented Control Section
SP	Settlement Plate
P	Pressure plate
L	Lateral pressure plate
EXT	Extensometer

AL	Accelerometer - Longitudinal
AT	Accelerometer - Transverse
AV	Accelerometer - Vertical
MS	Moisture Sensor
PP	Pore Pressure transducer
G	in Ground
SC	Subgrade/Capping interface
CB	Capping/Ballast interface
BS	Ballast/Sleeper interface
S	Sleeper
B	Ballast
©	Camera reading
M	Manual readings

10.7 Laboratory and Field Investigations

10.7.1 Particle Size Distribution and Proctor Curve

Figure 10. 15(a) shows that the capping material contains around 15% of fine particles (i.e., the percentage passing through 0.75μm is 15%). The optimum moisture content (OMC) and maximum dry density (MDD) were 6.6 % and 2.2 t/m³, respectively (Figure 10. 15(b)). It was expected to achieve more than 95% of Relative Compaction (RC) in the field.
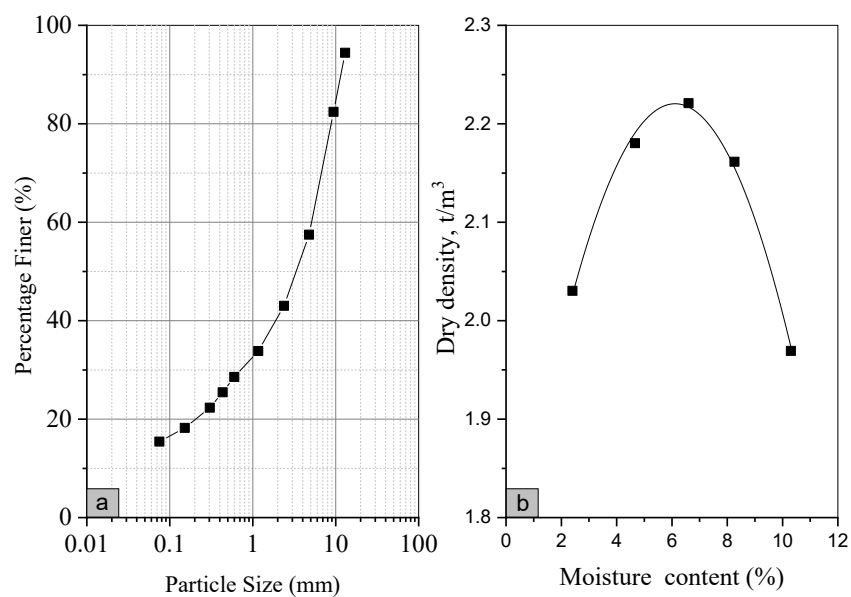
Figure 10. 15: Properties of Capping material (a) PSD and (b) Proctor compaction Test

10.7.2 38-mm Diameter Cored Samples (Compacted Capping)

Cored samples were taken to the laboratory to measure the dry density of compacted capping (Figure 10. 16).

Figure 10. 16: (a) Coring samples at different locations, (b) Cored specimen inside the cylindrical tube, and (c) Extruded specimen for laboratory testing
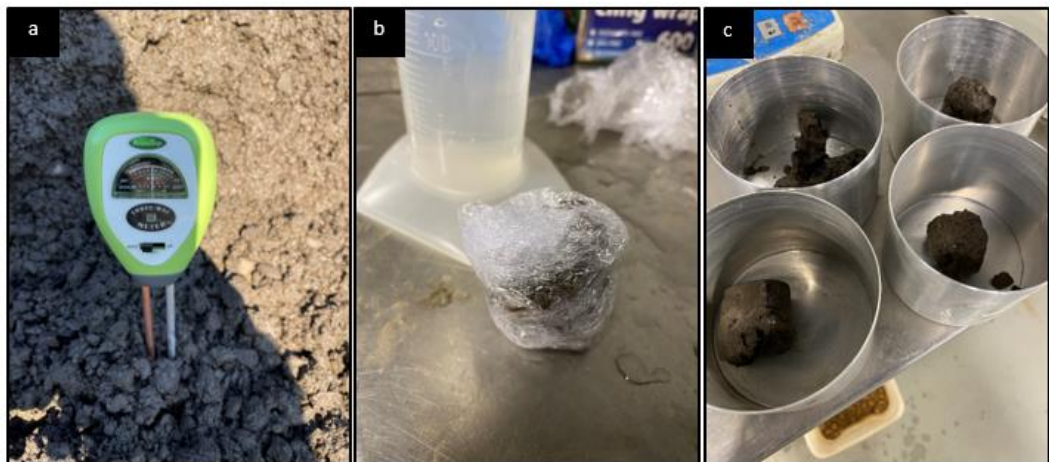
Figure 10. 17: (a) Measuring the water content, (b) Soil specimens collected from the field ,and (c) Determining the moisture content and density in the laboratory (Courtesy: Dr Mandeep Singh)

As Figure 10. 17(a) shows, a moisture meter (calibrated with actual field measurements) was used to determine the water content of stockpiles. Non-destructive density Test was performed on compacted capping to ensure 98% of RC (Figure 10. 18(a)). A DIGI Schmidt 2000 concrete tester was also used to measure the density of compacted capping.

Figure 10. 18: (a) Nuclear density gauge/Non-destructive density Test and (b) the Schmidt Test
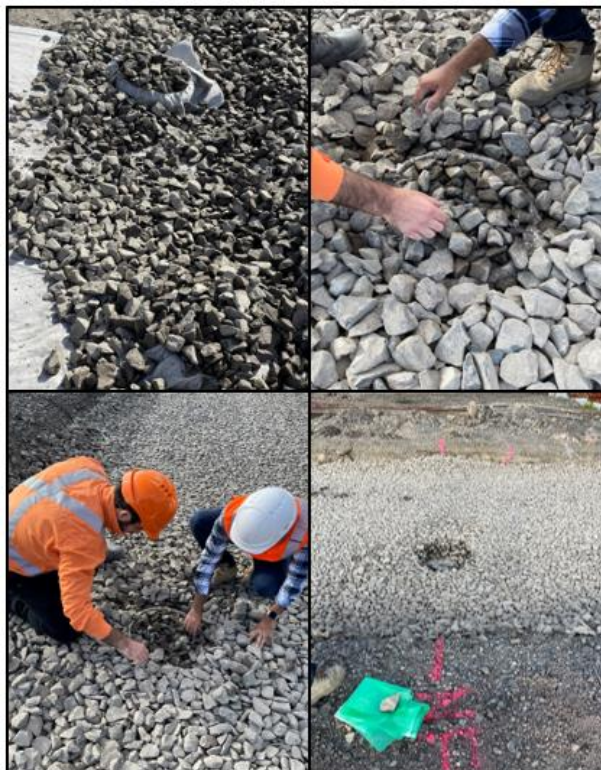
Figure 10. 19: Determining the bulk density of compacted ballast in the field (compaction of 150 mm thick layer)

10.7.3 Compacted Ballast Density

The target unit weight of 15.5-16.5 kN/m^3 was achieved by compacting the 250 mm thick ballast into two layers, i.e., the first and second layers were around 150 and 100 mm thick, respectively. The number of passes by a 7-tonne steel roller was calculated based on the packing density of the ballast layers, as shown in Figure 10. 19.

10.8 Track Construction – Instrumented Control Section

Once the 100 mm thick drainage layer had been compacted, a 150 mm thick layer of capping material was placed such that the top surface maintained a 2% slope towards the cess drain (Figure 10. 20). A layer of nonwoven geotextile (Bidim A44) was used as a separator at the capping/ballast interface to prevent the bottom ballast from digging into the capping surface (Figure 10. 21(a)). This means the coarser particles of ballast will not be contaminated by fines due to the inclusion of Bidim A44; it can also direct the water that percolates through the ballast layer and flows into the cess drain. After completing the capping layer, a 150 mm thick layer of ballast was laid and compacted in two stages to achieve a maximum dry density of 1600 kg/m^3, as explained in Section 10.6.3.

Figure 10. 20: Laying capping material on the drainage layer, and (b) Compaction of capping
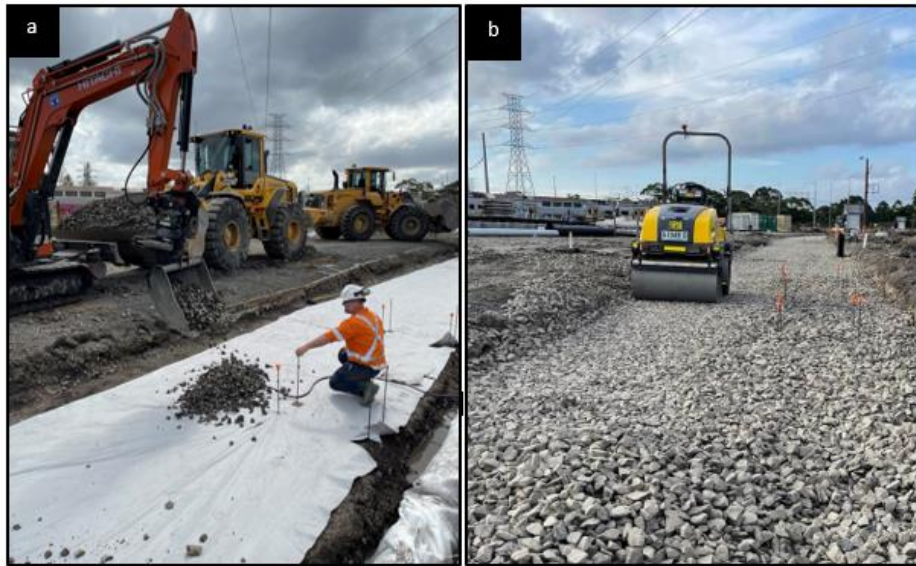
Figure 10. 21: (a) Pouring ballast on the instrumentation units, and (b) compaction of 150 mm thick ballast layer

Figure 10. 22: Final stages of track construction (a) Laying sleepers and rails, (b) Construct ballast shoulders, and (c) Tamping Ballast voids

The sleepers and rails were laid on a layer of compacted ballast, as shown in Figure 10. 22(a). The crib/shoulder ballast was constructed and levelled to improve the lateral sliding resistance, as shown in Figure 10. 22(b). A ballast tamper was used to pack the ballast in order to make the tracks more durable and level (Figure 10. 23(c)). As Figure 10. 23(a) shows, all the instruments were connected to the solar-powered data acquisition system at four locations; this system can continuously supply power to all the instruments during train loading.
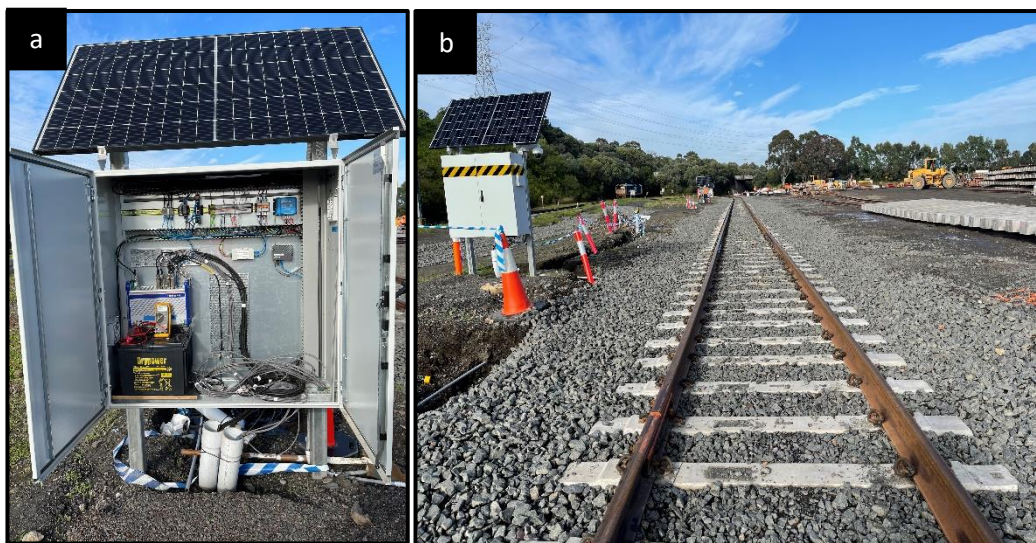
Figure 10. 23: (a) Solar powered data acquisition system and (b) Completed track at Chullora

10.9 Test Outcomes and Contributions

Due to the COVID-19 restrictions in NSW, Australia, the Chullora track construction was significantly affected, which delayed loading the live train and the field data measurements. The field measurements and data analysis can be done by other PhD students involved in this project. I want to express my sincere thanks to my supervisors, Industry Partners, and some of our technical crew on-site, especially Dr Trung, Dr Mandeep, Dr Rakesh, Chathuri and Anees for helping me collect soils and overseeing quite a lot of the site activities.

10.10 Chapter Summary

This chapter describes the design and construction stages of the Chullora field trial and the inclusion of geocomposite material in the field to reduce the risk of severe particle migration and mud pumping under adverse hydro-dynamic conditions. It also concludes the laboratory field observations and problems encountered during the construction phases. Furthermore, the effectiveness of geocomposites and other geosynthetics applied in the field were discussed based on the outcomes of laboratory testing and field trial construction. This collaborative research between academia and industry incorporated sophisticated laboratory tests, FEM modelling, and field studies to promote innovation and growth in technology.

CHAPTER 11: CONCLUSIONS AND RECOMMENDATIONS

11.1 General Synopsis

In railway tracks, the finer particles of subgrade soil can be softened and pumped up towards the uppermost layers under critical dynamic loads; this phenomenon is commonly known as mud pumping and mostly occurs in low-lying saturated subgrade. Although some studies have highlighted the adverse effects of mud pumping, the governing mechanism and critical factors which lead to subgrade instability, advanced geotechnical soil characterisations, and cost-effective solutions, have not been well established (Chapter 2). Track instability can generally be controlled by installing a compacted capping layer (sand blanket) beneath the ballast to reduce the dynamic stress that is transferred towards the subgrade soil, or by installing geosynthetics that can provide enough drainage to eliminate the excessive hydraulic gradients that develop under cyclic loads. Overly compacted capping or a sand blanket cannot dissipate the rapid generation of EPWPs and sometimes fails to prevent subgrade fluidisation (Nguyen et al. 2019). Undrained and free drainage tests were carried out in this study to determine the key factors that contribute to subgrade fluidisation (Chapter 5). While geotextiles can be used to prevent particle migration and enhance drainage capacity at the interface, fine particles that become trapped inside the pores can still affect the drainage properties of geosynthetics. Geotextiles with different filtration and drainage properties in terms of aperture opening sizes were therefore investigated to assess their performance under cyclic loading (Chapter 6). The

characteristics of vulnerable soft soils and the design criteria for effective filters should be investigated prior to the track construction (Chapter 7). Of the different techniques used to improve the stability of foundations, prefabricated vertical drains are a recent addition to alleviate the rapid generation of EPWPs and subgrade fluidisation in tracks that experience critical dynamic loads (Chapter 8). The combination of PVD and geotextile could be an appropriate technique to dissipate the accumulated pore water pressure at shallower depths (Chapter 9). Different types of geosynthetics were installed at the Chullora field trial to alleviate the occurrence of subgrade instability during the passage of heavy haul trains (Chapter 10).

11.2 Conclusions

The following salient findings evolving from the outcomes of this study are highlighted below.

11.2.1 Factors Causing Subgrade Fluidisation in Railway Tracks

Excessive cyclic excess pore pressure can undoubtedly cause instability in soft and saturated subgrade soils with high water content during the passage of trains. For example, an undrained test showed a rapid development of EPWP in less than 500 cycles and remained without any significant reduction afterwards ($>EPP_{T1}$). The tests also showed that the generation of EPWPs deeper in the subgrade soil profile (80-120 mm below the interface) without further reduction over time can lead to adverse hydraulic conditions.

11.2.1.1 Excess Pore Pressure Gradient (EPPG)

The EPPG under cyclic load plays a key role in inducing fines to migrate from the middle region towards the upper region. For instance, in the undrained tests, the EPPG that developed approximately 100 mm below the interface was more than 35 after only 500

cycles (i.e., with less than 2 minutes of train loading). A rapid generation of high EPPG can lead to soil softening and significant increases in the water content can cause a rapid reduction in track stiffness, localised deformation, and overall instability.

11.2.1.2 Loading Characteristics

The increasing cyclic deviator stress hinders the effectiveness of capping layer/geosynthetics and induces particle migration. For instance, during the passage of heavy-haul trains with an axle load of 40 tonnes (σ_{max} of 140 kPa), the ability of geocomposite (G1) to prevent particle migration decreased. Moreover, the EPPG was above 35 ($EPPG_{T1}$) in the middle layers of soil up to 40,000 cycles, and reached 5% of axial strain before 75,000 cycles in Test G-100-5 (approximately 35 tonnes axle load).

11.2.1.3 Characteristics of Soft Subgrade

Many researchers have investigated the characteristics of subgrade soil subjected to subgrade fluidisation in railway tracks (Indraratna et al. 2020; Nguyen & Indraratna 2021; Nguyen et al. 2019). The characteristics of subgrade, such as the consistency and degree of compaction of the soil, are among the key factors that contribute to subgrade fluidisation. Field investigations followed by geotechnical tests showed that low plasticity soils with a PI between 10 to 30% and LL of less than 50% were more vulnerable to subgrade fluidisation and associated mud pumping; this type of subgrade therefore needs more attention (Chapter 8).

11.2.1.4 Abrupt Change in Water Content

The water content of the tested specimens was measured from top to bottom at three different locations, after the cyclic tests. For example, the liquidity index (LI) at the top part (subgrade surface) was almost 1, which represents a state of liquidity, but this

decreased to about 0.2 at the bottom of the subgrade specimen. This represented inhomogeneous behaviour after the soil become fluidised because the water content and void ratio varied considerably along the height.

11.2.1.5 Pumping of Fine Particles

The upward migration of fines is also caused by the moisture content being redistributed due to cyclic loading. For instance, undrained tests experienced an abrupt change in the water content along the height of the specimen, and a finer fraction of less than 75 μm pumped up from underneath soil became slurry at the top. A particle with a large specific surface area (i.e., the finest particles) would absorb more water, which explains how the moisture content of soil redistributed during the migration of fine particles. Under free drainage tests, repetitive cyclic loading intensified the potential occurrence of subgrade fluidisation, which may then result in the overlying coarser particles penetrating the now softened subgrade layer.

11.2.2 Application of Geosynthetics in Preventing Subgrade Fluidisation

Prevention techniques for subgrade fluidisation are needed, especially when soft vulnerable soils are subjected to heavy haul train loading. The installation of geotextiles, geocomposites, prefabricated vertical drains (PVDs), and a combined PVD-Geocomposite system has proven to be a good method for reducing the accumulation of pore water pressure. Based on the series of tests carried out to quantify the risk of mud pumping under cyclic loading using dynamic filtration apparatus, the following conclusions were drawn, as shown below:

    a) Geocomposite (G1 and G5) alleviated the EPWPs that developed at or close to the interface as the cycles increased. At a maximum vertical cyclic stress of 70 kPa (undrained), the considerable upward migration of fine particles and a corresponding increase in the moisture content induced the subgrade surface to

become a slurry under undrained conditions. However, there was a dramatic decrease in the water content (26%) when geocomposite was placed at the interface, and the subsequent penetration of ballast particles into the subgrade soil (free drainage test) was prevented. This proves that this geocomposite could minimise the migration of fine particles in the middle region and prevent the slurry formation at the uppermost layer.

b) The EPWP that developed for G2, G3, and G4 were higher than EPP_{T1} (>22 kPa) after 10,000 cycles, and the rate of dissipation was not significant until the end of the cyclic test. Although the aperture opening size of filters (G1 and G5) was less than 10 μm (Chapter 3), they could still prevent particle migration and dissipate the EPWP under cyclic loading. However, the larger pores in geotextiles (G2 and G4) could not prevent particle migration and they finally became clogged with pumped-up fine particles. This indicated that geocomposites with a filter membrane could reduce the accumulation of EPWPs at the subgrade surface and prevent migration of fines.

c) The excess pore pressure gradient (EPPG) plays a key role in inducing fines to migrate from the middle region towards the subgrade surface. However, the inclusion of G1 and G5 reduced the EPPG by 90% after 1000 cycles in the middle layer compared to the undrained tests. This significant reduction in EPPGs reduced the migration of fines by 35% compared to the other geotextiles (G2, G3, and G4). These results imply that geocomposites with a filter reduced the EPPG that developed inside the subgrade soil and thus prevented finer particles from separating from the soil matrix.

d) Soil under increased axle loads may become more prone to subgrade fluidisation. An increase in the cyclic stress led to the development of axial strain and EPWPs, despite the inclusion of geocomposites, when the cyclic deviator stress was more than 55 kPa. The PSD curves also showed that the migration of fine particles

increased as the cyclic stress increased. These results suggest that the potential for fine migration can decrease as the cyclic stress decreases, and fluidisation can also be triggered at lower frequencies in tracks with poor drainage conditions.

e) The combined PVD-geocomposite system prevented the rapid accumulation in EPWP from the beginning of the cyclic test. The inclusion of PVDs could control the EPWP, even under higher axle loads and larger frequencies. For instance, the EPWP that developed at 20 and 80 mm from subgrade interface fell to less than 30 kPa after 100,000 cycles under increased axle loads (30-35 tonnes) and reached less than 2.5% of axial strain in Test PG-85-5. The migration of fine particles towards the top surface was insignificant with a PVD-geocomposite system compared to other tests. This indicates that under higher axle loads and speeds, the generation of EPWPs at the middle/lower regions could be curtailed with the inclusion of a combined system of PVD and geocomposite.

11.2.3 Numerical Modelling

Techniques for preventing mud pumping focus mainly on stabilising the weak subgrade soil by geosynthetic inclusions. The FE simulations carried out in PLAXIS 2D show that the inclusion of geotextiles can reduce the build-up of EPWPs at the subgrade surface. PVDs can help to reduce the peak of EPWPs at shallow depths, unlike in undrained conditions. These numerical simulations essentially proved that a combined PVD-geotextile system could continuously alleviate the formation of EPWPs under dynamic loading conditions. For instance, the maximum EPWPs that developed under 20 -tonne loads were less than 45 kPa at 0.5 m depth until 1500 cycles. The combination of PVD and geotextile could reduce the critical EPWP generation in the shallow subgrade more uniformly even after the train loading thereby increasing the stability of railway foundations.

11.2.4 Chullora Field Trial

The subgrade soil in Chullora field trial had a high fine content and was more prone to mud pumping under heavy haul train loading. Due to the heavy rainfall, the entire site was flooded and was filled up with surface runoff water. The geocomposite with a filter membrane was used for the instrumented railway track because it could prevent particle separation and the migration of fines through the pore openings of the filter membrane. The geocomposite was placed at the subgrade level, over which a 100 mm thick drainage layer was placed to provide adequate drainage during heavy rainfall and prevent soil fluidisation. A suite of instruments laid on the subgrade, capping, ballast, sleeper, and rail interfaces can measure the generation of pore pressure, cyclic stress distribution, differential settlements, and the acceleration of motion of a structure.

11.3. Industry Implications

This present research focused on understanding how geosynthetics prevent particle migration and associated mud pumping under heavy haul train loading. The laboratory results indicated that fine particles soften and form a slurry during cyclic loading, which is then pumped upwards when the moisture content approaches its liquid limit. However, the inclusion of geosynthetics alleviates the rapid accumulation of EPWP and reduces the potential for upward mud pumping and higher water content at the subgrade surface. The impact on industry as a result of this research can be summarised:

- The plasticity characteristics of subgrade govern the occurrence of mud pumping. Subgrade soils with low/medium plasticity show prominent signs of mud pumping in railway tracks, whereas cohesive soils with high plasticity may not experience mud pumping. In essence, cohesive soil with a high clay content can resist fabric instability by preventing the segregation of fine particles and the migration of moisture.

244

- The application of geosynthetics can be an effective way to stabilise railway tracks by preventing the migration of particles and continuously dissipating excess pore water pressure, especially near the subgrade surface. The geocomposites with a filter membrane can act as a filter and a separator to prevent particle migration and provide adequate drainage (Chapter 9). However, the inclusion of geotextiles without appropriate drainage and filtration characteristics can lead to subgrade instability in the long term.

- The inclusion of short PVDs can significantly reduce and delay the rapid generation of EPWPs in deeper subgrade soil, while geocomposite can provide adequate surficial drainage at the interface. From a practical perspective, the stabilisation of rail tracks with a PVD-geocomposite system can prevent the occurrence of subgrade instability and fluidisation in the field.

11.4 Limitations of the Study

The following limitations apply to the current study.

- The laboratory equipment can mostly be used for testing small-scale soil specimens compared to the actual field scale. Therefore, scale and boundary effects will influence the laboratory data in relation to the actual field behaviour. The drain dimensions and soil thickness tested in the current equipment can still provide realistic pore water pressures and gradients (Indraratna & Redana 1997, 1998). However, there will always be boundary effects which cannot be totally eliminated, and the rate of pore pressure dissipation in the laboratory with much smaller seepage path lengths is expected to be faster than typical field conditions (Baral et al. 2018)

- The effect of principal stress rotation under moving load was not considered within the scope of this study. It is expected that the behaviour of soft subgrade involving principal stress rotation and the influence of intermediate principal stress can affect the pore pressure response of soft soils especially at high train speeds (Bian et al. 2020; Gräbe & Clayton 2014). In this study, the experimental data obtained for low loading frequency (1-3 Hz) is more applicable for heavy haul trains operating at relatively low speeds (< 80 km/h).

- The geotextiles and geocomposites were placed between the subgrade surface and ballast layer; no sub-ballast layer (compacted sand layer) was placed over the geosynthetics. The filtration behaviour of subballast, the influence of cyclic load on the design of a combined geosynthetics and capping layer were not considered within the scope of this study.

- The current laboratory observations will need to be corroborated further to more extensive field monitoring of potential mud pumping sites to gain further insight into rise and dissipation of EPWP and corresponding EPPG under cyclic loading. Such information will be required to extend FE analysis and design standards to include quantified methods of analysis for subgrade fluidisation and to implement preventive measures such as PVD-geocomposite systems.

11.5 Recommendations for Future Research Work

Further research work could be undertaken in the following areas:

- The relative compaction (RC) of compacted soil used in this study was 95%, but a series of tests could still be carried out with varying RCs (70-95%) to examine how the degree of compaction induces subgrade fluidisation in railway tracks. To assess the potential for subgrade fluidisation, a range of soil samples (with varying soil properties) can be collected/tested from different mud pumping sites.

- A large-scale triaxial test could be the best way to carry out cyclic tests under confining pressure. By following the similar test procedures described for dynamic filtration tests, large-scale cylindrical triaxial tests (300-500 mm diameter by 600-1000 mm high) could be carried out. It would be good to measure how the critical EPWPs would dissipate over time and how the hydraulic gradient contributes to pumping up fine particles. Further work needs to consider the smear zone, well resistance, and mandrel effects.

- A numerical model could be used to observe the behaviour of particle migration associated with subgrade fluidisation. This could also be extended to various cyclic loadings under various drainage conditions, so that particle dislocation and migration could be captured using the coupled discrete element method (coupled CFD-DEM/LBM-DEM simulations).

12. REFERENCES

AASHTO M288 - 08 2008, Standard Specification for Geotextile Specification for Highway Application, Virginia, VA, USA.

Abeywickrama, A., Indraratna, B. & Rujikiatkamjorn, C. 2019, "Excess Pore-Water Pressure Generation and Mud Pumping in Railways Under Cyclic Loading", Geotechnics for Transportation Infrastructure, pp. 371-83.

Abeywikrama, A.L. 2020, "Investigation of subgrade fluidization under cyclic train loads and mitigation measures", PhD Thesis, University of Wollongong, Australia, p. 186.

Aboshi, H., Sutoh, Y., Inoue, T. & Shimizu, Y. 2001, "Kinking deformation of PVD under consolidation settlement of surrounding clay", Soils and foundations, vol. 41, no. 5, pp. 25-32.

Abuel-Naga, H.M., Pender, M.J. & Bergado, D.T. 2012, "Design curves of prefabricated vertical drains including smear and transition zones effects", Geotextiles and Geomembranes, vol. 32, pp. 1-9.

Ai-Qadi, I.L. & Appea, A.K. 2003, "Eight-year field performance of secondary road incorporating geosynthetics at subgrade-base interface", Transportation research record, vol. 1849, no. 1, pp. 212-20.

Al-Qadi, I.L., Brandon, T.L., Smith, T.E. & Lacina, B.A. 1994, "How do geosynthetics improve pavement's performance", Proceedings of the 3rd Materials Engineering Conference, ASCE, pp. 606-16.

Al-Soud, M.S. 2016, "Numerical analysis of prefabricated vertical drains improved soft soil beneath an embankment during staged construction", Journal of Engineering and Sustainable Development, vol. 20, no. 1, pp. 151-63.

Alobaidi, I. & Hoare, D. 1994, "Factors affecting the pumping of fines at the subgrade subbase interface of highway pavements: a laboratory study", Geosynthetics International, vol. 1, no. 2, pp. 221-59.

Alobaidi, I. & Hoare, D. 1998a, "The role of geotextile reinforcement in the control of pumping at the subgrade-subbase interface of highway pavements", Geosynthetics International, vol. 5, no. 6, pp. 619-36.

Alobaidi, I. & Hoare, D. 1999, "Mechanisms of pumping at the subgrade-subbase interface of highway pavements", Geosynthetics International, vol. 6, no. 4, pp. 241-59.

Alobaidi, I. & Hoare, D.J. 1996, "The development of pore water pressure at the subgrade-subbase interface of a highway pavement and its effect on pumping of fines", Geotextiles and Geomembranes, vol. 14, no. 2, pp. 111-35.

Alobaidi, I. & Hoare, D.J. 1998b, "Qualitative criteria for anti-pumping geocomposites", Geotextiles and Geomembranes, vol. 16, no. 4, pp. 221-45.

Alobaidi, I.M. 1991, "Some aspects of the role of geocomposites in controlling pumping of fines", PhD Thesis, University of Birmingham, United Kingdom, p. 360.

Andersen, K.H., Rosenbrand, W.F., Brown, S.F. & Pool, J.H. 1980, "Cyclic and static laboratory tests on Drammen clay", Journal of the Geotechnical Engineering Division, vol. 106, no. 5, pp. 499-529.

Ansal, A.M. & Erken, A. 1989, "Undrained behavior of clay under cyclic shear stresses", Journal of Geotechnical Engineering, vol. 115, no. 7, pp. 968-83.

ARA 2020, The value of freight rail, Australian Railway Association.

AREMA 2003, "Practical Guide to Railway Engineering", American Railway Engineering and Maintenance-of-way Association, Simmons-Boardman Publishing Corporation, Maryland.

Arivalagan, J., Indraratna, B., Rujikiatkamjorn, C. & Warwick, A. 2022, "Effectiveness of a Geocomposite-PVD system in preventing subgrade instability and fluidisation under cyclic loading", Geotextiles and Geomembranes, vol. 50, no. 4, pp. 607-17.

Arivalagan, J., Rujikiatkamjorn, C., Indraratna, B. & Warwick, A. 2021, "The role of geosynthetics in reducing the fluidisation potential of soft subgrade under cyclic loading", Geotextiles and Geomembranes, vol. 49, no. 5, pp. 1324-38.

ARTC 2013, Mud Hole Management Guideline ETH-10-01.

ARTC 2018, New Track Construction (Inland Rail), ETC-00-02.

ARTC 2019, Ballast Specification, ETA-04-01.

Arulrajah, A., Abdullah, A., Bo, M.W. & Leong, M. 2015, "Geosynthetic applications in high-speed railways: a case study", Proceedings of the institution of civil engineers-ground improvement, vol. 168, no. 1, pp. 3-13.

ASTM D5856-95 2002, Standard test method for measurement of hydraulic conductivity of porous material using a rigid-wall, compaction-mold permeameter, West Conshohocken, PA, USA: American Society for Testing and Materials.

ASTM D422-63 2007, Standard Test Method for Particle-Size Analysis of Soils, ASTM International West Conshohocken, PA.

ASTM D638-03 2003, Standard Test Method for Tensile Properties of Plastics, ASTM International, 100 Barr Harbor Drive, PO Box C700, West Conshohocken, PA 19428-2959, United States.

ASTM D698-00 2000, Standard Test Methods for Laboratory Compaction Characteristics of Soil Using Standard Effort (12,400 ft-lbf/ft3 (600 kN-m/m3)), Annual Book of ASTM Standards.

ASTM D854-02 2002, Standard test method for specific gravity of soil solids by water pycnometer, American Society for Testing and Materials West Conshohocken, PA.

ASTM D3774-96 1996, Standard Test Method for Width of Textile Fabric, ASTM, 100 Barr Harbor Drive, West Conshohocken, PA 19428-2959, United States.

ASTM D3999-91 2003, Standard Test Methods for the Determination of the Modulus and Damping Properties of Soils using the Cyclic Triaxial Apparatus, Annual Book of ASTM standards.

ASTM D4318-00 2003, Standard Test Methods for Liquid Limit, Plastic Limit, and Plasticity Index of Soils, Annual Book of ASTM Standards, American Society For Testing and Materials, West Conshohocken, PA.

ASTM D4491-99 1999, Standard test method from water permeability of Geotextiles by permitivity, American Society for Testing Materials, West Conshohocken, PA.

ASTM D4716-00 2000, Standard Test Method for Determining the (In-plane) Flow Rate per Unit Width and Hydraulic Transmissivity of a Geosynthetic Using a Constant Head, ASTM International, United States.

ASTM D4751-99 1999, Standard Test Method for Determining Apparent Opening Size of a Geotextile, ASTM, 100 Barr Harbor Drive, West Conshohocken, PA 19428-2959, United States.

ASTM D5199-01 2001, Standard Test Method for Measuring the Nominal Thickness of Geosynthetics, ASTM, 100 Barr Harbor Drive, West Conshohocken, PA 19428-2959, United States.

ASTM F316-03 2011, Standard Test Methods for Pore Size Characteristics of Membrane Filters by Bubble Point and Mean Flow Pore Test, ASTM International, West Conshohocken, PA, 2003.

Attya, A., Indraratna, B. & Rujikiatkamjorn, C. 2007a, "Cyclic behaviour of PVD-soft soil subgrade for improvement of railway tracks", Common Ground Proceedings, 10th Australia New Zealand Conference on Geomechanics Brisbane, pp. 36-41.

Attya, A., Indraratna, B. & Rujikiatkamjorn, C. 2007b, "Effectiveness of vertical drains in dissipating excess pore pressures induced by cyclic loads in clays", Proceedings of the 16th Southeast Asian Geotechnical Conference, Yee, K, et al. (eds), Selangor, Malaysia, pp. 447-51.

Austin, R. & Gilchrist, A. 1996, "Enhanced performance of asphalt pavements using geocomposites", Geotextiles and Geomembranes, vol. 14, no. 3-4, pp. 175-86.

Australian Trade and Investment Commission, Cutting-edge technology, products and services, Australian Government, Australia.

Aw, E.S. 2007, "Low cost monitoring system to diagnose problematic rail bed: Case study of mud pumping site", PhD Thesis, Massachusetts Institute of Technology, p. 203, pp. 1-203.

Aydilek, A.H., Oguz, S.H. & Edil, T.B. 2002, "Digital image analysis to determine pore opening size distribution of nonwoven geotextiles", Journal of Computing in Civil Engineering, vol. 16, no. 4, pp. 280-90.

Aydilek, A.H., Oguz, S.H. & Edil, T.B. 2005, "Constriction size of geotextile filters", Journal of Geotechnical and Geoenvironmental Engineering, vol. 131, no. 1, pp. 28-38.

Ayres, D. 1986, "Geotextiles or geomembranes in track? British railways' experience", Geotextiles and Geomembranes, vol. 3, no. 2-3, pp. 129-42.

Baral, P., Rujikiatkamjorn, C., Indraratna, B. & Kelly, R. 2018, "Radial consolidation characteristics of soft undisturbed clay based on large specimens", Journal of Rock Mechanics and Geotechnical Engineering, vol. 10, no. 6, pp. 1037-45.

Barron, R.A. 1948, "Consolidation of Fine-Grained Soils by Drain Wells", Transactions of the American Society of Civil Engineers, vol. 113, no. 1, pp. 718-42.

Basu, D. & Madhav, M. 2000, "Effect of prefabricated vertical drain clogging on the rate of consolidation: A numerical study", Geosynthetics International, vol. 7, no. 3, pp. 189-215.

Basye, C. & Li, D. 2015, "Remediation of a railway embankment involving soft soils and ballast pockets under heavy axle loads", International Heavy Haul Conference, Perth, Australia, pp. 1071-7.

Bergado, D., Manivannan, R. & Balasubramaniam, A. 1996, "Proposed criteria for discharge capacity of prefabricated vertical drains", Geotextiles and Geomembranes, vol. 14, no. 9, pp. 481-505.

Bhatia, S. & Smith, J. 1996, "Geotextile characterization and pore-size distribution: Part II. A review of test methods and results", Geosynthetics International, vol. 3, no. 2, pp. 155-80.

Bhatia, S.K. & Huang, Q. 1995, "Geotextile filters for internally stable/unstable soils", Geosynthetics International, vol. 2, no. 3, pp. 537-65.

Bian, X., Li, W., Qian, Y. & Tutumluer, E. 2020, "Analysing the effect of principal stress rotation on railway track settlement by discrete element method", Géotechnique, vol. 70, no. 9, pp. 803-21.

Bo, M., Bawajee, R. & Choa, V. 1998, "Smear effect due to mandrel penetration", Proceedings of the 2nd International Conference on Ground Improvement Techniques, CI Premier, Singapore, pp. 83-92.

Bo, M.W., Arulrajah, A., Horpibulsuk, S., Chinkulkijniwat, A. & Leong, M. 2016, "Laboratory measurements of factors affecting discharge capacity of prefabricated vertical drain materials", Soils and Foundations, vol. 56, no. 1, pp. 129-37.

Boomintahan, S. & Srinivasan, G. 1988, "Laboratory studies on mud-pumping into ballast under repetitive rail loading", Indian Geotechnical Journal, vol. 18, no. 1, pp. 31-47.

Brons, B.B. 1987, "Stabilization of very soft clay using geofabric", Geotextiles and Geomembranes, vol. 5, no. 1, pp. 17-28.

Brown, S., Lashine, A.K. & Hyde, A. 1975, "Repeated load triaxial testing of a silty clay", Geotechnique, vol. 25, no. 1, pp. 95-114.

Brown, S. & Selig, E. 1991, "The design of pavement and rail track foundations", Chapter 6 in Cyclic loading of soils: from theory to design, Blackie, Glasgow and London, pp. 249-305.

Bruzek, R., Stark, T.D., Wilk, S.T., Thompson, H.B. & Sussmann Jr, T.R. 2016, "Fouled ballast definitions and parameters", ASME/IEEE Joint Rail Conference, vol. 49675, Article V001T01A007.

Cai, X., Cai, X., Liu, K., Wang, H. & Guo, L. 2015, "Study on mud pumping mechanism of subgrade surface layer in slab ballastless track zone", Sensors & Transducers, vol. 186, no. 3, pp. 154-60.

Cai, Y., Wu, T., Guo, L. & Wang, J. 2018, "Stiffness degradation and plastic strain accumulation of clay under cyclic load with principal stress rotation and deviatoric stress variation", Journal of Geotechnical and Geoenvironmental Engineering, vol. 144, no. 5, Article 04018021.

Cantrell, D. 2009, "Drainage, better drainage, and more drainage", In Proceedings of the AREMA 2009 Annual Conference. American Railway Engineering and Maintenance-of-Way Association, Chicago, Illinois.

Carlos, D.M., Carneiro, J.R., Pinho-Lopes, M. & de Lurdes Lopes, M. 2015, "Effect of soil grain size distribution on the mechanical damage of nonwoven geotextiles under repeated loading", International Journal of Geosynthetics and Ground Engineering, vol. 1, no. 1, p. 9.

Carrillo, N. 1942, "Simple two and three dimensional case in the theory of consolidation of soils", Journal of Mathematics and Physics, vol. 21, no. 1-4, pp. 1-5.

Carroll, R. 1983, Geotextile filter criteria, Transportation Research Record, No. 916, 46-53.

Chai, J.-C. & Miura, N. 1999, "Investigation of factors affecting vertical drain behavior", Journal of Geotechnical and Geoenvironmental Engineering, vol. 125, no. 3, pp. 216-26.

Chai, J.-C., Miura, N. & Nomura, T. 2004, "Effect of hydraulic radius on long-term drainage capacity of geosynthetics drains", Geotextiles and Geomembranes, vol. 22, no. 1-2, pp. 3-16.

Chai, J.-C., Miura, N., Sakajo, S. & Bergado, D. 1995, "Behavior of vertical drain improved subsoil under embankment loading", Soils and Foundations, vol. 35, no. 4, pp. 49-61.

Chai, J. & Miura, N. 2000, "A design method for soft subsoil improvement with prefabricated vertical drain", Proceedings of International Seminar on Geotechnics in Kochi, Japan, pp. 161-6.

Chai, J., Miura, N. & Bergado, D. 2008, "Preloading clayey deposit by vacuum pressure with cap-drain: analyses versus performance", Geotextiles and Geomembranes, vol. 26, no. 3, pp. 220-30.

Chawla, S. & Shahu, J. 2016a, "Reinforcement and mud-pumping benefits of geosynthetics in railway tracks: Model tests", Geotextiles and Geomembranes, vol. 44, no. 3, pp. 366-80.

Chawla, S. & Shahu, J. 2016b, "Reinforcement and mud-pumping benefits of geosynthetics in railway tracks: numerical analysis", Geotextiles and Geomembranes, vol. 44, no. 3, pp. 344-57.

Christopher, B.R. & Fischer, G.R. 1992, "Geotextile filtration principles, practices and problems", Geotextiles and Geomembranes, vol. 11, no. 4-6, pp. 337-53.

Christopher, B.R. & Holtz, R.D. 1985, "Geotextile engineering manual", National Technical Information Service, pp. 86-203.

Christopher, B.R., Schwartz, C.W., Boudreaux, R. & Berg, R.R. 2006, "Geotechnical aspects of pavements", United States. Federal Highway Administration, Publication No. FHWA NHI-05-037.

Chu, J., Bo, M. & Choa, V. 2004, "Practical considerations for using vertical drains in soil improvement projects", Geotextiles and Geomembranes, vol. 22, no. 1-2, pp. 101-17.

Chu, J., Bo, M. & Choa, V. 2006, "Improvement of ultra-soft soil using prefabricated vertical drains", Geotextiles and Geomembranes, vol. 24, no. 6, pp. 339-48.

Chu, J., Indraratna, B., Yan, S. & Rujikiatkamjorn, C. 2014, "Overview of preloading methods for soil improvement", Proceedings of the Institution of Civil Engineers-Ground Improvement, vol. 167, no. 3, pp. 173-85.

Chu, J. & Raju, V. 2012, "Prefabricated vertical drains", Ground Improvement (Kirsch K and Bell A (eds)), 3rd edn. CRC Press, Florida, USA, pp. 87-167.

Coelho, B., Hölscher, P., Priest, J., Powrie, W. & Barends, F. 2011, "An assessment of transition zone performance", Proceedings of the Institution of Mechanical Engineers, Part F: Journal of Rail and Rapid Transit, vol. 225, no. 2, pp. 129-39.

Dash, H. & Sitharam, T. 2016, "Effect of frequency of cyclic loading on liquefaction and dynamic properties of saturated sand", International Journal of Geotechnical Engineering, vol. 10, no. 5, pp. 487-92.

Degoutte, G. 1987, "Practical examples of geotextile used in small earth dams", Geotextiles and Geomembranes, vol. 5, no. 4, pp. 239-50.

Deng, Y.-B., Liu, G.-B., Lu, M.-M. & Xie, K.-h. 2014, "Consolidation behavior of soft deposits considering the variation of prefabricated vertical drain discharge capacity", Computers and Geotechnics, vol. 62, pp. 310-6.

Do, T.M. 2021, "Excess pore water pressure generation in fine granular materials under cyclic loading - A laboratory study", Licentiate Thesis, Luleå University of Technology.

Duong, T.V., Cui, Y.-J., Tang, A.M., Dupla, J.-C., Canou, J., Calon, N., Robinet, A., Chabot, B. & De Laure, E. 2014a, "Physical model for studying the migration of fine particles in the railway substructure", Geotechnical Testing Journal, vol. 37, no. 5, pp. 895-906.

Duong, T.V., Cui, Y.J., Tang, A.M., Dupla, J.C., Canou, J., Calon, N. & Robinet, A. 2014b, "Investigating the mud pumping and interlayer creation phenomena in railway sub-structure", Engineering Geology, vol. 171, pp. 45-58.

Duong, T.V., Tang, A.M., Cui, Y.-J., Trinh, V.N., Dupla, J.-C., Calon, N., Canou, J. & Robinet, A. 2013, "Effects of fines and water contents on the mechanical behavior of interlayer soil in ancient railway sub-structure", Soils and foundations, vol. 53, no. 6, pp. 868-78.

Eller, B. & Fischer, S. 2019, "Review of the modern ballasted railway tracks'substructure and further investigations", Science and Transport Progress. Bulletin of Dnipropetrovsk National University of Railway Transport, no. 6 (84), pp. 72-85.

Elsharief, A.M. & Lovell, C. 1996, "A probabilistic retention criterion for nonwoven geotextiles", Geotextiles and Geomembranes, vol. 14, no. 11, pp. 601-17.

Elvidge, C. & Raymond, G. 1999, "Laboratory survivability of nonwoven geotextiles on open-graded crushed aggregate", Geosynthetics International, vol. 6, no. 2, pp. 93-117.

EN ISO 9863-1 2005, Geosynthetics–Determination of thickness at specified pressures. Part 1: Single Layers, CEN, Brusel.

EN ISO 10319 2008, Geosynthetics–Wide-width tensile test. , International Organization for Standardization, Geneva, Switzerland.

EN ISO 11058 2019, Geotextiles and geotextile-related products — Determination of water permeability characteristics normal to the plane, without load, ISBN 978 0 580 93628 9.

EN ISO 12236 2006, Geosynthetics—Static Puncture Test (CBR Test), European Committee for Standardization, Brussels, Belgium.

Fatahi, B., Khabbaz, H. & Liem Ho, H. 2011, "Effects of geotextiles on drainage performance of ballasted rail tracks", Australian Geomechanics, vol. 46, no. 4, p. 91.

Faure, Y.-H., Baudoin, A., Pierson, P. & Ple, O. 2006, "A contribution for predicting geotextile clogging during filtration of suspended solids", Geotextiles and Geomembranes, vol. 24, no. 1, pp. 11-20.

Feldman, F. & Nissen, D. 2002, "Alternative testing method for the measurement of ballast fouling: percentage void contamination", CORE 2002, Cost Efficient Railways through Engineering, Conference on Railway Engineering, Wollongong, New South Wales.

Feng, W.-Q., Lalit, B., Yin, Z.-Y. & Yin, J.-H. 2017, "Long-term non-linear creep and swelling behavior of Hong Kong marine deposits in oedometer condition", Computers and Geotechnics, vol. 84, pp. 1-15.

Feng, W.-Q., Li, C., Yin, J.-H., Chen, J. & Liu, K. 2019, "Physical model study on the clay–sand interface without and with geotextile separator", Acta Geotechnica, vol. 14, no. 6, pp. 2065-81.

Fernandes, G., Palmeira, E.M. & Gomes, R.C. 2008, "Performance of geosynthetic-reinforced alternative sub-ballast material in a railway track", Geosynthetics International, vol. 15, no. 5, pp. 311-21.

Fiberweb 2012, Product data sheets. Fiberweb Geosynthetics Ltd, Blackwater Industrial Estate, The Causeway, Maldon, CM9 4GG.

Fuggini, C., Zangani, D., Wosniok, A., Krebber, K., Franitza, P., Gabino, L. & Weigand, F. 2016, "Innovative approach in the use of geotextiles for failures prevention in railway embankments", Transportation Research Procedia, vol. 14, pp. 1875-83.

Gao, Y.B. & Zhang, Z. 2020, "Vertical compression of soft clay within PVD-improved zone under vacuum loading: Theoretical and practical study", Geotextiles and Geomembranes, vol. 48, no. 3, pp. 306-14.

Gerry, B.S. & Raymond, G.P. 1983, "The in-plane permeability of geotextiles", Geotechnical Testing Journal, vol. 6, no. 4, pp. 181-9.

Ghandeharioon, A., Indraratna, B. & Rujikiatkamjorn, C. 2010, "Analysis of soil disturbance associated with mandrel-driven prefabricated vertical drains using an elliptical cavity expansion theory", International Journal of Geomechanics, vol. 10, no. 2, pp. 53-64.

Ghandeharioon, A., Indraratna, B. & Rujikiatkamjorn, C. 2012, "Laboratory and finite-element investigation of soil disturbance associated with the installation of mandrel-driven prefabricated vertical drains", Journal of Geotechnical and Geoenvironmental Engineering, vol. 138, no. 3, pp. 295-308.

Ghataora, G., Burns, B., Burrow, M. & Evdorides, H. 2006, "Development of an index test for assessing anti-pumping materials in railway track foundations", Proceedings of the First International Conference on Railway Foundations, Railfound06, University of Birmingham, UK, pp. 355-66.

Ghataora, G., Burrow, M., Kamalov, R., Wehbi, M. & Musgrave, P. 2017, "Migration of fine particles from subgrade soil to the overlying ballast", Railway Engineering, pp. 21-32.

Ghosh, C. & Yasuhara, K. 2004, "Clogging and flow characteristics of a geosynthetic drain confined in soils undergoing consolidation", Geosynthetics International, vol. 11, no. 1, pp. 19-34.

Ghosh, C. & Yasuhara, K. 2021, "Ultrasonic Removal of Clogging and Evaluation of Flow Capacity of Geotextile Drain", Indian Geotechnical Journal, vol. 51, pp. 539-51.

Ghoshal, A. & Som, N. 1993, "Geotextiles and geomembranes in India—State of usage and economic evaluation", Geotextiles and Geomembranes, vol. 12, no. 3, pp. 193-213.

Giroud, J.-P. 2010, "Development of criteria for geotextile and granular filters", Proceedings of the 9th international conference on geosynthetics, Guaruja, Brazil, vol. 2327, p. 4564.

Giroud, J. 1996, "Granular filters and geotextile filters", Geofilters 96, Proc. of 2nd Int. Conf." Geo-filters", pp. 565-680.

Giroud, J.P. 1982, "Filter criteria for geotextiles", Proc. 2nd Int. Conference on Geotextiles, Las Vegas, USA, vol. 1, pp. 103-8.

Głuchowski, A., Soból, E., Szymański, A. & Sas, W. 2019, "Undrained Pore Pressure Development on Cohesive Soil in Triaxial Cyclic Loading", Applied Sciences, vol. 9, no. 18, p. 3821.

Gräbe, P. & Clayton, C. 2014, "Effects of principal stress rotation on resilient behavior in rail track foundations", Journal of Geotechnical and Geoenvironmental Engineering, vol. 140, no. 2, p. 04013010.

Greenwood, J. & Brady, K. 1992, "Geotextiles in aggressive soils", Construction and Building Materials, vol. 6, no. 1, pp. 15-8.

Gül, S. 2020, "An experimental study on geotextile-soil filter system", Degree of Master of Science, Middle East Technical University, p. 136.

Gundavaram, D. & Hussaini, S.K.K. 2021, "Influence of Coal Fouling on the Shear Behavior of Elastan-Treated Railroad Ballast", Journal of Materials in Civil Engineering, vol. 33, no. 9, p. 04021239.

Guo, L., Cai, Y., Jardine, R.J., Yang, Z. & Wang, J. 2018a, "Undrained behaviour of intact soft clay under cyclic paths that match vehicle loading conditions", Canadian Geotechnical Journal, vol. 55, no. 1, pp. 90-106.

Guo, L., Wang, J., Cai, Y., Liu, H., Gao, Y. & Sun, H. 2013, "Undrained deformation behavior of saturated soft clay under long-term cyclic loading", Soil Dynamics and Earthquake Engineering, vol. 50, pp. 28-37.

Guo, W., Chu, J. & Nie, W. 2018b, "An observational method for consolidation analysis of the PVD-improved subsoil", Geotextiles and Geomembranes, vol. 46, no. 5, pp. 625-33.

Hameiri, A. 2000, "Soil/geotextile filtration behavior under dynamic conditions of cyclic flow and vibration", PhD Thesis, University of British Columbia, Department of Civil Engineering, BC, Canada.

Hansbo, S. 1979, "Consolidation of clay by bandshaped prefabricated drains", Ground Engineering, London, vol. 12, no. 5, pp. 16-27.

Hansbo, S. 1981, "Consolidation of fine-grained soils by prefabricated drains", Proc. 10th Int. Conf. Soil Mech. and Found. Engrg., Vol. 3, International Society of Soil Mechanics and Foundation Engineering, Stockholm, vol. 3, pp. 677-82.

Hansbo, S. 1983, "How to evaluate the properties of prefabricated drains", Proc. 8th Eur. Conf. Soil Mech. and Found. Engrg. Balkema, Rotterdam, The Netherlands, vol. 2, pp. 621-6.

Hansbo, S. 1997, "Aspects of vertical drain design: Darcian or non-Darcian flow", Geotechnique, vol. 47, no. 5, pp. 983-92.

Haque, A., Kabir, E. & Bouazza, A. 2007, "Cyclic filtration apparatus for testing subballast under rail track", Journal of Geotechnical and Geoenvironmental Engineering, vol. 133, no. 3, pp. 338-41.

Hausmann, M., Ring, G. & Pitsis, S. 1990, "Abrasion of geotextiles in railway track applications", Proceedings of the Fourth International Conference on Geotextiles, Geomembranes and Related Products, The Hague, the Netherland, pp. 193-6.

Hawlader, B.C., Imai, G. & Muhunthan, B. 2002, "Numerical study of the factors affecting the consolidation of clay with vertical drains", Geotextiles and Geomembranes, vol. 20, no. 4, pp. 213-39.

Hayashi, S. & Shahu, J. 2000, "Mud pumping problem in tunnels on erosive soil deposits", Geotechnique, vol. 50, no. 4, pp. 393-408.

Hendry, M.T., Martin, C.D. & Barbour, S.L. 2013, "Measurement of cyclic response of railway embankments and underlying soft peat foundations to heavy axle loads", Canadian Geotechnical Journal, vol. 50, no. 5, pp. 467-80.

Henry, K.S. 1990, Laboratory investigation of the use of geotextiles to mitigate frost heave, Cold Regions Research and Engineering Lab Hanover NH.

Holtz, R., Christopher, B. & Berg, R. 1997, "Geosynthetic Engineering", Bitech Publishers Ltd., Richmond, British Columbia, Canada, p. 452.

Holtz, R.D., Jamiolkowski, M., Lancellotta, R. & Pedroni, R. 1991, Prefabricated Vertical Drains: Design and Performance, Construction Industry Research & Information Assoc, London : CIRIA ; Oxford : Butterworth-Heinemann.

Holz, R., Christopher, B.R. & Berg, R.R. 1998, "Geosynthetic design and construction guidelines", Report No. FHWA-NHI-07-092, U.S. Department of Transportation, Federal Highway Administration, Washington DC, 2008, p. 612

Hosseinpour, I., Almeida, M. & Riccio, M. 2015, "Full-scale load test and finite-element analysis of soft ground improved by geotextile-encased granular columns", Geosynthetics International, vol. 22, no. 6, pp. 428-38.

Hudson, A., Watson, G., Le Pen, L. & Powrie, W. 2016, "Remediation of mud pumping on a ballasted railway track", Procedia Engineering, vol. 143, pp. 1043-50.

Hudson, K. & East, G. 1991, "Geotextiles", Transit New Zealand Research Report, Wellington, New Zealand.

Hyodo, M., Yasuhara, K. & Hirao, K. 1992, "Prediction of clay behaviour in undrained and partially drained cyclic triaxial tests", Soils and Foundations, vol. 32, no. 4, pp. 117-27.

Idriss, I.M., Dobry, R. & Singh, R.D. 1978, "Nonlinear behavior of soft clays during cyclic loading", Journal of the Geotechnical Engineering Division, vol. 104, no. 12, pp. 1427-47.

Indraratna, B. 2010, "Recent Advances in the Appplication of Vertical Drains and Vacuum Preloading in Soft Soil Stabilisation", Australian Geomechanics Journal, 45(2), 2010, 1-43., vol. 45, no. 2, pp. 1-43.

Indraratna, B. 2017, "Recent advances in vertical drains and vacuum preloading for soft ground stabilisation", Proceedings of 19th International Conference on Soil Mechanics and Geotechnical Engineering, Seou,(London: International Society for Soil Mechanics and Geotechnical Engineering), pp. 145-70.

Indraratna, B., Attya, A. & Rujikiatkamjorn, C. 2009, "Experimental investigation on effectiveness of a vertical drain under cyclic loads", Journal of Geotechnical and Geoenvironmental Engineering, vol. 135, no. 6, pp. 835-9.

Indraratna, B., Dilema, E. & Vafai, F. 1996, "An experimental study of the filtration of a lateritic clay slurry by sand filters", Proceedings of the Institution of Civil Engineers-Geotechnical Engineering, vol. 119, no. 2, pp. 75-83.

Indraratna, B., Ionescu, D. & Christie, H. 1998, "Shear behavior of railway ballast based on large-scale triaxial tests", Journal of Geotechnical and Geoenvironmental Engineering, vol. 124, no. 5, pp. 439-49.

Indraratna, B., Israr, J. & Li, M. 2018a, "Inception of geohydraulic failures in granular soils–an experimental and theoretical treatment", Geotechnique, vol. 68, no. 3, pp. 233-48.

Indraratna, B., Korkitsuntornsan, W. & Nguyen, T.T. 2020a, "Influence of Kaolin content on the cyclic loading response of railway subgrade", Transportation Geotechnics, vol. 22, p. 100319.

Indraratna, B., Navaratnarajah, S.K., Nimbalkar, S. & Rujikiatkamjorn, C. 2014a, "Use of shock mats for enhanced stability of railroad track foundation", Australian Geomechanics Journal, vol. 49, no. 4, pp. 101-11.

Indraratna, B. & Ngo, T. 2018, Ballast railroad design: smart-uow approach, CRC Press, London, p. 176.

Indraratna, B., Ngo, T., Ferreira, F.B., Rujikiatkamjorn, C. & Shahkolahi, A. 2020b, "Laboratory examination of ballast deformation and degradation under impact loads with synthetic inclusions", Transportation Geotechnics, vol. 25, p. 100406.

Indraratna, B., Ni, J., Rujikiatkamjorn, C. & Zhong, R. 2015, "A partially drained model for soft soils under cyclic loading considering cyclic parameter degradation", Aust. Geomech Journal, vol. 50, no. 4, pp. 89-95.

Indraratna, B. & Nimbalkar, S. 2013, "Stress-strain degradation response of railway ballast stabilized with geosynthetics", Journal of Geotechnical and Geoenvironmental Engineering, vol. 139, no. 5, pp. 684-700.

Indraratna, B., Nimbalkar, S., Christie, D., Rujikiatkamjorn, C. & Vinod, J. 2010a, "Field assessment of the performance of a ballasted rail track with and without geosynthetics", Journal of Geotechnical and Geoenvironmental Engineering, vol. 136, no. 7, pp. 907-17.

Indraratna, B., Nimbalkar, S. & Rujikiatkamjorn, C. 2012, "Future of Australian rail tracks capturing higher speeds with heavier freight", Sixteenth annual Symposium of Australian Geomechanics Society, Advances in Geotechnics of Roadsand Railways, Sydney, Australia, pp. 1-24.

Indraratna, B., Nimbalkar, S. & Rujikiatkamjorn, C. 2014b, "Enhancement of rail track performance through utilisation of geosynthetic inclusions", Geotechnical Engineering Journal of the SEAGS & AGSSEA, vol. 45, no. 1, pp. 17-27.

Indraratna, B., Nimbalkar, S.S. & Tennakoon, N. 2010b, 'The behaviour of ballasted track foundations: track drainage and geosynthetic reinforcement', GeoFlorida 2010: Advances in Analysis, Modeling & Design, pp. 2378-87.

Indraratna, B. & Radampola, S. 2002, "Analysis of critical hydraulic gradient for particle movement in filtration", Journal of Geotechnical and Geoenvironmental Engineering, vol. 128, no. 4, pp. 347-50.

Indraratna, B. & Raut, A.K. 2006, "Enhanced criterion for base soil retention in embankment dam filters", Journal of Geotechnical and Geoenvironmental Engineering, vol. 132, no. 12, pp. 1621-7.

Indraratna, B. & Redana, I. 1997, "Plane-strain modeling of smear effects associated with vertical drains", Journal of Geotechnical and Geoenvironmental Engineering, vol. 123, no. 5, pp. 474-8.

Indraratna, B. & Redana, I. 1998, "Laboratory determination of smear zone due to vertical drain installation", Journal of Geotechnical and Geoenvironmental Engineering, vol. 124, no. 2, pp. 180-4.

Indraratna, B. & Redana, I. 2000, "Numerical modeling of vertical drains with smear and well resistance installed in soft clay", Canadian Geotechnical Journal, vol. 37, no. 1, pp. 132-45.

Indraratna, B., Rujikiatkamjorn, C., Ewers, B. & Adams, M. 2010c, "Class A prediction of the behavior of soft estuarine soil foundation stabilized by short vertical drains beneath a rail track", Journal of Geotechnical and Geoenvironmental Engineering, vol. 136, no. 5, pp. 686-96.

Indraratna, B., Rujikiatkamjorn, C., Nguyen, V.T. & Raut, A. 2014c, "Analytical solutions for filtration process based on the constriction size concept", Geo-Congress 2014: Geo-characterization and Modeling for Sustainability, pp. 999-1006.

Indraratna, B., Rujikiatkamjorn, C. & Ni, J. 2011a, "Cyclic behaviour of soft soil subgrade improved by prefabricated vertical drains", International Symposium on Deformation Characteristics of Geomaterials, September 1~3, 2011, Seoul, Korea 5, pp. 559-64.

Indraratna, B., Rujikiatkamjorn, C. & Sathananthan, I. 2005, "Analytical and numerical solutions for a single vertical drain including the effects of vacuum preloading", Canadian Geotechnical Journal, vol. 42, no. 4, pp. 994-1014.

Indraratna, B., Rujikiatkamjorn, C. & Walker, R.T. 2007, "Radial consolidation theories and numerical analysis of soft soil stabilisation via prefabricated vertical drains", International Workshop on Constitutive Modelling, Hong Kong, pp. 155-67.

Indraratna, B., Salim, W. & Rujikiatkamjorn, C. 2011b, Advanced rail geotechnology-ballasted track, CRC press/Balkema, Rotterdam, p. 333.

Indraratna, B., Singh, M. & Nguyen, T.T. 2020c, "The mechanism and effects of subgrade fluidisation under ballasted railway tracks", Railway Engineering Science, vol. 28, pp. 113-28.

Indraratna, B., Singh, M., Nguyen, T.T., Leroueil, S., Abeywickrama, A., Kelly, R. & Neville, T. 2020d, "Laboratory study on subgrade fluidization under undrained

cyclic triaxial loading", Canadian Geotechnical Journal, vol. 57, no. 11, pp. 1767-79.

Indraratna, B., Sun, Q., Heitor, A. & Grant, J. 2018b, "Performance of Rubber Tire-Confined Capping Layer under Cyclic Loading for Railroad Conditions", J. Mater. Civ. Eng, ASCE, vol. 30, no. 3, Article 06017021.

Ionescu, D. 2004, "Ballast degradation and measurement of ballast fouling", Seventh Railway Engineering Conference, Commonwealth Institute, London, vol. 2, pp. 12-8.

ISO/TR 20432 - 07 2007, Guidelines for the determination of the long-term strength of geosynthetics for soil reinforcement, International Organization for Standardization.

Israr, J. 2016, "Internal instability of granular filters under cyclic loading", PhD Thesis, University of Wollongong, Australia, p.248.

Israr, J. & Indraratna, B. 2017, "Internal stability of granular filters under static and cyclic loading", Journal of Geotechnical and Geoenvironmental Engineering, vol. 143, no. 6, p. 04017012.

Israr, J. & Indraratna, B. 2018, "Assessment of internal stability of filters under static and cyclic loading: an experimental and theoretical treatment", Australian Geomechanics Society Journal, vol. 53, no. 4, pp. 102-15.

Israr, J., Indraratna, B. & Rujikiatkamjorn, C. 2016, "Laboratory investigation of the seepage induced response of granular soils under static and cyclic loading", Geotechnical Testing Journal, vol. 39, no. 5, pp. 795-812.

Israr, J. & Zhang, G. 2021, "Geometrical assessment of internal instability potential of granular soils based on grading entropy", Acta Geotechnica, vol. 16, no. 6, pp. 1961-70.

Ito, T. 1984, "Actual situation of mud pumping and its countermeasures", Quarterly Reports of the Railway Technical Research Institute, vol. 25, no. 4, pp. 117-23.

266

Jiang, M., Cai, Z., Cao, P. & Liu, D. 2010, "Effect of cyclic loading frequency on dynamic properties of marine clay", In: GeoShangi international conference, Shanghai, China, pp. 240-5.

Jiang, M., Konrad, J. & Leroueil, S. 2003, "An efficient technique for generating homogeneous specimens for DEM studies", Computers and Geotechnics, vol. 30, no. 7, pp. 579-97.

Kagawa, T. 1992, "Moduli and damping factors of soft marine clays", Journal of Geotechnical Engineering, vol. 118, no. 9, pp. 1360-75.

Kamruzzaman, A., Haque, A. & Bouazza, A. 2008, "Filtration behaviour of granular soils under cyclic load", Geotechnique, vol. 58, no. 6, pp. 517-22.

Kaniraj, S.R. & Rao, G.V. 1994, "Trends in the use of geotextiles in India", Geotextiles and Geomembranes, vol. 13, no. 6-7, pp. 389-402.

Karol, R.H. 2003, Chemical grouting and soil stabilization, revised and expanded, vol. 12, Crc Press.

Karunaratne, G. 2011, "Prefabricated and electrical vertical drains for consolidation of soft clay", Geotextiles and Geomembranes, vol. 29, no. 4, pp. 391-401.

Kenny, T. 1985, "Internal stability of granular filters", Can. Geotech. J., vol. 22, pp. 215-25.

Kermani, B., Stoffels, S. & Xiao, M. 2020, "Evaluation of effectiveness of geotextile in reducing subgrade migration in rigid pavement", Geosynthetics International, vol. 27, no. 1, pp. 97-109.

Kermani, B., Stoffels, S.M. & Xiao, M. 2019, "Assessment of geotextile effectiveness in decreasing subgrade pumping and increasing service life in rigid pavements using scaled model mobile load simulator", American Society of Civil Engineers Reston, VA, pp. 357-67.

Kermani, B., Xiao, M., Stoffels, S.M. & Qiu, T. 2018, "Reduction of subgrade fines migration into subbase of flexible pavement using geotextile", Geotextiles and Geomembranes, vol. 46, no. 4, pp. 377-83.

Khan, M., Dawson, A. & Marshall, A. 2018, "A dynamic gradient ratio test apparatus", Geotextiles and Geomembranes, vol. 46, no. 6, pp. 782-9.

Khan, M., Dawson, A. & Marshall, A. 2022, "Filtration performance of non-woven geotextiles with internally-stable and-unstable soils under dynamic loading", Geotextiles and Geomembranes, vol. 50, no. 2, pp. 293-311.

Kim, P., Kim, T.-C., Kim, Y.-G., Myong, H.-B., Jon, K.-S. & Jon, S.-H. 2021, "Nonlinear consolidation analysis of soft soil with vertical drains considering well resistance and smear effect under cyclic loadings", Geotextiles and Geomembranes, vol. 49, no. 5, pp. 1440-6.

Koerner, G.R. & Koerner, R.M. 1990, "The installation survivability of geotextiles and geogrids", Geotextiles, Geomembranes, and Related Products: Canals, reservoirs and dams. Waste disposal. Geomembrane properties and testing. Mechanical damage. Creep and durability. Miscellaneous tests. Special products and applications, vol. 2, p. 597.

Koerner, R.M. 2012, Designing with geosynthetics-Vol. 1, vol. 1, Xlibris Corporation.

Koerner, R.M., Bove, J.A. & Martin, J.P. 1984, "Water and air transmissivity of geotextiles", Geotextiles and Geomembranes, vol. 1, no. 1, pp. 57-73.

Koerner, R.M., Hwu, B.-L. & Wayne, M.H. 1987, "Soft soil stabilization designs using geosynthetics", Geotextiles and Geomembranes, vol. 6, no. 1-3, pp. 33-51.

Konrad, J.-M. & Wagg, B. 1993, "Undrained cyclic loading of anisotropically consolidated clayey silts", Journal of Geotechnical Engineering, vol. 119, no. 5, pp. 929-49.

Korkitsuntornsan, W. 2020, "Mechanisms of Mud pumping and the Effects of the Fines content", PhD Thesis, University of Wollongong, Australia, p. 190.

Kumar, P.S. & Rajkumar, R. 2012, "Effect of geotextile on CBR strength of unpaved road with soft subgrade", Electronic Journal of Geotechnical Engineering, vol. 17, no. 1, pp. 1355-63.

Kuo, C. 2021, "Ground-penetrating radar to investigate mud pumping distribution along a railway line", Construction and Building Materials, vol. 290, p. 123104.

Kuo, C., Hsu, C., Wu, C., Liu, P. & Chen, D. 2017, "Study on the Piping Path and Mechanism of Mud-pumping in Railway Subgrade", The 19th international conference on soil mechanics and geotechnical engineering, Seoul, South Korea, pp. 1051-4.

Lafleur, J., Eichenauer, T. & Werner, G. 1996, "Geotextile filter retention criteria for well graded cohesionless soils", Geofilters'96 – Proceedings. Montreal: Ecole Polytechnique, pp. 429-38.

Larew, H. & Leonards, G. 1962, "A strength criterion for repeated loads", In Proceedings of the 41st Annual Meeting, Highway Research Board, Washington, DC, vol. 41, pp. 529-56.

Latvala, J., Nurmikolu, A. & Luomala, H. 2016, "Problems with railway track drainage in Finland", Procedia Engineering, vol. 143, pp. 1051-8.

Lawson, C.R. 1982, "Filter criteria for geotextiles: relevance and use", Journal of the Geotechnical Engineering Division, vol. 108, no. 10, pp. 1300-17.

Lee, C.-J. & Sheu, S.-F. 2007, "The stiffness degradation and damping ratio evolution of Taipei Silty Clay under cyclic straining", Soil Dynamics and Earthquake Engineering, vol. 27, no. 8, pp. 730-40.

Lei, H., Li, B., Lu, H. & Ren, Q. 2016, "Dynamic deformation behavior and cyclic degradation of ultrasoft soil under cyclic loading", Journal of Materials in Civil Engineering, vol. 28, no. 11, p. 04016135.

Lenart, S., Bizjak, K.F., Noren-Cosgriff, K., Kaynia, A.M., Kramar, M., Vajdić, M., Chen, K. & Clarke, J. 2018, "Guidelines on the use of novel construction and maintenance

techniques within the operational railway environment", DESTination RAIL – Decision Support Tool for Rail Infrastructure Managers.

Li, D., Hyslip, J., Sussmann, T. & Chrismer, S. 2015, Railway geotechnics, CRC Press.

Li, D. & Selig, E. 1995, "Evaluation of railway subgrade problems", Transportation Research Record, vol. 1489, p. 17.

Li, D. & Selig, E.T. 1998, "Method for railroad track foundation design. I: Development", Journal of Geotech. and Geoenvironmental Engineering, vol. 124, no. 4, pp. 316-22.

Li, D. & Wilk, S. 2020, "Recent studies on railway-track substructure at TTCI", Transportation Safety and Environment, vol. 3, no. 1, pp. 36-49.

Li, X. & Vanapalli, S.K. 2021, "Simulation of progressive shear failure in railway foundation", Transportation Geotechnics, vol. 29, p. 100550.

Liu, D., Fu, H.L., Zhu, X.Z., Liu, Y.S. & Rao, J.Y. 2013, "Study on the Remediation of Mud-Pumping", vol. 275, Trans Tech Publ, pp. 1560-3.

Liu, J. 2006, "Subgrade Engineering",The Architecture and Building Industry Publishing House of China, Beijing.

Liu, J. & Xiao, J. 2010, "Experimental study on the stability of railroad silt subgrade with increasing train speed", Journal of Geotechnical and Geoenvironmental Engineering, vol. 136, no. 6, pp. 833-41.

Long, P., Bergado, D., Nguyen, L. & Balasubramaniam, A. 2013, "Design and performance of soft ground improvement using PVD with and without vacuum consolidation", Geotechnical Engineering Journal of the SEAGS & AGSSEA, vol. 44, no. 4, pp. 36-51.

Lorenzo, G., Bergado, D., Bunthai, W., Hormdee, D. & Phothiraksanon, P. 2004, "Innovations and performances of PVD and dual function geosynthetic applications", Geotextiles and Geomembranes, vol. 22, no. 1-2, pp. 75-99.

Luettich, S., Giroud, J. & Bachus, R. 1992, "Geotextile filter design guide", Geotextiles and Geomembranes, vol. 11, no. 4-6, pp. 355-70.

Mamou, A., Powrie, W., Priest, J. & Clayton, C. 2017, "The effects of drainage on the behaviour of railway track foundation materials during cyclic loading", Géotechnique, vol. 67, no. 10, pp. 845-54.

Marinucci, A. 2010, "Effect of prefabricated vertical drains on pore water pressure generation and dissipation in liquefiable sand", PhD Dissertation, The University of Texas at Austin.

Martinek, K. 1986, "Geotextiles used by the German Federal Railway—experiences and specifications", Geotextiles and Geomembranes, vol. 3, no. 2-3, pp. 175-200.

Martínez, E., Patiño, H. & Galindo, R. 2017, "Evaluation of the risk of sudden failure of a cohesive soil subjected to cyclic loading", Soil Dynamics and Earthquake Engineering, vol. 92, pp. 419-32.

Matsui, T., Ohara, H. & Ito, T. 1980, "Cyclic stress-strain history and shear characteristics of clay", Journal of the geotechnical Engineering Division, vol. 106, no. 10, pp. 1101-20.

Meccai, K.A. & Hasan, E.a. 2004, "Geotextiles in transportation applications", Second Gulf Conference on Roads, Abu Dhabi, Citeseer, p. 13.

Michael, H. 2014, "Rethinking geotextile filter design", 10th International Conference on Geosynthetics (10ICG), Berlin. Essen: DGGT.

Miller, G., Teh, S., Li, D. & Zaman, M. 2000, "Cyclic shear strength of soft railroad subgrade", Journal of Geotechnical and Geoenvironmental Engineering, vol. 126, no. 2, pp. 139-47.

Mission, J.L., Kim, H.-J. & Won, M.-S. 2012, "Ground Improvement Optimization with Prefabricated Vertical Drains (PVD) and Surcharge Preloading", World Congress on Advances in Civil, Environmental, and Materials Research (ACEM'12) Seoul, Korea, pp. 2817-20.

Miszkowska, A. & Koda, E. 2017, "Change of water permeability of nonwoven geotextile exploited in earthfill dam", Proceedings of the 24th international PhD students conference, Brno, Czech Republic, pp. 790-5.

Mlynarek, J., Lafleur, J. & Lewandowski, J. 1990, "Field study on long term geotextile filter performance", Proceedings of the Fourth International Conference on Geotextiles. Geomembranes and Related Products. The Hague, Netherlands, pp. 259-62.

Modarres, A. & Nosoudy, Y.M. 2015, "Clay stabilization using coal waste and lime—Technical and environmental impacts", Applied Clay Science, vol. 116, pp. 281-8.

Mohammadinia, A., Arulrajah, A., Disfani, M.M. & Darmawan, S. 2019, "Small-Strain Behavior of Cement-Stabilized Recycled Concrete Aggregate in Pavement Base Layers", Journal of Materials in Civil Engineering, vol. 31, no. 5.

Montero, C.M. & Overmann, L.K. 1990, "Geotextile filtration performance test", Geosynthetic testing for waste containment applications, ASTM STP 108.

Mortezaie, A.R. & Vucetic, M. 2013, "Effect of frequency and vertical stress on cyclic degradation and pore water pressure in clay in the NGI simple shear device", Journal of Geotechnical and Geoenvironmental Engineering, vol. 139, no. 10, pp. 1727-37.

Muramoto, K. & Nakamura, T. 2011, "Development of the countermeasure against roadbed degradation under ballastless tracks for existing lines", 9th World Congress on Railway Research, pp. 1-10.

Muramoto, K., Sekine, E. & Nakamura, T. 2006, "Roadbed degradation mechanism under ballastless track and its countermeasures", Quarterly Report of RTRI, vol. 47, no. 4, pp. 222-7.

Narejo, D. 2004, 'Design, Performance and Economics of Separation Geotextiles in Pavements', Geotechnical Engineering for Transportation Projects, pp. 1042-9.

Narejo, D.B. 2003, "Opening size recommendations for separation geotextiles used in pavements", Geotextiles and Geomembranes, vol. 21, no. 4, pp. 257-64.

Navaratnarajah, S.K., Indraratna, B. & Ngo, N.T. 2018, "Influence of under sleeper pads on ballast behavior under cyclic loading: experimental and numerical studies", Journal of Geotechnical and Geoenvironmental Engineering, vol. 144, no. 9, p. 04018068.

Ngo, D.H., Horpibulsuk, S., Suddeepong, A., Hoy, M., Udomchai, A., Doncommul, P., Rachan, R. & Arulrajah, A. 2020, "Consolidation behavior of dredged ultra-soft soil improved with prefabricated vertical drain at the Mae Moh mine, Thailand", Geotextiles and Geomembranes, vol. 48, no. 4, pp. 561-71.

Nguyen, B.-P. 2021, "Nonlinear analytical modeling of vertical drain-installed soft soil considering a varied discharge capacity", Geotechnical and Geological Engineering, vol. 39, no. 1, pp. 119-34.

Nguyen, T.T. & Indraratna, B. 2019, "Micro-CT scanning to examine soil clogging behavior of natural fiber drains", Journal of Geotechnical and Geoenvironmental Engineering, vol. 145, no. 9, p. 04019037.

Nguyen, T.T. & Indraratna, B. 2021, "Rail track degradation under mud pumping evaluated through site and laboratory investigations", International Journal of Rail Transportation, pp. 1-28.

Nguyen, T.T., Indraratna, B., Kelly, R., Phan, N.M. & Haryono, F. 2019, "Mud pumping under railtracks: mechanisms, assessments and solutions", Aust Geomech J, vol. 54, no. 4, pp. 59-80.

Nguyen, V.T., Rujikiatkamjorn, C. & Indraratna, B. 2013, "Analytical solutions for filtration process based on constriction size concept", Journal of Geotechnical and Geoenvironmental Engineering, vol. 139, no. 7, pp. 1049-61.

Ni, J. 2012, "Application of geosynthetic vertical drains under cyclic loads in stabilizing tracks", PhD Thesis, University of Wollongong, Australia, p. 210.

Ni, J., Indraratna, B., Geng, X.-Y., Carter, J.P. & Chen, Y.-L. 2015, "Model of soft soils under cyclic loading", International Journal of Geomechanics, vol. 15, no. 4, p. 04014067.

Ni, J., Indraratna, B., Geng, X.-Y., Carter, J.P. & Rujikiatkamjorn, C. 2013, "Radial consolidation of soft soil under cyclic loads", Computers and Geotechnics, vol. 50, pp. 1-5.

Nithin, S., Rajagopal, K. & Veeraragavan, A. 2015, "The Use of Natural Geotextiles in Reinforcing the unpaved roads", The 6th International Geotechnical Symposium on Disaster Mitigation in Special Geoenvironmental Conditions, September, India.

Palmeira, E., Fannin, R. & Vaid, Y. 1997, "A study on the behaviour of soil geotextile systems in filtration tests", Canadian Geotechnical Journal, vol. 33, no. 6, pp. 899-912.

Palmeira, E. & Gardoni, M. 2000, "The influence of partial clogging and pressure on the behaviour of geotextiles in drainage systems", Geosynthetics International, vol. 7, no. 4-6, pp. 403-31.

Palmeira, E., Gardoni, M. & Bessa da Luz, D. 2005, "Soil–geotextile filter interaction under high stress levels in the gradient ratio test", Geosynthetics International, vol. 12, no. 4, pp. 162-75.

Palmeira, E. & Trejos Galvis, H. 2017, "Opening sizes and filtration behaviour of nonwoven geotextiles under confined and partial clogging conditions", Geosynthetics International, vol. 24, no. 2, pp. 125-38.

Palmeira, E. & Trejos Galvis, H. 2018, "Evaluation of predictions of nonwoven geotextile pore size distribution under confinement", Geosynthetics International, vol. 25, no. 2, pp. 230-41.

Palmeira, E.M. 2009, "Soil–geosynthetic interaction: Modelling and analysis", Geotextiles and Geomembranes, vol. 27, no. 5, pp. 368-90.

Palmeira, E.M. & Gardoni, M.G. 2002, "Drainage and filtration properties of non-woven geotextiles under confinement using different experimental techniques", Geotextiles and Geomembranes, vol. 20, no. 2, pp. 97-115.

Palmeira, E.M., Melo, D.L. & Moraes-Filho, I.P. 2019, "Geotextile filtration opening size under tension and confinement", Geotextiles and Geomembranes, vol. 47, no. 4, pp. 566-76.

Palmeira, E.M., Tatto, J. & Araujo, G.L. 2012, "Sagging and filtration behaviour of nonwoven geotextiles overlying different bedding materials", Geotextiles and Geomembranes, vol. 31, pp. 1-14.

Parsa-Pajouh, A., Fatahi, B., Vincent, P. & Khabbaz, H. 2014, "Trial embankment analysis to predict smear zone characteristics induced by prefabricated vertical drain installation", Geotechnical and Geological Engineering, vol. 32, no. 5, pp. 1187-210.

Paul, M., Sahu, R.B. & Banerjee, G. 2015, "Undrained pore pressure prediction in clayey soil under cyclic loading", International Journal of Geomechanics, vol. 15, no. 5, p. 04014082.

Phan, M.N., Indraratna, B. & Nguyen, T.T. 2019, "The response of granular soil to increasing hydraulic gradient through LBM-DEM coupling", Faculty of Engineering and Information Sciences - Papers: Part A.

Plaxis_Manual 2021, Material Models Manual, Bently, CONNECT Edition V21.01.

Portelinha, F., Bueno, B. & Zornberg, J. 2013, "Performance of nonwoven geotextile-reinforced walls under wetting conditions: laboratory and field investigations", Geosynthetics International, vol. 20, no. 2, pp. 90-104.

Powrie, W. 2014, "On track: the future for rail infrastructure systems", vol. 167, Thomas Telford Ltd, pp. 177-85.

Powrie, W., Yang, L. & Clayton, C.R. 2007, "Stress changes in the ground below ballasted railway track during train passage", Proceedings of the Institution of Mechanical Engineers, Part F: Journal of Rail and Rapid Transit, vol. 221, no. 2, pp. 247-62.

Pradhan, T. 1993, "Experimental Study on the Equivalent Diameter of a Prefabricated Band-Shaped Drains", Eleventh Southeast Asian Geotechnical Conference, pp. 391-6.

Priest, J., Powrie, W., Yang, L., Grabe, P. & Clayton, C. 2010, "Measurements of transient ground movements below a ballasted railway line", Géotechnique, vol. 60, no. 9, pp. 667-77.

Procter, D.C. & Khaffaf, J.H. 1984, "Cyclic triaxial tests on remoulded clays", Journal of Geotechnical Engineering, vol. 110, no. 10, pp. 1431-45.

Punetha, P., Maharjan, K. & Nimbalkar, S. 2021, "Finite Element Modeling of the Dynamic Response of Critical Zones in a Ballasted Railway Track", Frontiers in Built Environment, vol. 7, p. 42.

Raut, A.K. & Indraratna, B. 2008, "Further advancement in filtration criteria through constriction-based techniques", Journal of Geotechnical and Geoenvironmental Engineering, vol. 134, no. 6, pp. 883-7.

Raut, A.S., Dahiwade, A.A., Jangale, K.R., Lawhale, P.O. & Ghodmare, S.D. 2016, "Performance and Evaluation of Pavement Design with and without using Geotextiles", International Journal for Scientific Research & Development|, vol. 4, no. 3, pp. 438-41.

Rawes, B. 1997, "Critical parameters for specification of prefabricated vertical drains", Geosynthetics International, vol. 4, no. 1, pp. 51-64.

Raymond, G. 1984, "Research on geotextiles for heavy haul railways", Canadian Geotechnical Journal, vol. 21, no. 2, pp. 259-76.

Raymond, G. 1999, "Railway rehabilitation geotextiles", Geotextiles and Geomembranes, vol. 17, no. 4, pp. 213-30.

Raymond, G.P. 1986a, "Geotextile Application for a branch line upgrading", Geotextiles and Geomembranes, vol. 3, no. 2-3, pp. 91-104.

Raymond, G.P. 1986b, "Installation factors that affect perfromance of railroad geotextiles", Transportation Research Record, no. 1071.

Razouki, S.S. 2016, "Radial consolidation clay behaviour under haversine cyclic load", Proceedings of the Institution of Civil Engineers-Ground Improvement, vol. 169, no. 2, pp. 143-9.

Read, D., Hyslip, J. & McDaniel, R. 2011, "Heavy axle load revenue service mud-fouled ballast investigation", Technical Report. Federal Railroad Administration U.S. Department of Transportation.

Richardson, G.N. 1998, "Field evaluation of geosynthetic survivability in aggregate road base", Geotechnical Fabrics Report, vol. 16, pp. 34-9.

Rixner, J., Kraemer, S. & Smith, A. 1986, "Prefabricated vertical drains," Engineering Guideline, FHWA/RD-86/168, Federal Highway Administration, Virginia, vol. 1.

Road and Rail Freight 2018, "Supporting paper No.3: Inquiry into National Freight and Supply Chain Priorities", Australian Government, ISBN: 978-1-925701-16-6.

Rollin, A. & Lombard, G. 1988, "Mechanisms affecting long-term filtration behavior of geotextiles", Geotextiles and Geomembranes, vol. 7, no. 1-2, pp. 119-45.

Rollin, J.L., L, A. & Mlynarek, J. 1990, "Clogging of geotextiles under pumping loads", Geotextiles, Geomembranes, and Related Products: Steep slopes and walls. Embankments on soft soil. Roads and railroads. Filtration and drainage. Erosion control, vol. 1, p. 189.

Rosete, A., Mendonça Lopes, P., Pinho-Lopes, M. & Lopes, M. 2013, "Tensile and hydraulic properties of geosynthetics after mechanical damage and abrasion laboratory tests", Geosynthetics International, vol. 20, no. 5, pp. 358-74.

Rowe, R.K. 2020, "Protecting the Environment with Geosynthetics: 53rd Karl Terzaghi Lecture", Journal of Geotechnical and Geoenvironmental Engineering, vol. 146, no. 9, p. 04020081.

Rujikiatkamjorn, C. & Indraratna, B. 2007, "Analytical solutions and design curves for vacuum-assisted consolidation with both vertical and horizontal drainage", Canadian Geotechnical Journal, vol. 44, no. 2, pp. 188-200.

Rujikiatkamjorn, C., Indraratna, B. & Meng, G. 2011, "Experimental study on the effectiveness of prefabricated vertical drains under cyclic loading", International Conference on Advances in Geotechnical Engineering, Perth, Australia, ISBN: 978-0-646-55142-5.

Sabiri, N.-E., Caylet, A., Montillet, A., Le Coq, L. & Durkheim, Y. 2020, "Performance of nonwoven geotextiles on soil drainage and filtration", European Journal of Environmental and Civil Engineering, vol. 24, no. 5, pp. 670-88.

Samarasinghe, A.M., Huang, Y.H. & Drnevich, V.P. 1982, "Permeability and consolidation of normally consolidated soils", Journal of the Geotechnical Engineering Division, vol. 108, no. 6, pp. 835-50.

Sangrey, D., Henkel, D. & Esrig, M.I. 1969a, "The effective stress response of a saturated clay soil to repeated loading", Canadian Geotechnical Journal, vol. 6, no. 3, pp. 241-52.

Sangrey, D.A., Henkel, D.J. & Esrig, M.I. 1969b, "The effective stress response of a saturated clay to repeated loading", Canadian Geotechnical Journal, vol. 6, no. 3, pp. 241-52.

Sañudo, R., Miranda, M., García, C. & García-Sanchez, D. 2019, "Drainage in railways", Construction and Building materials, vol. 210, pp. 391-412.

Seah, T.H. 2006, "Design and construction of ground improvement works at Suvarnabhumi Airport", Geotechnical Engineering, vol. 37, no. 3, p. 171.

Selig, E., DelloRusso, V. & Laine, K. 1992, "Sources and causes of ballast fouling", Association of American Railroads,Technical Center, Chicago.

Selig, E.T. & Li, D. 1994, "Track modulus: Its meaning and factors influencing it", Transportation Research Record, no. 1470.

Selig, E.T. & Waters, J.M. 1994, Track Geotechnology and Substructure Management, Thomas Telford, London, U.K.

Sharma, J. & Xiao, D. 2000, "Characterization of a smear zone around vertical drains by large-scale laboratory tests", Canadian Geotechnical Journal, vol. 37, no. 6, pp. 1265-71.

Sharpe, P. 1988, "Track foundation reinforcement–The performance of six experimental track foundations", Technical Memorandum, British Rail Research, Derby, Ref TM TM 035.

Sharpe, P., Roskams, T. & Valero, S.N. 2014, "The development of a geocomposite to prevent mud pumping", In Proceedings of the Conference on Railway Excellence: Railway Transport for Vital Economy (RTSA), Adelaide, Australia, pp. 346-53.

Shen, Y., Xu, H., Tao, M., Wang, B. & Song, S. 2017, "Settlement of soft clay subgrade under coupled effects of vibration frequency and dynamic stress ratio caused by high-speed train loads", Soil Mechanics and Foundation Engineering, vol. 54, no. 2, pp. 87-96.

Shire, T. & O'Sullivan, C. 2013, "Micromechanical assessment of an internal stability criterion", Acta Geotechnica, vol. 8, no. 1, pp. 81-90.

Singh, M. 2021, "Subgrade instability and fluidisation under cyclic railway loading", PhD Thesis, University of Wollongong, Australia, p. 172.

Singh, M., Indraratna, B. & Nguyen, T.T. 2021, "Experimental insights into the stiffness degradation of subgrade soils prone to mud pumping", Transportation Geotechnics, vol. 27, p. 100490.

Singh, M., Indraratna, B. & Rujikiatkamjorn, C. 2019, 'Use of geosynthetics in mitigating the effects of mud pumping: a railway perspective', Geotechnics for Transportation Infrastructure, Springer, pp. 609-18.

Singh, M., Indraratna, B., Rujikiatkamjorn, C. & Kelly, R. 2020a, "Cyclic response of railway subgrade prone to mud pumping", Australian Geomechanics Journal, vol. 55, no. 1, pp. 43-54.

Singh, R.P., Nimbalkar, S., Singh, S. & Choudhury, D. 2020b, "Field assessment of railway ballast degradation and mitigation using geotextile", Geotextiles and Geomembranes, vol. 48, no. 3, pp. 275-83.

Skempton, A. & Brogan, J. 1994, "Experiments on piping in sandy gravels", Geotechnique, vol. 44, no. 3, pp. 449-60.

Subaida, E., Chandrakaran, S. & Sankar, N. 2009, "Laboratory performance of unpaved roads reinforced with woven coir geotextiles", Geotextiles and Geomembranes, vol. 27, no. 3, pp. 204-10.

Sudarsanan, N., Mohapatra, S.R., Karpurapu, R. & Amirthalingam, V. 2018, "Use of natural geotextiles to retard reflection cracking in highway pavements", Journal of Materials in Civil Engineering, vol. 30, no. 4, p. 04018036.

Sun, Q.D., Indraratna, B. & Nimbalkar, S. 2016, "Deformation and degradation mechanisms of railway ballast under high frequency cyclic loading", Journal of Geotechnical and Geoenvironmental Engineering, vol. 142, no. 1, p. 04015056.

Sussmann, T.R., Ruel, M. & Chrismer, S.M. 2012, "Source of ballast fouling and influence considerations for condition assessment criteria", Transportation Research Record, vol. 2289, no. 1, pp. 87-94.

Takatoshi, I. 1997, "Measure for the stabilization of railway earth structure", Japan Railway Technical Service, vol. 290.

Tang, X.W. & Onitsuka, K. 2001, "Consolidation of double-layered ground with vertical drains", International Journal for Numerical and Analytical Methods in Geomechanics, vol. 25, no. 14, pp. 1449-65.

Tavakoli Mehrjardi, G. & Amjadi Sardehaei, E. 2019, "Design graphs to estimate reduction factor of nonwoven geotextiles due to installation process", European Journal of Environmental and Civil Engineering, vol. 23, no. 9, pp. 1069-82.

Tennakoon, N. & Indraratna, B. 2014, "Behaviour of clay-fouled ballast under cyclic loading", Géotechnique, vol. 64, no. 6, pp. 502-6.

Tennakoon, N., Indraratna, B. & Rujikiatkamjorn, C. 2014, "Effect of ballast contamination on the behaviour of track substructure", Aust. Geomech. Journal, vol. 49, pp. 111-23.

Tennakoon, N., Indraratna, B., Rujikiatkamjorn, C., Nimbalkar, S. & Neville, T. 2012, "The role of ballast-fouling characteristics on the drainage capacity of rail substructure", Geotechnical Testing Journal, vol. 35, no. 4, pp. 629-40.

Thian, S. & Lee, C. 2017, "Cyclic stress-controlled tests on offshore clay", Journal of Rock Mechanics and Geotechnical Engineering, vol. 9, no. 2, pp. 376-81.

Toyota, H. & Takada, S. 2021, "Soil element assessment of cyclic-load-induced settlement considering combination of vertical, horizontal, and shear stresses in cohesive soil", Soils and Foundations, vol. 61, no. 3, pp. 752-64.

Trani, L.D.O. & Indraratna, B. 2010a, "Assessment of subballast filtration under cyclic loading", Journal of Geotechnical and Geoenvironmental Engineering, vol. 136, no. 11, pp. 1519-28.

Trani, L.D.O. & Indraratna, B. 2010b, "Experimental investigations into subballast filtrations behaviour under cyclic conditions", Aust. Geomech. Journal, vol. 45, no. 3, pp. 123-33.

Trani, L.D.O. & Indraratna, B. 2010c, "Use of impedance probe for estimation of porosity changes in saturated granular filters under cyclic loading: calibration and

application", Journal of Geotechnical and Geoenvironmental Engineering, vol. 136, no. 10, pp. 1469-74.

Transport for NSW 2016, Track Reconditioning Guidelines, T HR CI 12120 GU, Transport Asset Standards Authority, NSW.

Trinh, V.N., Tang, A.M., Cui, Y.-J., Dupla, J.-C., Canou, J., Calon, N., Lambert, L., Robinet, A. & Schoen, O. 2012, "Mechanical characterisation of the fouled ballast in ancient railway track substructure by large-scale triaxial tests", Soils and Foundations, vol. 52, no. 3, pp. 511-23.

Truong, M.H., Indraratna, B., Nguyen, T.T., Carter, J. & Rujikiatkamjorn, C. 2021, "Analysis of undrained cyclic response of saturated soils", Computers and Geotechnics, vol. 134, p. 104095.

Tutumluer, E., Dombrow, W. & Huang, H. 2008, "Laboratory characterization of coal dust fouled ballast behavior", In AREMA 2008 Annual Conference & Exposition, pp. 21-4.

USACE 2000, (U.S. Army Corps of Engineers), Railroad design and construction, TI 850–02, 32-1125(I), Washington, DC.

Voottipruex, P. & Roongthanee, J. 2003, "Prevention of mud pumping in railway embankment a case study from Baeng Pra-pitsanuloke, Thailand", The Journal of KMITB, vol. 13, no. 1, pp. 20-5.

Vucetic, M. & Dobry, R. 1991, "Effect of soil plasticity on cyclic response", Journal of Geotechnical Engineering, vol. 117, no. 1, pp. 89-107.

Wang, J., Guo, L., Cai, Y., Xu, C. & Gu, C. 2013, "Strain and pore pressure development on soft marine clay in triaxial tests with a large number of cycles", Ocean Engineering, vol. 74, pp. 125-32.

Wang, L., Zhang, G. & Zhang, J.-M. 2011, "Centrifuge model tests of geotextile-reinforced soil embankments during an earthquake", Geotextiles and Geomembranes, vol. 29, no. 3, pp. 222-32.

Wang, M., Kong, L., Zhao, C. & Zang, M. 2012, "Dynamic characteristics of lime-treated expansive soil under cyclic loading", Journal of Rock Mechanics and Geotechnical Engineering, vol. 4, no. 4, pp. 352-9.

Wang, T.-l., Song, H.-f., Yue, Z.-r., Hu, T.-f., Sun, T.-c. & Zhang, H.-b. 2019, "Freeze–thaw durability of cement-stabilized macadam subgrade and its compaction quality index", Cold Regions Science and Technology, vol. 160, pp. 13-20.

Wheeler, L.N., Take, W.A. & Hoult, N.A. 2017, "Performance assessment of peat rail subgrade before and after mass stabilization", Canadian Geotechnical Journal, vol. 54, no. 5, pp. 674-89.

Wichtmann, T., Andersen, K., Sjursen, M. & Berre, T. 2013, "Cyclic tests on high-quality undisturbed block samples of soft marine Norwegian clay", Canadian Geotechnical Journal, vol. 50, no. 4, pp. 400-12.

Williams, N.D. & Abouzakhm, M.A. 1989, "Evaluation of geotextile/soil filtration characteristics using the hydraulic conductivity ratio analysis", Geotextiles and Geomembranes, vol. 8, no. 1, pp. 1-26.

Wong, R., Thomson, P. & Choi, E. 2006, "In situ pore pressure responses of native peat and soil under train load: a case study", Journal of Geotechnical and Geoenvironmental Engineering, vol. 132, no. 10, pp. 1360-9.

Wu, H., Yao, C., Li, C., Miao, M., Zhong, Y., Lu, Y. & Liu, T. 2020, "Review of application and innovation of geotextiles in geotechnical engineering", Materials, vol. 13, no. 7, p. 1774.

Xiao, M. & Reddi, L.N. 2000, 'Comparison of fine particle clogging in soil and geotextile filters', Advances in Transportation and Geoenvironmental Systems Using Geosynthetics, pp. 176-85.

Yahaya, N.N., Ibrahim, A., Ahmad, A. & Rozli, M.I.F. 2020, "Case Study: Prevention Methods of Mud Pumping in Railway Track System", In Proceedings of Civil Engineering Colloquium 2020, p. 114.

Yang, Q., Tang, Y., Yuan, B. & Zhou, J. 2019, "Cyclic stress–strain behaviour of soft clay under traffic loading through hollow cylinder apparatus: effect of loading frequency", Road Materials and Pavement Design, vol. 20, no. 5, pp. 1026-58.

Yang, Z., Boogaard, A., Wei, Z., Liu, J., Dollevoet, R. & Li, Z. 2018, "Numerical study of wheel-rail impact contact solutions at an insulated rail joint", International Journal of Mechanical Sciences, vol. 138, pp. 310-22.

Yasuhara, K., Hirao, K. & Hyde, A.F. 1992, "Effects of cyclic loading on undrained strength and compressibility of clay", Soils and Foundations, vol. 32, no. 1, pp. 100-16.

Yasuhara, K., Yamanouchi, T. & Hirao, K. 1982, "Cyclic strength and deformation of normally consolidated clay", Soils and Foundations, vol. 22, no. 3, pp. 77-91.

Yean-Chin, T. & Peir-Tien, L. 2012, "Ground Treatment Design for 200km Electrified Double Tracks", Railway Project at Northern Peninsular Malaysia, pp. 32-44.

Yong, C.F., McCarthy, D.T. & Deletic, A. 2013, "Predicting physical clogging of porous and permeable pavements", Journal of Hydrology, vol. 481, pp. 48-55.

Yu, S., Wu-ming, L., Ji-dong, T., Ru-song, N. & Qi, Y. 2016, "Analysis of subgrade soil mud pumping model", Electronic Journal of Geotechnical Engineering, vol. 21, no. 24, pp. 7667-78.

Zeng, G.-X. & Xie, K.-H. 1989, "New development of the vertical drain theories", Proc., 12th Int. Conf. on Soil Mechanics and Foundation Engineering, Vol. 2, Rotterdam, The Netherlands, pp. 1435-8.

Zergoun, M. & Vaid, Y. 1994, "Effective stress response of clay to undrained cyclic loading", Canadian Geotechnical Journal, vol. 31, no. 5, pp. 714-27.

Zhang, S., Gao, F., He, X., Chen, Q. & Sheng, D. 2021a, "Experimental study of particle migration under cyclic loading: effects of load frequency and load magnitude", Acta Geotechnica, vol. 16, pp. 367-50.

Zhang, X., Pei, X., Zhang, Z. & Song, L. 2021b, "Study on pore pressure and fluidization evaluation method of unsaturated loess in vibration process", Bulletin of Engineering Geology and the Environment, pp. 1-13.

Zheng, G., Alimohammadi, H., Zheng, J. & Schaefer, V.R. 2021, 'Effectiveness of Geosynthetics in the Construction of Roadways: A Full-Scale Field Studies Review', IFCEE 2021, pp. 223-32.

Zhou, J. & Gong, X. 2001, "Strain degradation of saturated clay under cyclic loading", Canadian Geotechnical Journal, vol. 38, no. 1, pp. 208-12.

Zhu, D., Indraratna, B., Poulos, H. & Rujikiatkamjorn, C. 2020, "Field study of pile–prefabricated vertical drain (PVD) interaction in soft clay", Canadian Geotechnical Journal, vol. 57, no. 3, pp. 377-90.

Zornberg, J.G. & Thompson, N. 2012, Application guide and specifications for geotextiles in roadway applications, University of Texas at Austin. Center for Transportation Research.